ELUCIDATING THE FUNCTIONAL ROLE AND THERAPEUTIC POTENTIAL OF LA-RELATED PROTEIN 1B (LARP1B) IN CANCER AND ITS INTERPLAY WITH OTHER LARP FAMILY MEMBERS

UNIVERSITY OF OXFORD

Arussa Nawaz

A thesis submitted for the degree of Doctor of Philosophy

Department of Oncology

Lincoln College

University of Oxford

Michaelmas 2023

ELUCIDATING THE FUNCTIONAL ROLE AND THERAPEUTIC POTENTIAL OF LA-RELATED PROTEIN 1B (LARP1B) IN CANCER AND ITS INTERPLAY WITH OTHER LARP FAMILY MEMBERS

Arussa Nawaz

Thesis submitted for the degree of Doctor of Philosophy

Lincoln College, University of Oxford

Michaelmas 2023

Abstract

RNA binding proteins (RBPs) are indispensable regulators of gene expression with a growing body of evidence demonstrating their role in cellular acquisition of the hallmarks of cancer. By regulating the expression of hallmark regulatory genes, RBPs mediate key cancer phenotypes including sustained cell proliferation, evasion from apoptosis and the regulation of cellular energetics.

An exemplary group of RBPs known as the La-related proteins (LARPs) which include LARP1, LARP1B, La, LARP4, LARP4B, LARP6 and LARP7, are established regulators of mRNA translation and most are also known cancer effectors associated with cancer hallmarks. Whilst some LARPs such as LARP1 demonstrate pro-tumorigenic roles, others such as LARP7 exhibit anti-tumorigenic functions highlighting even intrafamilial diversity. To date, LARP1B has remained the "dark horse" of the family with little to no knowledge regarding the biological processes it regulates or participates in or its involvement in cancer. As such, this thesis provides a comprehensive analysis into the phenotypic and functional role of LARP1B in the context of cancer and to the best of our knowledge is the first study to do so.

Our interrogation of the LARP1B protein interactome revealed several novel candidates implicated in diverse biological processes ranging from cytoplasmic translation to metabolic processes and the regulation of mitochondrial gene expression. Within this, a striking finding

was the identification of many nuclear-localised proteins bound to LARP1B revealing previously unknown characteristics of nuclear-cytoplasmic shuttling, suggesting a diverse LARP1B-ribonucleoprotein (RNP) portfolio.

Importantly, we observed an affinity for LARP1B expression in testicular tissue and testicular germ cell tumour (TGCT) cells in which LARP1B appeared to regulate intracellular reactive oxygen species (ROS) levels and mitochondrial function. Following LARP1B depletion, we observed a significant impact on cellular fitness and growth which we attributed to oxidative stress and mitochondria dysfunction induced cytotoxicity and apoptosis. Given that testicular germ cells and surrounding tissue are highly sensitive to oxidative stress which can have severe adverse effects on sperm quality and function, these findings hint at an important role for LARP1B in the protection of testicular germ cells. Implications of this extend from male infertility to TGCT development which are often interlinked and are important considerations for the preservation of species.

Declaration of authenticity

I can confirm that all material presented in this thesis is the outcome of my own work, except in the following experiments and analyses which were kindly performed or supported by others:

- Immunohistochemistry staining of testis-specific tissue microarray shown in ***3*: Results Chapter 1** was performed by Molly Browne (Research and Laboratory Technician, Translational Histopathology lab, University of Oxford).
- Mass Spectrometry and analysis shown in **4: Results Chapter 2** and **supplementary** was performed with the help of Dr Robert Parker (Post Doctoral Researcher, Ternette Group, University of Oxford)
- LARP1B_Flag expression vector used throughout **5: Results Chapter *3*** was kindly provided by our long-term collaborator Dr Andrea Berman (Associate Professor, University of Pittsburgh, USA)
- MitoSOX live cell staining and quantification in **5: Results Chapter *3*** was performed with the support of Kendra Perez Smith (Research Assistant, Blagden Lab, University of Oxford)

To the best of my knowledge, no aspect of this thesis has been previously submitted for a degree, certificate or similar at the University of Oxford or elsewhere. This project was carried out under the supervision of Professor Sarah Blagden.

Arussa Nawaz

COVID-9 impact statement.

Before discussing the impact of the COVID-19 pandemic, it is important to note that the duration of this project was originally 3 years but due to the kindness of my peers, we were able to extend for an additional year in order to attempt making up for lost time during the pandemic.

This DPhil project was strongly impacted by the COVID-19 pandemic which began 5 months into the project and directly affected Years 1 and 2. During the first year, global lockdowns restricted access to the laboratory for approximately 5 months and so no experiments were completed during this time and no research tools were validated in preparation for experiments. During the lockdown I spent my time carrying out an extensive literature review in preparation for my return to the lab.

When access was finally granted to the building, the laboratory was open on a shift basis and with strict social distancing. These regulations meant that the time available to carry out experiments was cut short (up to 4 hours/day) affecting how and when certain experiments were carried out as they often take more than 4 hours to complete. The stringent rules also meant that experiments were carried out in isolation with little to no physical support or guidance available from far more experienced team members, which is of vital importance for DPhil students early on in their project. These regulations continued for the duration of the second year resulting in an approximately 50% reduction in time spent in the lab compared to what would be under normal working conditions.

The mental and emotional pressure applied due to the COVID-19 pandemic made the third year unexplainably more challenging as this was scheduled as the final year. Luckily half-way into the third year, we secured additional funding. Despite my gratitude for the opportunity to carry out research for an additional year, the impacts of the COVID-19 pandemic on the execution of this project affected my mental health and did not make completion of this project any easier. I also contracted COVID-19 which required self-isolation and I have felt effects of long COVID since.

Acknowledgements

My deepest gratitude goes to my creator Allah (swt) whose mercy and guidance has brought me where I am today. I have faced many challenges during the past 4 years, questioned every aspect of my life but the knowledge that this is all part of Allah's great plan for me has been my saving grace. Alhamdulillah.

I then extend my thanks to my supervisor Professor Sarah Blagden who took a chance on me 5 years ago. Your passion for science, support for women in STEM and ability to effortlessly multitask major projects is inspiring. I appreciate your support throughout my time here at Oxford in both my professional and personal life. I would also like to thank CRUK for the financial support I have received, without which this DPhil would not be possible.

To all members of the Blagden lab past and present, thank you for your continued support and contributions throughout this project. Each of you have the most unique personalities which make the Blagden lab extra special. Extra special thanks to Zinaida and James for thorough review of this thesis. To the friends I have made within the department, thank you for stimulating scientific conversations and always providing top-tier snacks! And to the Lincoln College MCR committee I was a part of, thank you for allowing me a platform to promote diversification and equality at Lincoln College; I have made positive changes I am extremely proud of and will continue to provide a lifetime of service to the MCR.

To the wonderful Barista's at Gail's, Summertown – I cannot thank you enough for the warm, friendly environment you always provided. The coffees and cakes were great too! This place became my second home during the final phase of my DPhil, and I will always remember the kindness of you all during such a difficult and stressful time.

My dearest friend Philippa, our friendship began during fresher's week whilst bonding over our love for the North. That bond has continued to grow over time and your friendship has been the most beautiful constant over the past 4 years. I will always remember our coffee dates contemplating trying every slice of cake that was on offer, our

girly nights out, sharing our big plans for the future and our pep talks – I hold these memories so close to my heart and our friendship means more to me than you know. Thank you for all that you are!

I've been lucky enough to have my family grow over the years with a wonderful big brother-in-law, mum- and dad-in-laws, sisters-in-laws and more who have all have been a continued support throughout my DPhil experience, for which I am extremely grateful. To my mother and father who have supported every decision of mine and are the reason for all that I am – words will never do justice for how thankful I am to you both. Baba, thank you for always reminding us of the importance of education.

To my oldest sister Maria. Only God knows how you manage being the most hands-on, super-mum to the most beautiful two babies and still find the time to check up on me. The FaceTime calls with Zavi and Millie, "just checking in" messages and hearing me rant about failed experiments alone, have gotten me through this challenging experience. You're more than a sister to me and will always be my female soulmate. I hope I make you a proud sister and an inspiring Maasi for Zaviyaan and Amelia.

Lastly, to my dearest husband Imran. Our first 4 years of marriage have coincided with this DPhil which have inevitably brought its challenges. From spending our honeymoon phase in a global lockdown, losing our best friend Bambi and being apart for weeks due to your work commitments all in addition to this PhD. We've really been through it all! I cannot thank you enough for your continued efforts in trying to understand what I do, supporting me through every hurdle, making me smile every single day and reminding me that I am more capable than I realise. I am eternally grateful for all that you do for us and can only hope to make you as proud as you make me.

I also want to take a moment to acknowledge just how difficult this experience has been. Completing a PhD was something I imagined but did not anticipate it becoming a reality at the University of Oxford. Nobody tells you just how isolating undertaking a PhD can be, particularly when you're the only scientist in your family unable to share your thoughts with anyone else. Not seeing family for months, having zero social life, working

consecutively for 45+ days without a break, late night weekend lab shifts, extreme dehydration…the list is endless! A PhD really is not for the faint hearted and I appreciate just how tough it can be much more now. I am proud for not giving up and losing heart and this PhD is a reminder to myself that I am capable of anything I put my mind to.

"Allah does not burden a soul beyond which it can bear" – Quran, 2:286

List of Figures

List of Tables

Abbreviations

5'/3'-UTR	5'/3'-Untranslated region
aa	Amino acids
ACC	Adrenocortical carcinoma
ADP	Adenosine diphosphate
ATP	Adenosine triphosphate
AMPK	AMPK activated protein kinase
BIS-AAF-R110	Bis-analyl-analyl-phenylanalyl-rhodamine 110
BLCA	Bladder urothelial carcinoma
BRCA	Breast invasive carcinoma
CDS	Coding sequence
CER	Cytoplasmic extraction reagent
CESC	Cervical squamous cell carcinoma and endocervical adenocarcinoma
CHOL	Cholangiocarcinoma
CI	Cell Index
COAD	Colon adenocarcinoma
cov	coverage
Cyto	Cytoplasmic
DAPI	4'-6-diamidino-2-phenylindole
DLBC	Lymphoid neoplasm diffuse large B-cell lymphoma
DNA	Deoxy-ribonucleic acid
ECAR	Extracellular acidification rate
ESCA	Esophageal carcinoma
FADH	Flavin Adenine Dinucleotide + Hydrogen
FBS	Foetal Bovine Serum
FCCP	Carbonyl cyanide-p-trifluoromethoxy phenylhydrazone
FFPE	Formalin-Fixed Paraffin-Embedded
GBM	Glioblastoma multiforme
GCT27	Germ Cell Tumour 27
GCT27CR	Germ Cell Tumour 27 Cisplatin Resistant
GCNIS	Germ cell neoplasia *in situ*
GE	Germinal Epithelium

GF-AFC	Glycyl-phenylanalyl-aminofluorocoumarin
GRSF1	G-rich RNA sequence binding factor 1
GSH	Glutathione
GSK-3 β	Glycogen synthase kinase-3 β
GTEx	Genotype-Tissue Expression
HEK293T	Human embryonic kidney 293t
HER2	Human epidermal growth factor receptor 2
HIF1α	Hypoxia inducible factor 1 subunit alpha
HNSC	Head and neck squamous cell carcinoma
HPA	Human Protein Atlas
HuD	Human antigen D
HuR	Human antigen R
IF	Immunofluorescence
IP	Immunoprecipitation
kDa	Kilodaltons
KH	K-homology (domain)
KICH	Kidney chromophobe
KIRC	Kidney renal cell carcinoma
KIRP	Kidney renal papillary cell carcinoma
KRAS	Kirsten Ras oncogene
LAM	La motif
LAML	Acute myeloid leukaemia
LARP	La-related protein
LARP1	La-related protein 1
LARP1B	La-related protein 1B
LARP1^{KO}	LARP1 knockout
LDS	Lithium dodecyl sulphate
LGG	Brain lower grade glioma
LIHC	Liver hepatocellular carcinoma
LUAD	Lung adenocarcinoma
LUSC	Lung squamous cell carcinoma
MS	Mass Spectrometry
MS/MS	Tandem MS
mTOR	Mammalian target of rapamycin

mTORC1	Mammalian target of rapamycin complex 1
NADH	Nicotinamide Adenine Dinucleotide + Hydrogen
NER	Nuclear extraction reagent
NFR2	Nuclear erythroid -related factor 2
NSGCT	Non-seminomatous germ cell tumour
nuc	Nuclear
OCR	Oxygen consumption rate
OS	Overall survival
OV	Ovarian serous cystadenocarcinoma
PAAD	Pancreatic adenocarcinoma
PABP	Poly(A) binding protein
PBS	Phosphate buffered saline
PCPG	Pheochromocytoma and paraganglioma
PCR	Polymerase chain reaction
PFA	Paraformaldehyde
PGCs	Primordial germ cells
pid	Percentage identity
PRAD	Prostate adenocarcinoma
PTM	Post-translational modification
QKI	Quaking
qRT-PCR	Real-time quantitative reverse transcription PCR
RBD	RNA-binding domain
RBP	RNA binding protein
READ	Rectum adenocarcinoma
RIPA	Radioimmunoprecipitation assay (buffer)
RIP-Seq	RNA IP sequencing
RNA	Ribonucleic acid
RNP	Ribonucleoprotein complex
ROS	Reactive oxygen species
RRM	RNA recognition motif
RTCA	Real Time Cell Analysis
SARC	Sarcoma
shRNA	Short hairpin RNA
siRNA	Small interfering RNA

SKCM	Skin cutaneous melanoma
SOD1	Superoxide dismutase 1
ST	Seminiferous Tubules
STAD	Stomach adenocarcinoma
TCA	The Citric Acid (Cycle)
TCGA	The Cancer Genome Atlas
TGCT	Testicular germ cell tumour
THCA	Thyroid carcinoma
THYM	Thymoma
TMA	Tissue microarray
TOMM20	Translocase of outer mitochondrial membrane 20
TP53	Tumour protein p53
TPM	Transcripts per million
TfR1	Transferrin receptor 1
UCEC	Uterine corpus endometrial carcinoma
UCS	Uterine carcinosarcoma
WCE	Whole Cell Extract

Nomenclature

Human proteins are written in upper case e.g., LARP1B

Human genes are written in upper case, italicised e.g., *LARP1B*

Yeast genes are written in lower case with the first letter capitalised e.g., Sro9

Vertebrate genes (*Xenopus* and Zebrafish) are written in lower case, italicised e.g., *larp1b*

Table of contents

1

INTRODUCTION

1.1 RNA binding proteins (RBPs)

More than 7.5% of all protein-coding genes in the human genome encode RBPs, with over 1500 RBPs being identified to date[1, 2]. RBPs belong to diverse functional categories[3] and are defined as such due to the ability to bind RNA regulatory elements within different RNA species including messenger RNA (mRNA) and microRNA (miRNA)[4]. By doing so, RBPs play key roles in co-transcriptional and post-transcriptional gene expression regulation to maintain normal cellular function and regulate biological processes including, but not limited to, cell differentiation, growth, proliferation and metabolism[5].

1.1.1 RBPs – master regulators of gene expression

Eukaryotic mRNA transcripts possess characteristic structural elements including the 5'cap and 3' poly(A) tail which determine mRNA-protein interactions and efficient translation. RNA binding proteins (RBPs) are one class of proteins involved in gene expression regulation, guiding the RNA from pre-mRNA splicing in the nucleus to the cytoplasm for further processing, translation, degradation, and storage **(Figure 1.1**). This way, RBPs are key to ensuring the balance of mRNA supply and demand and thus maintenance of cellular fate and function. [6, 7] Importantly, by regulating mRNA kinetics RBPs regulate downstream protein expression and localisation mediating biological processes and cell phenotypes[8].

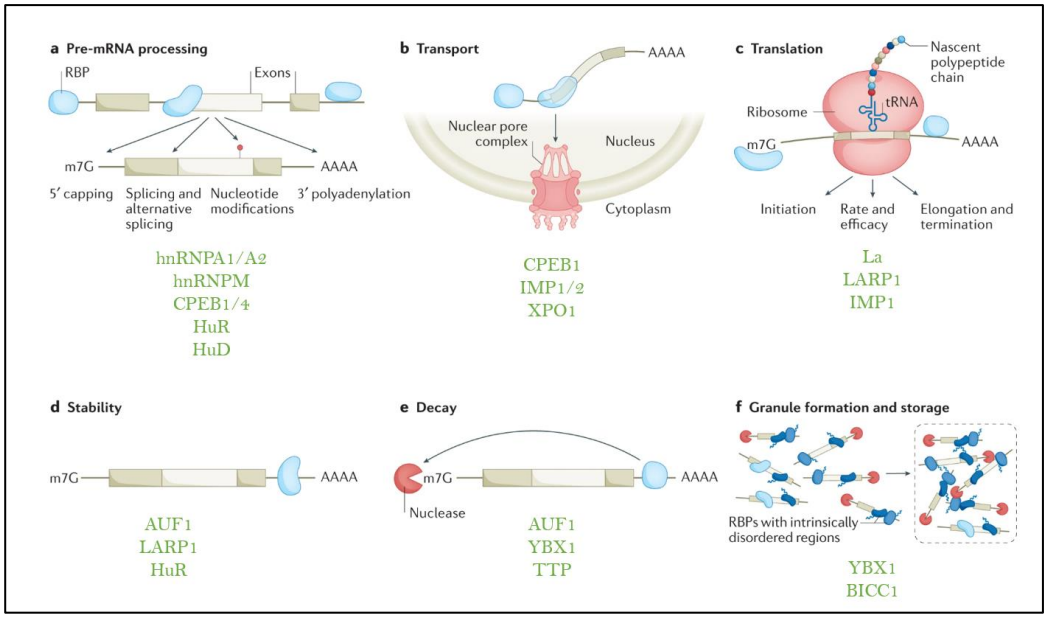

Figure 1.1: RBPs interact with mRNAs at every stage of the mRNA life cycle to regulate cellular fate and function. ***a.*** *RBPs are indispensable for pre-mRNA processing including 5'capping, splicing and 3'polyadenylation.* ***b.*** *RBPs enable mRNPs assembly and export of mRNAs from the nucleus into the cytoplasm through nuclear pore complexes.* ***c.*** *Once in the cytoplasm, RBPs regulate translation initiation and rate, transcript elongation and translation termination.* ***d.-e.*** *RBPs regulate mRNA stability and decay and* ***f.*** *aid in the formation of membrane-less organelles including stress granules and P-bodies for RNA storage. Example RBPs are listed in green. Diagram adapted from Seufert et al., 2022[9] and further information derived from Pereira et al., 2017[7].*

RBPs are typically modular in structure composed of multiple RNA binding domains (RBDs) responsible for binding to RBP recognition elements within the coding and non-coding regions of target mRNAs. A single RBP can possess one of many RBDs which collectively dictate RBP binding affinity and specificity; a number of RBDs have been identified including but not limited to the RNA recognition motif (RRM), K-Homology (KH) domain, and zinc finger domain. The resultant mRNA-RBP interactions are referred to as ribonucleoprotein complexes (RNPs). [7, 10, 11]

RBPs themselves are subject to tight regulation as any deviation from the norm can prove catastrophic. For example, the subcellular localisation of RBPs dictates which stage of the RNA life cycle it is regulating and ensures correct transition from one stage to the next[12]. Post-translational modifications (PTMs) such as methylation, phosphorylation and ubiquitination can also impact RBPs particularly if inflicted on RNA binding elements that are deemed "hotspots" for PTMs[7, 10, 12]. Such modifications can alter RBP localisation as well as binding affinities for target mRNAs or proteins, altering downstream effects[7, 13]. As such, any perturbation in RBP regulation can have major implications and is the core to the development and progression of a number of diseases ranging from neurological disorders to cancer. Our focus will be on the roles of RBPs in the development and progression of cancer.

1.1.2 RBPs in cancer

Cancer encompasses a set of diseases in which cells acquire the ability to uncontrollably grow and proliferate beyond their site of origin within the body (metastasis) due to the activation of oncogenes and/or deactivation of tumour suppressor genes[14]. It is typically understood that these diseases arise as a result of genetic and epigenetic changes which are either inherited or acquired over time[15]. However, post-transcriptional changes also contribute to cancer by promoting the acquisition of cancer hallmarks, of which RBPs are an emerging driving force[16]. There are a number of established key players in the development and progression of various cancers including the Tumour Protein P53 (*TP53*), Kirsten Ras oncogene (*KRAS*) and Human epidermal growth factor receptor 2 (*HER2*) genes with some like the *HER2* gene encoding a protein against which there is successful therapeutic intervention, namely Trastuzamab. Trastuzamab is administered as adjuvant therapy for HER2-positive early-stage breast cancer and is composed of a monoclonal antibody which binds to the HER2 transmembrane receptor thereby preventing receptor dimerization and downstream signalling cascades. The net result includes cell cycle arrest, disrupted DNA damage repair and apoptosis. [17, 18] Still, cancer remains the leading cause for mortality with over 19 million new cases recorded in 2020[19]. Despite continued efforts and achievements in understanding the pathophysiology of cancer and how best to treat them, numbers are on the rise.

Cancer cells are said to possess a unique set of characteristics termed hallmarks of cancer which enable their growth and survival; evading growth suppressors, sustained proliferative signalling, resisting cell death and induction of angiogenesis are just a few of the hallmarks defined by Hanahan and Weinberg[20]. We now know that acquisition of these hallmarks is a result of an altered genomic landscape in cancer, with the post-transcriptional modification of key regulatory genes being a known determinant for the development and progression of many cancers[21, 22]. Further research has led to the emergence of RNA binding proteins (RBPs) as key contributors to genomic alterations observed in the development and progression of cancer.

A number of studies have outlined the involvement of RBPs in the development and progression of different cancer types which are found to be over and under-expressed in

tumour tissue compared to normal tissue, depending on the cancer subtype analysed[1, 23]. Changes in RBP expression ultimately alters the normal functionality of these proteins, which can impact the expression and function of downstream tumour suppressor genes and oncogenes, promoting the acquisition of multiple cancer hallmarks (**Figure 1.2**)[23, 24]. For example, the Hu antigen R (HuR) RBP is upregulated in a number of cancers including lung and breast cancers where expression is associated with poor overall survival outcomes[25, 26]. HuR is known to bind adenine- and uridine-rich elements (ARE) within the 3'untranslated region (UTR) of target genes enhancing their stability and translation. As many HuR target mRNAs encode factors promoting cancer cell growth, proliferation, invasion and metastasis, HuR regulatory effects on these transcripts demonstrates a pro-tumorigenic role. [27, 28] Meanwhile, expression of RNA binding protein Quaking (QKI) is often downregulated in lung adenocarcinoma and confers a poor prognosis. QKI has been demonstrated to regulate the alternative splicing of *NUMB* pre-mRNA, inhibiting activation of the Notch signalling pathway and lung cancer cell proliferation. Thus, QKI demonstrates an anti-tumorigenic role. [7, 29] Although initially seen as "un-druggable" due to the lack of open binding pockets, RBPs are gaining traction as potential cancer therapeutic targets using novel approaches such as small molecular inhibitors, anti-sense oligonucleotides and siRNA (reviewed by Mohibi et al., 2019)[30].

Compelling recent evidence highlights the involvement of the La-related protein (LARP) family of RBPs in cancer, demonstrating diverse pro-tumorigenic and anti-tumorigenic roles.

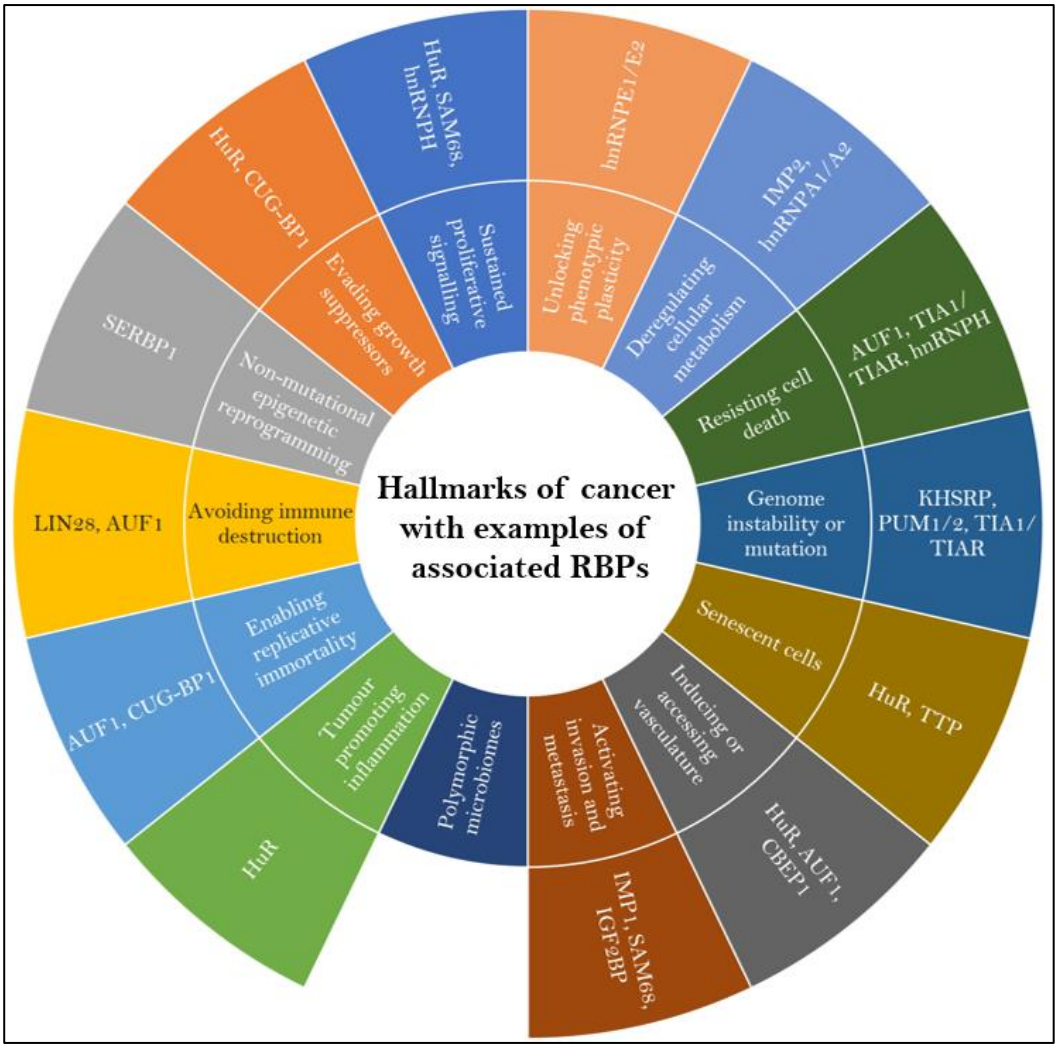

Figure 1.2: RBPs are associated with the acquisition of various hallmarks of cancer. *RBPs regulate various biological processes which during tumorigenesis can promote the acquisitions of multiple hallmarks of cancer. Figure adapted from Hallmarks of Cancer defined by Hanahan and Weinberg[31], with RBP annotations supported from[7, 10, 32-36]*

1.2 La-related Protein (LARP) family of RBPs

La protein (also known as LARP3) was discovered as an RNP target of autoimmune antibodies in Systemic Lupus Erythematosus (SLE) and pioneered research into the now established family of La-related proteins (LARPs)[37]. All LARPs possess the namesake "La-module" composed of the La-motif, interdomain linker and downstream RNA recognition motif (RRM)[38]. These proteins are established RBPs with key roles in regulating essentially all stages of the RNA cycle. [37]

1.2.1 LARP evolution, structure, and function

Whilst LARP proteins are evolutionarily conserved throughout eukaryotes[39], various La-motif containing proteins have been further characterised for example, in yeast there are three LARP orthologs termed Sro9p, Lhp1p and Slf1p exhibiting some similarity with the La motif with humans[40]. In humans, there are seven LARPs subdivided into five families: LARP1 (isoforms LARP1 and LARP1B), Genuine La/LARP3, LARP4 (LARP4/LARP4A and LARP5/LARP4B), LARP6 and LARP7 (**Figure 1.3**)[37]. Whilst LARP3 and LARP7 carry a canonical La-module, the remaining LARPs possess slightly altered variants due to their RRM-like (RRM-L) domains[37, 38, 41]. Furthermore, evolution has prompted the development of additional domains making each protein diverse in structure and functionality, with the La-module defining their RNA recognition and binding functions. LARP1 and LARP1B are distinct from the rest of the family as they possess another RBD, the DM15 domain. In-keeping with canonical functions of RBPs, the LARPs have established roles as regulators of the mRNA life cycle with contributions to essentially all stages. [37, 38]

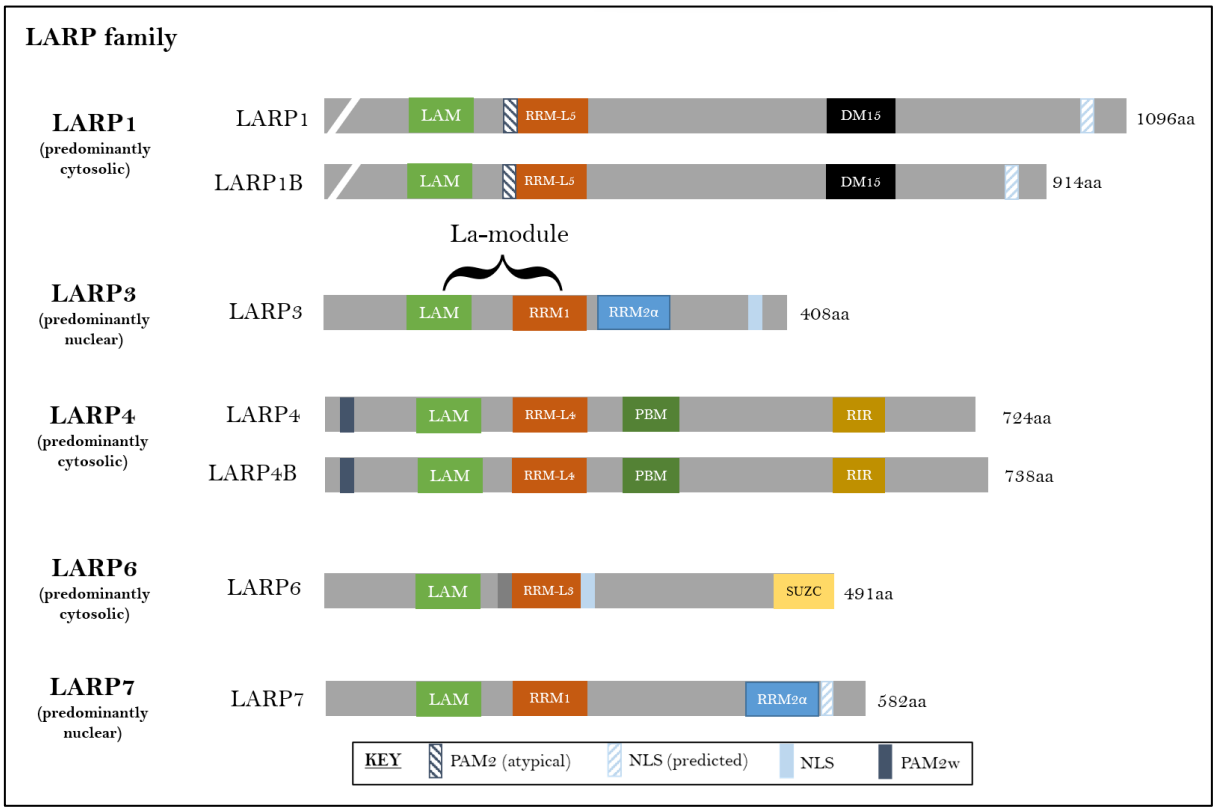

Figure 1.3: Schematic diagram of the LARPs adapted from Stavraka and Blagden., 2015[37] and Maraia et al., 2017[38]. *LAM: La motif, RRM/RRM-L: RNA recognition motif/RNA recognition motif-like, PBM: Poly(A) binding protein (PABP) -binding motif, RIR:*

RACK1 interaction region, PAM2/PAM2w: PABP-interacting motif 2, NLS: nuclear localisation sequence.

All LARP members have established characteristics as RBPs in gene expression regulation and some have further associations with the development and progression of various cancers. It is evident that LARP1B is lacking research with unknown roles in cancer, RNA targets and regulators compared to its siblings. To the best of our knowledge, this study is the first to provide an extensive characterisation of LARP1B in the context of cancer and how it interacts with paralog LARP1. Therefore, this work focuses on the LARP1 family encompassing LARP1 and LARP1B. **Table 1.1** outlines key characteristics of the LARP family members including roles in transcription and/or translation, oncogene, or tumour suppressor-like functions in cancer, target binding site and domain involved in RBP functions.

LARP	**Role in transcription and/or translation**	**Known mRNA or protein interactions and motifs or domains involved in the interactions**	**Known regulators**	**Cancers implicated (primary studies showing direct association)**	**Diseases or pathogens associated (primary studies showing direct association)**
LARP1	Translation: stabilises or de-stabilises mRNA transcripts to promote or repress translation[42]. LARP1 binds 5'terminal oligopyrimidine (TOP) sequences in a cap-independent manner[43] as well as other mRNAs[44–49] and interacts with poly(A) mRNA simultaneously[43].	We refer the reader to two key publications outlining the LARP1 mRNA interactome in HeLa[46] and HEK293T[50] which best describes LARP1 mRNA interactions. In summary: mTORC1, survival-associated, extracellular-matrix interactions, focal adhesion, actin cytoskeleton genes,	CDK9 phosphorylates LARP1[54] miR-129-5p[55], miR-615-5p [56], miR-374a[57], miR-144-5p[58],miR-330-5p[59], miR-26a/b[60], miR-326[61] and miR-185-5p/miR-214-3p[62] repressed LARP1 mRNA or protein expression and tumour promoting phenotypes	Pro-tumour role: Cervical cancer[51], ovarian cancer[44, 58], intrahepatic cholangiocarcinoma[64], prostate cancer[60], hepatocellular carcinoma[65, 66], hepatoblastoma[63], non-small cell lung cancer[57, 59], colorectal cancer[56, 67], osteosarcoma[55], lung adenocarcinoma[61] and clear cell renal carcinoma[62]	Non-alcoholic fatty liver disease[65], hepatitis C virus[68], HIV[69], influenza virus[70], dengue virus[71], SARS-COV-2[72] and diabetes[73]

		translation associated and ribosomal protein encoding genes were amongst mRNAs identified, in both cell lines. Key protein interactors include PABP, eIF4E, RAPTOR, mTORC pathway components[51, 52] La Module and PABP-interacting domains stabilise LARP1-mRNA interactions but are not necessary for	O-GlcNAc transferase prevented TRIM-25-mediated ubiquitination and proteolysis of LARP1[63] mTOR, Akt and S6K1 directly phosphorylate LARP1[50]		

		regulation; DM15 domain associates with 5'TOP sequences within target mRNAs[43, 45, 53]			
LARP1B	Translation: 5'Cap and TOP mRNA translation, similar to LARP1 but precise mechanism is unknown[48]	mTORC1, RAPTOR and PABP (exogenous LARP1B expression)[50, 74] . binding to PABP is mediated by the PAM2 domain[74]	Unknown	Unknown	β-thalassemia[75, 76] and diabetes[73]
LARP3	Transcription: La-module binds to the 3'UUU-OH region of nascent misfolded RNA polymerase III transcripts maintaining correct folding and protection from exonuclease digestion and tRNA assembly[37, 77] .	Cyclin D1-internal ribosome entry site (CCND1-IRES) mediated protein synthesis[78, 79]	Akt phosphorylation at T389 abrogates RNA chaperone activity and CCND1 IRES-mediated mRNA translation by LARP3[78]	Pro-tumour role: Cervical cancer[79], hepatocellular carcinoma[82, 83], head and neck squamous cell carcinoma[84]	Sjögren's syndrome[85], systemic lupus erythematosus[86], neonatal lupus sydrome[87]

	Translation: positively regulates IRES translation whilst repressing 5'TOP mRNA translation[37]		Casein kinase 2 (CK2) phosphorylation at S366 regulates LARP3 effects on IRES and 5'TOP translation[37, 80, 81]		
LARP4	Translation: binds to poly(A) RNA improving stabilisation to promote translation[88]	LARP4 PAM2w binds to the MLLE domain of PABP[88]	TNFα regulated LARP4 mRNA levels in a Tristetraprolin-dependent manner[89]	Pro-tumour role: Prostate cancer[90], osteosarcoma[90, 91], Anti-tumour role: Ovarian[92, 93], prostate[94, 95] and breast cancers[95]	Unknown
LARP4B	Translation: binds to AU-rich regions within the 3'UTR of mRNA to promote translation perhaps by bridging interactions with ribosomes[96]	PABPC1 and RACK1[96]; PABP interaction is mediated by N-terminal PAM2w motif and MLLE	miR-106b suppressed LARP4B expression in prostate cancer cell lines[98]	Pro-tumour role: Prostate cancer[90], osteosarcoma[90] and neurofibroma[99] Anti-tumour role:	Unknown

		domain within PABP[97]		Prostate cancer[98], glioma[100]	
LARP6	<u>Translation:</u> promotes local translation of ribosomal protein mRNA at actin-rich cell protrusions[101]. Promotes the translation of Collagen type I mRNAs[102-106]	Stem loop within the 5'UTR of collagen type I alpha-1 and alpha-2 via La-module[102, 106] C-terminal of STRAP protein to enable recruitment of STRAP to collagen mRNAs. Binding is initiated by the last 27 amino acids of LARP6 [107]. Binds to vimentin filaments via the La-domain to further	mTORC1, Akt and IGF1 mediate LARP6 phosphorylation to regulate Collagen type I expression[103-105]	<u>Pro-tumour role:</u> Colorectal (downregulated and associated with poor prognosis)[112], Breast cancer (upregulated and possibly associated with poor prognosis)[113]	Keloid skin fibroproliferative disease[114]

		stabilise collagen mRNAs[108] C-terminal region of LARP6 binds to RNA helicase A tethering it to the 5'stem loop of collagen mRNAs[109] FKBP3 binds to LARP6 to regulate type I collagen synthesis[110] Binds to non-muscle myosin to regulate type I collagen translation via C-terminal region[111]			
LARP7	<u>Transcription:</u> LARP7 stabilises circularises and	La-Module dictates binding to UUU-	ATM phosphorylation on	<u>Pro-Tumour role:</u> Breast cancer[117],	Alazami Syndrome[121]

	protects 7SK snRNP structures by binding to 5'capping protein MePCE and the 3'UUU-OH structures of 7SK RNA[37]. Overall LARP7 negatively regulates the transcription of polymerase II genes[115]	3'OH whilst C-terminal additional RRM2α is necessary for 7SK and P-TEFb binding[116] and recognition of stem loop 4 within 7SK RNA[116]	LARP7 promotes BRCA/BARD1 polyubiquitination of LARP7 and subsequent proteasomal degradation resulting in 7SK snRNP disassembly[117]	<u>Anti-Tumour role:</u> Breast cancer[118], papillary thyroid carcinoma[119] and gastric cancer[120]	

Table 1.1: Properties of the LARP family of RBPs. *This table highlights key characteristics of the LARP family with RNA binding function regarding transcription and/or translation, known mRNA or protein interactions, known regulators, cancers in which a direct role has been implicated and diseases in which a direct role has been implicated. Findings are accumulated from primary research papers and not predictions from online functional information databases. LARP1B is highlighted to emphasise the lack of research investigating the functions of LARP1B in normal physiology and cancer, particularly in comparison to LARP1.*

1.2.2 LARP1 family

LARP1 and LARP1B demonstrate an elevated level of sequence similarity overall and between functional domains such as the La motif and RRM (**Figure 1.4**). LARP1B evolved from LARP1 likely due to a duplication event, deeming them paralogs[39]. Whilst *LARP1* is located on chromosome 5, *LARP1B* is located on chromosome 4. Structurally, LARP1 and LARP1B possess the namesake La-module composed of the La motif and RRM-like domain at the N-terminus as well as a highly conserved C-terminal DM15 domain composed of three DM15 repeats (A, B and C). This domain has a number of key functions including 5'Cap motif recognition and binding and general RNA binding independent of RNA. [38, 45]

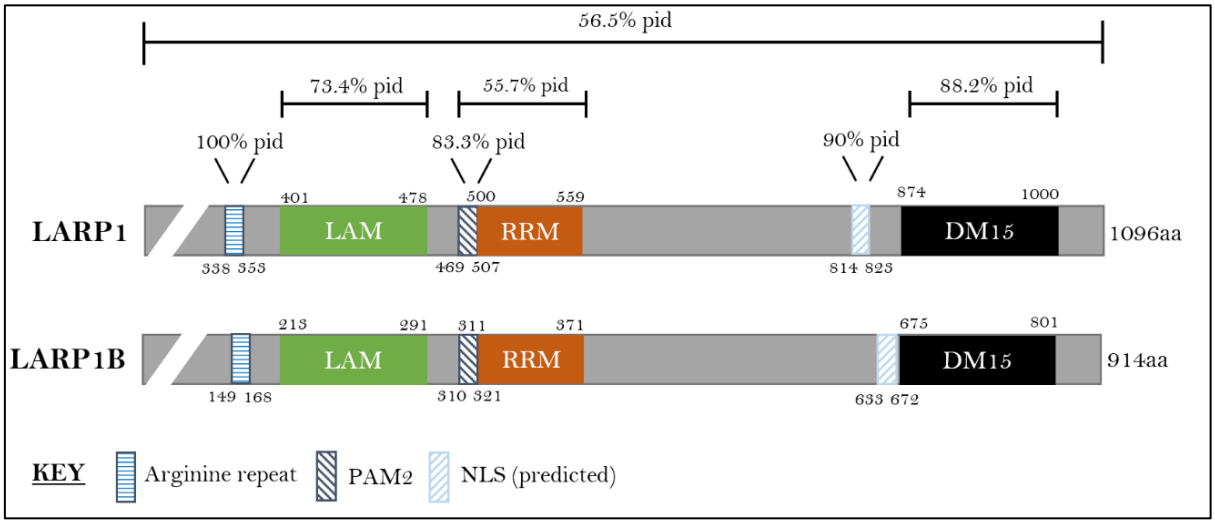

Figure 1.4: Depiction of LARP1 and LARP1B protein domains annotated with shared percentage identities (pid). *LARP1 and LARP1B amino acid sequences were aligned on Clustal Omega with known LARP1 domain sequences used to map LARP1B domains (results in supplementary Figures 8.1 and 8.2). These sequences were then submitted to MView to determine the percentage identity as a readout for sequence similarity between LARP1 and LARP1B. LAM: La module, RRM: RNA recognition motif, PAM2: poly(A) binding protein interacting motif 2, RRM: RNA recognition motif and NLS: Nuclear Localisation Sequence.*

1.2.3 LARP1 RNA binding function

LARP1 (also known as LARP1a, cytogenetic location: 5q34) is the more abundant and well established LARP1 family member with mRNA levels reported to be expressed up to 40x more than that of its paralog LARP1B in HeLa cells[51]. There are a number of validated

isoforms on NCBI which has caused some confusion within the field, leading to the classification of Isoform 2 (NP_291029.2) as the canonical isoform at 130kDa/1096aa[42].

The best-established RBP functionality for LARP1 is in translation regulation, particularly of mRNA transcripts containing a 5'terminal oligopyrimidine (5'TOP) motif, which encode components involved in translation processes. These include translation factors and ribosomal proteins regulated by mTOR kinases, particularly mTORC1 which induces translation of these mRNAs thus initiating ribosomal and global protein synthesis as well as cell growth[74]. When LARP1 is phosphorylated by mTORC1, the DM15 domain of LARP1 releases binding to the 5'cap of the 5'TOP mRNA thereby permitting eIF4E binding and translation initiation[45, 52, 74, 122]. However, LARP1 is also known to bind a number of non-5'TOP mRNAs with interactions at the 5'UTR, 3'UTR and within coding regions[46, 50, 123]. While this binding appears to promote mRNA stability, whether it promotes or represses translation seems to be highly context dependent. This is a known matter of debate and ongoing area of research within the field of LARP1, discussed in a recent publication[42].

Figure 1.5 summarises the hypothesised functions of LARP1 in the regulation of TOP and non-TOP mRNAs, likely depending on nutrient availability and mTORC1 status. Where mTORC1 is inactive, LARP1 DM15 is un-phosphorylated preventing eIF4E binding to the 5' cap and so translation is repressed. Active mTORC1 phosphorylates LARP1 DM15 displacing the eIF4E complex and allowing translation activation. At the same time, PABP and La module binding promotes mRNA stabilisation (**Figure 1.5A**). With regards to non-TOP mRNAs, alternative kinases may also phosphorylate LARP1 which regulates mRNA stabilisation and/or localisation (**Figure 1.5B**). Precisely which LARP1 domains are involved in non-TOP interactions is not yet clearly defined. [42]

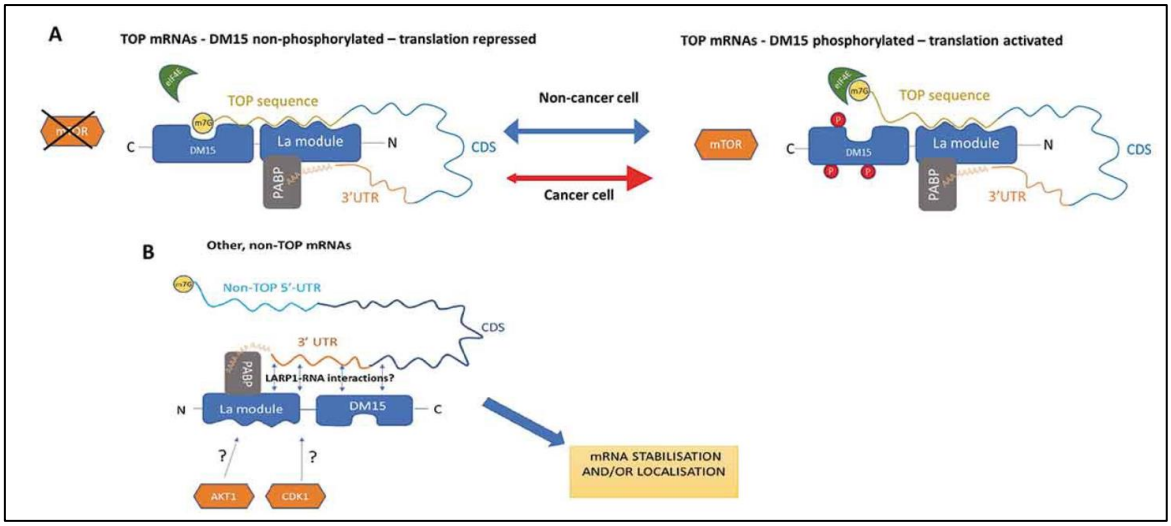

Figure 1.5: Proposed model of LARP1 functions in translation repression, activation, and mRNA stability. A. *Regulation of TOP and* ***B.*** *non-TOP mRNAs by LARP1 is largely dictated by mTORC1 and other kinase activity on the DM15 domain. The end results are translation repression or activation and mRNA stabilisation. Figure extracted from Berman et al., 2021*[42]

1.2.4 LARP1 in cancer

A number of studies have sought to identify the mRNA targets and protein interactors of LARP1 in a cancer setting. The cumulative findings are that LARP1 is in complex with proteins necessary for translation, protein synthesis, cytoskeletal composition, cell signalling, apoptosis, migration and invasion, cell cycle regulation and metabolism. By post-transcriptionally regulating the expression of transcripts involved in these biological processes, LARP1 promotes a proto-oncogenic phenotype. In fact, a LARP1 RNA immunoprecipitation chip (RIP-ChIP) in HeLa cervical cancer cell lines identified over 3000 mRNAs in complex with LARP1 which were augmented for cancer-associated pathways[46]. Across five independent studies aiming to identify the LARP1 interactome in different cellular contexts, a considerable level of variability in the mRNA binders was observed, demonstrating the ability of LARP1 to module its binding targets in response to different cellular context and upstream signalling. [46, 50, 123-125]

Altered expression of LARP1 mRNA and/or protein has been implicated in various cancers culminating in a number of phenotypes and acquisition of multiple cancer hallmarks (reviewed here[7, 37]). Through loss of function and gain of function studies *in vitro* and *in*

vivo, LARP1 has been deemed a pro-tumorigenic RBP promoting cell survival, chemoresistance, migration and invasion whilst repressing apoptosis, mitotic cell cycle arrest and chemosensitivity (these studies are highlighted in **Table 1.1**). The precise mechanism behind these findings have not been established in all cases, however in an ovarian cancer cell model Hopkins et al., 2015 attributed LARP1 pro-survival capacities to LARP1 preferentially stabilising anti-apoptotic *BCL2* mRNA transcripts whilst de-stabilising pro-apoptotic *BIK* mRNA transcripts to promote or repress their translation, respectively[44]. The end result was enhanced ovarian cancer cell survival and so it is possible that LARP1 plays similar post-transcriptional regulatory functions on pro-tumorigenic mRNAs in other cancers also such as those highlighted in **Table 1.1**.

1.2.4 LARP1B RNA binding function

LARP1B (also known as LARP2; cytogenetic location: 4q28.2) is a paralog of LARP1, both sharing 60% sequence homology and the highly conserved DM15 domain; in fact, LARP1 and LARP1B are the only proteins within the human proteome to possess the DM15 domain. A number of isoforms are annotated on NCBI (**Table 1.2**) with Isoform 1 deemed the canonical isoform by UniProt. There are two key publications exploring the RNA-binding function of LARP1B which have highlighted key roles in translation regulation, similar to LARP1[48, 74].

Isoform and Accession no.	Exons	Amino acids	kDa
Isoform 1; NM_018078/NP_060548.2	20	914	105
Isoform 2; NM_178043.3/NP_835144.1	11	522	60
Isoform 3; NM_032239.4/NP_115615.2	9	358	41
Isoform 4; NM_001278604.2/NP_001265533.1	8	335	39
Isoform 5; NM_001350531.2/NP_001337460.1	17	634	73
Isoform 6; NM_001410786.1/NP_001397715.1	19	902	104

Table 1.2: LARP1B isoforms annotated on NCBI gene database with Accession numbers, exon numbers, amino acids, and molecular weight in kilodalton (kDa). *Isoform 1 is deemed the canonical isoform (highlighted grey).*

A key study published by Philippe et al., 2020 illustrated how the dynamics between LARP1 and mTORC1 controls gene expression and established LARP1 as a master regulator of TOP mRNA translation[48]. The authors also investigated the role of LARP1B in this context and concluded that LARP1B is a minor regulator of TOP mRNA translation in HEK293T cells. They found that LARP1B binds to TOP sequences and the 5'cap and controls the translation of TOP reporter mRNAs but is not a major regulator of TOP mRNA translation in HEK293T cells unlike LARP1 which is deemed a primary TOP regulator. This study, however, presents some limitations: firstly, the role of LARP1B was assessed in a LARP1/LARP1B double deficient cell model and not a single LARP1B knockout model and so the results are an effect of combined depletion. Secondly, the expression or function of endogenous LARP1B was not analysed and instead a Myc/FLAG-LARP1B expression vector was utilized to detect ectopically expressed LARP1B. Thirdly, LARP1B was detected using an anti-Flag antibody and not an anti-LARP1B antibody. Use of a LARP1B-specific antibody for the detection and pulldown of endogenous LARP1B would yield more physiologically relevant results compared to an anti-FLAG antibody which may produce non-physiological interactions.[48] This reflects the challenges faced in this project with a lack of validated or optimized research tools required for investigation into the function of LARP1B.

LARP1B was found to interact with Poly(A) binding protein via the PAM2-like domain suggesting a role in translation regulation[74]. The authors also observed a weak/negligible interaction with mTORC1 which contrasted the robust interaction of LARP1 with mTORC1 and associated partners. However, in another study an interaction between LARP1B, mTORC1 and RAPTOR was observed, albeit weaker than LARP1[50]. Both of these studies observed these findings following ectopic expression of LARP1B (Myc/Flag-LARP1B) and/or ectopic Flag-mTOR/HA-RAPTOR and used anti-Flag antibodies for protein immunoprecipitation, both of which would promote non-physiological interactomes due to various "tag" proteins. The combined use of different LARP1B expression vectors and different tag proteins could be a possible explanation for contrasting results in the LARP1B-mTORC1 interaction observed in these studies.

1.2.5 The role of LARP1B in human disease

As highlighted, our current knowledge on the physiological role of LARP1B is scarce, with little to no exploration into its target transcripts, regulators, post-translational modifications or function in both health and disease, despite the high level of sequence similarity to LARP1. As highlighted in previously in **Table 1.1**, LARP1 is implicated in a number of biological processes with physiological relevance, in stark contrast to LARP1B emphasising a significant research gap within the field of LARP research. Nevertheless, further review of the available literature reveals clear involvement in hematological diseases, metabolism, cancer, embryonic development, and testicular function.

Beta (β) thalassemia: Two cohort studies demonstrated hypermethylation of the LARP1B promoter region in β-thalassemia patients. Through bisulfite sequencing of patient DNA extracted from blood samples of normal individuals and β-thalassemia patients, Gao et al., 2012 identified 209 differentially methylated genes[75]. Within this dataset, LARP1B was hypermethylated in β-thalassemia compared to normal blood which also correlated with lower *LARP1B* mRNA expression. Similarly, Haiyuni et al 2019., identified partial methylation of LARP1B promoter region in HbE/β-thalassemia which was associated with variable *LARP1B* mRNA expression as 75% of cases exhibited reduced expression when compared to controls[76]. The same study demonstrated that in β-thalassemia major, the *LARP1B* promoter region was unmethylated and was associated with a significant upregulation when compared to normal controls.

Liver disease or Hepatocellular carcinoma (HCC): A Korean cohort study identified chromosomal region 4q28.2 which hosts *LARP1B*, as having a significant correlation with HCC compared to normal patients. Specifically, low copy number was frequently observed in normal controls which was associated with an increased risk for HCC and liver cirrhosis.[126] In an alternative study, bioinformatics analysis of two publicly available datasets identified *LARP1B* as a differentially expressed gene in in non-alcoholic fatty liver disease (NFALD). Specifically, *LARP1B* expression was lower in steatosis and non-alcoholic steatohepatitis tissue when compared to healthy controls.[127] *LARP1B* was also identified as a differentially expressed gene in HCC which was associated with a high risk and reduced overall survival rate in HCC patients, compared to healthy controls.[128]

Diabetes: Analysis of mRNA expression of LARP1 and LARP1B from publicly available databases revealed high expression of *LARP1* and *LARP1B* expression in fetal and purified pancreatic β-cells. Single cell transcriptome profiling of human β-cells in healthy and type 2 diabetes subjects further revealed a 30% significant increase in *LARP1* mRNA expression and 100% significant increase in *LARP1B* mRNA expression in type 2 diabetes. This was attributed to potentially higher levels of translation in accordance with increased mTORC1 activity observed in diabetes.[73] In another study, transcriptome profiling identified LARP1B as upregulated in gestational diabetes mellitus samples compared to healthy subjects.[129] Two further independent studies identified LARP1B as a high confidence protein-protein interactor of glycogen synthase kinase-3 β (GSK-3 β) using BioID proximity labelling in HEK293T cells[130, 131]. GSK-3β is a regulator of glycogen synthesis which is key in maintaining blood glucose levels and dictating insulin resistance or deficiency[132]. Studies have demonstrated increased expression of GSK-3β in diabetes and involvement in diabetes-associated complications including diabetic cardiomyopathy[133] and diabetic nephropathy[134] in mice.

Embryonic development: In a mouse embryo knockout model deficient in maternal and zygotic Stella expression (protein necessary for embryonic pre-implantation development), qPCR analysis revealed a significant reduction in *LARP1B* mRNA expression when compared to wildtype oocytes and embryos. Stella knockout was associated with partial failure of maternal-to-zygotic transition of the embryonic genome. [135] qPCR analysis of soluble and insoluble fractions of fully grown *Xenopus* oocytes and mature eggs identified significant upregulation of *larp1b* in insoluble fractions following oocyte maturation. This finding suggests *larp1b* is amongst a group of RNAs undergoing soluble-to-insoluble phase transition during oocyte maturation.[136] Single cell RNA sequencing and RNA *in situ* hybridization of zebrafish testicular cells identified *larp1b* enrichment in round spermatids, deeming it a novel marker for zebrafish testicular cell types[137]. Global transcriptomic analysis of murine embryonic stem cell-derived brachyury$^+$ (T) cells identified upregulation of *LARP1B* mRNA expression in mesodermal brachyury$^+$ and bone morphogenic protein-2 (BMP-2) positive embryonic stem cells. Further, LARP1B siRNA knockdown in murine embryonic stem cells significantly downregulated the expression of

late mesodermal marker BMP-2 suggesting a role for LARP1B in regulating BMP-2 expression. [138]

LARP1B alternative splicing as a risk factor for cancer: Two studies analyzing publicly available transcriptomic data have identified a correlation between *LARP1B* splicing events and patient risk or survival outcome. In testicular germ cell tumour (TGCT) *LARP1B* alternative splicing events were deemed risk factors for TGCT (HR 7.42E05, *P*=0.007)[139]. Similarly, in prostate cancer, *LARP1B* splicing events were negatively associated with disease-free survival[140]. No further investigation into *LARP1B* splicing was performed in either study.

During our search of available literature, we also searched for 4q28.2 deletions and identified a medical report by Torrado et al 1982., who presented growth abnormalities in an 11-year-old boy with loss of chromosomal region 4q27-q31. Amongst short stature, minor anomalies of the skull and face and various physical abnormalities, the patient presented with abnormally small testes.[141] Although this chromosomal region houses many genes, it is interesting that *LARP1B* is also located at this site. We identified two alternative studies in which female infants with similar interstitial deletion in the middle portion of chromosome 4 (4q27-q31.22 and q27-q282.) presented with various growth malformations[142, 143]. These findings suggest a cluster of development-related genes within this region of chromosome 4 surrounding *LARP1B*.

Collectively, these studies suggest diverse functionalities of LARP1B in normal physiology and disease. Intriguingly, the described pathologies have an element of cellular metabolic or mitochondrial dysfunction as an etiology or associated pathologies. For example, in β-thalassemia, mitochondria-mediated respiration (oxidative phosphorylation) and apoptosis are dysregulated in differentiated erythrocytes of β-thalassemia patients and can contribute to chronic anemia – a symptom of β-thalassemia[144, 145]. Mitochondrial dysfunction regulates redox homeostasis and cellular metabolism, contributing to progression and therapeutic resistance in HCC[146]. Whilst in diabetes, mitochondrial dysfunction leads to reduced ATP and increased reactive oxygen species production which induces insulin resistance and diabetes progression[147]. Even in embryonic development, cellular

metabolism plays a key role in maintaining and responding to changes in energy demand supporting embryonic development and growth[148]. Together, these findings hint at the involvement of LARP1B in participating in cellular metabolic processes.

1.3 Mitochondrial function and dysfunction in normal physiology and cancer

Mitochondria are highly complex organelles responsible for cellular ATP production through the Krebs cycle and electron transport chain (ETC)[149]. Mitochondrial proteins are encoded by nuclear and mitochondrial genomes and adequate mitochondrial function is reliant on tight communications between mitochondrial and nuclear compartments. Deregulated mitochondrial functions due to mitochondrial DNA mutations have been implicated in the development and progression of a number of cancers including gastric[150] and hepatocellular carcinoma[151].

1.3.1 Mitochondrial function in normal physiology and cancer

The primary functions of the mitochondria are cellular metabolism, programmed cell death (apoptosis) and generation of reactive oxygen species (ROS)[151]. Perhaps the most understood function of mitochondria is oxidative phosphorylation (OXPHOS) by which the food we consume is oxidized to generate ATP which is then transported to the cytoplasm for use in various downstream biological processes[152].

Deregulation of cellular metabolism is an emerging cancer hallmark manifesting through several biological processes. Indeed, as cancer cells acquire the abilities to sustain proliferation and growth, increasing energy demands need to be met to ensure cell growth.[20] Under normal aerobic conditions, cells rely on OXPHOS to sustain the majority of their energetic demands (**Figure 1.6**). In brief, glucose is converted into pyruvate, NADH and ATP during glycolysis; pyruvate is further metabolized into acetyl CoA and fed into the citric acid cycle (TCA cycle) to generate the electron donor NADH as well as biosynthetic precursors for amino acids. Finally, mitochondrial respiration occurs through the electron transport chain (ETC) using electrons from NADH and $FADH_2$, to generate a proton gradient which can drive the oxidative phosphorylation of ADP to ATP via ATP synthase. As molecular oxygen acts as the final electron acceptor in this process, efficient

mitochondrial respiration is dependent on normoxic conditions. Under normal but anaerobic conditions, pyruvate is reduced to lactate in the cytoplasm where glycolysis produced the majority of the cell's ATP, in lieu of oxidative phosphorylation. In a cancer setting, despite the presence of oxygen, the cell metabolizes up to 85% of available glucose into pyruvate and lactate in the cytoplasm instead of through oxidation. [153, 154, 155]

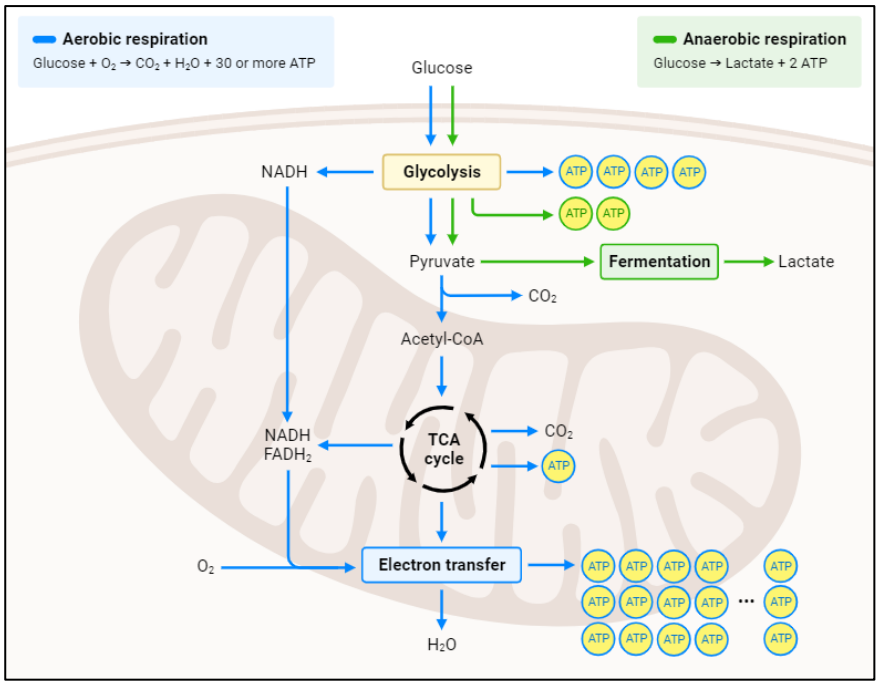

Figure 1.6: Schematic of cellular respiration processes in mitochondria. *Summary of glycolysis, the citric acid (TCA) cycle and electron transfer chain by which mitochondria generate cellular ATP. A summary of the process is provided in the text above. Briefly, glucose is converted into NADH, pyruvate or ATP during glycolysis. Pyruvate is converted into acetyl-CoA and fed into the TCA cycle to generate NADH/$FADH_2$, CO_2 and ATP. Electrons from NADH and FADH and cellular O_2 are used during the electron transport chain to drive oxidative phosphorylation of ADP to ATP.* [153, 154, 155] *Original diagram generated using Biorender.*

Otto Warburg was the first to recognize the switch in cellular metabolism and bioenergetics in cancer cells leading to the discovery of the "Warburg effect." Whilst the original hypothesis was that cancer cells possess defective mitochondria, we now know that many cancer cells possess functional mitochondria that play key roles in cancer cell proliferation and survival[156]. The original hypothesis and since observed cancer cell

metabolisms continue to raise questions and have given rise to further key discoveries based on Otto Warburg's original conclusion, further reviewed here[157].

Several cancer types present with up or down-regulation of OXPHOS with varying contribution to disease progression and survival. Cancers in which OXPHOS is downregulated as a result of mitochondrial DNA mutation or reduction of mitochondrial DNA and encoded mitochondrial protein (such as those encoding OXPHOS subunits I to V), are usually associated with a poor clinical outcome and metastatic disease[158]. In other cancers, OXPHOS is upregulated and contributes to cancer cell proliferation, therapeutic resistance and metastasis[159]. Another important phenomenon exhibited by cancer cells is metabolic plasticity which allows cells to switch between oxidative phosphorylation and glycolysis to continue meeting the extensive demands of rapidly proliferating cancer cells and the ever-changing tumour microenvironment[160]. Key metabolic regulators including hypoxia-inducible factor 1 (HIF-1) and AMP-activated protein kinase (AMPK) are recently emerged contributors to metabolic plasticity responding to cellular changes in energy and nutrient demands[161, 162].

1.3.2 Reactive oxygen species (ROS) in normal physiology and cancer

The mitochondria are a key source of ROS, generated as a by-product of normal mitochondrial oxidative metabolism produced by leaked electrons from the electron transport chain[152, 163]. ROS is an umbrella term referring to a family of oxidants produced from molecular oxygen and includes hydrogen peroxide (H_2O_2), superoxide anion (O_2^-) and hydroxyl radicals ($OH^•$)[164, 165]. ROS function as signaling factors mediating biological processes including cell growth[166], apoptosis[167] and differentiation[168]. For example, in SARS-CoV-2 infected HEK293T and epithelial cells, ROS suppressed PI3K/AKT/mTOR signaling, thereby inducing an inflammatory response which led to apoptosis[167]. ROS species, particularly H2O2 are also capable of regulating gene expression by promoting transcription[165].

Intracellular ROS levels are carefully regulated by antioxidant systems which maintain ROS at levels which ensure the smooth running of biological processes whilst preventing ROS-induced damage[163]. Excessive ROS levels as a result of impaired antioxidant systems

or accumulation of ROS by other means is thought to induce enzymatic inactivation, DNA damage, lipid peroxidation and apoptosis, contributing to aging and aging-related diseases if the damage is not repaired[152, 169, 170].

Rapidly proliferating cancer cells exhibit increased metabolic demands to support their growth and proliferation and so generally produce more ROS than normal cells[171]; this is a result of deregulated cellular energetics defined as a key hallmark of cancer[20]. There are conflicting findings regarding the effects of ROS on tumour growth as some studies demonstrate a pro-tumour role whilst others an anti-tumour role. For example, in pancreatic ductal adenocarcinoma (PDAC), mitochondria-derived ROS are necessary for transferrin receptor 1 (TfR1) mediated PDAC cell growth with downregulation of TfR1 abrogating cell viability and cellular ROS levels, which was partially rescued with H_2O_2 addition[172]. In prostate cancer CWR22RV1 cells, H_2O_2 induced apoptosis via an Akt and von Hippel-Lindau protein/Hypoxia inducible factor subunit alpha (pVHL/HIF1α) mediated pathway[173].

ROS mediated apoptosis is one means by which chemotherapeutic agents such as cisplatin induce cancer cell death[174-176]. In line with these findings, various studies have demonstrated the effects of antioxidants in promoting cisplatin resistance via upregulation of key redox regulating factors such as glutathione (GSH) and nuclear erythroid -related factor 2 (NRF2)[177, 178]. These findings further highlight the key role of intracellular redox homeostasis in tumorigenesis and therapeutic responses.

1.3.3 The role of RBPs in mitochondrial function and ROS generation

Mitochondria are highly unique organelles in that they rely on the coordinated expression of nuclear and mitochondrial encoded genes for the assembly and function of respiratory complexes necessary for energy production and mitochondrial biogenesis[179]. As previously discussed, the subcellular localisation of RBPs strongly dictates their function and this is also true for mitochondrially-localised RBPs. Those situated at the outer mitochondrial membrane (OMM) often initiate local translation of mitochondrial proteins whilst RBPs located within mitochondrial RNA granules aid mitochondrial DNA processing and translation[180, 181]. And so RBPs also play a key role in regulating the expression of mitochondrial proteins necessary for mitochondria homeostasis and function with the

depletion of RBPs known to impact localised protein translation and OXPHOS capacities[182]. An exemplary RBP is G-rich RNA sequence binding factor 1 (GRSF1) which coordinates the storage, handling, and translation of mitochondrial RNAs including those encoding mitochondrial ribosomal proteins. As a result, GRSF1 depletion in human fibroblasts led to defected OXPHOS complex and mitochondrial ribosome assembly.[183]

Given that RBPs are key regulators of gene expression, ROS mediated oxidative stress is one condition under which RBPs alter the cellular proteome to regulate responses to oxidative stress. In fact, RBPs can rapidly respond to changes in the intra and extracellular environment by altering the mitochondrial proteome to respond to such changes[181]. RBPs may do this by directly acting on target mRNAs, promoting or inhibiting their decay and translation thus mediating the cellular response to oxidative stress[184, 185]. A recent study exploring the oxidative stress response in human neuroblastoma SH-SY5Y cells, identified RNA binding protein Human antigen D (HuD) to positively regulate the translation of antioxidant, neuronal Superoxide dismutase 1 (SOD1) in response to H2O2-induced oxidative stress. Thus demonstrating HuD as a regulator of cellular antioxidant responses by post-transcriptionally regulating SOD1 expression. [186]

1.4 Testes and testicular germ cell tumours (TGCT)

TGCTs represent the most frequent solid malignancy in young males aged between 20-40 years of age, most prevalent in Caucasian populations. Worldwide incidence is slowly on the rise despite TGCTs demonstrating a high survival rate of over 95%. Current treatment options include radical orchiectomy or lymph node dissection followed by chemotherapy and/or radiotherapy, with cisplatin-based chemotherapeutic agents demonstrating a high level of success. Nevertheless, a small percentage of patients present with disease recurrence which is associated with a poorer disease outcome and reduced response to combined therapies. [187-189]

1.4.1 Structural composition of mammalian testicular tissue

The primary function of the testes is for sperm development and maturation, collectively termed spermatogenesis. They are composed of distinct tubular structures termed

seminiferous tubules which is made up of the germinal epithelium and inner lumen (**Figure 1.7**). The germinal epithelium contains Sertoli cells and germ cells undergoing various stages of development and differentiation into mature spermatozoa, or sperm. The tubules themselves are held by basal lamina containing extracellular matrix materials which not only compartmentalise the tubules, separating them from the surrounding interstitial space but also provide structural integrity to the tubules. Sertoli cells provide structural integrity to the germ cells during their stages of differentiation from spermatogenic stem cells termed spermatogonia, to spermatocytes and then spermatids. Sertoli cells also communicate with Leydig cells located within the interstitial space to regulate the release of androgens, necessary for spermatogenesis. [190, 191] Thus the interplay between all cell types within and surrounding the tubules is key to maintaining testicular function and spermatogenesis.

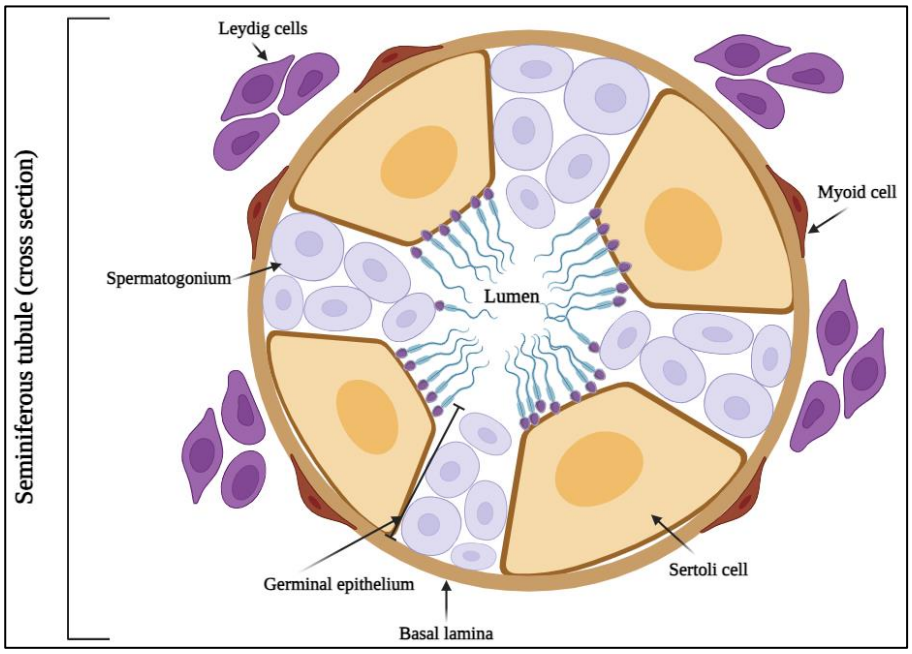

Figure 1.7: Schematic cross section of testicular seminiferous tubule. *Adapted from Paxton et al., 2003*[191].

1.4.2 TGCT etiology and pathophysiology

TGCTs account for up to 95% of testicular cancers, the other 5% termed "non-germ cell tumours". TGCTs are subdivided into two categories based on histological subtype: seminoma or non-seminoma which can be further characterized as yolk sac tumors (YST),

teratomas, choriocarcinoma and embryonal carcinoma (EC). In rare instances, a combination of these types can manifest giving rise to mixed germ cell tumours.[192, 193] Although the precise etiology is not known, a combination of environmental and genetic risk factors are considered to contribute to the development of TGCT including cryptorchidism, infertility, inguinal hernia and delayed puberty[193, 194]. The combination of such genetic and environmental factors can alter the fetal development of gonads giving rise to Testicular Dysgenesis Syndrome (TDS) which has been linked to the abrogation of normal germ cell differentiation – the primary cause of TGCTs[193, 195].

Testicular cancers develop from germ cell neoplasia *in situ* (GCNIS) composed of primordial germ cells (PGCs) that have bypassed normal cell differentiation *in utero*, failing to develop into spermatogonia and so GCNIS represent embryonic germ cells (**Figure 1.8**)[193, 195]. Under normal physiological conditions, PGCs undergo various rounds of differentiation to form gonocytes, spermatogonia with intermediate spermatocytes, spermatids and sperm largely dictated by KITLG/KIT signalling[193, 196]. In TGCT, PGCs escape these stages of differentiation, instead obtaining genetic mutations including chromosome 12p gain or *KIT* mutations giving rise to TGCT subtypes[196].

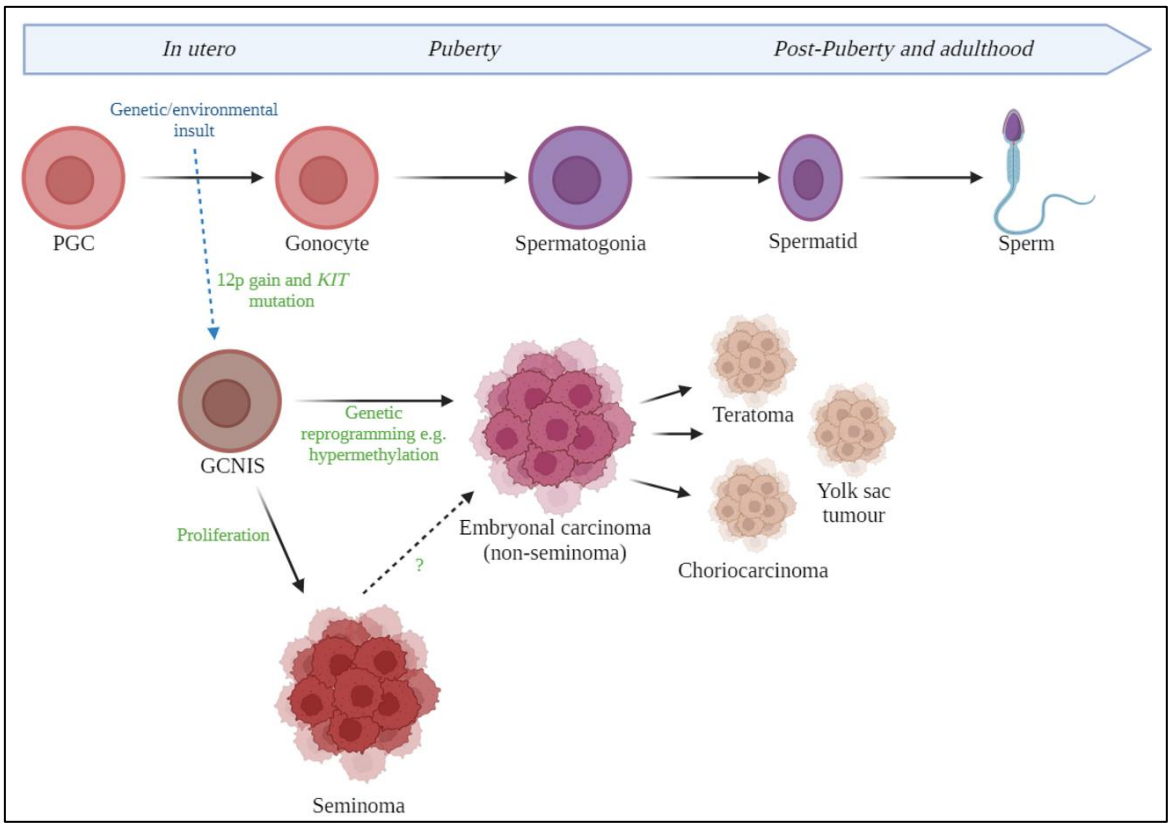

Figure 1.8: Schematic diagram of normal testicular germ cell differentiation and

TGCT development. *The pathophysiology of TGCT involves failed differentiation of PGCs because of genetic and/or environmental factors, resulting in GCNIS. Further proliferation or genetic reprogramming such as hypermethylation gives rise to seminoma or non-seminomas. Embryonal carcinoma represents the primary non-seminoma subtype which can further differentiate into teratoma, yolk sac tumours or choriocarcinoma. Diagram adapted from Fukawa et al., 2018[196] and Das et al., 2022[197]. PGC: Primordial germ cell and GCNIS: Germ cell neoplasia in situ.*

GCNIS was first characterized in 1987 by Skakkebaek et al.[198], who characterized GCNIS as malignant gonocytes with the capacity to differentiate into totipotent embryonic cells to further give rise to non-seminoma germ cell tumours. The population of germ cells unable to differentiate into totipotent embryonal cells are termed seminomas[198]. GCNIS are a noninvasive neoplasia localised within the basal layer of seminiferous tubules. They are often diagnosed in patient groups carrying a high risk for TGCT development and manifest as a precursor legion within the seminiferous tubules directly adjacent to testicular tumours in up to 90% of cases. [199]

Seminomas account for over 50% of TGCT cases resembling GCNIS. There are two main stages to seminoma in which disease is confined to the testicular region or involves lymphatic metastasis. Although demonstrating a high proliferative rate, seminomas are highly curable. Non-seminomas represent malignant stem cells arising from embryonal carcinomas which can further differentiate into teratoma, yolk sac tumour or choriocarcinoma which represent cell and tissue types at various stages of germ cell differentiation. [200]

1.4.3 TGCT current treatment options and sensitivity to cisplatin

The current treatment options for TGCT include surgery with adjuvant chemo- or radiotherapy[201]. TGCTs are unique in their high level of response to cisplatin-based therapies (particularly non-seminoma) with the precise mechanism underlying this characteristic still not known[202]. Possible reasons for successful chemotherapeutic response include the low frequency of somatic mutations, reduced expression of DNA damage repair genes and wildtype TP53 expression; combined these factors promote chemotherapy hypersensitivity in TGCT[202, 203]. Indeed Bragado et al., 2007 demonstrated that cisplatin-

induced apoptosis was more pronounced in cancer cell lines expressing wildtype *TP53* compared to those expressing mutant *TP53*[204].

1.4.4 Regulation of metabolism and oxidative stress in testicular tissue and TGCT

Testicular spermatogonia generate high quantities of ATP through glycolysis whilst spermatocytes and spermatids generate ATP primarily through OXPHOS[205]. Germ cell differentiation and sperm production are dependent on functioning mitochondria to undergo OXPHOS and provide a continued ATP supply. Inadequate OXPHOS capacities and ATP levels due to mitochondrial dysfunction are associated with reduced sperm quality and male infertility.[206, 207] One example of such a phenomena is testicular torsion in which the spermatic cord is twisted causing testicular ischemic injury and reperfusion injury; further resulting in oxidative damage and reduced spermatogenesis due to germ cell apoptosis[208].

Another key role for the mitochondria in spermatogenesis is the production of ROS; low physiological levels are necessary for sperm capacitation and sperm-oocyte fusion[209, 210]. In fact, normal germ cell development in the testis is known to generate high levels of ROS as a result of their metabolism[211]. Thus antioxidant systems within the testicular microenvironment are necessary to ensure these function and not induce cellular damage or sperm apoptosis[210]. The effects of ROS on testicular and sperm function are many and thoroughly reviewed here[212]. In summary, excessive oxidative stress in testicular tissue induces extensive morphological changes within the seminiferous tubules resulting in testicular atrophy and reduced sperm quality and count[212, 213]. Meanwhile, the effects of oxidative stress on sperm involves changes in structure and sperm DNA damage which can lead to implantation failure[212, 214]. The surrounding Leydig cells are also susceptible to ROS-induced oxidative stress and contribute to downstream complications because of reduced androgen synthesis and secretion which is required for spermatogenesis[215]. To summarize, ROS induced oxidative stress induced destruction to testicular tissue and sperm structural integrity, all of which can also contribute to male infertility[211].

As a reproductive organ with the primary role of species maintenance, the testes have in place an antioxidant defense system that protects testicular tissue from free radical damage

and oxidative stress. This antioxidant system may come in the form of antioxidant enzymes such as superoxide dismutase (SOD)[212] or ROS scavengers such as Cytochrome C[216]. Either way, antioxidants are key to the maintenance of testicular homeostasis, spermatogenesis and further down the line, embryogenesis. Regulators of oxidative stress are therefore incredibly important in testicular tissue homeostasis and so we wondered whether the indicated high expression of LARP1B in the testicular tissue might indicate a role in the regulation of oxidative stress or ROS scavenging.

Although there is little data exploring the metabolism of TGCTs, evidence suggests TGCTs favor the more energy inefficient glycolytic pathway for ATP production. Silva et al., 2018 identified overexpression of lactate transporters monocarboxylate transporter 1 and 4 (MCT1/4) along with their chaperone CD147 in TGCT tissue compared to benign tissue samples. Expression of these factors was associated with a hyper glycolytic phenotype and a worse patient prognosis.[217] In a similar study, TGCT tissues exhibited upregulation of CD44 and GLUT1 compared to paired normal tissue; CD44 is an additional MCT1/4 chaperone whilst GLUT1 is a glucose transporter often upregulated during metabolic reprogramming[218]. MCT1/4, CD44 and CD147 are all associated with the Warburg effect[217, 218].

1.5 Hypothesis and Project Aims

Based on our preliminary research findings summarized above, we hypothesized that LARP1B influences cellular metabolism to maintain cell fitness. Further, LARP1B exhibits tissue-specific roles occasionally in a manner contrasting LARP1 with which LARP1B shares over 50% sequence similarity. Specifically, as LARP1B appeared to play a key role in testicular tissue evidenced by high LARP1B protein expression in male tissues we hypothesized a key function of LARP1B in maintaining testicular homeostasis.

To the best of our knowledge, no study has carried out an extensive characterization of LARP1B and its role in cancer. Specifically, we aimed to identify an appropriate cancer research model based on LARP1B expression which would be used to determine the phenotypic and functional role of LARP1B. Most importantly, we wanted to explore the effects of LARP1B depletion on cell fitness and metabolism in cancer given that its paralog

LARP1 is a recognized driver of cancer metabolism and prior studies have implicated a role for LARP1B in metabolism-associated biological processes. Lastly, we set out to understand the interplay between LARP1B and LARP1 investigating their interaction and begin understanding the redundancy or compensatory kinetics between the two proteins.

2

MATERIALS AND METHODS

2.1 Materials

2.1.1 Tissue Culture reagents and media supplements

Medium	Specifics	Supplier (product code)
Dulbecco's Modified Eagle Medium (DMEM)	High Glucose, GlutaMAX	Thermo Scientific (10566016)
RPMI-1640	Glutamine	Thermo Scientific (11875093)
Trypsin-EDTA (1X)	N/A	Sigma-Aldrich (59030C-100ML)
Phosphate Buffer Solution (PBS, 1X)	pH 7.4	Thermo Scientific (10010056)
Dimethyl Sulfoxide (DMSO)	N/A	Sigma-Aldrich (D8418)
Opti-MEM Reduced Serum Medium	N/A	Thermo Scientific (31985062)
Foetal Bovine Serum (FBS)	Qualified, United States	Thermo Scientific (26140079)
Penicillin-Streptomycin	5000U/ml	Thermo Scientific (15070063)
XF Seahorse Calibrant Solution	N/A	Agilent Technologies (100840-000)
XF Seahorse DMEM medium, pH 7.4	N/A	Agilent Technologies (103575-100)
1.0 M Glucose Solution	Seahorse medium supplement	Thermo Scientific (A2494001)
100mM Pyruvate Solution	Seahorse medium supplement	Thermo Scientific (11360070)
200mM Glutamine Solution	Seahorse medium supplement	Thermo Scientific (A2916801)

2.1.2 Mammalian cell lines

Cell line	**TGCT subtype**	**Response to cisplatin**	***TP53* status**
HEK293T	Human embryonic kidney cells expressing the SV40 large T antigen	Cisplatin sensitive	Wildtype
HEK293T LARP1^{KO}	LARP1 knockout of the parental HEK293T	Cisplatin sensitive	Wildtype
GCT27	Embryonal Carcinoma	Cisplatin sensitive,	Wildtype
GCT27CR	Embryonal Carcinoma	Cisplatin resistant (in vitro resistance)	Wildtype
2102EP	Embryonal Carcinoma	Cisplatin sensitive	Wildtype
OVCAR8	Ovarian adenocarcinoma	Cisplatin sensitive	Mutant
OVCAR8 LARP1^{KO}	LARP1 knockout of the parental OVCAR8	Cisplatin Sensitive	Mutant

2.1.3 Buffers and Reagents

Buffer/Reagent (supplier and product code)	**Application**	**Components/supplements**	**Supplier (product code)**
Pierce RIPA lysis buffer	Cell lysis and protein extraction	N/A	Thermo Scientific (89900)

Supplemented RIPA lysis buffer for general cell lysis	Cell lysis and protein extraction	cOmplete Protease Inhibitor Cocktail Phosphatase Inhibitor Cocktail 2 Phosphatase Inhibitor Cocktail 2 1x PhoSTOP phosphatase inhibitor 1 mM Sodium fluoride	Merck (11697498001) Merck (P5726-1ML) Merck (P0044-1ML) Merck (04906837001) Fisher Scientific (15463049)
Supplemented RIPA lysis buffer for co-IP	Cell lysis and protein extraction	cOmplete Protease Inhibitor Cocktail 1x PhoSTOP phosphatase inhibitor 1 mM Sodium fluoride	Merck (11697498001) Merck (P0044-1ML) Merck (04906837001)
LDS sample buffer	Protein sample reconstitution	Bolt LDS sample buffer Sample Reducing Agent (10X)	Life Technologies (B0008) Life Technologies (B0009)
1X Tris/Glycine/SDS electrophoresis buffer	TGX PAGE electrophoresis	100 ml 10X Tris/Glycine/SDS buffer 900 ml dH_2O	Bio-Rad (1610772)
1X Tris/Glycine transfer buffer (1 L)	Western blot transfer	100 ml 10X Tris/Glycine buffer 200 ml Methanol	Bio-Rad (1610771)

		700 ml filtered H_2O	
1X TBST	Western blot membrane washes	500 ml 10X TBS 25 ml 20% Tween-20 Up to 5 L filtered H_2O	10X TBS: Thermo Scientific (J60764.K2)
20% Tween-20 solution (500 ml)	Supplement to buffers and washes	Tween-20 500 ml filtered H_2O	Sigma Aldrich (P1379-1L)
1% Fish gelatine blocking buffer (500ml)	Western blot membrane block and antibody diluent	5g Fish gelatine 500ml TBS	Sigma Aldrich (G7041-500G)
Pre-extraction Buffer	Immunofluorescence	0.1% NP40 in PBS	Thermo Scientific (85124 and 10010023)
Fixative	Immunofluorescence	4% Paraformaldehyde in PBS	Thermo Scientific (043368.9M)
First wash	Immunofluorescence	0.1% Triton X-100 in PBS	Thermo Scientific (85111)
Second wash	Immunofluorescence	0.2% Tween-20 in PBS	Merck (P1379-1L)
Hanks Balanced Salt Solution (HBSS)	MitoSOX	Calcium, magnesium, no phenol red	Thermo Scientific (14025092)

2.1.4 Experimental kits and components

Kit	**Application**	**Supplier (product code)**
Microplate BCA Protein Assay Kit – Reducing Agent Compatible	Protein quantitation (kit and standards)	Thermo Scientific (23252)

Quick Start Bovine Serum Albumin Standard Set		Bio-Rad (5000207)
Promega ReliaPrep RNA miniprep system	RNA extraction	Promega (Z6012)
Fast SYBR Green Master mix	qPCR (real time PCR)	Thermo Scientific (4385612)
High-Capacity Reverse transcription kit	First strand cDNA synthesis	Thermo Scientific (4368813)
Protein A Dynabeads	Co-IP	Invitrogen (10001D)
Nitrocellulose membrane	Western blot transfer	Bio-Rad (1620097)
NE-PER Nuclear and Cytoplasmic Extraction reagents	Subcellular protein fractionation	Thermo Scientific (78835)
xCELLigence RTCA E-plate 96 PET	Real-time cell analysis	Agilent Technologies (300600910)
Cyquant NF Cell Viability	Cell Viability	Invitrogen (C35007)
ApoTox-Glo Triplex Assay	Cell viability, Cytotoxicity and Apoptosis	Promega (G6320)
Seahorse XF Cell Mito-stress test kit (also used for Glycolysis stress test assay)	Mito-stress test	Agilent Technologies (103015-100)
Xfe96 FluxPak	Mito-stress test	Agilent Technologies (102416-100)
Pierce Silver Stain Kit	co-IP gel stain	Thermo Scientific (24612)
S-TRAP micro column	co-IP bead digestion	Protifi (C02-micro-10)
MitoSOX red	MitoSOX Mitochondrial superoxide indicator/live cell staining	Invitrogen (M36008)
Menadione	MitoSOX positive control for ROS induction	Fisher Scientific (ICN10225925)

2.1.5 Chemical reagents

Reagent	Application	Supplier (product code)
Lipofectamine RNAiMAX transfection Reagent	siRNA transfection/RNAi	Thermo Scientific (13778075)
X-tremeGENE 360 Transfection Reagent	shRNA transfection/RNAi	Roche (XTG-360-RO)
Fugene 6 Transfection Reagent	DNA transfection/Vector expression	Promega (E2691)
Ampicillin Sodium Salt	Bacterial growth	Thermo Scientific (J63807.06)

2.1.6 Primary and Secondary antibodies

Primary antibodies		
Target (host species)	**Working concentration**	**Supplier (product code)**
LARP1 (rabbit)	1:1000 (WB), 4mg/ml (co-IP)	Abcam (ab86359)
LARP1B (rabbit)	1:1000 (WB), 4mg/ml (co-IP)	Proteintech (17277-1-AP)
β-Actin (rabbit)	1:2000 (WB)	Santa Cruz Technology (sc-47778)
IgG Isotype control (rabbit)	1:10000 (co-IP)	Cell Signalling Technology (3900S)
Lamin A/C (mouse)	1:500 (WB)	Cell Signalling Technology (4777s)
α-Tubulin (mouse)	1:2000 (WB)	Cell Signalling Technology (3873s)
Secondary antibodies		
Target (host species)	**Working concentration**	**Supplier (product code)**
IR Dye 800CW Goat anti-Rabbit IgG H+L (goat)	1:10,000	LI-COR (926-32211)
IR Dye 680RD Goat anti-mouse IgG H+L (goat)	1:10,000	LI-COR (926-68070)

Alexa Fluor Goat anti-Rabbit-488	1:1000	Thermo Scientific (R37116)
Alexa Fluor Goat anti-Rabbit-647	1:1000	Thermo Scientific (A-21244))
Alexa Fluor Goat anti-Mouse-488	1:1000	Thermo Scientific (R37120)
Alexa Fluor Goat anti-Mouse-647	1:1000	Thermo Scientific (A32728)
4',6-diamidino-2-phenylindole (DAPI)	1:500	Thermo Scientific (D1306)

2.1.7 qRT-PCR primers

Primer target	**Primer sequence**	**Supplier (product code)**
LARP1	Forward: 5'-GGAGATCGTTGATGAGAAAG-3' Reverse: 5'-TCTGTCTCCTTTTGGTAGTG-3'	Invitrogen by Thermo Fisher
LARP1B	Forward: 5'-CTTTTGCTCACATACAGAGTC-3' Reverse: 5'-AGAAAAATGGCCAATTCCAG-3'	Invitrogen by Thermo Fisher
OAZ1	Forward: 5'-ATAGTCAGAGGGATCACAATC-3' Reverse: 5'-CGTTAGTTCCTCTGTTACATTC-3'	Invitrogen by Thermo Fisher

2.1.8 Oligonucleotide sequences

Oligonucleotide target	**Oligonucleotide sequence**	**Supplier (product code)**
LARP1	RNAi siRNA, siQ2c sense: 5'-CAUGACUCUUGACAUCCUAtt-3' siQ2c antisense: 3'-UAGGAUGUCAAGAGUCAUGga-5'	Ambion by Life Technologies

	RNAi siRNA, si2 sense: 5'-UGAUGUCUGGCUUGAGUCU [dT][dT]-3' si2 antisense: 3'-AGACUCAAGCCAGACAUCA[dT][dT]-5'	Invitrogen by Thermo Fisher
Scrambled	Propriety information	Ambion by life technologies

2.1.9 shRNA plasmid DNA

shRNA target	**shRNA sequence**	**Supplier (product code)**
LARP1B	sh_33: 5'-GCCTGAGAAATAGACTCTTAT-3' sh_202: 5'-CCACTCCACTTAGATGTTGTA-3'	Merck (SHC001)
tGFP	sh_tGFP: 5'-CCGGCGTGATCTTCACCGACAAGATCTC-GAGATCTTGTCGGTGAAGATCACGTTTTT-3'	Merck (SHC004)

2.1.10 Tissue Microarray (TMA)

Tissue Type	**Supplier (product code)**
Human Testicular spectrum tissue (x3)	US, Biomax Inc (TE810)

2.1.11 Machinery

Machinery	**Application**	**Supplier**
ProFlex PCR System	First strand cDNA synthesis and PCR	Applied Biosystems by Life Technologies
Branson Digital Sonifier	Cell disruption/homogenisation	Branson

NanoDrop One/One Microvolume UV/Vis Spectrophotometer	RNA quantitation	Thermo Scientific
PolarStar Omega Plate Reader	BCA assay/Protein quantitation	BMG Labtech
Bio-Rad GelDoc/ChemiDoc	Gel imaging	Bio-Rad
Licor	Licor Odyssey	LICOR
xCELLigence RTCA SP and DP	Cell proliferation and cell migration and invasion (real time cell analysis)	Agilent Technologies
Inverted Zeiss LSM 718 confocal microscope	Immunofluorescence	Zeiss
Zoe Fluorescent Imager	Fluorescent cell imaging	Bio-Rad
xCELLigence RTCA SP-Single Plate	Real-time cell analysis	Agilent Technologies
Seahorse XF Analyser	Seahorse XF Mito Cell stress test and Glycolysis stress test	Agilent Technologies

2.1.12 Software

Software	**Application**	**Supplier or Developer**
RStudio	Data analysis	Posit, Joseph J. Allaire
GraphPad Prism 9	Data analysis	Dotmatics
xCELLigence RTCA software Pro	Real-time cell analysis and report generator	Agilent Technologies
QuPath	TMA staining and MitoSOX staining quantification	JavaFX
MaxQuant	MS/MS data analysis	Max-Planck-Institute of Biochemistry

2.2 Methods

2.2.1 Cell culture

Testicular Germ Cell Tumour GCT27 and GCT27CR ("CR" referring to cisplatin resistance) cell lines and Human Embryonic Kidney Cell lines (HEK293T) were cultured and maintained in Dulbecco's Modified Eagle's Medium (DMEM) supplemented with 10% foetal calf serum (v/v), penicillin (100 units/ml) and streptomycin (100ug/ml). Ovarian cancer OVCAR8 and OVCAR8 LARP1 knockout cell lines (OVCAR8 LARP1^{KO}) were maintained in RPMI 1640 medium supplemented with 10% foetal calf serum (v/v), penicillin (100 units/ml) and streptomycin (100ug/ml). All cells were maintained in a humidified incubator at 37°C and 5% atmospheric CO_2.

2.2.2 Routine cell passaging

Once cells had reached approximately 70% confluency, they were washed with room temperature PBS and detached with 4-5 ml of 0.25% Trypsin-EDTA for 3-5 minutes. Cells were then diluted in 8-10ml of fresh medium, centrifuged at 400 G for 4 minutes and re-seeded at a density of 1:10 in 12-24 ml of complete culture medium.

2.2.3 Cryopreservation and cell resuscitation

For long term storage, cells were trypsinised and centrifuged as mentioned previously. Cell pellets were then re-suspended in 1 ml of freezing medium (complete medium supplemented with 10% DMSO) and frozen in 1 ml cryovials stored in a Mr. Frosty freezing container at -80°C overnight. Cryovials were then transferred to storage boxes in liquid nitrogen. To resuscitate frozen cell lines, cryovials were collected on dry ice and rapidly thawed in a 37°C water bath. Cells were then transferred to a T75 flask containing 12 ml of complete growth medium and incubated to reach optimal confluency with a medium change overnight.

2.2.4 Cellular protein extraction

For protein extraction, cells were kept on ice at all times whilst reagents and washing buffers were chilled to 4°C. Cells were washed twice with 1-5 ml of PBS and lysed in RIPA buffer supplemented with protease (1:25) and phosphatase (1:100) inhibitors. Cells were

scraped into 1.5 ml Eppendorf tubes, retained on ice for 15 minutes and sonicated once using a probe sonicator at 10% intensity for 5 seconds. Samples were then centrifuged at 16,000 G for 15 minutes at 4°C after which the supernatant was retained and used for protein concentration quantitation.

2.2.5 Subcellular protein fractionation

For extraction of subcellular protein fractions cells were grown to confluency in 10 cm-15 cm dishes with buffers scaled accordingly depending on the total packed cell volume. Generally, for whole cell lysates, cells were harvested in supplemented RIPA buffer as mentioned in **2.2.4**. Cytoplasmic and nuclear extraction was performed using the NE-PER Nuclear and Cytoplasmic Extraction reagents, according to the manufacturer's protocol. Briefly, cells were collected in 1ml of ice-cold PBS and centrifuged at 500 G for 3 minutes at 4°C. The supernatant was discarded and 1000 µl of CER I reagent supplemented with protease inhibitor cocktail (1:25) was added to the pellet. Samples were vortexed at maximum speed for 15 seconds and incubated on ice for 10 minutes. 55 µl of CER II reagent was added to the sample, vortexed at maximum speed for 5 seconds and incubated on ice for 1 minute. Samples were vortexed again as before and centrifuged at 14,000 G for 5 minutes at 4°C. The supernatant (cytoplasmic fraction) was transferred into a pre-chilled 1.5 ml Eppendorf tube. 50 µl of ice-cold NER reagent supplemented with protease inhibitor cocktail (1:25) was added to the insoluble pellet, vortexed for 15 seconds at maximum speed and maintained on ice; this was repeated every 10 minutes for a total of 40 minutes. Samples were then centrifuged at 14,000 G for 10 minutes at 4°C and the supernatant (nuclear extract) was transferred to a pre-chilled 1.5 ml Eppendorf tube. Proteins samples were quantified, normalised, and subjected to SDS-PAGE western blotting as explained further below.

2.2.6 Cellular protein quantitation and sample normalisation

Protein lysate concentrations were determined by Bicinchoninic acid (BCA) assay. To generate a standard curve, six dilutions of bovine serum albumin (BSA) at concentrations ranging from 0-4 mg/ml were added to wells of a 96 well plate containing 50 µl of PBS, at concentrations of 1:25 in duplicates. Protein lysates were added to respective wells containing 50 µl of PBS at concentrations of 1:25 in duplicates. BCA reagent B was

combined with BCA reagent A at a 1:49 ratio and 150 µl of this reagent mix was added to the wells containing the BSA standard curve or our collected protein lysate. The plate was incubated in a 70°C water bath for approximately 25 minutes after which the absorbance was analysed at an optical density of 562 nm using the BMG Labtech PolarStar Omega Plate Reader. Protein concentrations were calculated using the standard curve analysis tool available on the OMEGA Mars analysis software. Lysates were then normalised to the lowest concentration with sample reducing agent and 4X LDS sample loading buffer. All samples were reconstituted to a final concentration of 1-2 µg.

2.2.7 TGX PAGE gel electrophoresis and western blotting

Protein samples reconstituted in 4X LDS sample buffer were boiled at 70°C for 10 minutes before equal volumes (20-40 µl) were loaded into wells of 4-15% TGS PAGE gels. Proteins were separated at 150 volts for 1 hour in 1X Tris/Glycine/SDS electrophoresis buffer alongside a pre-stained protein marker to distinguish protein molecular weights. Proteins were then transferred onto nitrocellulose membranes at 60 volts for 2 hours in 1X Tris/Glycine transfer buffer and then blocked in 1% fish gelatine/TBS buffer for 1 hour at room temperature on a rocker. Membranes were then incubated in the appropriate primary antibody diluted in 1% fish gelatine/TBS on a roller at 4°C, overnight. Following 3x15 minutes washes in TBST on a rocker at room temperature, membranes were incubated with fluorescently tagged LI-COR secondary antibodies diluted in 1% fish gelatine/TBS supplemented with 0.2% Tween 20, for 1 hour on a rocker at room temperature. Membranes were washed in TBST as before and imaged using the LI-COR Odyssey Imager and Image Studio software.

2.2.8 RNA extraction

RNA was extracted using the Promega ReliaPrep RNA miniprep system according to the manufacturer's protocol. In summary, 250 µl of BL+TG lysis buffer was added directly to plated cells and incubated on ice for 1 minute to promote cell lysis. Lysates were then collected into microcentrifuge tubes and briefly vortexed. 85ul of 100% Isopropanol was added and further vortexed for 5 seconds. Lysates were then bound to a ReliaPrep minicolumn and washed accordingly with kit-specific wash buffers containing ethanol. To eliminate DNA, lysates were subjected to on column DNase I digestion for 15 minutes at

room temperature followed by removal of contaminants with wash solutions. Pure total RNA was eluted in 30 µl of nuclease-free H_2O and quantified using the NanoDrop One/One Microvolume UV/Vis Spectrophotometer. All centrifugations were performed at 14,000 G at room temperature. RNA was stored at -20°C until required for downstream cDNA synthesis.

2.2.9 First strand cDNA synthesis

cDNA was generated using the High-Capacity cDNA reverse transcription kit according to their protocol. In short, 1000 ng of RNA was transcribed into cDNA under the following conditions: 25oC, 10 minutes; 37oC, 120 minutes; 85oC 5 minutes; 4oC, ∞. Samples were then diluted in 80µl of nuclease-free H_2O and stored at -20°C until required for downstream qPCR analysis.

2.2.10 Real time polymerase chain reaction (qPCR)

cDNA was amplified into double-stranded DNA using the FAST SYBR Green Master Mix kit, according to the manufacturers protocol and the Applied Biosystems Step One Plus Real Time PCR system. In summary, 100 ng of cDNA was amplified under the following conditions: 95oC, 20 seconds (holding stage); 95oC, 3 seconds followed by 60°C 30 seconds (cycling stage x40); 95°C, 15 seconds followed by 60°C, 1 minute and 95°C, 15 seconds (Melt curve stage). Melt curve and amplification analysis was carried out using the Applied Biosystems Step One Plus software whilst data was plot using GraphPad Prism 7.

2.2.11 Co-Immunoprecipitation (Co-IP)

Cells were grown to confluency in 15cm dishes and lysed in RIPA buffer supplemented with sodium fluoride, protease, and phosphatase inhibitors. Lysates were sonicated at an intensity of 10% for 15 seconds on ice and centrifuged at maximum speed for 15 minutes at 4°C. The supernatant was retained for protein concentration quantitation by BCA assay as previously mentioned and normalised to 2-4mg protein/1ml.; from this, 100 µl was retained at "input". Remaining lysates were immunoprecipitated with Dynabeads Protein A according to the manufacturer's protocol. In summary, 2-4 µg/ml of the desired antibody was bound to the beads by rotation at room temperature for 20 minutes and then washed

in PBS-Tween wash buffer. 1 ml of protein lysate containing the target antigen was immunoprecipitated with Dynabead Protein A on rotation at 4°C for 1 hour. The immunoprecipitated complexes were washed 3 times in PBS-Tween wash buffer and re-suspended in 80 µl of supplemented LDS. Samples were boiled at 70°C for 10 minutes and separated by SDS-PAGE electrophoresis, as previously mentioned.

2.2.12 LARP1B shRNA-mediated gene silencing

Cells were cultured in 6 well plates or 10 cm dishes to 70% confluency prior to transfection using X-tremeGENE 360 Transfection Reagent. Briefly, 2-10 µg of shRNA plasmid DNA (depending on usage of a 6-well plate or 10 cm dish) plus 6-30 µl X-tremeGENE 360 was added to 200-1000 µl of Opti-MEM and incubated for 30 minutes at room temperature. The entire transfection mix was added dropwise to the cells, with 2-10 ml of antibiotic-free medium. Cells were incubated for 48 hours after which they were lysed for protein and RNA extraction in the appropriate lysis buffers or collected and re-seeded for further phenotypic analysis. shRNA plasmids used were a control shRNA later referred to as sh_ctrl or a combination of anti-LARP1B shRNAs later referred to as sh_LARP1B.

2.2.13 LARP1 siRNA-mediated gene silencing

Cells were cultured in 6 well plates to 70% confluency prior to transfection. Briefly, 9 µl of Lipofectamine RNAiMAX transfection reagent was added to 150 µl of Opti-MEM. In a separate tube, 1.5 µl of non-targeting (scrambled) or LARP1 (si2 or siQ2) siRNA was diluted in 150 µl of Opti-MEM. The two mixtures were combined at a 1:1 ratio and incubated at room temperature for 5 minutes. 250 µl of this transfection mix was added dropwise to the cells in addition to 1.75 ml of antibiotic-free DMEM medium to give a final concentration of 15 nM. Cells were incubated for 72 hours after which they were lysed for protein and RNA extraction in the appropriate lysis buffers.

2.2.14 LARP1B-Myc/Flag overexpression

HEK293T cells were cultured in 6 well plates or 10 cm dishes to 70% confluency prior to transfection using Fugene 6 Transfection Reagent. Briefly, 6-12 µl of Fugene 6

Transfection Reagent (depending on use of a 6 well plate or 10cm dishes) was added to 100-200 µl of Opti-MEM and incubated at room temperature for 5 minutes. Purified plasmid DNA at a concentration of 2-4 µg was then added to the complex and further incubated for 20 minutes. The complete DNA: Fugene 6: media complex was added dropwise to the cells and supplemented with 2-10 ml of antibiotic-free DMEM and incubated for 48 hours until lysed for western blot or qPCR analysis or re-seeded into 96 well assay plates for further phenotypic analysis.

2.2.15 Real-time cell proliferation assay

To determine cell proliferation following LARP1B knockdown, we utilised the xCELLigence Real-Time Cell Analysis (RTCA) system (Agilent). This system allows measuring of real-time cell proliferation and growth of adherent cells over the surface of custom-made 96 well plates based with gold electrodes. The assay was performed according to the manufacturer's protocol. In brief, 48 hours following knockdown of LARP1B, xCELLigence E-plate 96 were equilibrated with 100 µl of antibiotic-free DMEM medium per well for 30 minutes at room temperature. Transfected cells were collected via trypsinisation and re-seeded into the equilibrated plates at a density of 40,000 cells/well in antibiotic-free DMEM medium. The E-plate was then inserted and locked into the RTCA device within an incubator maintaining an atmosphere of 37°C and 5% CO_2 for a further 48 hours measuring "sweeps" every hour. The average Cell Index and standard deviation for each sample was calculated and plotted on the RTCA Software (Agilent). An example of a cell index (CI) plot generated by the xCELLigence system is depicted in **Figure 2.1** below and results from a preliminary experiment optimising cell seeding number is shown in **Figure 2.2**.

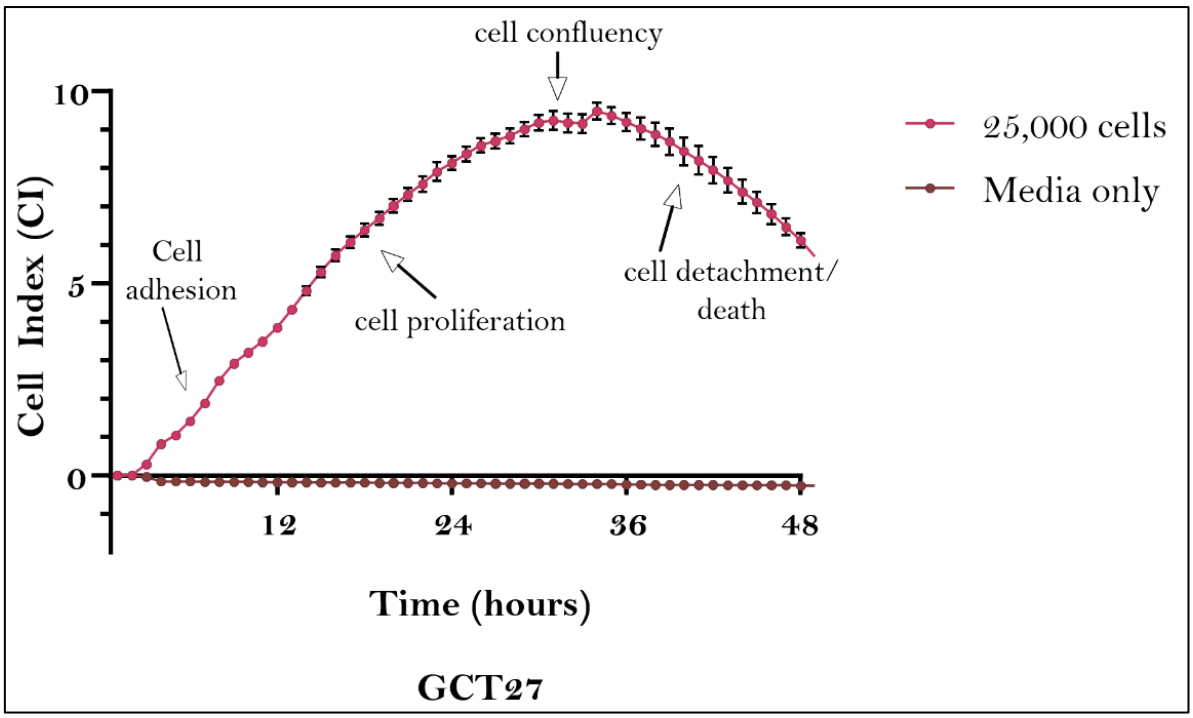

Figure 2.1: Depiction of a cell index (CI) plot generated by the xCELLigence system with annotated cell growth phases over 48 hours. *GCT27 cells as a cell number of 25,000 cells/well vs DMEM media only control was used as an example.*

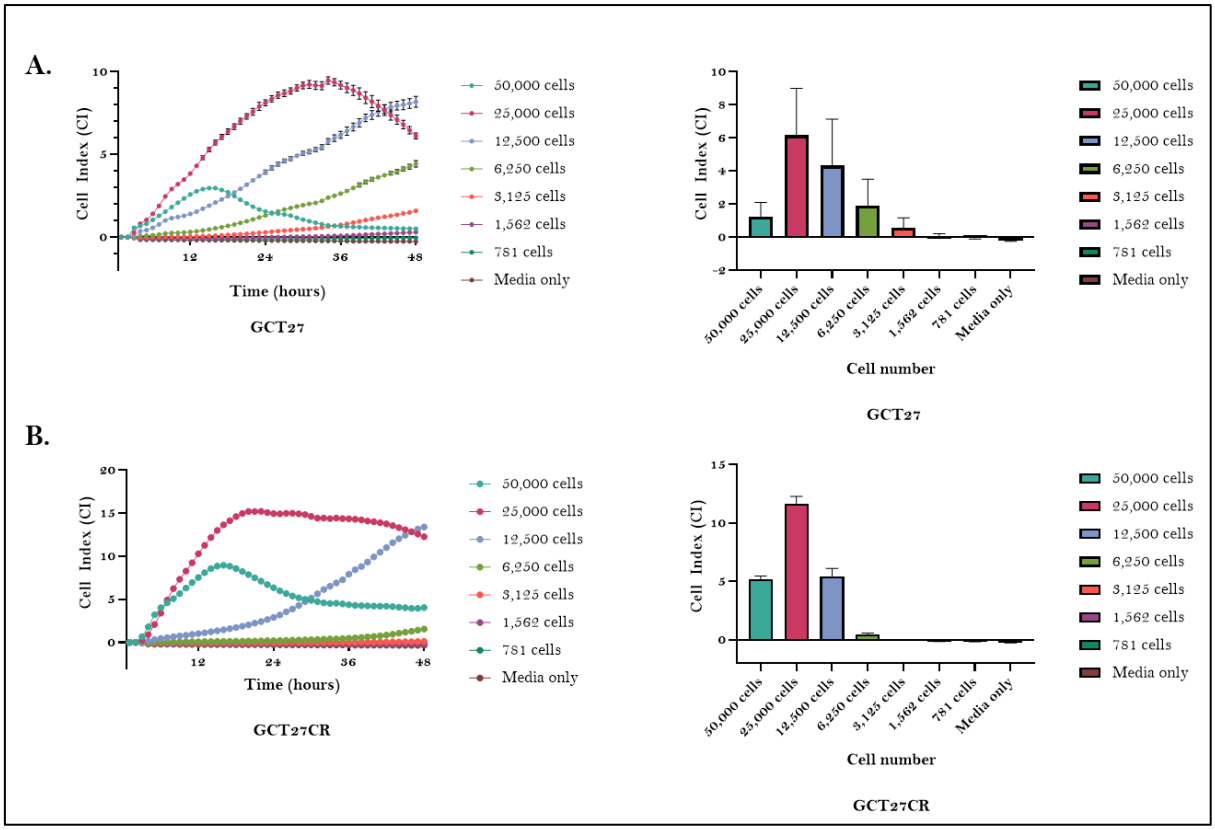

Figure 2.2: Optimal cell seeding densities for GCT27 and GCT27CR were determined prior to phenotypic analysis. A. *Serial dilutions of GCT27 and* ***B.*** *GCT27CR were prepared and seeded into specialised gold surface plated 96 well assay plates at the indicated seeding densities and analysed for 48 hours using the xCELLigence RTCA system. Error bars represent the standard error of mean across technical triplicates.*

2.2.16 Cell viability for cell number normalisation

For experiments outlined in the following sections, equivalent experiments were set up for cell viability analysis to enable cell number normalisation. For this, we carried out the Cyquant NF Cell proliferation assay according to the manufacturer's protocol. Following 48-hour knockdown of LARP1B, cells were re-seeded in 96 well plates at densities of 30,000-40,000 cells/well and allowed to adhere overnight. At the appropriate time the following day, spent media was removed from the wells and replaced with 100 µl of 1X dye binding solution composed of 22 µl of Cyquant NF dye reagent and 11 ml of 1X HBSS buffer. The microplate was incubated for 1 hour at 37°C after which fluorescence intensity was measured. After normalising relative fluorescence to background fluorescence and

extrapolating relative viability, this data was utilised for cell number normalisation of experiments outlined in 2.2.17.

2.2.17 Seahorse XF cell Mito stress test and glycolysis cell stress test

Mitochondrial oxygen consumption rate (OCR) as a measure of mitochondrial respiration and function were assessed using the Seahorse XF Mito Stress Test Kit (Agilent) and Seahorse XF96 cell culture microplates (Agilent). Following 48-hour knockdown of LARP1B, cells were re-seeded into Seahorse XF96 cell culture microplates at a density of 30,000 cells per well in 6 technical replicates, in antibiotic-free DMEM medium and allowed to adhere overnight. In addition, 100 µl of XF Calibrant Solution was added per well of a sensor cartridge overnight in a non-CO_2 incubator. Prior to the assay the next day, cells were maintained in Seahorse XF base medium supplemented with 5 mM Glucose, 4 mM L-Glutamine and 5 mM Sodium Pyruvate in a non-CO_2 incubator for 1 hour. During analysis of mitochondrial OCR, Oligomycin (1 µM), FCCP (0.8 µM), Antimycin A (2 µM) and Rotenone (2 µM) were added to relevant ports within the sensor cartridge and injected sequentially during the assay. In parallel, 30,000 cells were seeded into a 96 well plate and subjected to the same changes in culture medium and incubation in a non-CO_2 incubator for 1 hour for Cyquant NF assay as explained in 2.2.16.

2.2.18 Viability, Cytotoxicity and Apoptosis

In order to assess viability, cytotoxicity, and caspase 3/7 activation and cleavage as a marker of apoptosis, the ApoTox-Glo Triplex assay (Promega) was implemented according to the manufacturer's protocol. Following 48-hour knockdown of LARP1B, cells were re-seeded into opaque 96 well plates (in triplicate) at a density of 40,000 cells/well and allowed to adhere overnight. Briefly, 20 µl of Viability/Cytotoxicity Reagent containing GF-AFC and bis-AAF-R110 substrates was added to all wells, briefly mixed on an orbital shaker at 500 rpm for 30 seconds and incubated at 37°C for 30 minutes. Fluorescence was then measured at two separate wavelength sets: $400_{Ex}/505_{Em}$ for Viability and $485_{Ex}/520_{Em}$ for Cytotoxicity. After which, 100 µl of Caspase-Glo 3/7 Reagent was added to all wells, mixed on an orbital shaker at 500 rpm for 30 seconds and incubated at room temperature for 30 minutes. Luminescence was measured to detect caspase activation.

2.2.19 Immunofluorescence (IF)

Sterilisation of glass coverslips was performed by exposure to ultraviolet light in the tissue culture hood for 20 minutes. Cells were then grown to approximately 80% confluency on the coverslips in 6 well plates. At the time of staining, the coverslips were briefly rinsed 5 times in pre-extraction buffer and fixed in 1ml 4% Paraformaldehyde in PBS at room temperature for 20 minutes. Coverslips were then washed in 1 ml First wash at room temperature, on a rocker for 10 minutes and twice more in PBS only for 5 minutes. Fixed cells were then blocked in 1% fish gelatine at room temperature for 30 minutes in a humidified chamber. Fixed cells were then incubated in 100 µl primary antibody at room temperature for 1 hour in a humidified chamber. Primary antibody solution was washed briefly by immersing coverslips in Second wash 15 times and applied directly to 150 µl secondary antibody for 1 hour at room temperature in a humidified chamber. Fixed cells were washed as before and mounted onto glass coverslips in 15 µl of mounting media and imaged using the Zeiss LSM 710 confocal microscope after 24 hours.

2.2.20 MitoSOX Red Mitochondrial Superoxide live cell staining, visualisation, and analysis

GCT27 and GCT27CR cells were seeded in Ibidi 8 well chamber slides to 70% confluency and transfected with sh_ctrl or sh_LARP1B shRNA as mentioned previously, for 72 hours. 2 hours prior to cell staining, 50 µM menadione was added to half of the wells. After 2 hours, spent media was removed and cells were gently washed with pre-warmed HBSS. 1 µM MitoSOX Red in fresh culture medium was added to all wells and left to incubate for 30 minutes at 37°C and 5% atmospheric CO_2. MitoSOX Red solution was removed, and cells were washed as before in HBSS, thrice. Cells were imaged within 2 hours of staining under the Zeiss 710 confocal microscope. MitoSOX staining quantification was performed using ImageJ.

2.2.21 Testicular Tissue Microarray (TMA) immunohistochemistry (IHC) staining, scoring and digital analysis

Human Testicular tissue spectrum TMA slides were purchased in triplicate from TissueArray.com LLC (formerly US Biomax Inc). Automated staining was performed using the Leica BOND-MAX auto stainer under the following conditions: antigen retrieval

at 1°C for 20 minutes with epitope retrieval solution 1 (AR9961, Leica Biosystems), primary antibody solution incubation with LARP1 (Abcam, 1:2000) and LARP1B (Proteintech, 1:2000) for 30 minutes and detected using the BOND™ Polymer Refine Detection System (DS9800, Leica Biosystems) according to the manufacturers protocol. Slides were analysed and scored using the QuPath Pathology and Bioimage analysis open-source software. The percentage of LARP1B and LARP1 positive (%) cells and staining intensity were evaluated using the positive cell detection command on QuPath. For positive cell detection the following parameters were set: Detection image – Haematoxylin OD; Requested pixel size – 0.5 μm; Nucleus Background radius – 18 μm; Median filter radius – 0 μm; Sigma – 1.5 μm; Minimum area – 10 μm^2; Maximum area – 400 μm^2. Intensity parameters were set as follows: Threshold – 0; Max background intensity – 2; Cell expansion 5μm (include cell nucleus); Score compartment Cytoplasm: DAB OD mean; Threshold 1+ 0.2; Threshold 2+ 0.4; Threshold 3+ 0.6. For each tissue core the H-score (intensity) was calculated using the following command: 1 x (percentage of 1+ cells) + 2 x (percentage of 2+ cells) + 3 x (percentage of 3+ cells).

2.2.22 TGX gel silver stain

Immunoblotting was performed as previously mentioned (**2.2.7**) whilst silver staining of the gel was performed using the Pierce Silver Stain Kit, according to the manufacturers protocol with constant gentle shaking at room temperature throughout. Briefly, following protein separation the TGX gel was washed in ultrapure H_2O twice for 5 minutes each. The gel was fixed in 30% ethanol:10% acetic acid solution twice for 15 minutes each. The gel was then washed in 10% ethanol twice for 5 minutes each, followed by ultrapure H_2O twice for 5 minutes each. Sensitizer working solution composed of 1 part Silver Stain Sensitizer to 500 parts ultrapure water for 1 minutes and then washed twice for 2 minutes. the gel was then incubated in Stain Working Solution composed of 1 part Silver Stain Enhancer to 50 parts Silver Stain for 30 minutes. Gels were briefly washed with ultrapure H_2O for 1 minute and then incubated in Developer Working Solution until bands appeared after which 5% acetic acid solution was added as a Stop Solution for 10 minutes. The gel was then imaged using the Bio-Rad ChemiDoc Imaging System.

2.2.23 S-Trap™ micro spin column digestion of co-IP samples

Immunoprecipitation were performed as mentioned previously (2.2.11) using anti-LARP1B and anti-IgG (Rabbit species) antibodies. Following IPs, 10% of the bead slurry was retained for western blot and silver stain gel analysis in order to confirm successful pull downs. The remaining 90% of beads were stored at -80°C overnight to retain complexes and then subjected to column digestion using S-TRAP micro columns, according to the manufacturers protocol. Briefly, 23 µl of 1X lysis buffer was added to sedimented beads and vortexed briefly to dissolve proteins. Samples were clarified of debris and separated from the beads by ultracentrifugation for 8 minutes at 130,000 G and transferred to fresh 1.5 ml tubes. To reduced proteins, 1 µl of reductant (5 mM Tris(2-carboxyethyl) phosphine) was added to each sample and incubated at 55°C for 15 minutes. 1 µl of alkylator (20mM Methyl methanethiosulfonate) was added and incubated at room temperature for 10 minutes. 2.51 µl of acidifier composed of 27.5% phosphoric acid in H_2O was added and vortexed briefly. 165 µl of wash buffer was added, briefly mixed and transferred to a S-Trap micro column inside a 1.7 ml Eppendorf tube. columns were centrifuged at 4,000 G for 30 seconds at room temperature to trap proteins. To clean the protein, 150 µl of wash buffer was added and centrifuged at 4,000 G for 30 seconds at room temperature 3 times and then centrifuged at 4,000 G for 1 minute to remove all traces of wash buffer. The S-Trap column was transferred to a fresh 17 ml Eppendorf tube and 20 µl of digestion buffer containing trypsin proteases was added at a 1:10 weight: weight ratio onto the column and incubated for 1 hour at 47°C. Following incubation, 40 µl of elution buffer 1 was added to the column and centrifuged at 4,000 G for 1 minute, sequentially followed by 40 µl elution buffer 2 and elution buffer 3 under the same conditions. Eluted peptides were then resuspended in 20 µl of buffer composed of 5% acetonitrile and 0.1% formic acid and dried on a speed vacuum overnight in preparation for MS analysis.

2.2.24 MS/MS and data analysis

MS analysis was performed by Dr Robert Parker using the Dionex Ultimate 3000 nHPLC and Q-Exactive mass spectrometer. MS1 spectra with a resolution of 60,000 was acquired at 200 m/z. Maxquant quantitative proteomics software was used for the identification and label-free quantification of MS/MS data using the UniProt human reviewed proteome (2020 update). We performed standard statistical testing instead of label-free quantification (MaxLFQ) for protein quantification due to a lack of triplicate samples. Minimum peptide

length was set to 7 and minimum unique peptides was set to 1. The default cleavage enzyme Trypsin/P was used, and the maximum number of missed cleavages was set to 1. Carbamidomethyl (C) was selected for fixed modifications. The data files were then further analysed using standard Microsoft Office tools and further analysed using The Gene Ontology Resource software for functional analysis of enriched proteins. We also used Metascape Gene Annotation and Analysis Resource to determine the subcellular localisation of enriched LARP1B-bound proteins. To determine enriched proteins, intensity scores in LARP1B IPs were normalised to IgG control IP of which the log2 fold change ≥2 was calculated.

2.3 LARP1B antibody and RNAi validation

Due to the novelty of this project, there was a significant lack of validated anti-LARP1B antibodies and RNAi tools within our lab or amongst our collaborators within the LARP society. Our collaborator Professor Andrea Berman kindly provided us with a human wildtype LARP1B pCMV6 LARP1B-Myc/Flag expression construct. Two key studies have investigated the binding and function of LARP1B with the use of LARP1B Myc/Flag expression constructs, but used an anti-Flag antibody to detect LARP1B expression[48, 74]. Thus, it was necessary to validate a suitable LARP1B-specific antibody for further LARP1B studies.

RNAi experiments are useful tools for understanding the phenotype and function of the target of interest, however there is not always a good quality antibody available to validate successful knockdown at the protein level (as we experienced in this project) particularly when characterising novel targets. If an adequate antibody is not available, investigations rely on assessing knockdown efficacy by analysing mRNA levels only, by qRT-PCR as siRNA mediated RNAi is a method of post-transcriptional interference leading to mRNA degradation[219]. We also used this approach due to difficulties in validating depletion of LARP1B protein. A key drawback of this however, is that mRNA and protein levels do not always correlate and so assessment of mRNA levels only, does not provide the complete picture.

In attempts to overcome these issues, we conducted a comprehensive evaluation of six commercially available LARP1B antibodies whilst simultaneously verifying LARP1B

RNAi tools and construct based LARP1B expression. A flow chart of our optimisation and antibody selection processes is shown in **Figure 2.3**. In summary, our aim was to validate at least one LARP1B antibody based on the ability to 1) detect endogenous LARP1B Isoform 1 protein at the predicted molecular weight of 105kDa or thereabouts (there is often a difference in the predicted and observed molecular weight of proteins), 2) demonstrate changes in LARP1B protein levels following RNAi or construct based experiments which to some extent corresponded with mRNA expression and 3) does not cross-react with LARP1 which is possible due to their high level of sequence similarity.

Initial studies ruled out Elabsciences, Atlas Antibodies and Novus Biologicals LARP1B antibodies based on their inability to detect endogenous LARP1B with minimal non-specific binding. From this point onwards, our work in validating the remaining Origene, Everest and Proteintech LARP1B antibodies involved thorough investigation into the suitability of each antibody through extensive, repeated RNAi and construct-based expression studies. We interrogated LARP1B protein expression in a number of cell lines, using various RNAi and LARP1B constructs expression methods at different timepoints. During this intensive exercise, we found the inability of most antibodies in detecting a reduction or increase in LARP1B protein levels despite corresponding changes in LARP1B mRNA expression. This was attributed to either inability of the antibody in detecting endogenous LARP1B or the binding of the antibody to an immunogen present in LARP1B expression constructs and not endogenous protein. Continued investigation culminated in validation of the Proteintech LARP1B antibody as it fulfilled our criteria and generated the results presented throughout this thesis.

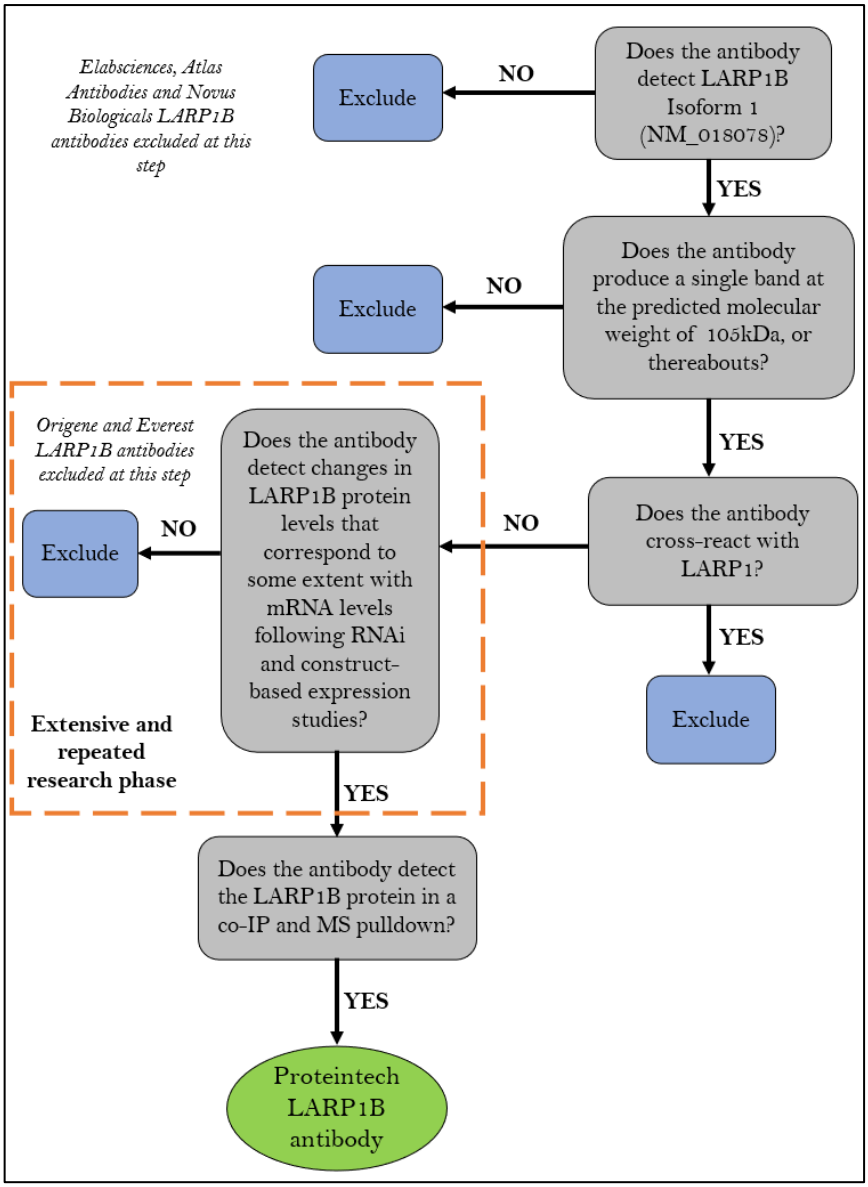

Figure 2.3: Flow chart highlighting steps taken in validating LARP1B antibodies.

3

RESULTS CHAPTER 1: LARP1B AND LARP1 EXPRESSION IN A SUBSET OF CANCERS

3.1 Introduction

Blagden lab alongside others, have demonstrated the tumour-promoting role of LARP1. LARP1 mRNA and/or protein levels are upregulated in a number of cancers and are associated with worse prognosis in ovarian[44, 46], cervical[46], colorectal[67], hepatocellular[66] and renal carcinoma[62]. In these studies, LARP1 depletion significantly abrogated cancer cell proliferation, migration, invasion and enhanced chemosensitivity supporting a hypothesised oncogenic role for LARP1.

LARP1 shares 56.5% sequence similarity with LARP1B, both containing the same highly conserved domains including the LARP1 specific DM15 RBD[37] suggesting that they may share cellular functions. However, LARP1B remains largely unexplored and its cellular roles in the development and progression of cancer, are unknown warranting further investigation.

This project provided us with a blank page to begin exploring the phenotypic role and function of LARP1B in cancer and how this compared to LARP1. The primary aim of this chapter was to understand the expression profile of LARP1B in different cancer types using online databases and research tools such as The Cancer Genome Atlas (TCGA) and The Genotype-Tissue Expression (GTEx) projects. Crucially, these tools can be used to interrogate the roles of genes with no functional annotation like LARP1B and would support our second aim of identifying a clinically relevant cancer research model in which the function of LARP1B could be explored.

Finally, we set out to verify LARP1B and LARP1 expression in human normal and cancerous tissue to confirm our *in-silico* findings.

3.2 Results

3.2.1 *LARP1B* and *LARP1* mRNA show contrasting expression patterns in a subset of cancer types

To investigate the expression of LARP1B and LARP1 in cancer we performed transcriptome analysis using normal and matched tumour samples from cancer patients in the TCGA and GTEx Pan Cancer cohorts. This data was accessed from Gene Expression Profiling Interactive Analysis (GEPIA)[220] and included analysis of 31 tissue types as per their TCGA annotation. Due to the lack of *LARP1B* expression data for a number of

normal tissue types within the TCGA database, we compared tumour tissue from the TCGA database with paired normal tissue from both the TCGA and GTEx cohorts which allowed for a greater number of datasets to be analysed.

As shown in **Figure 3.1**, expression levels of *LARP1B* and *LARP1* mRNA was variable across the different cancer types. Generally, *LARP1* expression was highest with median expression reaching 107.8 transcripts per million (TPM) in acute myeloid leukaemia (LAML) samples (**Figure 3.1B.**) whereas *LARP1B* gene expression reached a median TPM value of 51.39 in testicular germ cell tumour (TGCT) normal control samples (**Figure 3.1A.**). We also observed that in 12/31 tissue types analysed, both *LARP1B* and *LARP1* had opposite expression patterns, for example in cholangiocarcinoma (CHOL), *LARP1B* expression was higher in normal than tumour tissue whilst *LARP1* expression was higher in tumour than normal tissue. We identified opposing expression patterns of *LARP1B* and *LARP1* in over 30% of the tissue types analysed but identical expression patterns in the remaining cancer types including bladder urothelial carcinoma (BLCA), breast invasive carcinoma (BRCA) and cervical squamous cell carcinoma (CESC).

The most striking finding with regards to *LARP1B* mRNA expression was observed in TGCT with a median expression of 51.39 TPM in normal tissue compared to a 24.77 median TPM in tumour tissue, suggesting a significant reduction in *LARP1B* expression during TGCT development. Further investigation revealed an opposite expression pattern for *LARP1* in TGCT with elevated expression in tumour tissue compared to normal controls (**Figure 3.2**). Analysis of the two primary subtypes of TGCT, seminoma and non-seminoma, revealed a significant decrease in *LARP1B* mRNA expression in non-seminoma tissue compared to normal testicular tissue and a similar non-significant trend in seminoma (**Figure 3.3**).

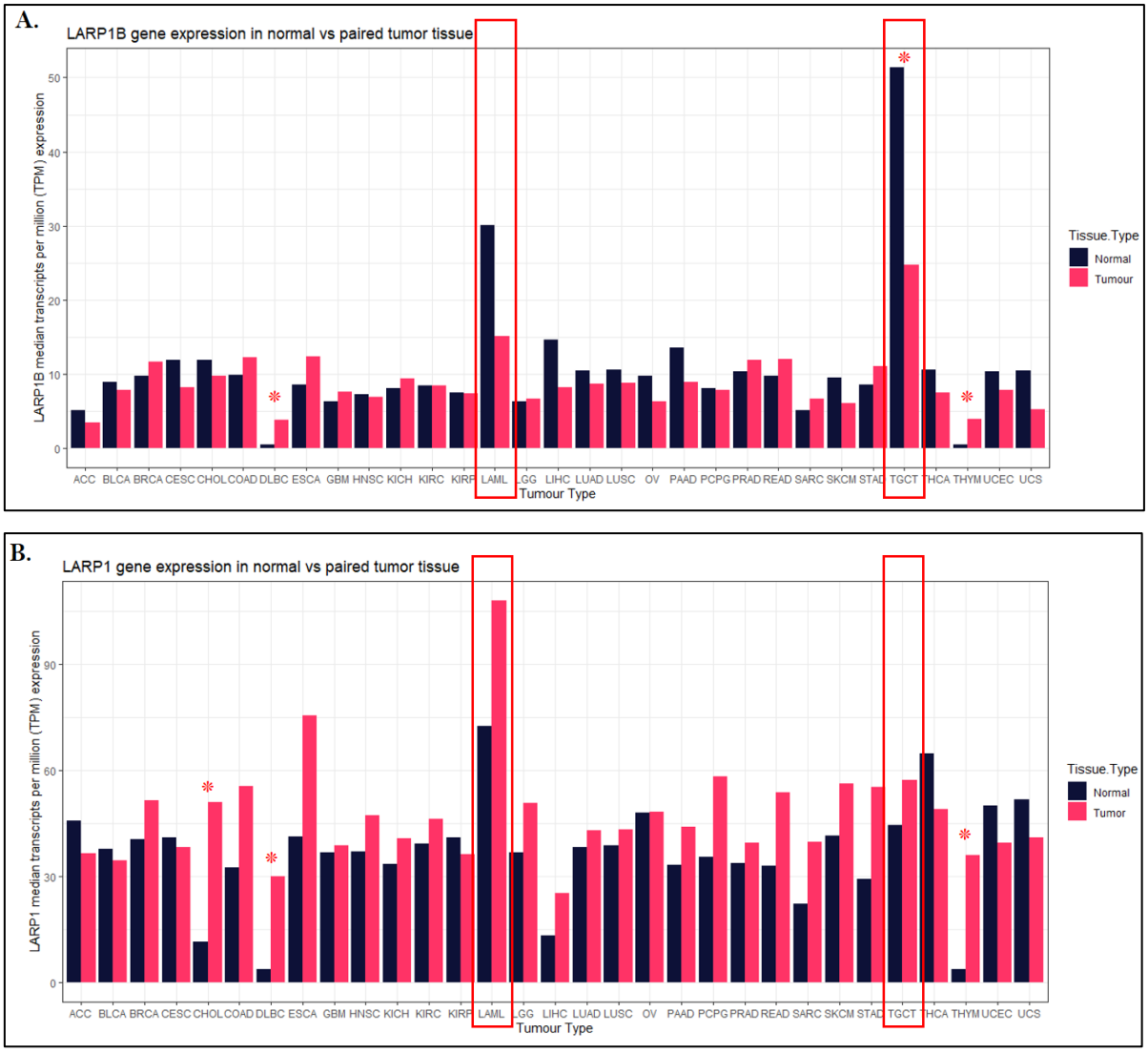

Figure 3.1: LARP1B and LARP1 median TPM expression in indicated cancer types. ***A.*** *LARP1B median TPM expression was highest in LAML and TGCT (red-boxed regions) but reduced in tumour compared to normal samples.* ***B.*** *LARP1 median TPM expression in LAML and TGCT showed an opposite expression pattern to LARP1B with increased expression in tumour compared to normal samples (red-boxed regions). Significant differences between normal and tumour samples are highlighted with an Asterix (*). * P Value ≤ = 0.01.*

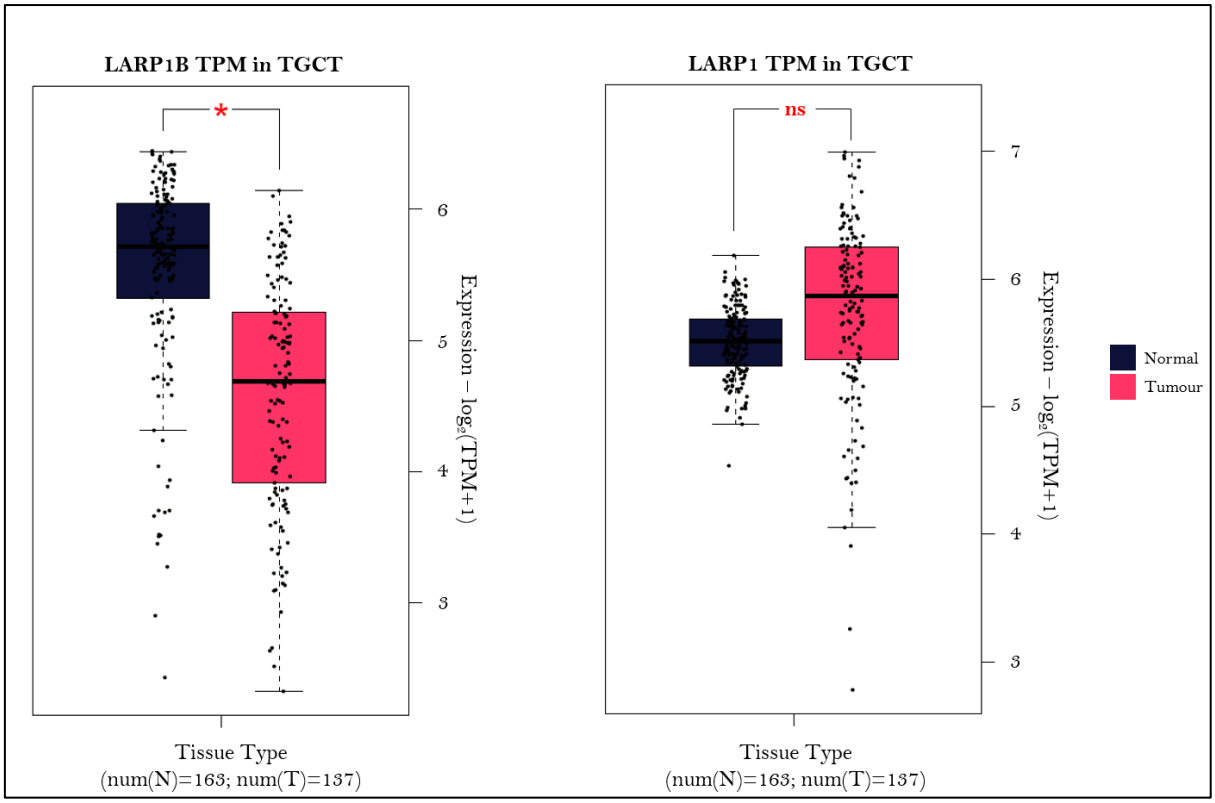

Figure 3.2: LARP1B mRNA expression is reduced between normal testicular and TGCT tissue whilst expression of LARP1 is increased. *LARP1B mRNA expression was highest in normal testicular tissue with a significant reduction of expression in TGCT tumour tissue. LARP1 expression was higher in TGCT compared to normal testicular tissue, although data was not significant. N: Normal tissue, T: Tumour/TGCT tissue, "num": number of cases. Log₂ scale used; * P Value ≤ = 0.01, ns = non-significant.*

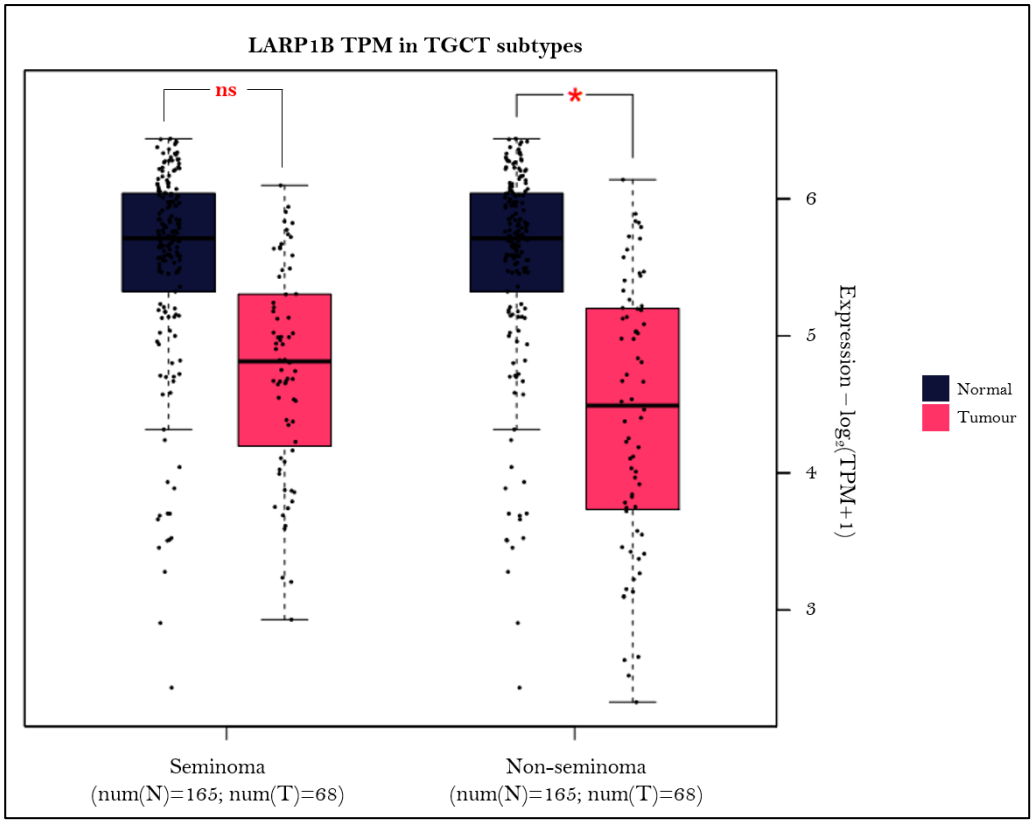

Figure 3.3: LARP1B gene expression is reduced between normal testicular and seminoma or non-seminoma tumour tissue. *LARP1B gene expression was highest in normal testicular tissue with a significant reduction of expression in non-seminoma tumour tissue. LARP1B expression was also lower in seminoma tissue compared to normal testicular tissue, although data was not significant. N: Normal tissue, T: Tumour/TGCT tissue, "num": number of cases. Log_2 scale used; * P Value ≤ = 0.01, ns = non-significant.*

3.2.2 Co-expression of *LARP1B* and *LARP1* mRNA varies between normal and tumour tissues of different cancer types

Analysis of Pan Cancer databases revealed heterogeneous expression patterns for both *LARP1B* and *LARP1* mRNA expression. In 12/31 tissue types analysed on GEPIA, *LARP1B* and *LARP1* presented with contrasting expression patterns with the remaining 19/31 cases showing identical changes in expression during tumour development. We then analysed co-expression of *LARP1B* and *LARP1* mRNA across the same tissue and cancer types to provide further insight into their co-expression patterns. As shown in **Figure 3.4**, *LARP1B* and *LARP1* mRNA expression across the same 31 tissue types as those shown

previously, demonstrated a weak positive correlation in expression in both normal and tumour tissue (R=0.43; *P*=0.00001 and R=0.41; *P*=0.00001, respectively).

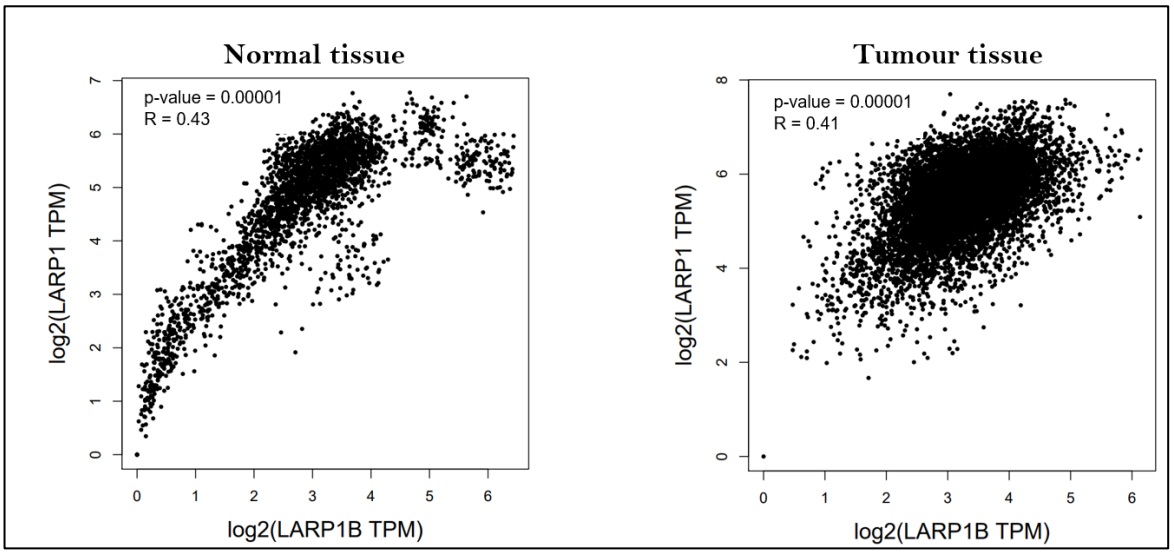

Figure 3.4: LARP1B and LARP1 mRNA demonstrate weak positive expression correlation amongst TCGA and GTEx normal and paired tumour samples. *mRNA expression correlation data between LARP1B and LARP1 was extrapolated from the GEPIA database and analysed for gene co-expression. Pearson correlation coefficient was used to measure linear correlation as indicated by "R" values in the top left corner. Normal tissue: R = 0.43; P Value = 0.00001 and Tumour tissue: R = 0.41; P Value = 0.00001.*

Given that we showed a significant reduction in *LARP1B* mRNA expression during TGCT development but a non-significant reduction in *LARP1* mRNA expression, we also investigated their co-expression in TGCT. Interestingly, we found different correlative patterns between normal and tumour tissue (**Figure 3.5**). In normal testicular tissue we identified a weak negative correlation between *LARP1B* and *LARP1* mRNA expression (R=-0.24; *P*=0.0023) suggesting that there was little to no correlation between the expression of *LARP1B* and *LARP1* in normal testicular tissue. In TGCT tumour tissue we identified a strong positive correlation in expression (R=0.62; *P*=8.9e-16) between the two genes.

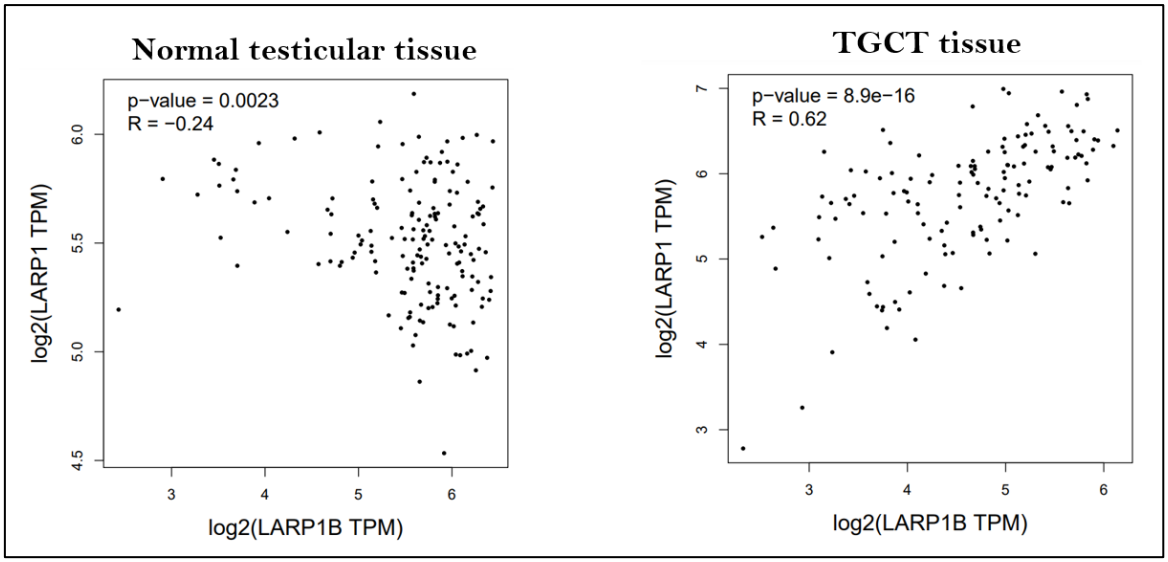

Figure 3.5: LARP1B and LARP1 show a weak negative correlation in expression in normal testicular tissue but a strong positive correlation in TGCT tumour tissue. *mRNA expression correlation data between LARP1B and LARP1 was extrapolated from the GEPIA database and analysed for gene co-expression in TGCT and paired normal tissue. Pearson correlation coefficient was used to measure linear correlation as indicated by "R" values in the top left corner. Normal testicular tissue: R = -0.24; P Value = 0.0023 and TGCT tissue R = 0.62; P Value = 8.9e-16.*

3.2.3 The correlation between *LARP1B* mRNA expression and patient overall survival varies amongst lung, gastric and colon cancers

To understand the functional importance of altered *LARP1B* expression in cancer, we examined the correlation between mRNA expression with overall survival (OS) of cancer patients, alongside *LARP1*. Due to the lack of sufficient TGCT cases for the analysis of patient survival outcomes in the TCGA project we used kmplot.com as an alternative data source. We selected cancers with mRNA gene chip expression of *LARP1B* and *LARP1* data of which there were seven in total (breast[221], ovarian[222], lung[223], gastric[224], colon[225], AML[222] and myeloma[224] cancers) and investigated correlation with overall survival. We selected overall survival due to availability of this data for all cancer types analysed whilst progression-free survival, palliative performance scale and first progression scores were only available for a select few cancer types. It is important to note that there were fewer patient samples available for the analysis of *LARP1B* expression compared to *LARP1* (**Table 3.1**) which is just one of many examples of the disparity in the research tools available for LARP1B and LARP1, which has been a major challenge of this project.

	Number of cases in each mRNA gene chip dataset						
	Breast Cancer	**Ovarian Cancer**	**Lung Cancer**	**Gastric Cancer**	**Colon Cancer**	**AML**	**Myeloma**
LARP1B	943	655	1411	631	304	734	1152
LARP1	1879	1656	2166	875	550	1608	1416

Table 3.1: Number of patient samples per cancer type available for overall survival analysis associated with LARP1B and LARP1 mRNA expression. *There were fewer samples available for analysis of LARP1B expression compared to LARP1 within the mRNA gene chip datasets on kmplot.com.*

We discovered a notable correlation between elevated LARP1B mRNA expression and positive survival outcome in lung, gastric and myeloma cancers (*P*=1.5e-6, *P*=2.4e-5 and *P*=0.012, respectively) but a significantly worse overall survival in colon cancer (*P*=0.0036). (**Figure 3.6A.).** Non-significant trends towards improved overall survival were observed in breast and AML (*P*=0.33 and *P*=0.066, respectively) whilst a non-significant trend towards worse overall survival was observed in ovarian cancer (*P*=0.51). Higher *LARP1* mRNA expression was associated with a positive overall survival outcome in ovarian, gastric and AML cancers (*P*=0.023, *P*=0.0011 and *P*=0.00012) whilst a non-significant trend was observed in colon cancer (*P*=0.34) (**Figure 3.6B.**). Higher *LARP1* expression was associated with a poorer overall survival in breast and myeloma cancers (*P*=0.011 and *P*=0.027, respectively) whilst a non-significant trend was observed in lung cancer (*P*=0.33). It is interesting to observe different survival outcomes for *LARP1B* and *LARP1* in the same cancer for example in myeloma high *LARP1B* expression correlated with a better overall survival whilst high *LARP1* expression correlated with a poor overall survival (**Figure 3.6**).

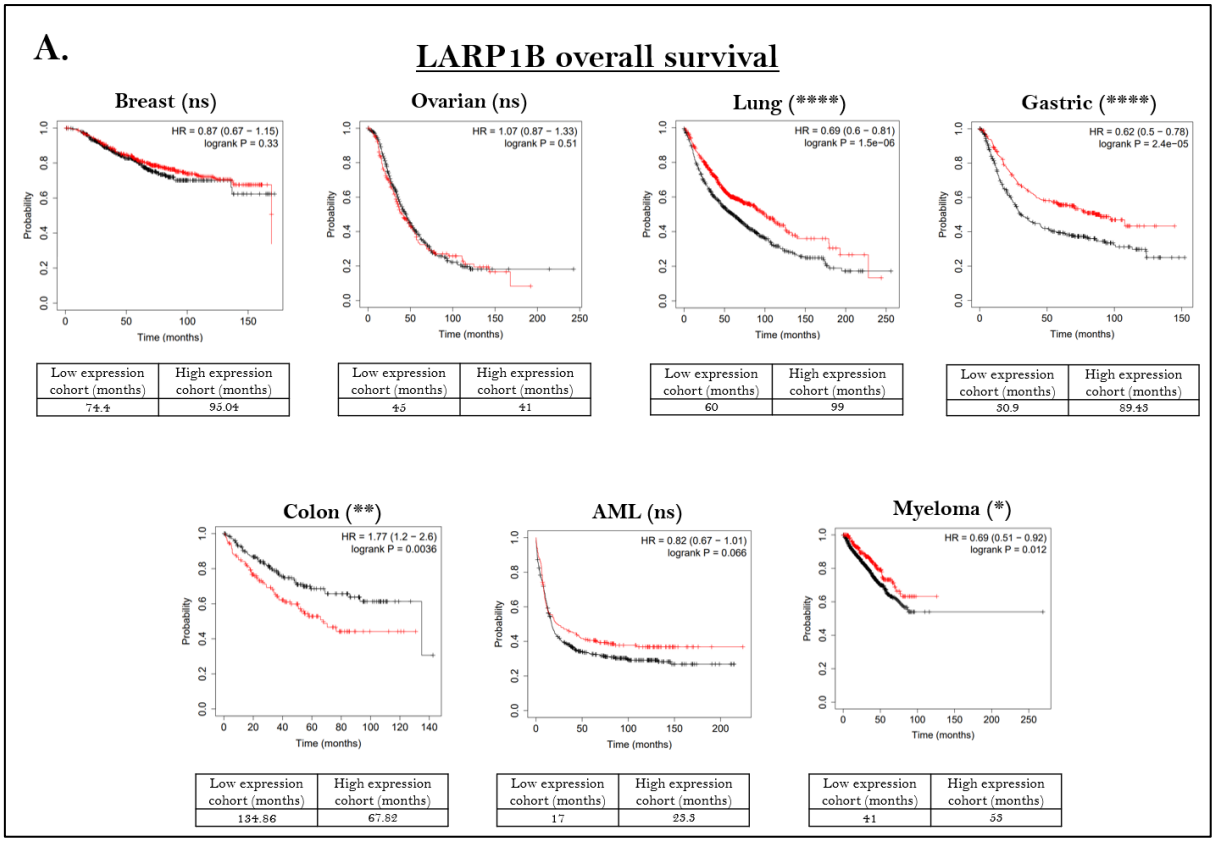

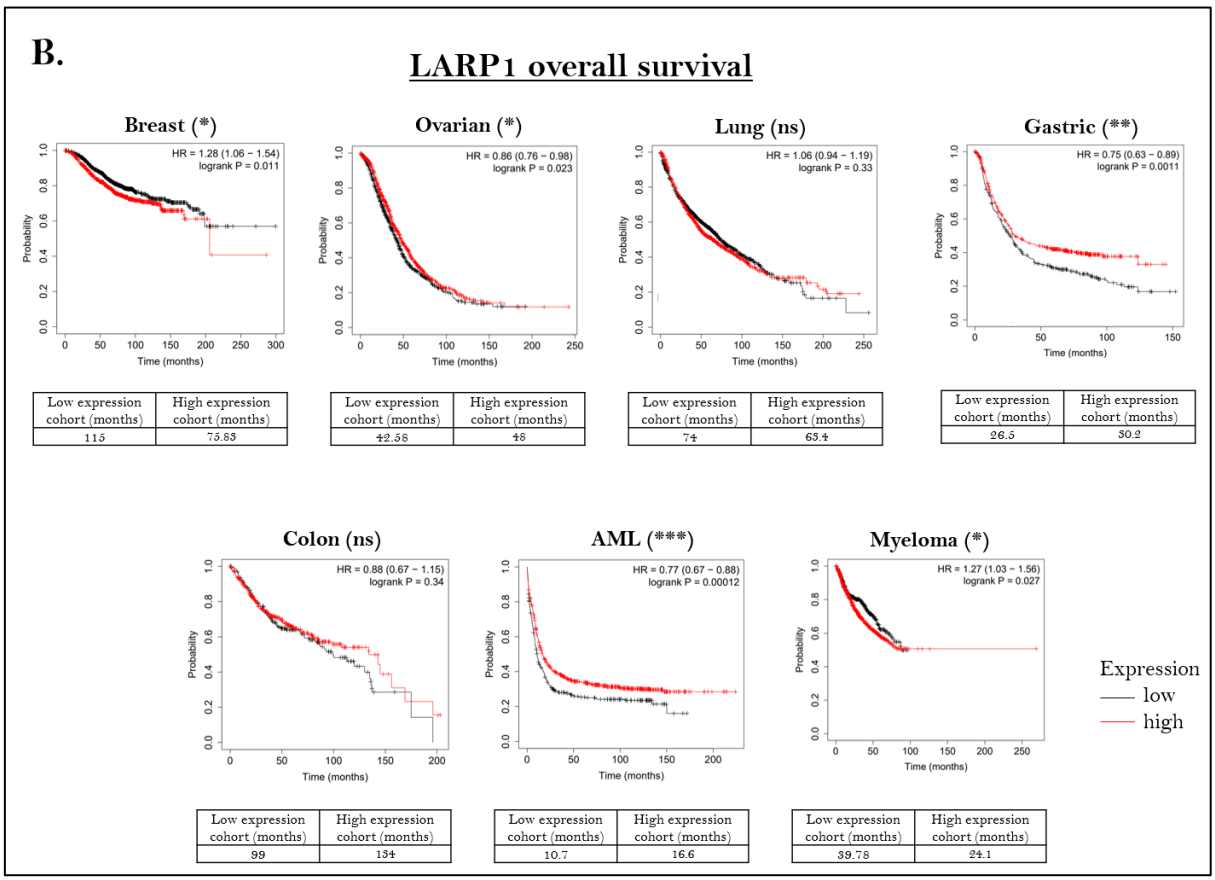

Figure 3.6: LARP1B and LARP1 expression levels are associated with variable overall survival outcomes in cancer. *Cancer survival curves were obtained from kmplot.com*

for LARP1B and LARP1. High LARP1B mRNA expression was significantly associated with a positive outcome in lung, gastric and myeloma cancers. High LARP1 mRNA expression was significantly associated with a positive overall survival outcome in ovarian, gastric and AML cancers. mRNA gene-chip datasets were selected for our analysis with significance defined at P Value =<0.05.

3.2.4 LARP1B and LARP1 protein exhibit different expression patterns in normal and cancerous testicular tissue

Following on from our *in-silico* findings (and earlier literature search findings) we further explored LARP1B and LARP1 protein expression in normal and cancerous testicular tissue. We acquired a testicular-specific tissue microarray (TMA) composed of 75 normal, tumour and "other" testicular tissue cores, details of which are highlighted in **Table 3.2**; briefly, normal testicular tissue, normal adjacent tissue, testicular atrophy and malignant tissue types were included. Malignant tissues were further sub-classified into teratoma, yolk sac tumour, embryonal carcinoma and seminoma which are all TGCT diagnoses. TMA slides were then stained with anti-LARP1B or anti-LARP1 antibody to determine their expression patterns in testicular tissue.

	n/75
Diagnosis:	
Normal testicular tissue	5
Normal adjacent tissue	10
Testicular atrophy	6
Malignant	54
Malignant:	
Teratoma	6
Yolk Sac Tumour	9
Embryonal Carcinoma	13
Seminoma	26
Stage at diagnosis:	
IA	22
IB	24
Not specifiied	29

Table 3.2: Testicular TMA content. *FFPE tissue cores were approximately 1.5mm in diameter and classified by tissue type followed by diagnosis to outline specific TGCT subtypes.*

Figures 3.7 and **3.8** show examples of a normal testicular tissue cores stained for LARP1B and LARP1 protein respectively (brown staining), with structures and cell types labelled. In **Figure 3.7** LARP1B was localised primarily within the cytoplasmic and membranous regions with scattered nuclear staining and was detected in all cell types at varying intensities. Strongest staining was within the secretory Leydig cells located within the interstitial space between the tubules (▲) whilst weakest staining was within the myoid cells and basal lamina surrounding the tubules (▲). All cells within the germinal epithelium (GE) stained positive for LARP1B with germ cells at later stages of differentiation such as the spermatocytes and spermatids exhibiting stronger staining than those in earlier stages such as the spermatogonia.

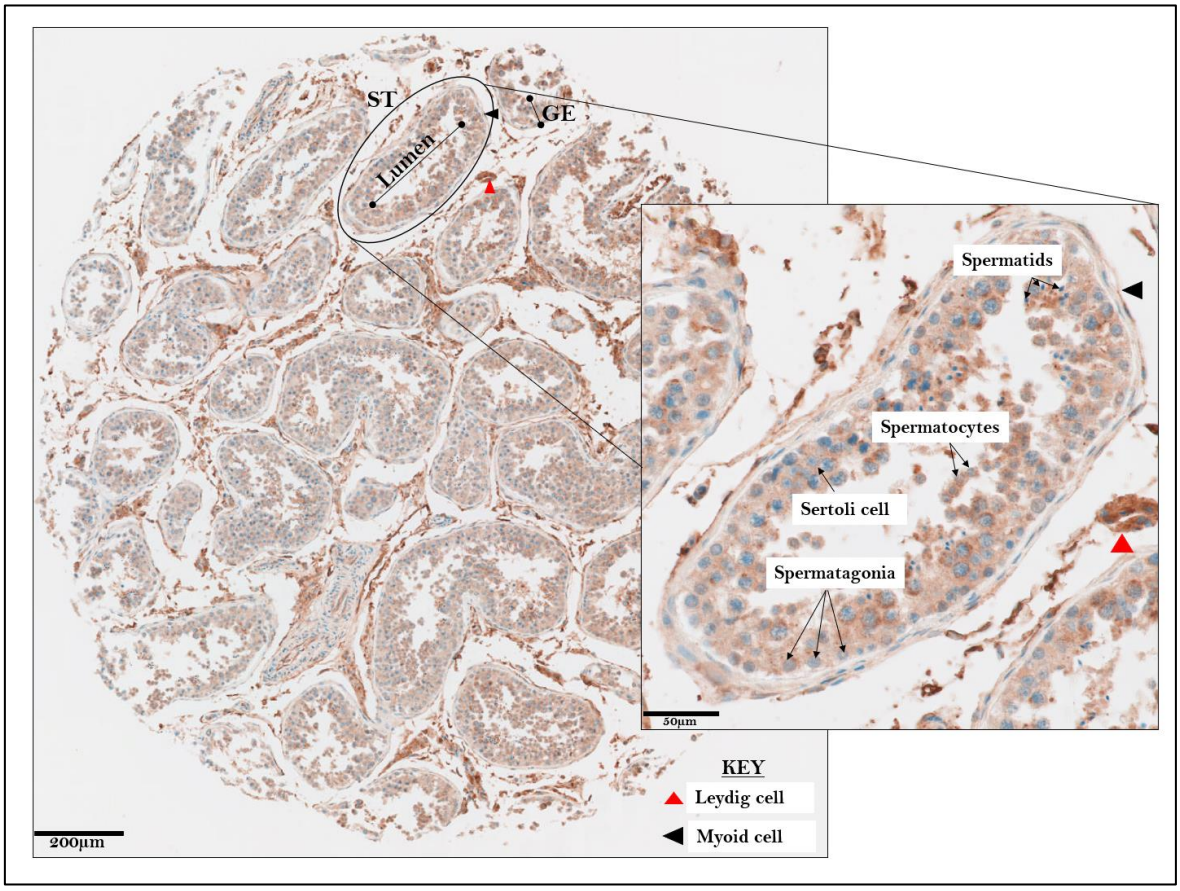

Figure 3.7: LARP1B expression was strongest in the Leydig cells and weakest in the basal lamina surrounding the seminiferous tubules. *FFPE normal testicular tissue was stained using and anti-LARP1B antibody. The key structures of the testicular tissue are highlighted as follows: Lumen, ST: Seminiferous tubule, GE: Germinal epithelium. Black arrowhead pointing to elongated myoid cells within the basal lamina surrounding the tubules. Red arrowhead pointing to the Leydig cells located within the interstitial space between the seminiferous tubules. Scale bar = 200µm and 50µm.*

Overall, we observed less intense antibody staining for LARP1 compared to LARP1B in normal testicular tissue (**Figure 3.8**). LARP1 was also localised to the cytoplasmic and membranous regions but with no observable nuclear staining throughout the core. Strongest staining for LARP1 was within the GE whilst weakest staining was in the basal lamina surrounding the tubules (▲). All cells within the GE stained positive for LARP1 with similar intensity.

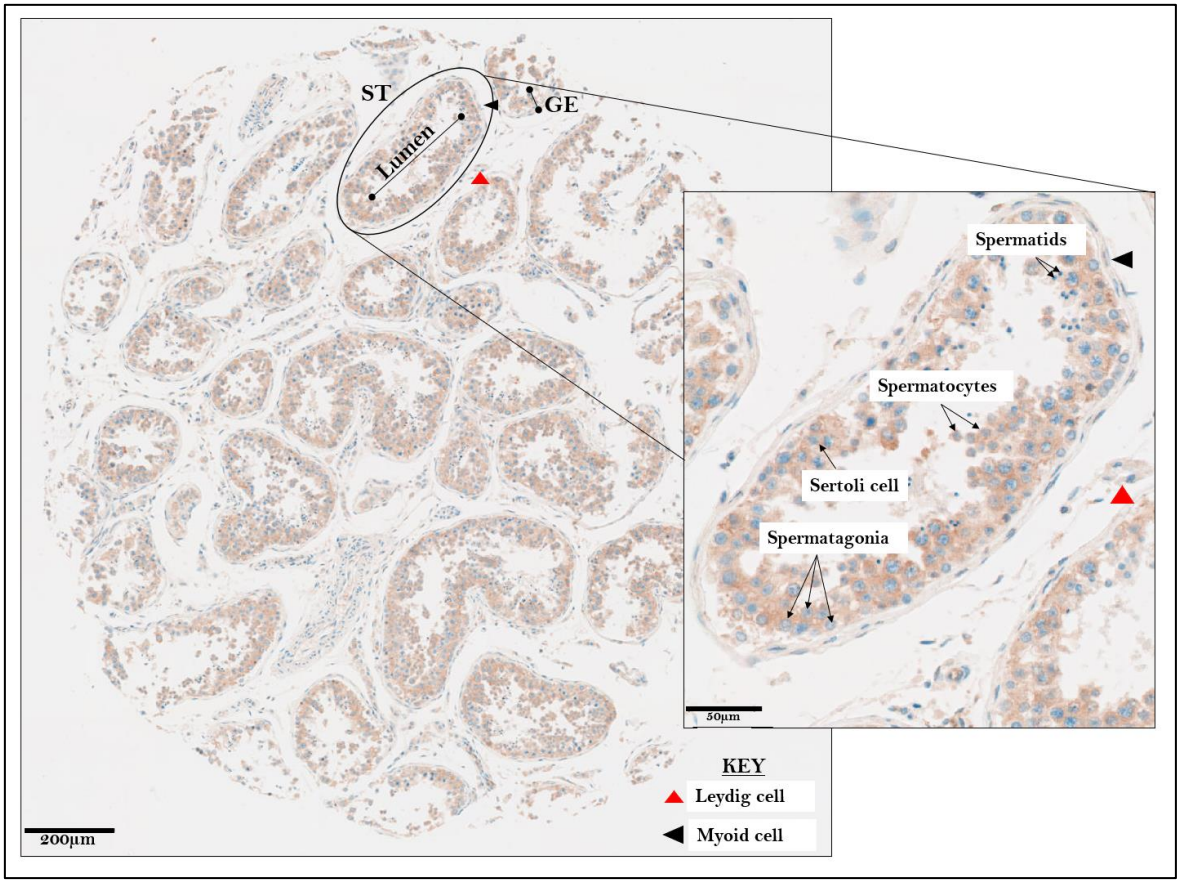

Figure 3.8: LARP1 expression was strongest in the germinal epithelium and weakest in the basal lamina surrounding the seminiferous tubules. *FFPE normal testicular tissue was stained using and anti-LARP1 antibody. The key structures of the testicular tissue are highlighted as follows: Lumen, ST: Seminiferous tubule, GE: Germinal epithelium. Black arrowhead pointing to elongated myoid cells within the basal lamina surrounding the tubules. Red arrowhead pointing to the Leydig cells located within the interstitial space between the seminiferous tubules. Scale bar = 200µm and 50µm.*

We then analysed the expression of LARP1B and LARP1 protein across the different tissue types by looking at the percentage of LARP1B and LARP1-positive cells and staining

intensity using QuPath as described in **Chapter 2: methods 2.2.21**. First, we compared the number of LARP1B-positive cells (cells stained for LARP1B) between normal tissue and normal adjacent tissue and found no change. However, we observed a significant reduction in the number of LARP1B-positive cells between normal and malignant tissue as detected by a reduction in brown staining (**Figure 3.9A. and B.**). This may be largely attributed to the anatomical and morphological changes in the tissue itself, including loss of distinct structures namely the seminiferous tubules which contain LARP1B-positive germ cells but also loss of the Leydig cells which stained strongest for LARP1B. To examine the difference in LARP1B staining intensity between tissue types, we compared the Histochemical-score (H-score) of cytoplasmic/membranous regions where LARP1B localised (**Figure 3.9**); H-score was used as it enables combined assessment of staining intensity and percentage of stained cells. We observed a similar pattern as before with no change in LARP1B staining intensity between normal and normal adjacent tissue but a significant reduction between normal and malignant tissue (**Figure 3.9C.**). The number of LARP1B-positive cells and staining intensity of atrophied tissue (as would occur after testicular torsion) was comparable to normal and normal adjacent tissue cores.

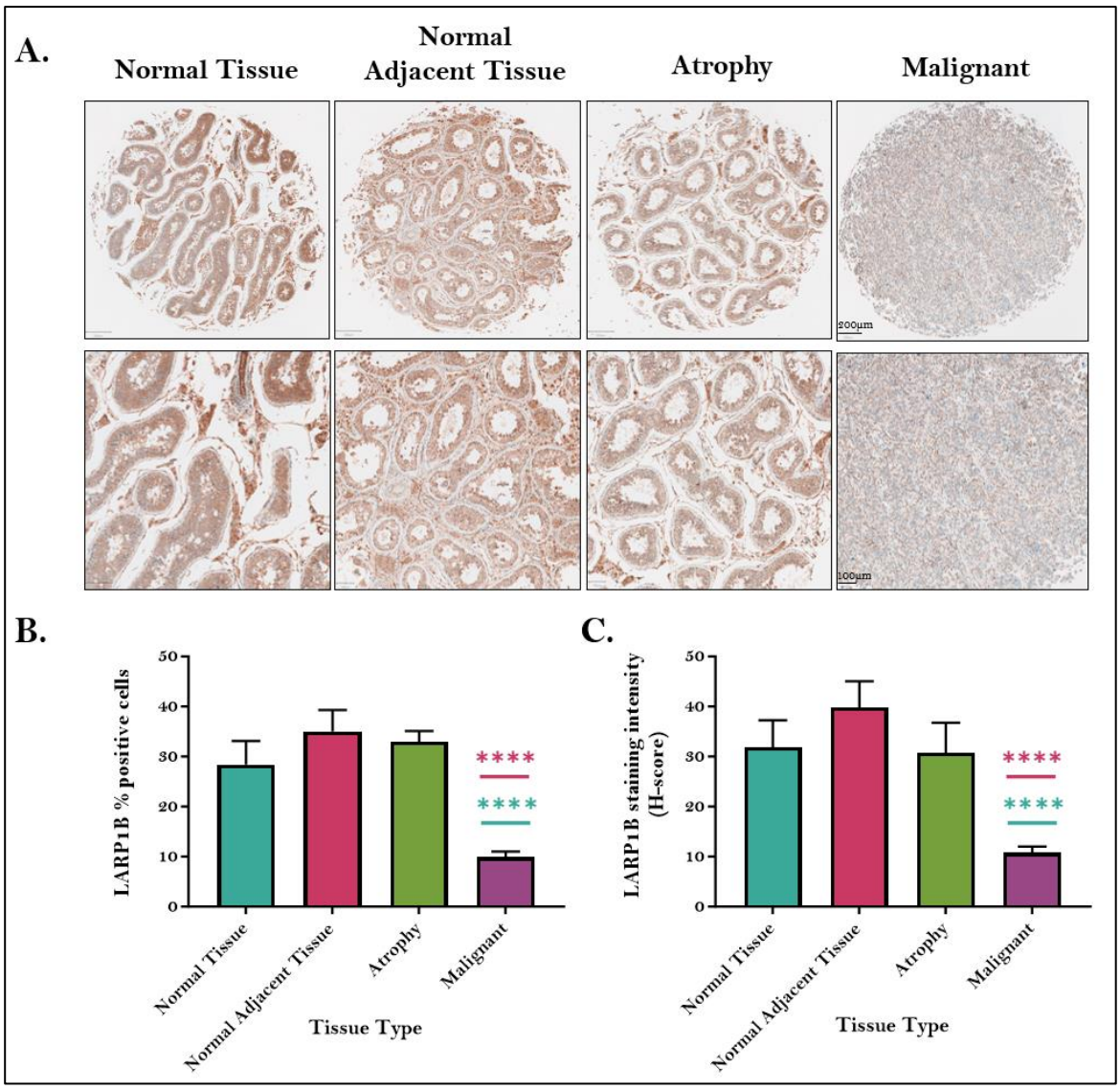

Figure 3.9: LARP1B protein expression was significantly lower in malignant testicular tissue compared to normal and normal adjacent tissue. A. *Representative images of FFPE testicular tissue cores were analysed for* ***B.*** *% of LARP1B-positive cells and* ***C.*** *LARP1B staining intensity (H-score) using QuPath. Scale bar = 200µm and 100µm. **** P Value= ≤0.0001; green Asterix (****) refer to statistical comparison to normal tissue whilst red Asterix (****) refer to statistical comparison to normal adjacent tissue. Unpaired t-test was used for statistical analysis.*

Interestingly, we observed the opposite pattern for LARP1. There was no significant change in the number of LARP1-positive cells between normal and normal adjacent tissue but a hint of more LARP1-positive cells in malignant tissue compared to normal testicular tissue, which did not reach significance (**Figure 3.10A. and B.**). This was despite the loss

of key structures such as the seminiferous tubules which were LARP1-positive. We also did not observe significant changes in LARP1 staining intensity (**Figure 3.10C.**)

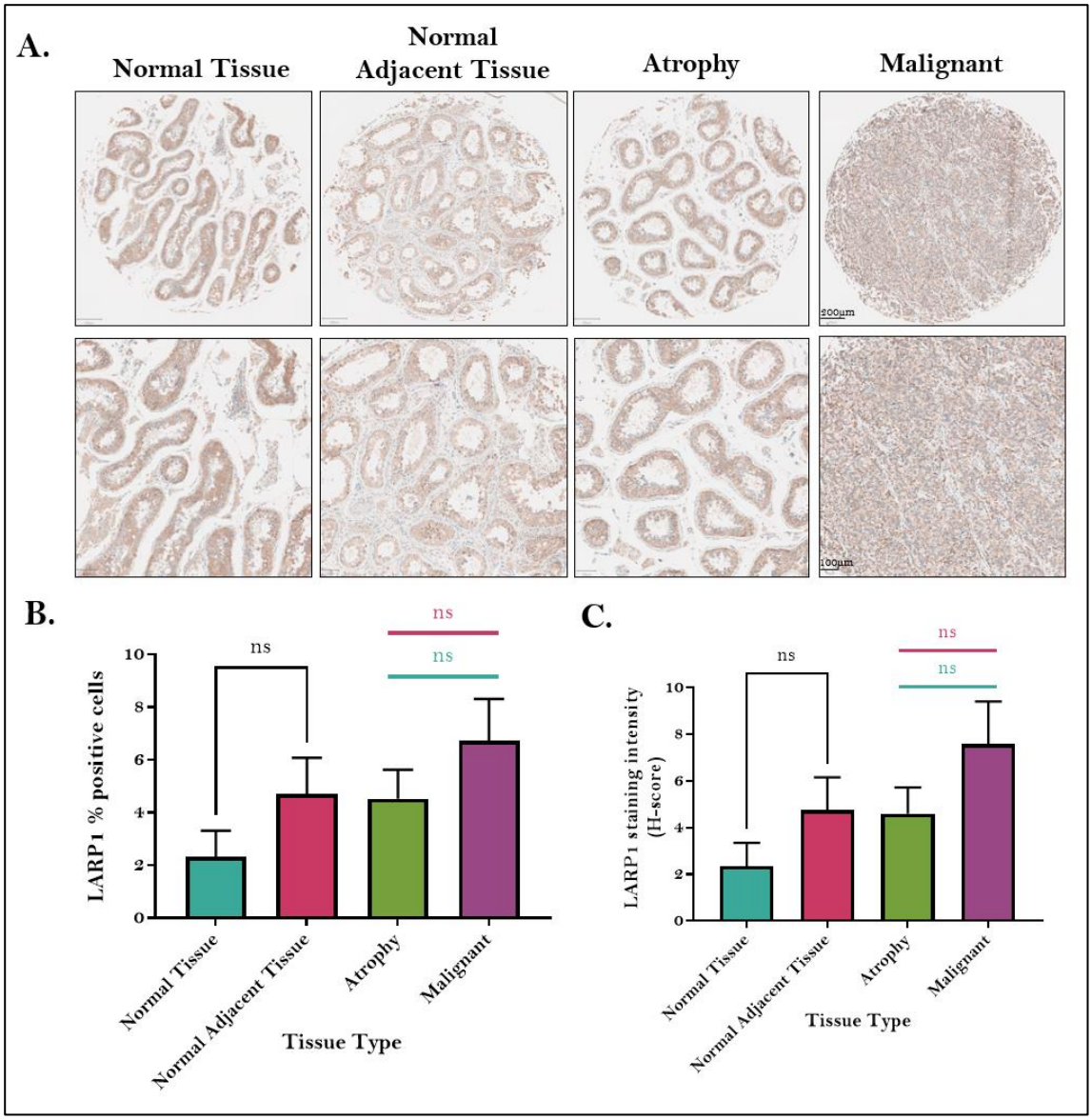

Figure 3.10: LARP1 protein expression was higher albeit not significant, in malignant testicular tissue compared to normal and normal adjacent tissue. A. *Representative images of FFPE testicular tissue cores were analysed for* ***B.*** *% of LARP1-positive cells and* ***C.*** *LARP1 staining intensity (H-score) using QuPath. Scale bar = 200µm and 100µm. Ns P Value= ≥0.05; green statistical analysis (ns) refers to comparison to normal tissue whilst red statistical analysis (ns) refers to comparison to normal adjacent tissue. Unpaired t-test was used for statistical analysis.*

We then analysed LARP1B and LARP1 protein expression in different TGCT subtypes compared to normal and normal adjacent tissue. We observed a similar pattern as before with significant reduction in the number of LARP1B-positive cells in TGCT tissues compared to normal and normal adjacent tissue (**Figure 3.11A. and B.**). The most significant reduction in LARP1B-positive cells was in teratoma which are characterised by their mixed population of cell and tissue types. Lower LARP1B expression in TGCT tissues may be due to the loss of distinct tubules which are rich in LARP1B-positive germ cells and loss of Leydig cells which stained strongest for LARP1B. Again, LARP1B staining intensity was significantly reduced in TGCT tissue (**Figure 3.11C.**).

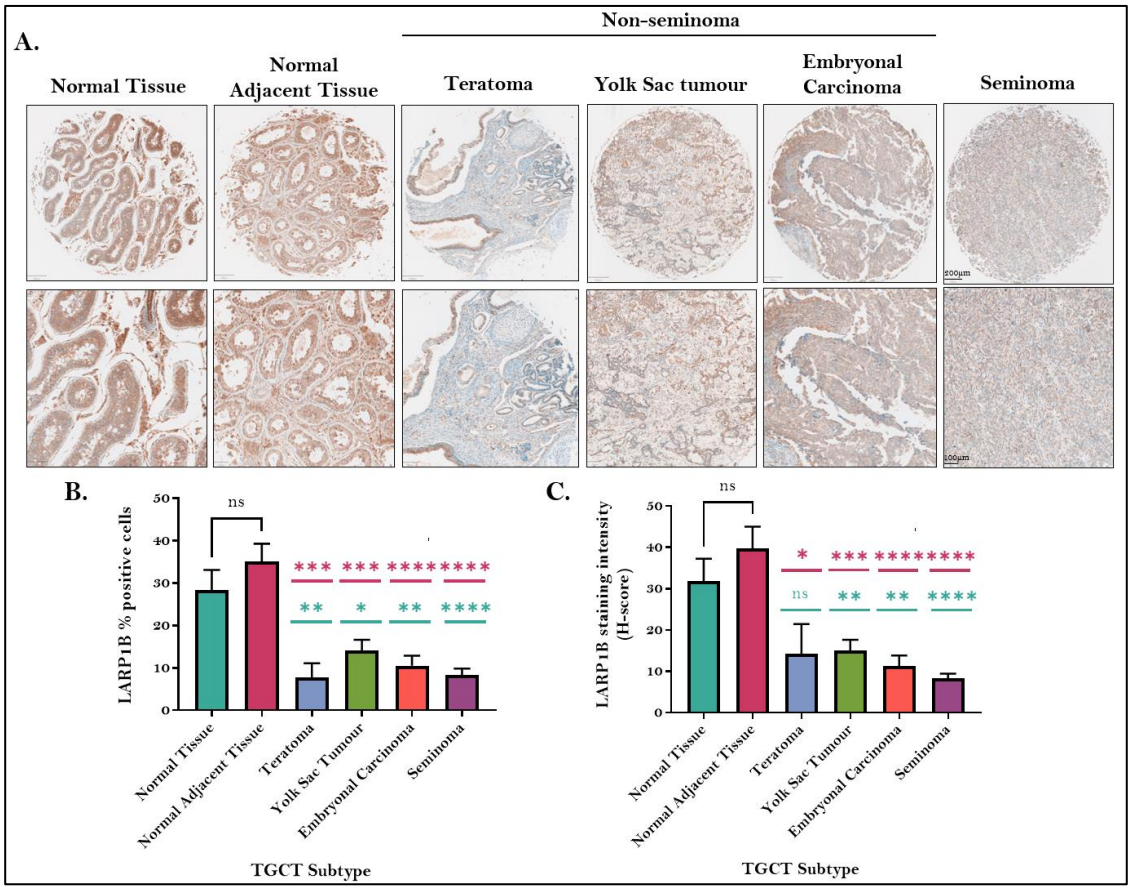

Figure 3.11: LARP1B protein expression was significantly reduced in TGCT subtypes compared to normal and normal adjacent tissue. A. *Representative images of FFPE testicular tissue cores were analysed for* ***B.*** *% of LARP1B-positive cells and* ***C.*** *LARP1B staining intensity (H-score) measured with QuPath. Scale bar = 200µm and 100µm. Ns P Value= ≥0.05, * P Value= ≤0.05, ** P Value= ≤0.01, *** P Value= ≤0.001, **** P Value= ≤0.0001; green Asterix (****) refer to statistical comparison to normal tissue whilst red Asterix (****) refer to statistical comparison to normal adjacent tissue. Unpaired t-test was used for statistical analysis.*

With regards to LARP1 protein, we observed a more varied expression pattern (**Figure 3.12**). Across the TGCT subtypes, LARP1 expression was comparable to normal tissue with the exception of embryonal carcinoma in which the number of LARP1-positive cells was higher than in normal testicular and normal adjacent tissue albeit not significant (**Figure 3.12B.**). Highest number of LARP1 positive cells and staining intensity was observed in embryonal carcinoma (**Figure 3.12C.**). Again, it is important to note the anatomical and morphological changes observed in TGCT tissues.

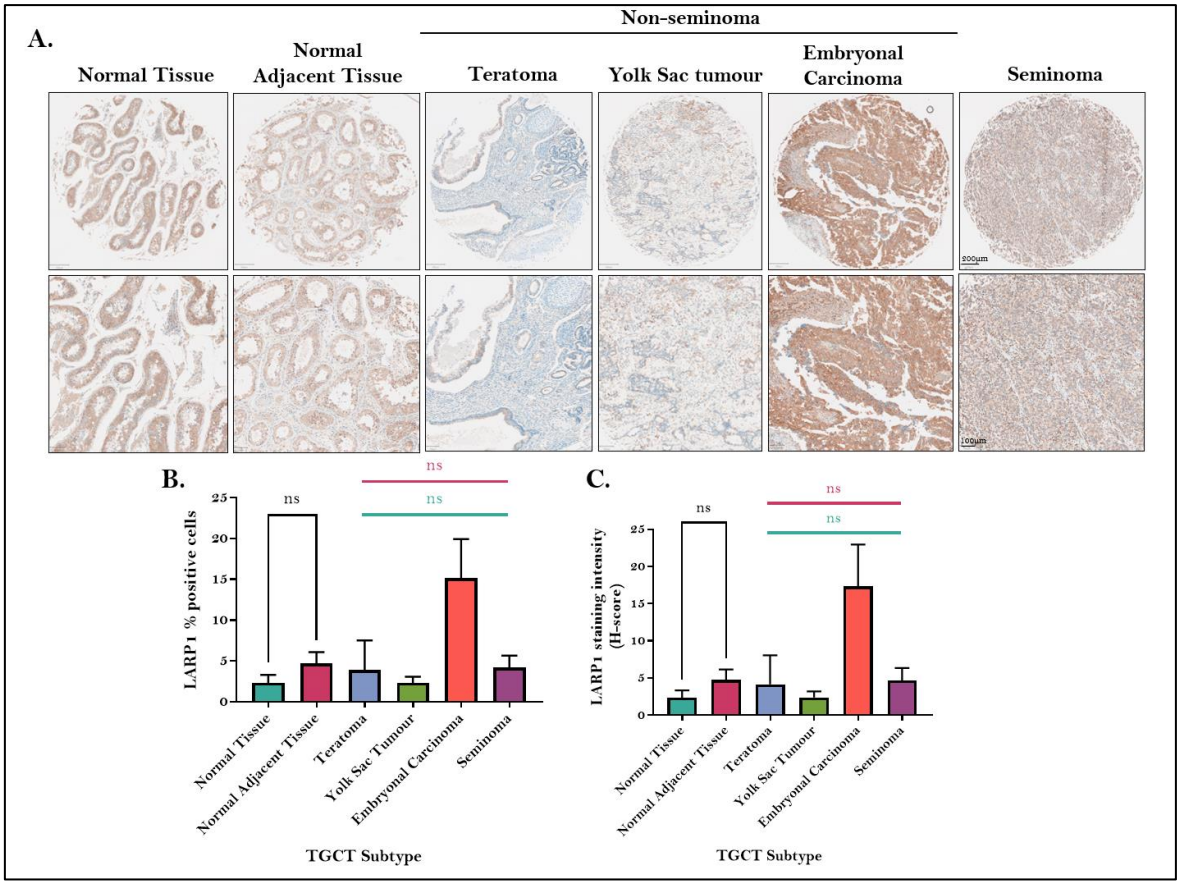

Figure 3.12: LARP1 protein expression varied across TGCT subtypes when compared to normal and normal adjacent tissue. A. *Representative images of FFPE testicular tissue cores were analysed for* ***B.*** *% of LARP1-positive cells and* ***C.*** *LARP1 staining intensity (H-score) using QuPath. Scale bar = 200µm and 100µm. Ns P Value= ≥0.05; green statistical analysis (ns) refers to comparison to normal tissue whilst red statistical analysis (ns) refers to comparison to normal adjacent tissue. Unpaired t-test was used for statistical analysis.*

3.3 Summary of findings

To begin understanding the functional and phenotypic role of LARP1B in cancer and its interplay with LARP1 we first performed *in-silico* analysis of publicly available databases for the expression of *LARP1B* and *LARP1* mRNA in normal and cancer tissues within the TCGA and GTEx cohorts. We found that in over 30% of the tissue types analysed, mRNA expression of *LARP1B* was reduced in tumour tissue compared to normal tissue (**Figure 3.1A.**). *LARP1* showed the same expression pattern as *LARP1B* in only 30% of the tissue types analysed (**Figure 3.1B.**) with the remaining tissue types exhibiting an increase in expression within tumour tissue. Of particular interest was the striking expression level of *LARP1B* mRNA in TGCT which is one of the tissue types in which *LARP1B* mRNA expression was significantly attenuated during tumour development (**Figure 3.2 and 3.3**). Reduced expression of LARP1B protein during TGCT development were also confirmed (**Figures 3.9 and 3.11**).

Given that LARP1B and LARP1 are paralogs sharing over 50% sequence homology and share the same mRNA expression pattern in 19/31 tissue types analysed, we investigated their co-expression. In the same 31 tissue types, there was a weak positive correlation between *LARP1B* and *LARP1* in both normal and tumour tissue (R=0.43; P =0.00001 and R=0.41; P =0.00001, respectively; **Figure 3.4**). We also observed that in testicular and TGCT tissue, *LARP1B* and *LARP1* presented with opposing gene-gene correlation patterns with a weak negative correlation in normal testicular tissue and a strong positive correlation in TGCT tissue (R=-0.24; P=0.0023 and R=0.62; P=8.9e-16 respectively; **Figure 3.5**).

To further understand the clinical relevance of LARP1B we investigated the correlation between *LARP1B* and *LARP1* mRNA expression and cancer patient survival outcome. Due to the lack of TGCT samples available for survival analysis in various cohorts, overall survival outcome was inconclusive. Investigation of all seven cancer types within the mRNA gene chip database of kmplot.com database revealed that in breast, lung, gastric, AML and myeloma cancers *LARP1B* expression correlated with a higher overall survival rate whilst in ovarian and colon cancers *LARP1B* expression correlated with a poor overall survival (**Figure 3.6A.**). Similarly, *LARP1* expression correlated with a higher overall survival rate in ovarian, gastric, colon and AML cancers whilst in breast cancer and myeloma *LARP1* expression correlated with a poor overall survival rate (**Figure 3.6B.**).

These findings demonstrate differences in the clinical relevance of *LARP1B* and *LARP1* amongst cancer types.

Due to the implicated association of LARP1B within the testicular tissue and TGCT, we adopted this as our primary research model to begin exploring its expression and function. Using a testicular-specific TMA composed of normal and abnormal testicular tissue due to atrophy or malignancy, we stained for LARP1B and LARP1 protein and again found contrasting expression profiles. Whilst LARP1B expression was higher in normal testicular tissue compared to TGCT tissue, LARP1 was higher in malignant testicular tissue compared to normal testicular tissue despite the profound morphological and anatomical alterations between the tissue types (**Figures 3.9 and 3.10**). It may be that the reduction in LARP1B expression between normal and disease tissue was attributed to the changes observed in TGCT tissue; specifically, the loss of LARP1B-rich Leydig cells and distinct seminiferous tubules which contained LARP1B-positive germ cells. For example, atrophic testicular tissue had anatomically normal seminiferous tubules and Leydig cells within the interstitial space and so LARP1B expression was comparable to normal tissue. In malignant TGCT tissue the loss of normal anatomy was accompanied with significantly reduced LARP1B expression and staining intensity (**Figure 3.11**). The same cannot be said for LARP1 which despite the anatomical changes stained stronger in TGCT tissue compared to normal tissues (**Figure 3.12**). This may be attributed to the increased abundance of germ cells which stained strongest with LARP1. Our TMA analysis supported our *in-silico* findings which demonstrated attenuated LARP1B expression with increased LARP1 expression during TGCT development.

Our findings also support those presented by the Human Protein Atlas (HPA; proteinatlas.org[226]) which demonstrate higher LARP1B protein expression in normal testicular tissue compared to TGCT tissue. Similar to our findings, they observed low to moderate LARP1B staining intensities in testicular cancer tissue within the cytoplasmic/membranous regions, compared to normal tissue. A clear difference between the datasets however is that in the HPA samples, LARP1B staining was localised to the spermatids and spermatocytes whilst we also observed LARP1B staining in all germ cells within the lumen, myoid cells and Leydig cells. The observed differences may be attributed to multiple factors including variances in the testicular tissue samples used for anti-LARP1B staining, different binding affinities of the antibodies employed and technical variations in the methods used for both staining and analysis.

4

RESULTS CHAPTER 2: INVESTIGATING THE LARP1B INTERACTOME AND SUBCELLULAR DISTRIBUTION

4.1 Introduction

A single RBP is capable of forming RNP complexes with a multitude of protein and RNA combinations. Depending on the RNPs formed, a number of biological processes and functions are executed to maintain cellular homeostasis. [7, 10] Although in the context of RBPs knowledge of the mRNAs they bind and regulate is of high importance, understanding the protein-protein interactions broadens our understanding of RBP functionality. We applied co-IP and mass spectrometry analysis to provide us with further functional insights into the functional role of LARP1B.

4.2 Results

4.2.1 LARP1B expression in TGCT cell lines

Our earlier *in-silico* findings outlined in the previous chapter revealed a heterogeneous expression pattern of *LARP1B* mRNA across different tissue and cancer types however, the most divergent result was of testicular germ cell tumours (TGCT) with a significant reduction in *LARP1B* mRNA expression in TGCT tissue compared to normal testicular tissue. We further substantiated these findings using a testicular-specific TMA in which LARP1B protein expression was significantly reduced in malignant testicular tissue compared to normal testicular tissue.

We therefore selected a panel of cisplatin sensitive and resistant TGCT cell lines including GCT27, GCT27CR and 2102EP cells for profiling of LARP1B protein expression by western blotting. GCT27 and 2102EP cell lines are cisplatin-sensitive whilst GCT27CR is cisplatin-resistant; all three are embryonal carcinoma (non-seminoma subtype) and *TP53* wildtype with no known *LARP1B* mutations. We also assessed LARP1B protein expression in HEK293T human embryonal kidney cells as a non-cancer model both wildtype and knockout for paralog LARP1 (generated in our laboratory by Dr James Chettle). As OVCAR8 ovarian cancer cell lines are our teams' primary research model for investigating the oncogenic function of LARP1, we also included these cell lines in our investigation.

As shown in **Figure 4.1**, expression of endogenous LARP1B and LARP1 protein was variable across the cell line panel. LARP1B expression was highest in HEK293T and

lowest in OVCAR8 cells. Interestingly, LARP1B expression was not visibly altered in HEK293T LARP1^{KO} cells compared to wildtype HEK293T; significance of these findings is discussed in later chapters. In TGCT cell lines, LARP1B expression was higher in GCT27 and GCT27CR cells compared to 2102EP cells. We also noted that LARP1B appeared at a higher molecular weight than expected at approximately 140kDa instead of 105kDa. This is not unusual as the expected vs observed molecular weight often differs, as is also the case for LARP1 (expected size is 130kDa but we observe bands at 150kDa). Further, our antibody may be detecting multiple isoforms or modified LARP1B proteins due to appearance of an additional band at approximately 135kDa.

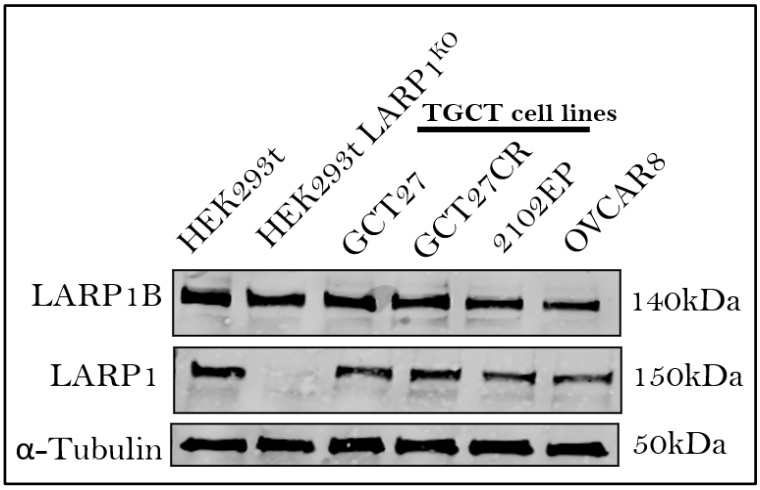

Figure 4.1: Endogenous LARP1B and LARP1 showed ubiquitous protein expression in a panel of cell lines. *Approximately 20µg of total protein was loaded/well.*

4.2.2 Investigating the LARP1B interactome in TGCT cell lines

We performed proteomic analysis using co-immunoprecipitation (co-IP) of endogenous LARP1B in GCT27 and GCT27CR cells followed by mass spectrometry (MS). co-IPs were performed as described in **Materials and Methods 2.2.11**, using anti-LARP1B to enrich for endogenous LARP1B and anti-IgG as a negative control. Successful pulldown was confirmed by western blotting (**Figure 4.2A.**). The LARP1B band at 140kDa is visibly faint due to applying only 10% of the sample for western blot analysis and retaining the rest for mass spectrometry (**Figure 4.2A, see** *). Silver staining of a protein gel ran in parallel showed the presence of bands that were not present in the IgG control IPs (**Figure 4.2B.**).

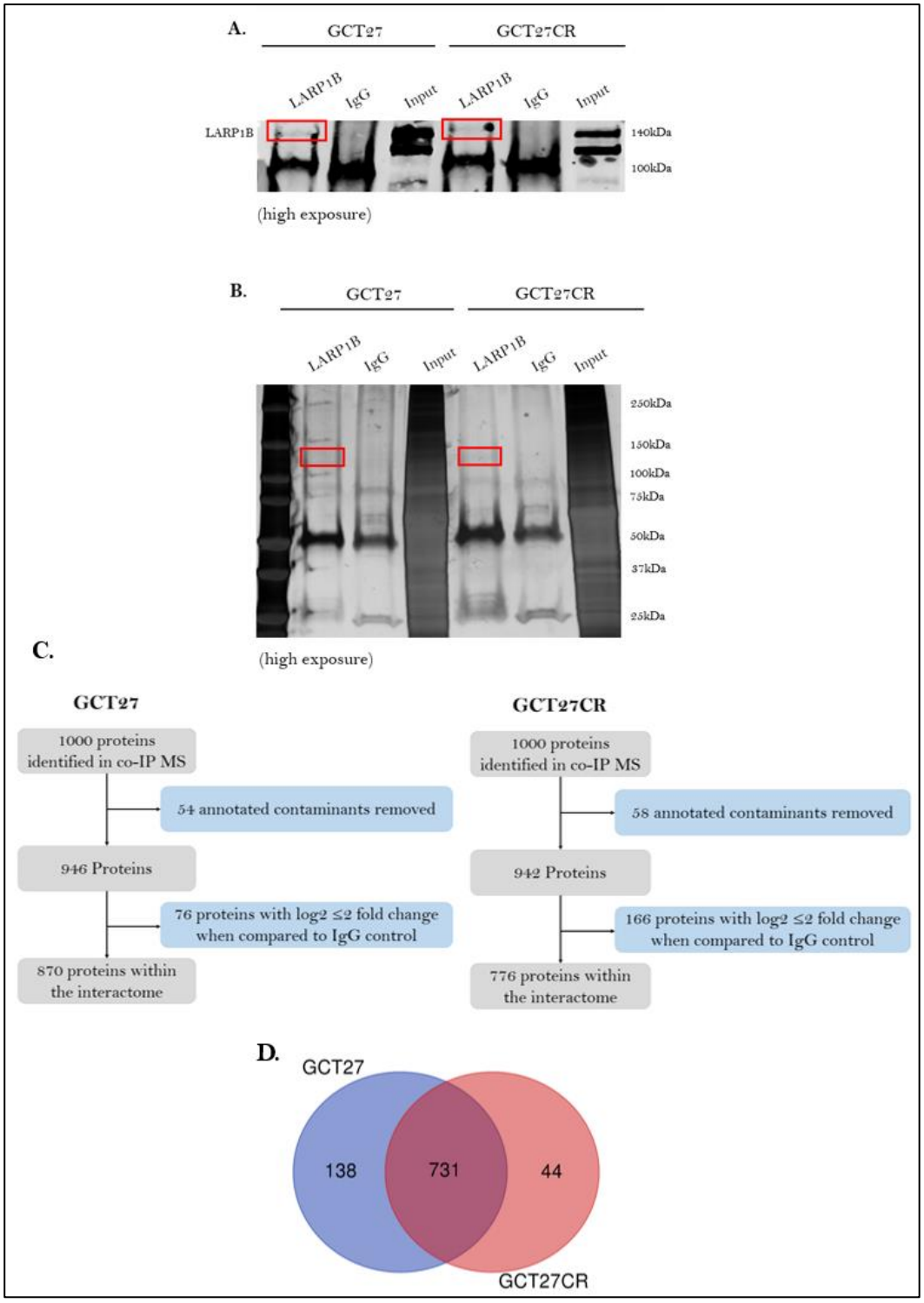

Figure 4.2: Co-immunoprecipitation and mass spectrometry revealed endogenous LARP1B protein interactors in TGCT cell lines. ***A.*** *Western blot shows detection of LARP1B in LARP1B-IP in GCT27 and GCT27CR cell lines.* ***B.*** *Silver stain of SDS-PAGE gel for LARP1B-IP products in GCT27 and GCT27CR cells.* ***C.*** *MS data analysis workflow for GCT27 and GCT27CR cells.* D. *Venn diagram analysis revealed an overlap of 731 LARP1B protein interactors shared between GCT27 and GCT27CR.*

The remaining immunoprecipitant was then processed for mass spectrometry analysis by column purification and digestion. Tandem mass spectrometry (MS/MS) analysis was then performed by Dr Robert Parker. From the results generated by MaxQuant we selected the intensity scores for each candidate which combines the number of peptides identified for each protein. We selected these datasets instead of label-free quantitative (LFQ) intensity scores which require multiple replicate readings and t-test statistics for accurate analysis, which we did not have.

Initial analysis of the protein interactome revealed 1000 candidates for each cell line from which up to 58 known contaminants, such as keratin and trypsin were removed. Missing values were imputed and the log2 ratio of LARP1B-IP to IgG-IP was calculated. Values which represented a ≥ 2-fold change in expression were selected, resulting in a total of 870 or 776 proteins within the LARP1B interactome for GCT27 and GCT27CR, respectively (**Figure 4.2C.**). We submitted the list of enriched proteins from GCT27 and GCT27CR cells into an online Venn diagram generator and found an overlap of 731 proteins between the cell lines whilst 138 proteins were present in GCT27 only and 44 proteins found in GCT27CR suggesting a high level of similarity within the LARP1B protein interactome of both cell lines (**Figure 4.2D.**).

4.2.3 LARP family members and canonical RBP-interacting proteins are amongst the LARP1B interactome

We first sought to detect LARP family members within the LARP1B interactome to uncover possible interactions between LARP1B and other LARP family members. As shown in **Table 4.1**, we identified LARP1, LARP1B and LARP7 in GCT27 cells with log2 fold change values of 32.84, 31.13 and 22.54, respectively. Similarly, we identified LARP1B and LARP1 in GCT27CR cells with log2 fold change values of 27.24 and 12.73, respectively.

LARP family members identified in the LARP1B interactome			
GCT27		**GCT27CR**	
Protein	**Log2 fold change**	**Protein**	**Log2 fold change**
LARP1	32.84	LARP1B	27.24
LARP1B	31.31	LARP1	12.73
LARP7	22.54		

Table 4.1: LARP1 and LARP7 were within the LARP1B interactome of TGCT cells

Amongst the LARPs, LARP1 and LARP4 have established interactions with cytoplasmic Poly(A) binding proteins, primarily PABPC1 via the PAM2 motif[227]. In fact, the LARP1-PABP interaction is one of the most established in the field of LARP1 research and is known to mediate LARP1 translation regulation[51, 52, 123]. We identified 3/6 possible isoforms that have been found in humans including cytoplasmic PABPC1 and PABPC4 and recently discovered nuclear PABPN1 (**Table 4.2**). In GCT27 cells, PABPC4 was most enriched with a log2 fold change of 31.81, in fact PABPC4 was the 9th most enriched protein in our LARP1B-IP (**supplementary materials Table 8.1**). PABPC1 exhibited a log2 fold change of 12.27 and PABPN1 with a log2 fold change of 8.76. A similar pattern was observed in GCT27CR cells with PABPC4 the 14th most enriched protein identified (**supplementary materials Table 8.2**) with a log2 fold change of 30.19. PABPN1 was the next most enriched isoform (27.52 log2 fold change) followed by PABPC1 (8.67 log2 fold change). Although we observed a slight difference in the levels of enrichment, in both cell lines LARP1B was found to interact with the same PABP isoforms.

PABP isoforms identified in the LARP1B interactome			
GCT27		**GCT27CR**	
Protein	**Log2 fold change**	**Protein**	**Log2 fold change**
PABPC4	31.81	PABPC4	30.19
PABPC1	12.27	PABPN1	27.52
PABPN1	8.76	PABPC1	8.67

Table 4.2: Various PABP isoforms including nuclear PABPN1 were amongst the LARP1B protein interactome.

4.2.4 LARP1B interacting partners are involved in novel biological processes

To unravel the functional association of the LARP1B interactome, gene ontology (GO) biological processes and molecular functional analysis in both TGCT cell lines was performed using The Gene Ontology Resource. Given that there was a large overlap of LARP1B protein interactors between the cell lines (**Figure 4.2D.**), it was not surprising to also find an overlap in biological processes and molecular functions. We selected the top 20 GO terms for both cell lines and combined them to generate a list of 27 biological processes of which 12 were shared, and 29 molecular functions of which 11 were shared between the cell lines (**Figure 4.3**). Amongst the top shared biological processes were cytoplasmic translation, peptide biosynthetic process, translation, peptide metabolic process and amide biosynthetic process (**Figure 4.3A.**). Macromolecule biosynthetic process, cellular biosynthetic process and regulation of protein stability were amongst the top 20 processes confined to GCT27 whilst mitochondrial translation and mitochondrial gene expression were confined to GCT27CR cells.

A similar level of overlap was observed in GO molecular function analysis with structural constituent of the ribosome, structural molecular activity, protein folding chaperone, ATP-dependent protein folding chaperone and unfolded protein binding being amongst the top 20 shared molecular functions (**Figure 4.3B.**). Ubiquitin protein ligase binding, organic acid binding and carboxylic acid binding were specific for GCT27 whilst unfolded protein binding, collagen binding and transporter activity were specific for GCT27CR cells. Overall, a number of novel and diverse biological processes and functions were annotated.

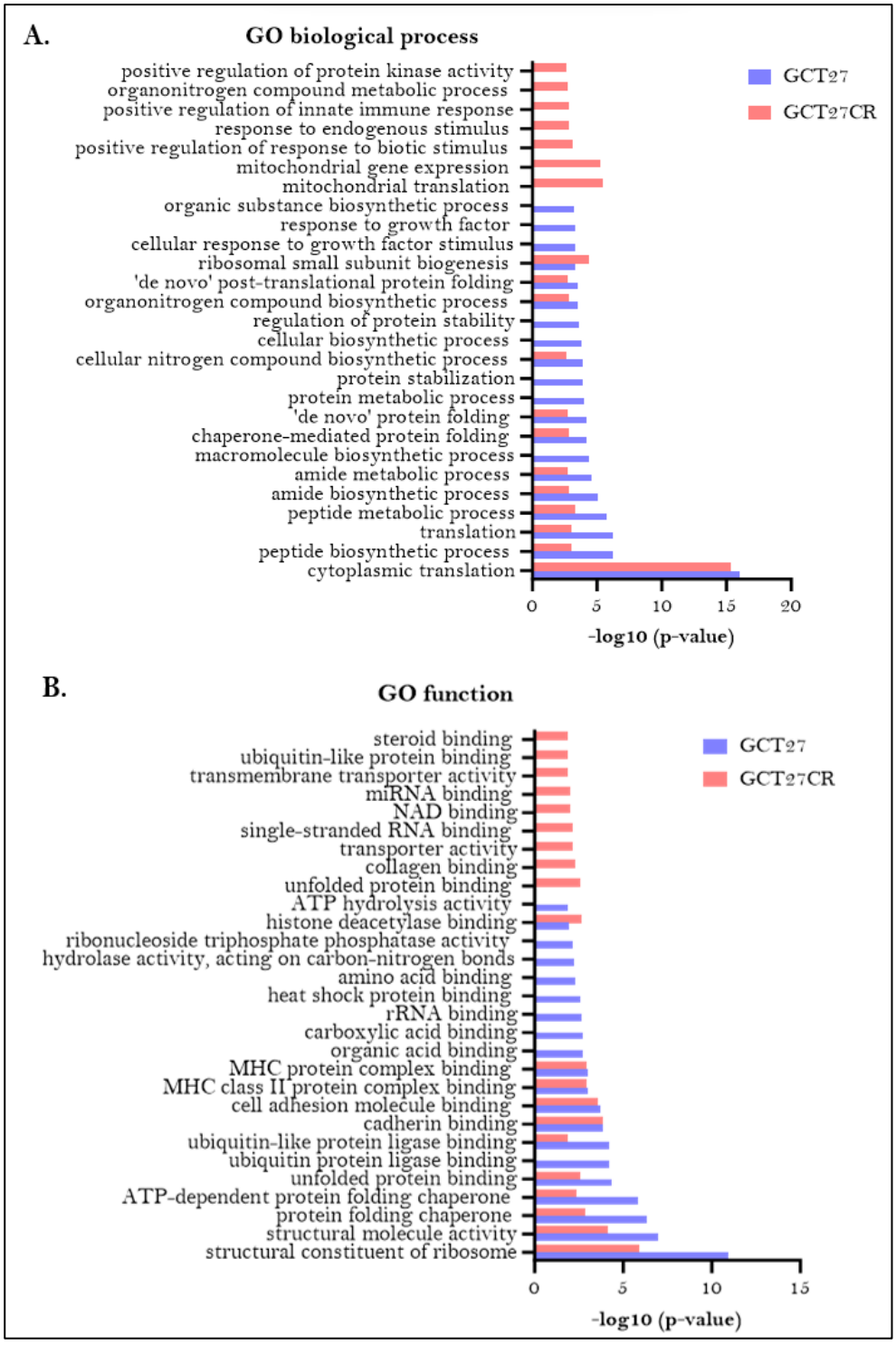

Figure 4.3: GO biological processes and molecular functional analysis for LARP1B-bound proteins in TGCT cell lines. A. *Top 20 GO annotated biological processes for GCT27 and GCT27CR were overlayed to reveal an overlap of 12 processes shared between the cell lines.* ***B.*** *Top 20 GO annotated molecular functions were overlayed to reveal an overlap of 11 functions shared between the cell lines.*

4.2.5 LARP1B protein interactors have diverse functions within the cell supporting cytoplasmic, nuclear, and mitochondrial functions of LARP1B

To further understand the functional role of LARP1B, we also performed GO subcellular component analysis of the LARP1B-IP interactors. Again, we found an overlap of 13 annotations between the top 20 GO terms between both cell lines including cytosolic ribosome, cell-substrate junction, focal adhesion, and cytosolic large and small ribosomal subunits (**Figure 4.4**). Subcellular components enriched in GCT27 included ribosome, polysome and the survival of motor neurons (SMN) complex whilst in GCT27CR mitochondrial ribosome components were present. These results suggest a potentially diverse functionality of LARP1B and interacting proteins.

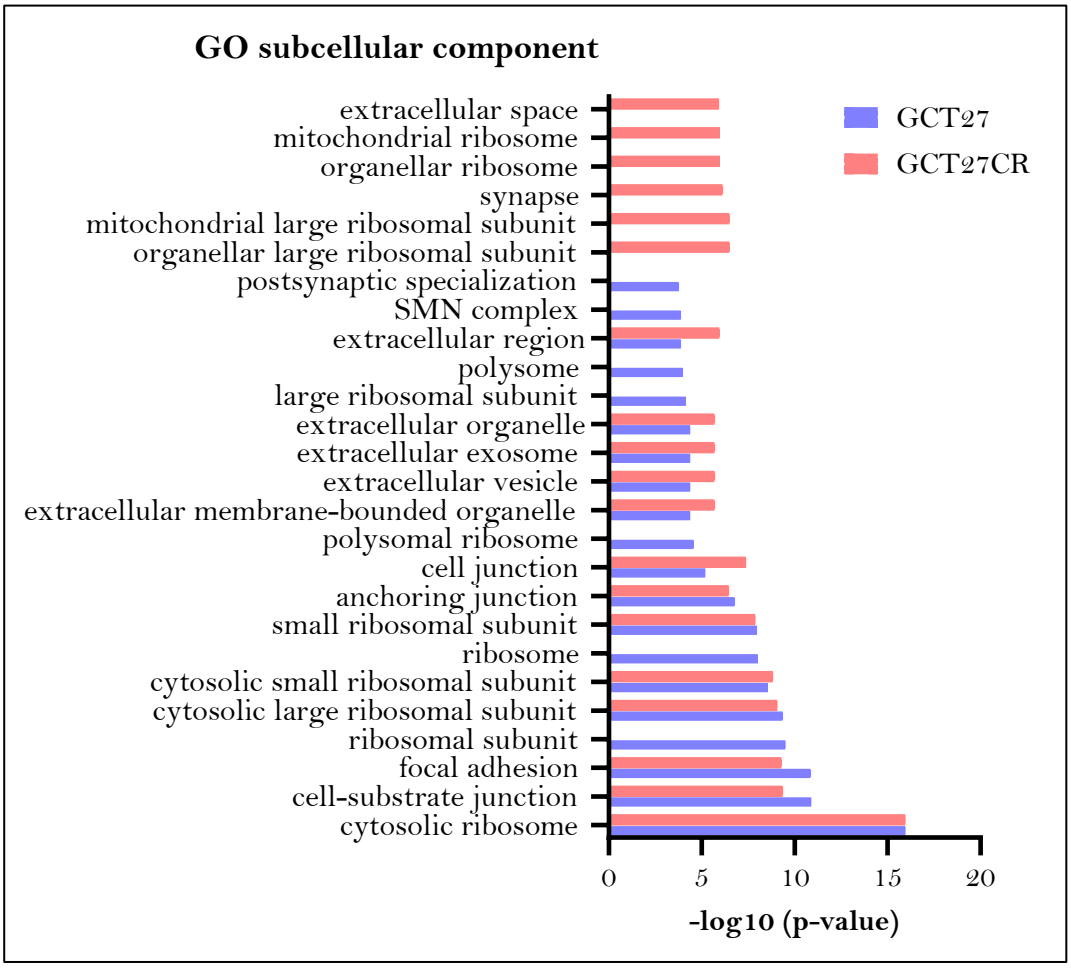

Figure 4.4: GO subcellular component analysis of LARP1B interactors reveal diverse localisation in GCT27 and GCT27CR cell lines, with predominant cytosolic ribosome localisation in both cell lines. *Top 20 GO subcellular components for GCT27 and GCT27CR were overlayed and revealed an overlap of 13 components shared between LARP1B interacting partners in both cell lines.*

Identification of nuclear PABP isoform, PABPN1 within the LARP1B interactome of both cell lines hinted at the ability of LARP1B in localising to the nucleus of mammalian cells. As such we decided to further explore our datasets for additional proteins which may corroborate these findings. It is known that the nuclear localisation of proteins involves identification of nuclear localisation sequences (NLSs) by members of the importin superfamily namely importin α and β subunits[228]. Similarly, nuclear export of proteins from the nucleus into the cytoplasm is executed by the exportin family of proteins the best characterised of which is CRM1/XPO1/exportin 1, which identify and bind to nuclear export sequences (NESs)[229]. We first started by searching for importin and exportin proteins within the LARP1B interactomes and identified various isoforms of both protein superfamilies (**Table 4.3**). It is important to note that these transportin proteins shuttle between the nucleus and cytoplasm and our interactome study does not confirm at which point this interaction is occurring.

Transportin proteins identified in the LARP1B interactome			
GCT27		**GCT27CR**	
Protein	**Log2 fold change**	**Protein**	**Log2 fold change**
Exportin-2 (CSE1L)	26.88	Exportin-2 (CSE1L)	23.33
Importin-5 (IPO5)	25.63	Importin-7 (IPO7)	21.1
Importin-7 (IPO7)	25.31	Exportin-T (XPOT)	21
Exportin-T (XPOT)	23.4	Importin-9 (IPO9)	21
Importin-9 (IPO9)	23.4	Exportin-5 (XPO5)	20.14
Importin-11 (IPO11)	23.4	Exportin-1 (XPO1)	6.75
Exportin-5 (XPO5)	22.26	Importin subunit alpha-1 (KPNA2)	5.86
Exportin-1 (XPO1)	9.5		
Importin subunit alpha-1 (KPNA2)	8.83		
Importin subunit beta-1 (KPNB1)	7.42		

Table 4.3: Multiple transportin protein isoforms were identified within the LARP1B interactome of TGCT cell lines. *We searched the LARP1B interactomes for transportin proteins and identified various importin and exportin isoforms in both TGCT cell lines, suggesting cytoplasmic and nuclear shuttling of LARP1B.*

We then decided to explore the LARP1B interactomes for specific nuclear proteins within our LARP1B-IP datasets which we also submitted into Metascape Gene Annotation and Analysis Resource, for subcellular localisation annotation of our enriched proteins. In total over 300 proteins were identified as localising to the nucleus or nuclear structures (**shown in supplementary materials Table 8.1 and 8.2**). To simplify our analysis for the purposes

of this chapter, we used "nuc" as a search term in our list to identify UniProt-annotated nuclear proteins enriched within the LARP1B interactomes of GCT27 and GCT27CR cells (**Table 4.4**). The complete list of proteins is outlined in **supplementary materials Table 8.1 and 8.2**. We identified a range of proteins including members of the heterogenous nuclear ribonucleoprotein family of RBPs, which are amongst the most abundantly expressed RBPs in mammalian cells. Again, it is important to note that not all of these proteins are exclusive to the nucleus but shuttle between the nucleus and cytoplasm. Nevertheless, the presence of these proteins within the LARP1B interactome strongly suggest nuclear functions of LARP1B.

Nuclear protein identified in the LARP1B interactome			
GCT27		**GCT27CR**	
Protein	**Log2 fold change**	**Protein**	**Log2 fold change**
HNRNPUL2	30.41	DDX21	31.31
HNRNPUL1	29.93	SNRNP200	30.83
ACIN1	29.71	HNRNPH3	30.47
DKC1	29.50	EFTUD2	30.14
SNRPA	29.49	HNRNPDL	29.99
NOP56	28.97	DKC1	29.78
HNRNPH2	28.8	HNRNPH1	29.69
NOP58	28.22	HNRNPF	28.86
SNRPF	28.22	RRP9	28.29
BPTF	28.14	SNRPE	28.09
SNRPC	27.86	GTPBP4	27.93
SNRNP40	27.68	HNRNPUL1	27.91
GTPBP4	27.62	SNRNP40	27.90
NUP210	27.19	BPTF	27.36
NCBP1	26.66	SNRPF	27.34
NUP93	26.21	NOP10	26.63
NOLC1	26.18	LYAR	26.33
NIFK	26.09	SNRPC	26.16
NUMA1	25.99	NOLC1	26.16
RRP9	25.87	NHP2	26.07
MRPL2	25.84	NOL6	25.95

GAR1	25.83	NUMA1	25.92
NOP10	25.80	NIFK	25.75
NHP2	25.79	GAR1	25.20
NUP205	25.62	UTP15	24.64
GNL3	25.48	ACIN1	24.56
NOL6	25.09	NCBP1	24.40
NUP160	24.77	NUP205	23.87
GNB2	24.18	NOL9	23.86
GNB1	24.09	NDE1	23.29
PRPF31	23.98	NOL11	23.21
UTP15	23.73	PRPF31	22.00
NDE1	23.56	NEMF	21.63
SNRPA1	22.78	SNRPA1	21.33
SNRPB2	22.70	SNRPB2	20.58
NUP188	22.02	NUP160	20.30
NOL11	21.90	NCOA5	11.64
NUP107	21.84	HNRNPA0	10.29
STRBP	21.76	HNRNPA3	10.28
NEMF	19.45	SYNCRIP	10.27
SYNCRIP	14.87	HNRNPD	10.27
SNRNP70	12.84	HNRNPL	10.15
EFTUD2	12.78	HNRNPAB	10.01
HNRNPR	12.22	HNRNPC	9.54
HNRNPF	11.52	HNRNPR	9.40
HNRNPA3	11.15	NOP56	8.94
SNRNP200	11.14	HNRNPA1;	8.46
HNRNPL	11.02	NOP58	8.27
HNRNPA0	10.90	HNRNPA2B1	7.86
HNRNPU	10.46	SNRPD1	7.62
HNRNPDL	10.08	SNRNP70	7.59
HNRNPC	9.86	HNRNPH2	7.20
HNRNPA2B1	9.58	SNRPD2	7.10
HNRNPD	9.58	HNRNPUL2	6.98

HNRNPAB	9.44	HNRNPK	6.73
DDX21	9.37	NCL	6.60
HNRNPH1	9.18	SNRPD3	6.53
HNRNPH3	9.16	HNRNPM	6.22
SNRPD3	9.08	SNRPN	6.19
SNRPD1	9.05	SNRPA	5.98
SNRPG	9.05	UTP18	5.95
SNRPN	8.83	NPM1	5.75
SNRPD2	8.71	RAN	4.68
HNRNPA1	8.65		
NRPE	8.46		
HNRNPK	8.05		
RAN	7.33		
LYAR	7.27		
NCL	7.05		
HNRNPM	6.85		
GNB2L1	6.70		
UTP18	3.98		
NPM1	3.75		

Table 4.4: The LARP1B interactomes were rich in nuclear proteins suggesting nuclear localisation and functions of LARP1B. *A simple search for nuclear proteins in the LARP1B interactomes returned a number of proteins which reside in the nucleus, strongly supporting the nuclear shuttling and/or localisation capacities of LARP1B.*

Further, our earlier GO analyses revealed numerous mitochondrial annotations including mitochondrial translation, mitochondrial gene expression and mitochondrial ribosome. Thus, we explored the LARP1B-IP datasets for mitochondrial proteins using "mitochondria" as a search term to identify UniProt-annotated mitochondrial proteins and cross-referenced this to our Metascape Gene list report which annotated proteins according to their subcellular localisation. As shown in **Table 4.5**, a number of mitochondrial ribosomal proteins were identified along with proteins involved in mitochondrial energy yielding pathways such as COX6C, COX5A and DLAT.

Mitochondrial proteins identified in the LARP1B interactome			
GCT27		**GCT27CR**	
Protein	**Log2 fold change**	**Protein**	**Log2 fold change**
DLAT	29.49	PGAM5	30.24
TOMM40	27.31	MRPL4	28.17
AIFM1	27.27	MRPL15	27.95
MRPL4	27.21	DLAT	27.69
C1QBP	26.86	MRPL39	27.57
VDAC3	26.56	MRPL44	27.23
COX6C	26.44	ATP5C1	27.02
ATP5L	26.17	MRPL49	26.92
SLC25A1	26.07	MRPL13	26.80
MRPL15	26.02	MRPL50	26.75
MT-CO2	25.88	MRPL21	26.75
CYC1	25.88	MRPL19	26.34
MRPL2	25.84	MRPL2	26.31
ATAD3A	25.68	MRPL43	26.27
MRPL49	25.56	MRPL22	26.26
AFG3L2	25.46	MRPL45	26.19
COX4I1	25.42	MRPL24	26.11
MRPL44	25.37	MRPL47	26.05
MRPL50	25.36	MRPL37	26.01
MTCH2	25.29	MRPL9	25.87
MRPL39	25.25	MRPL17	25.87
MRPL22	24.97	MRPL23	25.86
SLC2A1	24.87	ICT1	25.84
TOMM22	24.79	MRPL28	25.83
SLC1A5	24.73	SLC25A11	25.73
MRPL21	24.71	MRPL38	25.70
MRPL19	24.56	MRPL20	25.59
HADH	24.49	MRPL41	25.58
MRPL43	24.42	BRI3BP	25.52
MRPL13	24.31	AFG3L2	25.36

MRPL17	24.30	MRPL57	25.36
IDH3B	24.06	TOMM40	25.27
SLC25A4	24.05	ETFA	25.14
MRPL51	24.02	MRPS30	25.05
ICT1	23.93	MRPL51	24.91
NNT	23.82	MRPL52	24.66
MRPL23	23.82	MRPL12	24.41
HADHA	23.78	VDAC3	24.24
PYCR1	23.77	GADD45GIP1	24.07
SLC25A13	23.77	MCCC2	23.98
GRSF1	23.65	ATP5L	23.64
MCCC2	23.55	MTCH2	23.64
MRPL47	23.53	ATAD3A	23.49
PFKL	23.46	ATP5O	23.31
MRPL45	23.34	MRPS35	22.90
DHX30	23.28	CYC1	22.77
MRPL12	23.27	MRPS5	22.73
ALDH1B1	23.02	COX5A	22.48
MRPS35	22.94	DNAJA3	22.43
DNAJA3	22.92	REXO2	22.24
GADD45GIP1	22.88	MRPL40	22.20
MRPS5	22.76	HADHA	22.18
MRPL41	22.75	MRPS18A	22.11
MRPL38	22.74	GRSF1	22.05
ATAD3B	22.73	PFKL	21.93
MRPL20	22.17	SLC25A13	21.81
SDHA	22.14	NDUFA9	21.45
NDUFA9	22.06	HIGD1A	20.86
MRPL40	21.30	SLC25A1	20.46
MRPL30	21.26	DHX30	20.37
MRPL28	21.25	NGDN	20.30
MTX2	21.02	AIFM1	19.83
AK2	20.87	AIFM1	19.83

NGDN	20.82	ILF3	10.94
PTCD3	20.70	TUFM	6.42
OPA1	20.58	SLC25A5	5.52
ETFA	20.55	COX6C	5.39
ILF3	13.03	SLC25A6	5.27
PGAM5	10.85	VDAC2	5.07
SLC25A5	8.17	ATP5B	4.93
SLC25A11	8.16	PHB2	4.38
SLC25A3	7.73	SLC25A3	4.26
TUFM	7.44	ATP5A1	4.20
PHB2	7.04	MGST1	3.98
MGST1	6.91	PHB	3.12
ATP5C1	6.82	ATP5J2	2.82
ATP5J2	6.56		
LC25A6	6.41		
PHB	6.25		
ATP5A1	6.21		
VDAC2	6.20		
ATP5B	4.86		
COX5A	4.78		
ATP5O	4.26		
HSPD1	3.14		
HSPA9	3.12		
PRDX1	2.67		

Table 4.5: Mitochondrial ribosomal and respiratory chain-associated proteins were amongst the LARP1B interactomes in GCT27 and GCT27CR cells. *A simple search for mitochondrial proteins cross-referenced with our Metascape data list returned a number of mitochondrial proteins, the majority of which are mitochondrial ribosomal proteins mitochondrial respiratory chain-associated proteins in both cell lines.*

4.2.6 LARP1B localises to the cytoplasm and nucleus of TGCT and HEK293T cell lines

The diversity of the biological processes, functions and cellular distribution of LARP1B-bound proteins prompted us to explore the cellular localisation pattern of LARP1B and LARP1 in TGCT and HEK293T cell lines. We identified a number of transportin proteins bound to LARP1B including importin and exportin family members which are the primary complexes that enable intracellular movements between the cytoplasmic and nuclear regions[230, 231] (**Table 4.3**). We also performed *in-silico* analysis of LARP1B and LARP1 amino acid sequences to identify possible NLS and NES domains using various online prediction tools. These results identified putative NLS and NES domains further supporting the possibility that LARP1B is capable of nuclear-cytoplasmic shuttling and functions (**supplementary material Figures 8.6-8.11**).

To confirm the subcellular distribution patterns of LARP1B *in vitro*, we carried out subcellular fractionation of our cell lines to generate whole cell extracts (WCE), cytoplasmic (cyto) and nuclear (nuc) extracts followed by immunoblot analysis. Whole cell and cytoplasmic fractions were enriched in α-Tubulin whilst nuclear extracts were enriched in Lamin A/C. We detected LARP1B in whole cell, cytoplasmic and nuclear extracts in GCT27, GCT27CR and HEK293T cells (**Figure 4.5**). Further, LARP1B was enriched in nuclear extracts more than cytoplasmic fractions. LARP1 was detected in whole cell and cytoplasmic fractions as expected however a faint band referring to LARP1 was present in nuclear extracts also, albeit substantially less so than LARP1B.

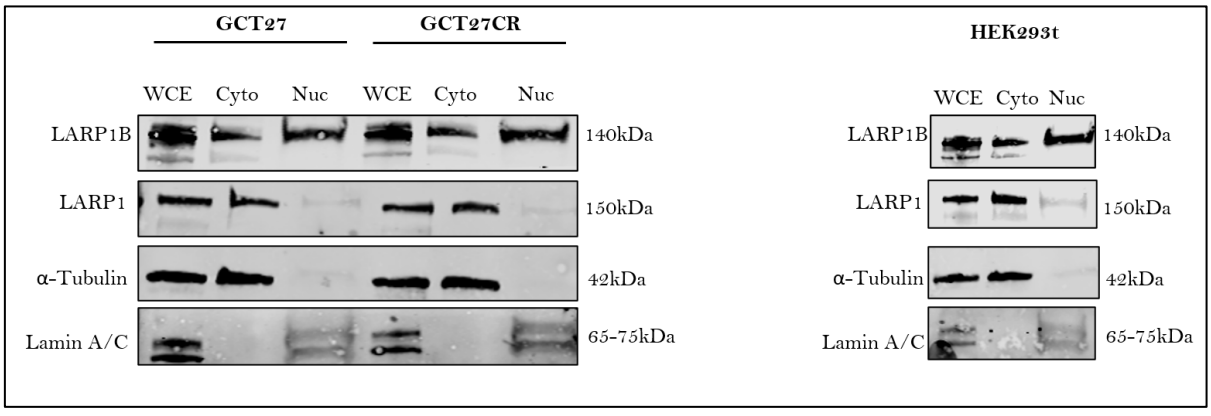

Figure 4.5: LARP1B localises to the cytoplasm and nucleus of TGCT and HEK293T cell lines whilst LARP1 resides primarily in the cytoplasm. *GCT27, GCT27CR and HEK293T cells were subjected to subcellular fractionation and immunoblotting to detect LARP1B*

and LARP1 protein localisation in these compartments. LARP1B was detected in whole cell (WCE), cytoplasmic (cyto) and nuclear (nuc) extracts whilst LARP1 resided primarily in the cytoplasm. Trace amounts of LARP1 protein were detected in nuc fractions.

We further carried out immunofluorescence (IF) analysis of our cell lines and observed a distinct overlap of LARP1B with DAPI nuclear stain (**Figure 4.6**) supporting our western blot findings which showed nuclear localisation of LARP1B. In fact, little cytoplasmic LARP1B was detected in our IF analysis. We also identified mostly in GCT27 and HEK293T cells, nuclear dots or speckles which may demonstrate LARP1B within nuclear granules however further confirmation with a specific nuclear speckle marker such as SC35 splicing factor[232], would be necessary to confirm this.

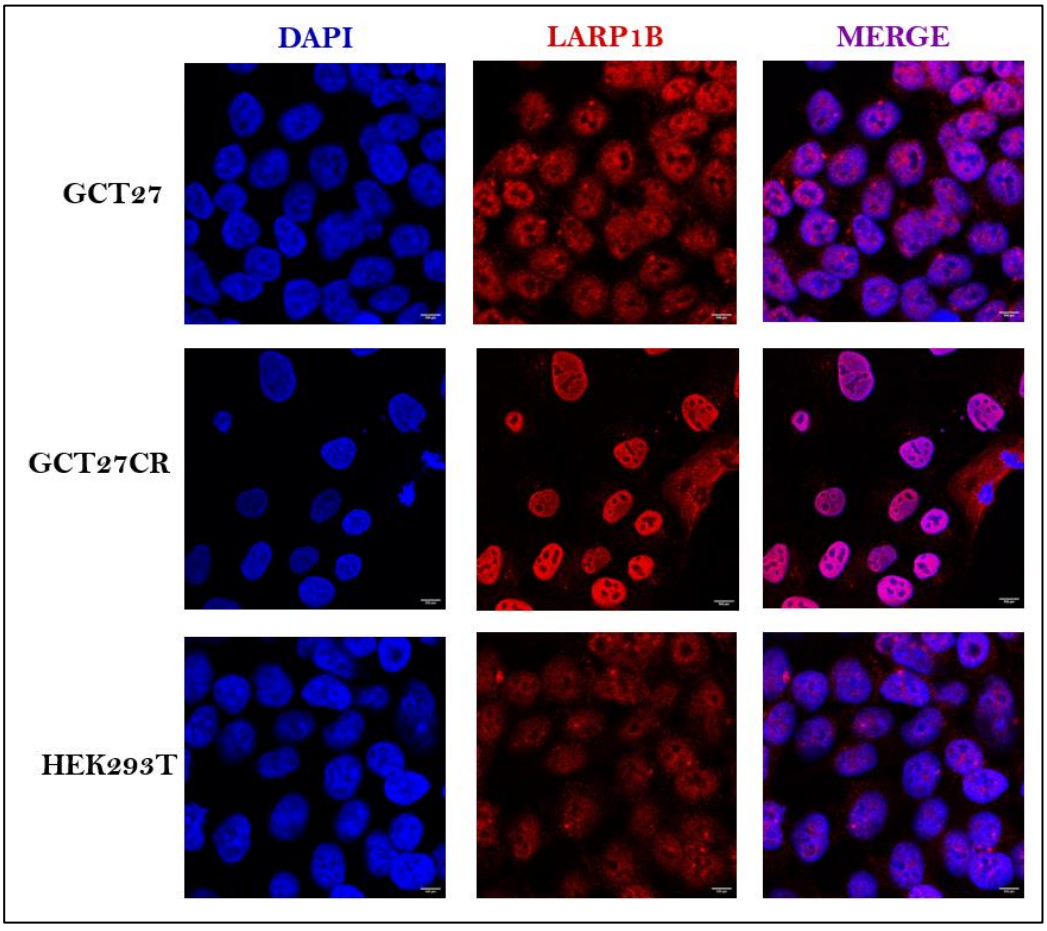

Figure 4.6: Immunofluorescence supports the predominant nuclear localisation pattern of LARP1B in TGCT and HEK293T cell lines. *TGCT and HEK293T cell lines were immuno-stained with anti-LARP1B antibody (red) and DAPI nuclear stain (blue) and*

visualised under the Zeiss LSM 710 confocal microscope. Images were processed using Fiji open-source image processing package. Scale bar = 500μm.

A number of LARP1B-bound candidates were annotated in our Metascape Gene List report as localising to the mitochondria and our search also revealed a number of mitochondrial ribosomal proteins and mitochondrial energetics associated candidates (**Table 4.5**). Thus, we interrogated whether LARP1B localises to the mitochondria by detecting the co-localisation of LARP1B with a mitochondrial protein, translocase of outer mitochondrial membrane 20 (TOMM20). Indeed, we identified co-localisation of LARP1B and TOMM20 in both TGCT cell lines as demonstrated by orange staining (**Figure 4.7**).

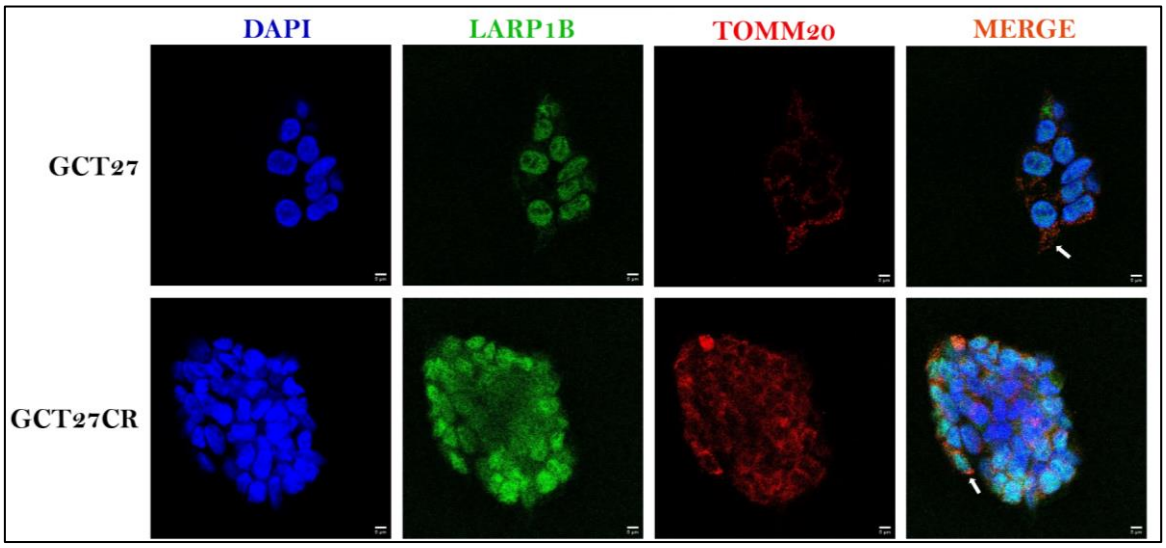

Figure 4.7: Co-localisation analysis of LARP1B and TOMM20 revealed LARP1B mitochondrial localisation in TGCT cell lines. *TGCT cell lines were immuno-stained with anti-LARP1B (green) and anti-TOMM20 (red) antibodies along with DAPI nuclear stain (blue) with merged signal producing an orange signal (clusters indicated by white arrow). Cells were visualised under the Zeiss LSM 710 confocal microscope and images were processed using Fiji open-source image processing package. Scale bar = 5μm.*

4.3 Summary of findings

To gain insight into the novel functionalities of LARP1B, we thought it imperative to explore the LARP1B protein interactome and the biological processes of the interactors. To achieve this, we performed co-IP followed by MS in GCT27 and GCT27CR cells. Our

MS analysis revealed over 700 proteins with a log2 fold change ≥2 in both cell lines. Gene ontology analyses of biological processes, function revealed enrichment of interacting partners in cytoplasmic translation, structural constituent of the ribosome and cytosolic ribosome respectively (**Figure 4.3**). GO subcellular component and Metascape Annotation analysis revealed distribution of LARP1B-bound proteins (**Figure 4.4**) to cytoplasmic, mitochondrial, and nuclear regions (amongst others highlighted in **supplementary materials table 8.1 and 8.2**).

With regards to LARP1B protein interactions with its siblings, we identified LARP1B, LARP1 and LARP7 in GCT27 cells whilst in GCT27CR we identified LARP1B and LARP1 suggesting some difference in LARP1B family interactions in different cell lines (**Table 4.1**). Interestingly, we also identified various members of the PABP family of proteins namely PABPC1, PABPC4 and PABPN1 (**Table 4.2**); cytoplasmic isoforms were expected due to the knowledge that other LARP family members including LARP1 also bind to these proteins however identification of PABPN1 was a novel finding. This further supports the possible nuclear-cytoplasmic shuttling of LARP1B. Building on this, we also explored our interactome datasets for transportin proteins that may aid in the nuclear-cytoplasmic movements of LARP1B and identified a range of importin and exportin isoforms including the best characterised importin-α and exportin 1(**Table 4.3**).

To gain some insight into the nuclear functions of LARP1B, we utilised Metascape annotations and "nuc" as a search term to identify enriched nuclear proteins within the LARP1B interactomes. Over 300 nuclear proteins in each cell line were identified accounting for over 1/3 of the total number of LARP1B-bound proteins involved in diverse nuclear functions. We also searched for mitochondrial proteins and identified up to 87 mitochondrial proteins in both cell lines cells. To further determine the cellular localisation pattern of LARP1B, we performed subcellular fractionation and western blot analysis of whole cell, cytoplasmic and nuclear extracts of TGCT and HEK293T cell lines and found strong cytoplasmic and nuclear localisation of LARP1B (**Figure 4.5**). This was in contrast to the predominantly cytoplasmic localisation of LARP1, with minimal nuclear localisation. Co-localisation analysis by IF revealed nuclear and mitochondrial LARP1B with distinct overlap of LARP1B staining with nuclear DAPI and clustered overlap with mitochondrial marker TOMM20 stain (**Figures 4.6 and 4.7**).

5

RESULTS CHAPTER 3: INVESTIGATING THE IMPACT OF LARP1B KNOCKDOWN ON TESTICULAR GERM CELL TUMOUR (TGCT) CELL LINE FITNESS AND METABOLISM

5.1 Introduction

LARP1B is part of the LARP family of established RNA binding proteins (RBPs) capable of regulating various stages of the mRNA life cycle[37]. LARP1 is an oncoprotein driving a number of key hallmarks of cancer including but not limited to sustained proliferative signalling, resisting cell death, and activating invasion and metastasis[44, 46, 51]. More recently, data generated within our lab outlined a key role of LARP1 in regulating metabolic plasticity. Upon LARP1 siRNA-mediated knockdown, a significant reduction in basal OCR was observed along with a significant reduction in ECAR suggesting that glycolysis was unable to compensate for the reduction in aerobic respiration induced by LARP1 depletion.[233]

TGCTs are uniquely rare accounting for only 1-2% of all male cancers[234] but have a high response rate and sensitivity to conventional surgical resection, radiotherapy and chemotherapy[201]. Still, approximately 15% of patients with TGCTs are insensitive to chemotherapy and develop recurrent aggressive disease with poor prognosis[235]. Interestingly, an analysis of differential gene expression in cisplatin resistant and sensitive TGCT cell lines identified *LARP1B* mRNA (NM_033229, isoform 3) as significantly upregulated in two cisplatin resistant TGCT cell lines (1411HP and 1777Nrpmet) compared to cisplatin sensitive TGCT cells (H12.1), with fold change values of 2.5 and 2.7, respectively[236]. Although the identified isoform of *LARP1B* is not the primary isoform annotated on NCBI (NM_018078, isoform 1) they share 100% percentage identity and 91% query cover when compared by BLAST nucleotide analysis. To our knowledge, this is the only study identifying differential expression of *LARP1B* gene expression in TGCT cell lines.

With evidence of LARP1B expression changes in TGCT tissue, we decided to explore LARP1B loss of function and gain of function phenotypes using shRNA and expression constructs in TGCT cell lines. Specifically, we aimed to determine whether LARP1B regulated cell viability, proliferation, apoptosis, and metabolism (phenotypes that are associated with LARP1) and whether these phenotypes could be reversed by exogenous LARP1B re-expression. Where applicable, we used HEK293T cells as a comparative cell line to validate our experiments.

5.2 Results

5.2.1 LARP1B knockdown induced morphological changes in TGCT cell lines

To investigate the phenotypic and functional role of LARP1B we first depleted LARP1B expression. To achieve this, we optimised LARP1B knockdown conditions in GCT27 and GCT27CR with different LARP1B shRNA concentrations, transfection reagents and timepoints (data not shown). We proceeded with a combination of two shRNA constructs targeting the 3'UTR and CDS of *LARP1B* henceforth referred to as "sh_LARP1B" alongside a control empty shRNA termed "sh_ctrl" for 24-72 hours. Changes in mRNA and protein expression of LARP1B following LARP1B knockdown for 24-72 hours are shown in **Figure 5.1**.

Partial gene knockdown was observed in both cell lines from 24 hours reaching approximately 50% expression after 48 hours. At the protein level, we observed a negligible reduction in LARP1B protein levels at all timepoints suggesting a high level of protein stability. Based on these observations, we decided to continue with a minimum of 48 hours LARP1B knockdown.

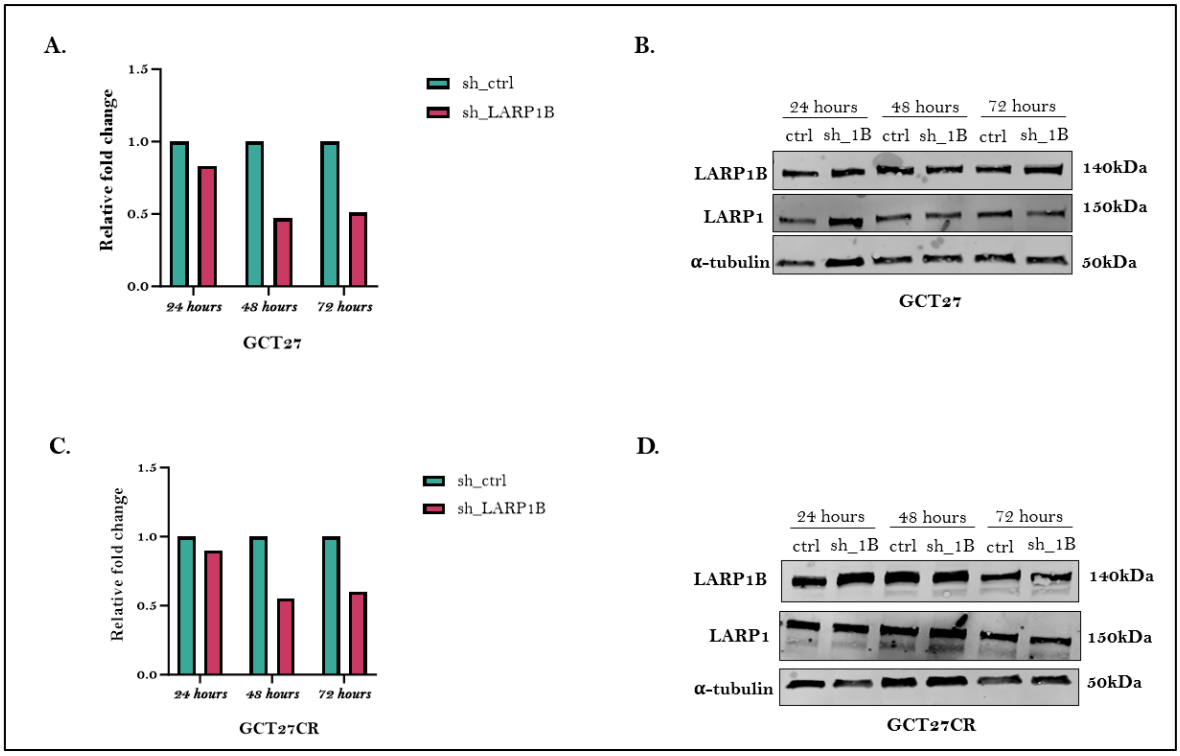

Figure 5.1: shRNA mediated LARP1B knockdown was apparent at the gene level but not at the protein level in TGCT cell lines. A. - B. *GCT27 and* ***C. – D.*** *GCT27CR wells were transfected with a combination of shRNA targeting LARP1B (sh_1B) or an empty shRNA (ctrl) for 24-72 hours and subjected to qPCR (left) and western blot analysis (right). Results revealed a visible reduction in LARP1B gene expression but no appreciable effect on LARP1B protein levels.*

Due to the lack of a phenotype associated with LARP1B, we also examined cell morphology following LARP1B depletion in TGCT cells. To do this, cells were transfected with sh_ctrl or sh_LARP1B for 24-72 hours and analysed using the Nexcelom Celigo Image Cytometer to visualise cells real time and generate brightfield images. At just 24 hours, sh_ctrl did not seem to impact cell morphology in either cell line whilst sh_LARP1B induced cell rounding and lifting. These phenotypes were present in later timepoints also, but to a further extent with visibly more round cells in suspension following sh_LARP1B transfection compared to sh_ctrl (**Figure 5.2 and Figure 5.3**). These features are characteristic of disrupted cell fitness, particularly apoptosis activation.

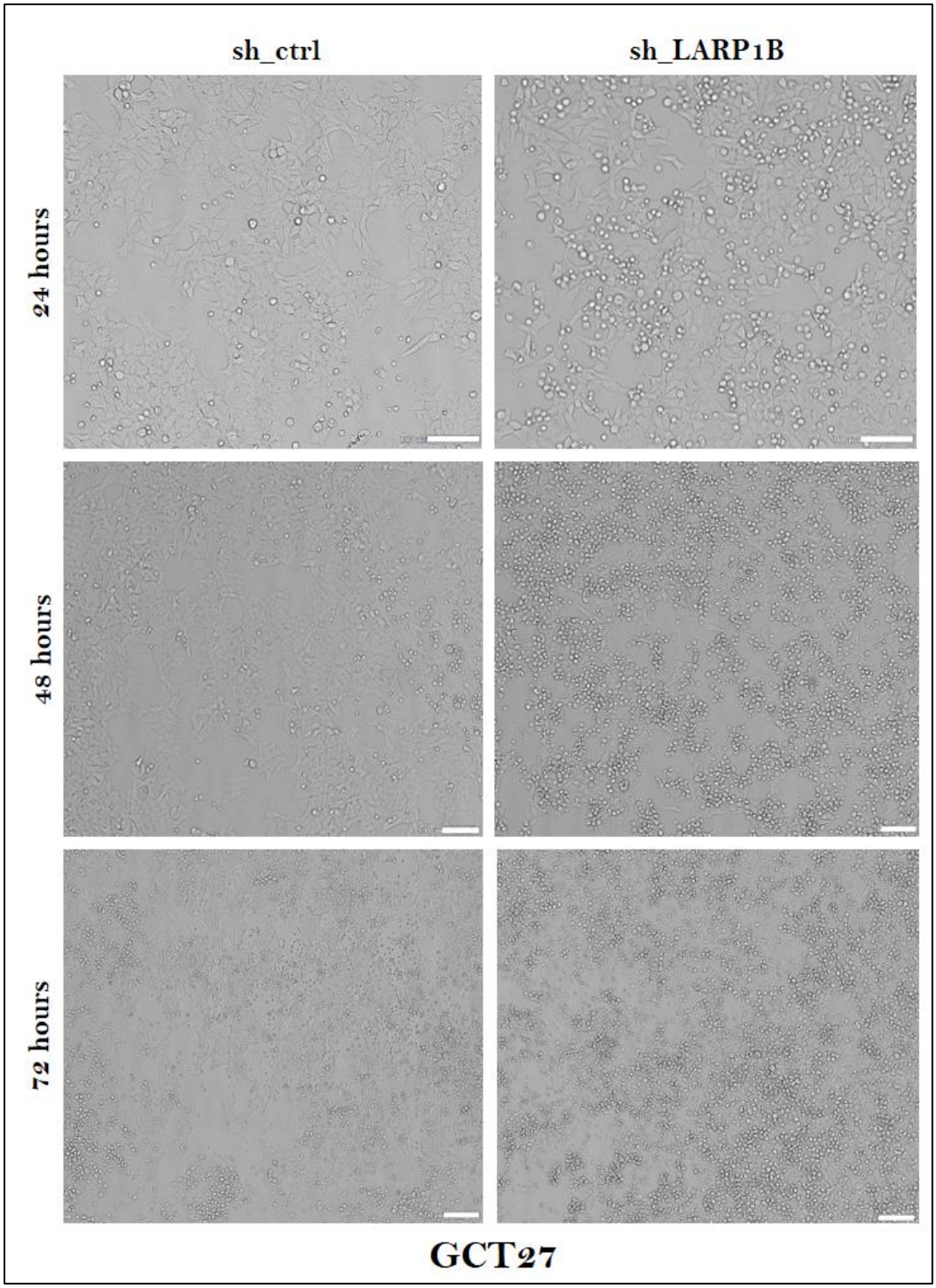

Figure 5.2: LARP1B depletion induced cell rounding and lifting over a course of 72 hours in GCT27 cells. *GCT27 cells were transfected with sh_ctrl or sh_LARP1B for 24-72 hours and assessed for morphological changes at 24 hours timepoints using the Nexcelom Celigo Image Cytometer. sh_LARP1B visibly altered normal cell morphology by causing cell rounding and lifting. Scale bar = 100µm*

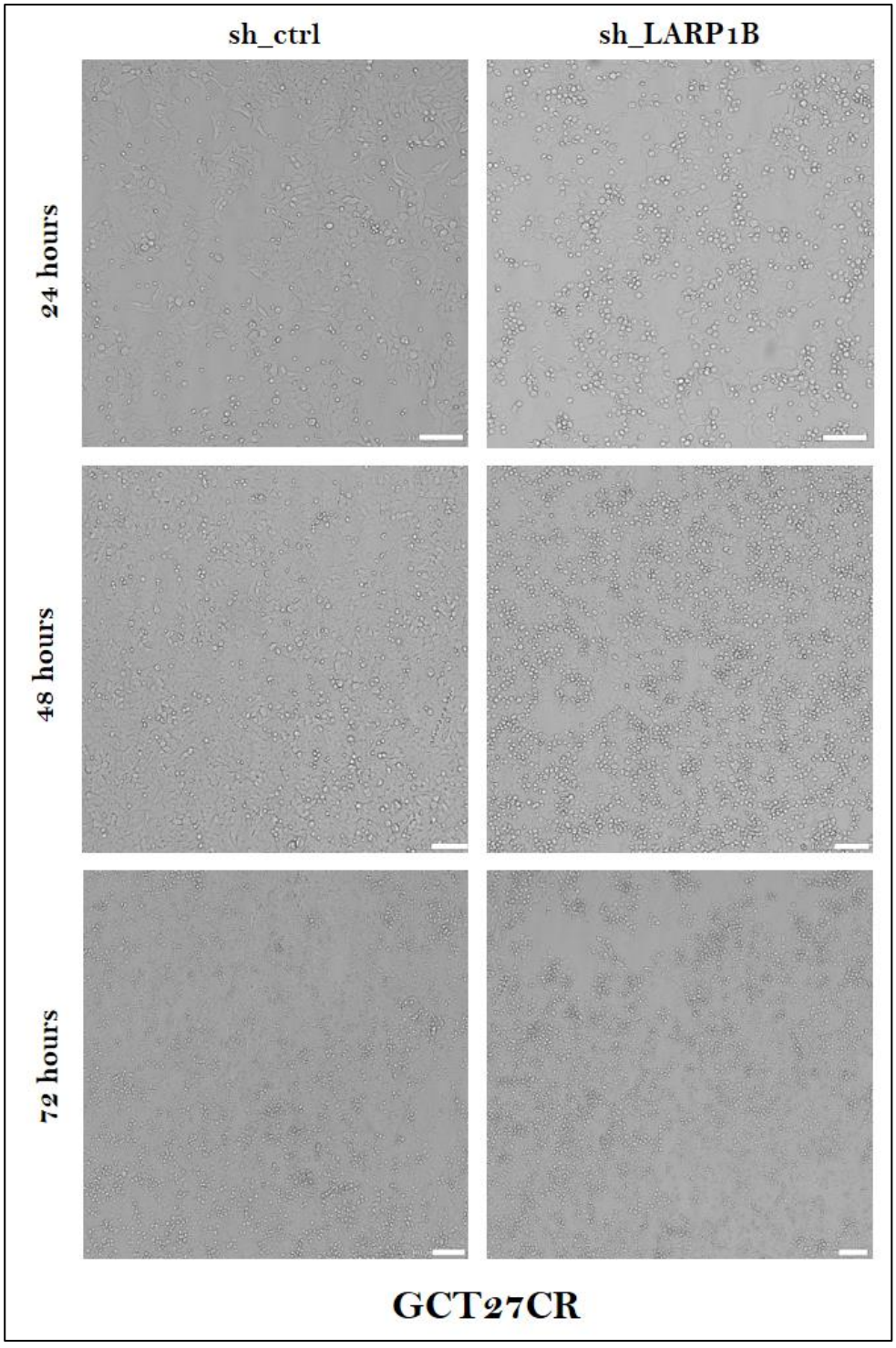

Figure 5.3: LARP1B depletion induced cell rounding and lifting over a course of 72 hours in GCT27CR cells. *GCT27CR cells were transfected with sh_ctrl or sh_LARP1B for 24-72 hours and assessed for morphological changes at 24 hours timepoints using the Nexcelom Celigo Image Cytometer. Sh_LARP1B visibly altered normal cell morphology by causing cell rounding and lifting. Scale bar = 100µm.*

5.2.2 LARP1B knockdown phenotype was not due to subsequent reduction in LARP1 expression

As we observed cell rounding and lifting following LARP1B knockdown, we wanted to observe effects on LARP1 expression to determine whether the exhibited characteristics were due to a reduction in LARP1 expression also. We performed LARP1B knockdown in GCT27 and GCT27CR cells and observed LARP1B knockdown at the mRNA level (Figure 5.5A. and C.) but also modestly at the protein level in both cell lines (Figure 5.5B. and D.). LARP1B depletion was accompanied by a slight increase in LARP1 mRNA expression (**Figure 5.5A and C, right panel**). No impact was observed on LARP1 protein levels.

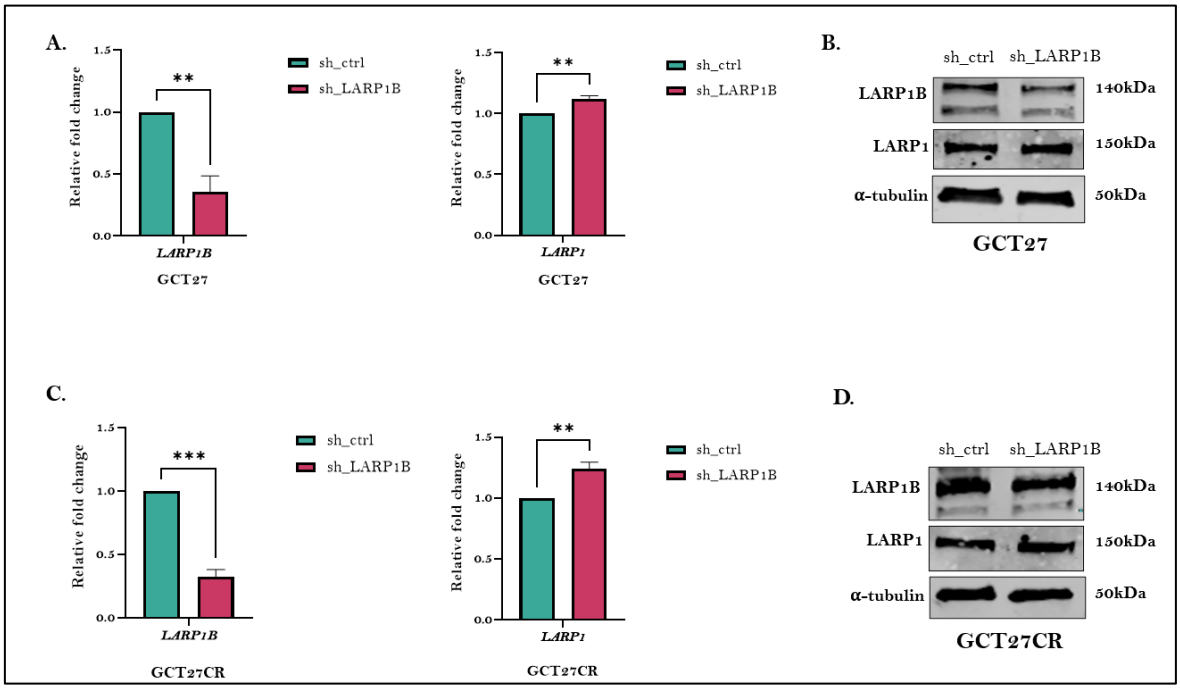

Figure 5.4: LARP1B knockdown in TGCT cell lines caused a small but significant increase in LARP1 mRNA expression. *GCT27 (A. and B.) and GCT27CR (C. and D.) cells were transfected with sh_ctrl or sh_LARP1B for 48 hours and subjected to qPCR and western blotting.* ***A.*** *sh_LARP1B significantly reduced LARP1B mRNA expression resulting in a significant increase in LARP1 mRNA expression in GCT27 cells.* ***B.*** *Parallel western blotting demonstrated minimal reduction of LARP1B following knockdown and no effect on LARP1 protein.* ***C.*** *sh_LARP1B significantly reduced LARP1B mRNA expression resulting in a significant increase in LARP1 mRNA levels in GCT27CR cells.* ***D.*** *Parallel western blotting demonstrated minimal reduction of LARP1B following knockdown and no effect on LARP1 protein. Western blot shown is a representative image of biological replicates. Error bars represent*

*the standard error of mean across biological triplicates. ** P Value= ≤0.01, *** P Value= ≤0.001. Unpaired student t-test was performed for statistical analysis.*

5.2.3 LARP1B knockdown significantly reduced TGCT cell proliferation

To measure the impact of LARP1B loss of function on cell proliferation, we utilised the xCELLigence RTCA system which detects, and measures cell number, morphology, adhesion, and viability as electronic readings referred to as cell impedance. Impedance is plotted as cell index (CI) which directly correlates to the number of cells attaching to the electrodes the plate surface and so is a readout for cell viability and proliferation. A simplified depiction of a CI plot is shown in **Methods 2.2.14 Figure 2.1**, with annotated phases of a cell growth curve.

As shown in **Figure 5.5A**, LARP1B knockdown significantly reduced the mean CI by 60% and thus proliferative rate and viability of GCT27 cells when compared to sh_ctrl. In GCT27CR cells (**Figure 5.5B.**), we observed a 37% reduction in mean CI with sh_LARP1B compared to sh_ctrl. With sh_LARP1B, both cell lines followed the same growth pattern as sh_ctrl at a visibly slower rate as shown in the growth curve. In LARP1B-depleted GCT27 cells we observed a slow growth rate over the 48 hours time course whilst in GCT27CR cells, we observed an exponential rate of cell adhesion and growth up to 24 hours, plateau from 24-26 hours and a slight reduction in CI by 48 hours. Although a decline phase after approximately 12 hours was observed with sh_ctrl in GCT27CR cells, we suspect this is due to the generally faster proliferation rate of these cells compared to GCT27, reaching over confluency as also observed in our optimisation study (**Methods 2.2.14 Figure 2.2**).

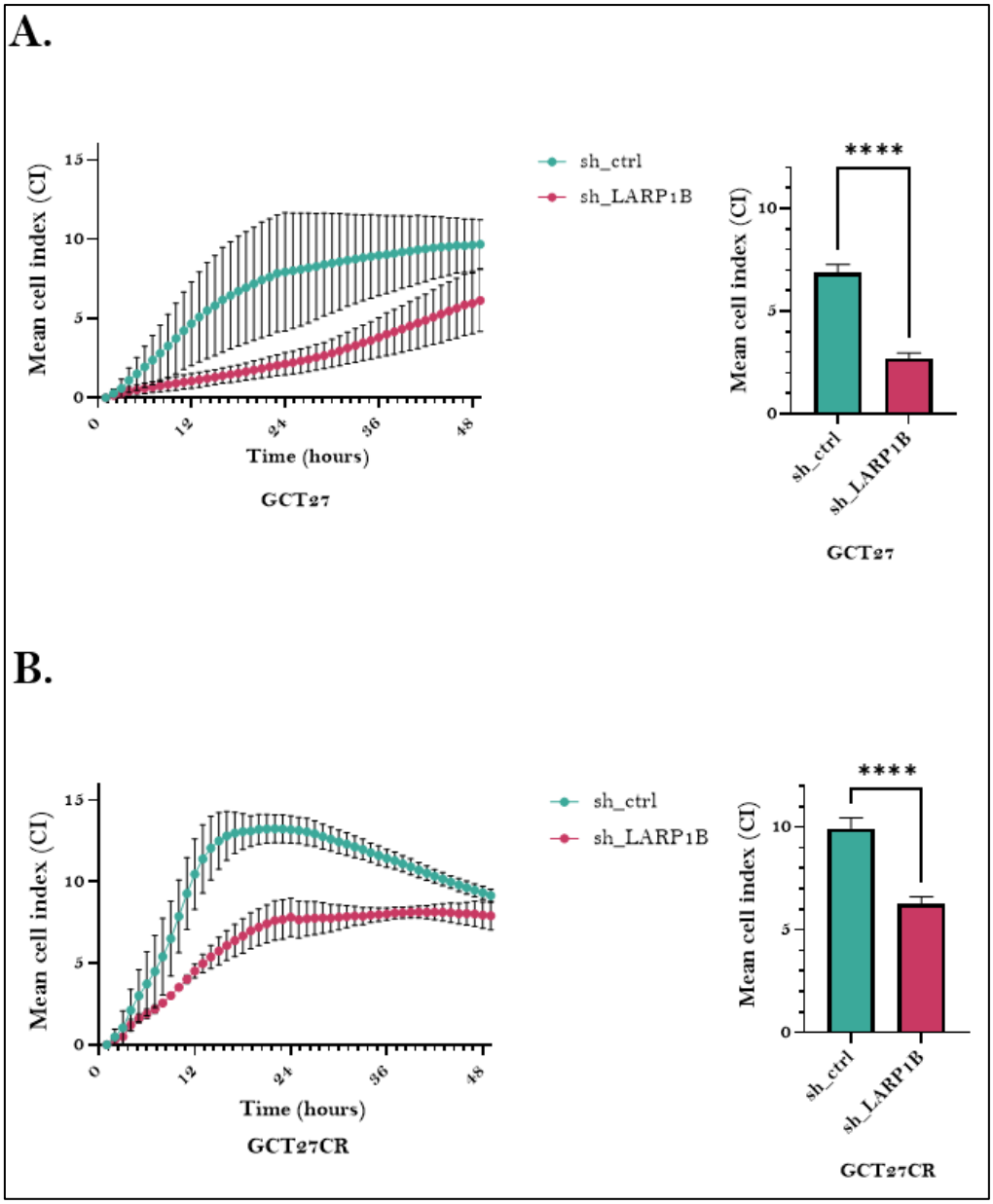

Figure 5.5: LARP1B knockdown caused a significant reduction in the proliferative potential of TGCT cell lines*. GCT27 and GCT27CR cells transfected with sh_ctrl or sh_LARP1B for 48 hours were subjected to RTCA for a further 48 hours.* ***A.*** *GCT27 cell growth curve and CI plot and* ***B.*** *GCT27CR cell growth curve and CI plot. Error bars represent the standard error of mean across biological triplicates. **** P Value= ≤0.0001. Unpaired student t-test was performed for statistical analysis.*

5.2.4 LARP1B knockdown significantly reduced TGCT cell viability

Based on significant abrogation of TGCT cell proliferation following LARP1B knockdown, we then measured cell viability, cytotoxicity, and apoptosis activation. To

achieve this, we first measured levels of a GF-AFC fluorogenic substrate (glycyl-phenyl-alanyl-aminofluorocoumarin) using the ApoTox-Glo Triplex assay. This substrate enters intact, viable cells where it is cleaved by live cell proteases to produce a fluorogenic signal and so fluorescent signal is directly proportional to the number of live or viable cells[237].

As before, GCT27 and GCT27CR cells were transfected with sh_ctrl or sh_LARP1B for 48 hours, re-seeded into opaque 96 well assay plates and viability was assessed after 24 hours giving an endpoint reading of 72 hours of LARP1B depletion. As shown in **Figure 5.6**, cell viability was significantly reduced in both cell lines in sh_LARP1B conditions, when compared to sh_ctrl. This effect was comparable in both GCT27 and GCT27CR cells with an approximate 70% reduction in both cell lines upon LARP1B knockdown compared to sh_ctrl. This supported our earlier findings in which LARP1B knockdown promoted cell rounding and lifting and significantly reduced cell proliferation (**Figure 5.2 and Figure 5.3**).

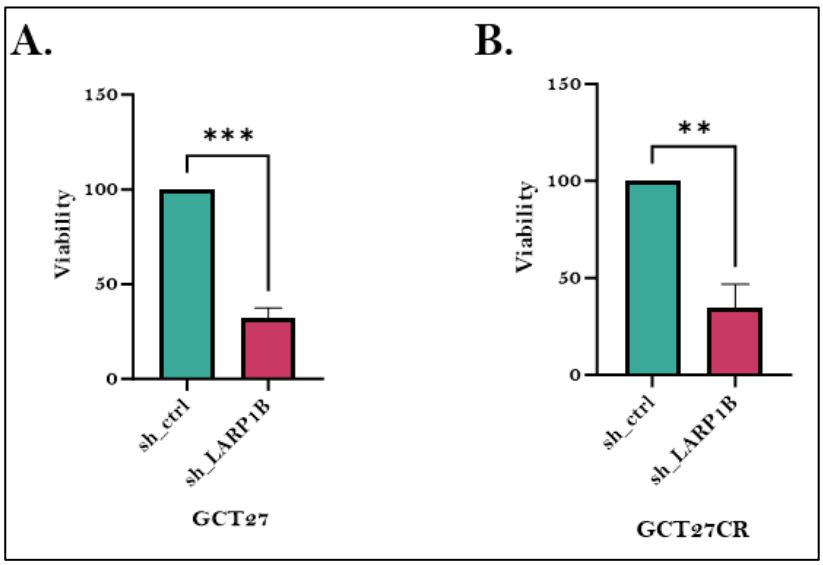

Figure 5.6: LARP1B knockdown significantly reduced the viability of TGCT cell lines. A. *GCT27 and* ***B.*** *GCT27CR cells were transfected with sh_ctrl or sh_LARP1B for 48 hours, and co-cultured with a GF-AFC substrate within the ApoTox-Glo Triplex assay kit. Fluorescent signal was measured which is directly proportional to the number of intact, viable cells. Error bars represent the standard error of mean across biological triplicates. ** P Value= ≤0.01, *** P Value= ≤0.001. Unpaired t-test was performed for statistical analysis.*

5.2.5 LARP1B knockdown induced cytotoxicity and caspase 3/7 activation in TGCT cell lines

As part of the ApoTox-Glo Triplex assay, cytotoxicity and apoptosis were also measured. Cytotoxicity was assessed using a fluorogenic substrate (bisAAF-R110: bis-alanylalanyl-phenylalanyl-rhodamine) which is a cell impermeant peptide substrate activated by dead cell protease activity, thus fluorescent signal is directly proportional to the number of dead cells with a disrupted cell memberane[237]. Apoptosis is detected by measuring caspase 3/7 activity using the luminogenic caspase 3/7 substrate containing the tetrapeptide sequence DEVD; when combined with dead cells, cell lysis and caspase cleavage of the substrate produces a luminescence signal which is directly proportional to the level of caspase activity (Promega technical manual). Evaluating cytotoxicity and caspase cleavage together enables us to understand whether apoptosis is activated and at what stage.

Firstly, in GCT27 cells (**Figure 5.7**) LARP1B knockdown resulted in a substantial increase in cytotoxicity and significant increase in caspase 3/7 cleavage when compared to sh_ctrl. Specifically, we observed a 78% increase in cytotoxicity and 282% increase in caspase 3/7 cleavage in sh_LARP1B conditions, which together suggests apoptosis activation.

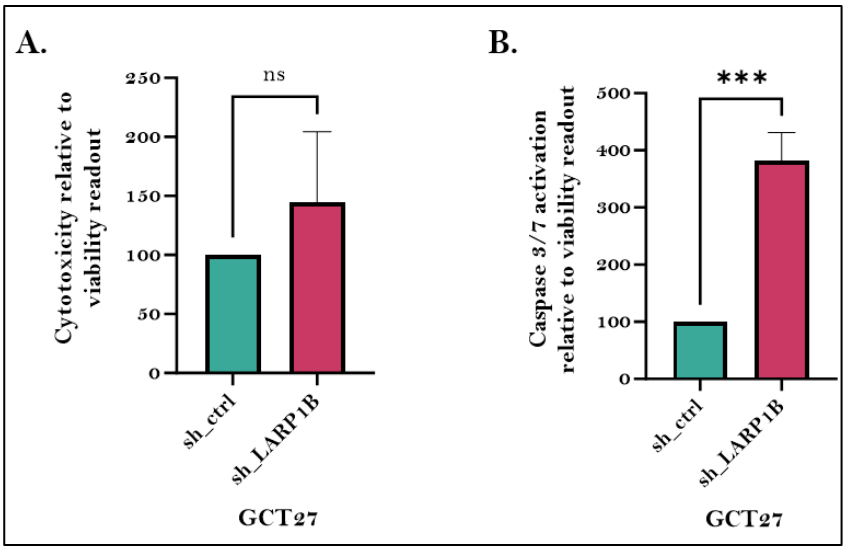

Figure 5.7: LARP1B knockdown in GCT27 cells resulted in apoptosis activation. A. *Cytotoxicity and* ***B.*** *Caspase 3/7 activation upon LARP1B knockdown were analysed as a percentage of sh_ctrl and compared to viability readout. Error bars represent the standard error of mean across biological triplicates. Ns P Value= ≥0.05, *** P Value= ≤0.001. Unpaired t-test was performed for statistical analysis.*

Similar phenotypes were observed in GCT27CR cells (**Figure 5.8**) which also showed a 600% significant increase in cytotoxicity and 500% increase in caspase 3/7 cleavage following LARP1B knockdown, suggestive of apoptosis activation.

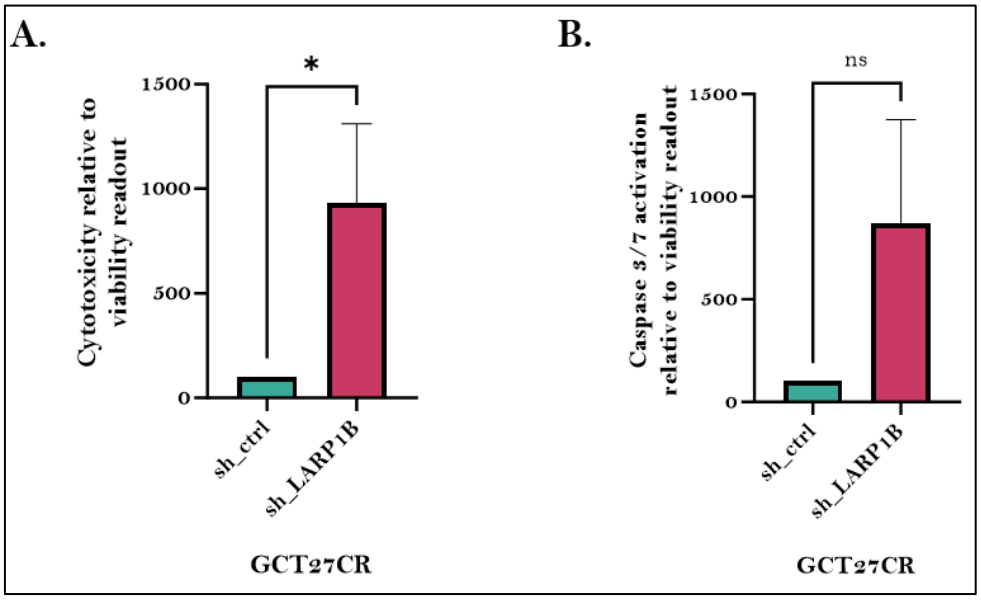

Figure 5.8: LARP1B knockdown in GCT27CR cells induced apoptosis activation. A. *Cytotoxicity and* ***B.*** *Caspase 3/7 activation upon LARP1B knockdown were analysed as a percentage of sh_ctrl and compared to viability readout. Error bars represent the standard error of mean across biological triplicates. Ns P Value= ≥0.05, * P Value= ≤0.05. Unpaired t-test was performed for statistical analysis.*

5.2.6 LARP1B exogenous expression reversed the anti-proliferative phenotype in HEK293T cells

We performed parallel experiments in HEK293T cells due to their ease of growth, use and transfect-ability and to provide a non-cancer equivalent model. qRT-PCR and western blotting analyses are shown in **Figure 5.9** verifying successful LARP1B knockdown at the mRNA level but no visible reduction in LARP1B protein expression with sh_LARP1B. These findings are consistent with those presented earlier in TGCT cell lines. Overexpression of LARP1B with LARP1B-Myc/Flag (**vector map in supplementary materials Figure 8.4**) is confirmed by qPCR and western blotting with a visible increase in LARP1B mRNA and protein levels as well as detection of the Flag tag with an anti-Flag antibody (**Figure 5.9C.**). We did not observe significant effects on LARP1 expression with LARP1B knockdown in HEK293T, contrasting the small but significant increase in

LARP1 expression in TGCT cells with sh_LARP1B. There was an increase in LARP1 mRNA levels following LARP1B overexpression however more biological replicates are necessary with LARP1B-Myc/Flag to determine the significance of these results.

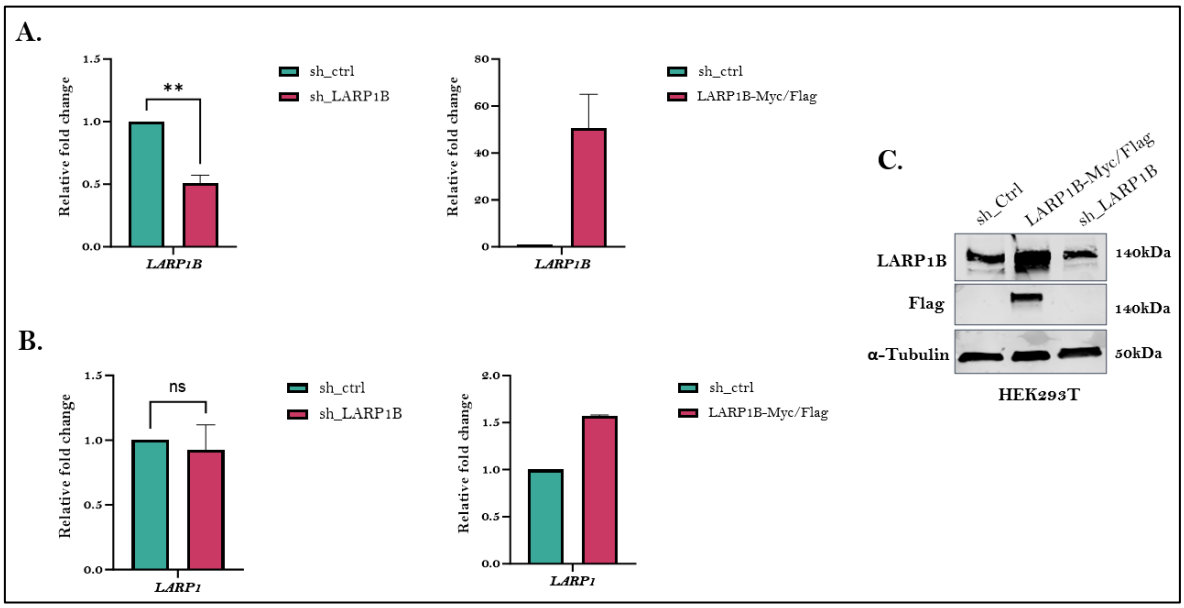

Figure 5.9: LARP1B knockdown in HEK293T cells did not induce changes in LARP1 mRNA expression whilst LARP1B overexpression increased LARP1 mRNA levels. *HEK293T cells were transfected with sh_ctrl, sh_LARP1B or LARP1B-Myc/Flag for 48 hours and harvested for western blot and qPCR analysis.* ***A.*** *qPCR confirmed LARP1B knockdown and construct expression with significant reduction and increased expression of LARP1B, respectively.* ***B.*** *sh_LARP1B had no effect on LARP1 mRNA expression whilst LARP1B construct expression elevated LARP1 mRNA levels.* ***C.*** *Western blotting confirmed LARP1B construct expression with anti-LARP1B and anti-Flag immunoblotting with no appreciable impact of sh_LARP1B. Error bars represent the standard error of mean across biological triplicates for knockdown and biological duplicates for LARP1B-Myc/Flag analysis. Western blots are representative of multiple experiments with approximately 25µg protein loaded/well. Ns P Value= ≥0.05, ** P Value= ≤0.01. Unpaired t-test was performed for statistical analysis.*

As with the TGCT cell lines, HEK293T cells transfected with sh_ctrl or sh_LARP1B or LARP1B-Myc/Flag expression construct, were subjected to xCELLigence RTCA analysis. As shown in **Figure 5.10**, sh_LARP1B had similar anti-proliferative effects as observed in TGCT cells, with a significant reduction in cell growth rate and mean CI when compared to controls. Specifically, LARP1B knockdown resulted in a 67% reduction of mean CI when compared to sh_ctrl. This phenotype was reversed in conditions with

overexpression of LARP1B with an apparent increase in growth rate and 76% increase in mean CI when compared to sh_ctrl. Cells in which LARP1B was overexpressed exhibited exponential growth for approximately 30 hours followed by a decline phase suggesting over-confluency of cells.

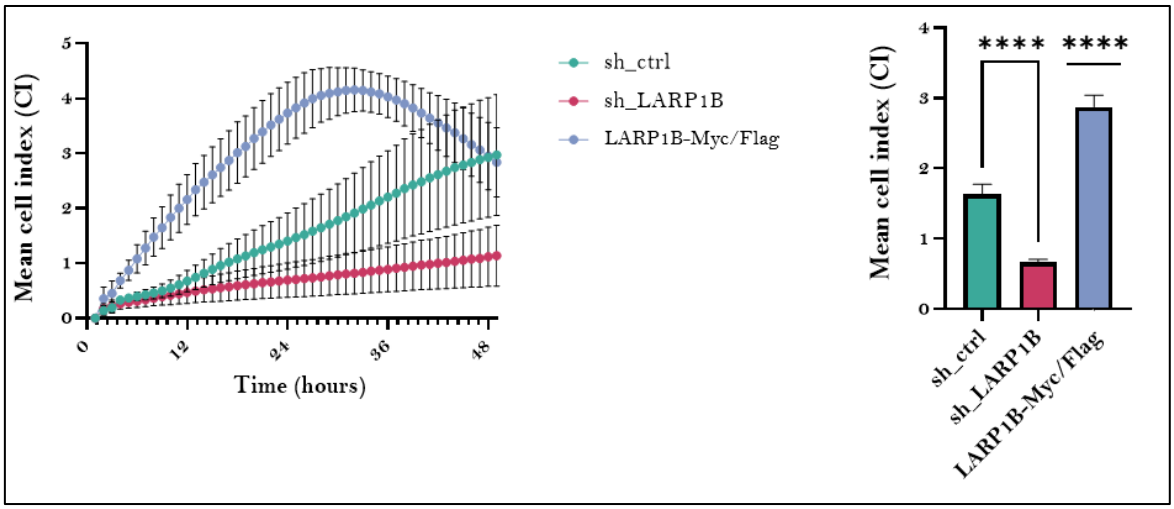

Figure 5.10: LARP1B knockdown significantly reduced the proliferative potential of HEK293T cells, with overexpression of LARP1B promoting proliferation. *HEK293T cells were transfected with sh_ctrl, sh_LARP1B or LARP1B-Myc/Flag for 48 hours, re-seeded into specialised 96 well assay plates and real time cell impedance was measured for a further 48 hours. Error bars represent the standard error of mean across biological triplicates. **** P Value= ≤0.0001. Unpaired t-test was performed for statistical analysis.*

We also evaluated viability alongside cytotoxicity and caspase 3/7 activation as before, to determine if these effects are also reversed with LARP1B overexpression. As shown in **Figure 5.11A.**, viability was significantly reduced in sh_LARP1B conditions by approximately 30% but unaffected in conditions of LARP1B overexpression. We did not observe induction of cytotoxicity or caspase 3/7 in either condition (**Figure 5.11B. and C.**).

Interestingly, LARP1B-Myc/Flag expression maintained HEK293T viability when compared to sh_ctrl, further supporting our hypothesis of LARP1B playing a key role in cell fitness, but also seemingly did not induce cytotoxicity or caspase 3/7 activation. Again, this coincided with our RTCA data (**Figure 5.10**) which demonstrated exponential cell growth and proliferation with LARP1B-Myc/Flag expression. Although we observed a

decline phase in conditions of LARP1B overexpression we did not detect cytotoxicity or caspase 3/7 activation.

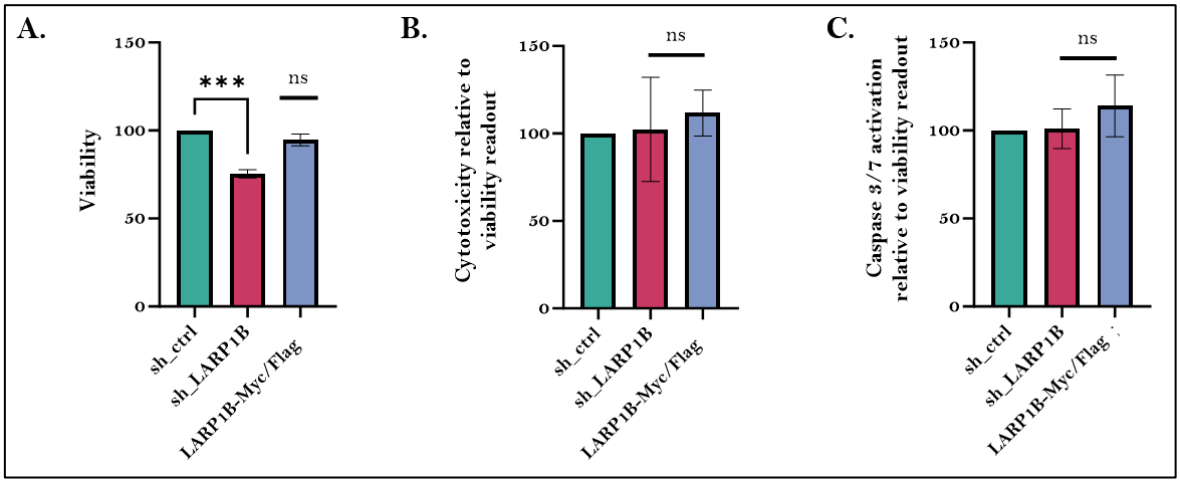

Figure 5.11: LARP1B knockdown significantly abrogated HEK293T cell viability without cytotoxicity or apoptosis induction whilst overexpression maintained these phenotypes. ***A.*** *sh_LARP1B significantly reduced HEK293T cell viability whilst LARP1B-Myc/Flag maintained cell viability levels comparable to sh_ctrl.* ***B.*** *Cytotoxicity and* ***C.*** *caspase 3/7 activation upon LARP1B knockdown or LARP1B-Myc/Flag construct expression was not impacted. Error bars represent the standard error of mean across biological triplicates. Student t-test was used during statistical analysis.*

5.2.7 LARP1B knockdown impaired mitochondrial respiration and energy consumption in TGCT cell lines

Given that we observed an enrichment of mitochondrial and metabolism associated proteins in the LARP1B interactomes (**outlined in Results Chapter 2**) and recent findings of LARP1 regulating cancer cell metabolism[233] we wanted to explore the role of LARP1B in TGCT cell metabolism. To do this we used the Seahorse XF Extracellular Flux Analyser to measure mitochondrial function of live cells. Specifically, we applied the Mito stress test with sequential injections of Oligomycin, FCCP and Antimycin/Rotenone to decrease or increase oxygen consumption rate (OCR; proxy for oxidative phosphorylation) and Extracellular Acidification rate (ECAR; proxy for glycolysis) ultimately providing a readout of mitochondrial function and cell fitness in response to LARP1B depletion. To account for well-to-well cell number variation, we carried out Cyquant cell proliferation assays in parallel and normalised Seahorse XF data to cell number.

As shown in **Figure 5.12A.**, LARP1B knockdown resulted in a significant reduction in basal OCR of both GCT27 and GCT27CR cells. Overall, GCT27CR cells were more metabolically active than their cisplatin-sensitive counterpart as shown by higher basal OCR levels in control conditions which also supports their general higher proliferative rate (**Figure 5.5B.**). Following LARP1B depletion, basal OCR was reduced by approximately 50% in GCT27 and 32% in GCT27CR cells. Alongside basal OCR, we found that LARP1B depletion caused a slight yet significant increase in basal ECAR in both cell lines (**Figure 5.12B.**). Although we observed only a 4.5% increase in GCT27 and 18.3% increase in GCT27CR this hinted at a switch from oxidative phosphorylation to glycolysis as a means of energy consumption. Emphasis of these metabolic changes was most apparent in the OCR/ECAR ratio (**Figure 5.12C.**) which concluded a significant reduction in basal OCR and shift towards glycolysis upon LARP1B depletion in both TGCT cell lines.

Interestingly, we also observed significant 54% and 48% reductions in ATP-linked respiration in GCT27 and GCT27CR cells, respectively (**Figure 5.12D.**) which also reflects a decrease in ATP synthesis. This was further coupled with a significant decrease in maximal respiratory capacities in both cell lines following LARP1B depletion (**Figure 5.12E.**). Specifically, maximal respiration was abrogated by approximately 57% in GCT27 and 60% in GCT27CR, suggesting that LARP1B depletion not only affected basal respiration, but also impaired the cells abilities to increase oxygen consumption and ATP synthesis in response to changes in cellular metabolic demands.

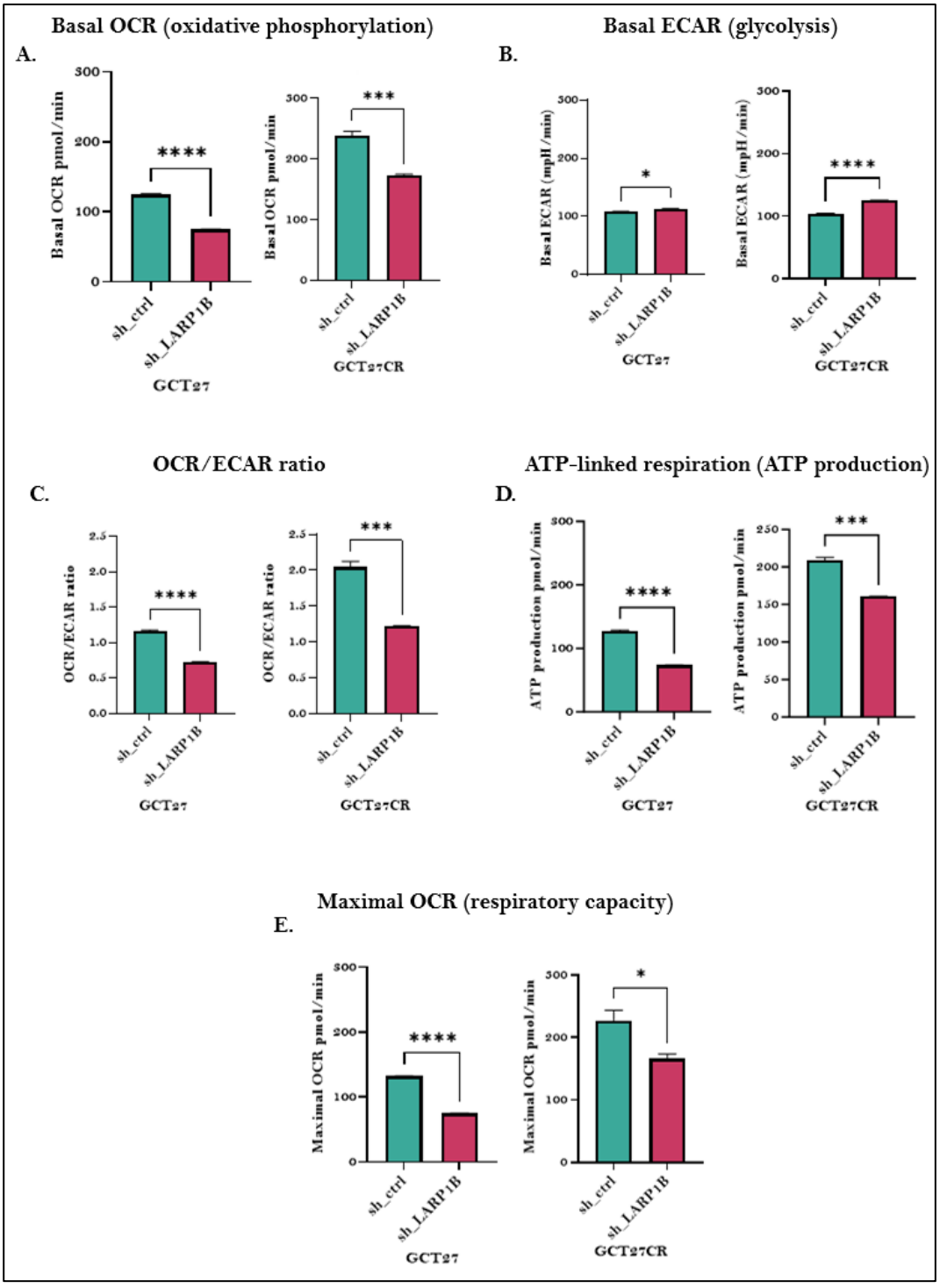

Figure 5.12: LARP1B knockdown reduced basal oxidative phosphorylation, ATP-linked respiration and maximal respiration whilst increasing basal glycolysis in TGCT cells. A. *Basal OCR (pmol/min) was significantly reduced in GCT27 and GCT27CR cells following LARP1B knockdown for 72 hours.* ***B.*** *Basal ECAR (mpH/min) showed a slight but significant increase upon LARP1B knockdown for 72 hours.* ***C.*** *OCR/ECAR ratio was significantly reduced following LARP1B knockdown for 72 hours suggesting a shift towards*

glycolysis for energy consumption. ***D.*** *ATP-linked respiration and thus ATP production was significantly reduced in GCT27 and GCT27CR cells following LARP1B knockdown for 72 hours.* ***E.*** *Maximal OCR was significantly reduced in GCT27 and GCT27CR cells following LARP1B knockdown for 72 hours. Error bars represent the standard error of mean across biological triplicates. * P Value= ≤0.05, ** P Value= ≤0.01, *** P Value= ≤0.001, **** P Value= ≤0.0001. Student t-test was used for statistical analysis.*

5.2.8 LARP1B knockdown promoted excessive ROS generation and oxidative stress in TGCT cell lines

ROS are well recognised activators of apoptosis following mitochondrial dysfunction[238]. As we observed significant apoptosis and a decrease in mitochondrial function following LARP1B depletion, we explored the level of intracellular mitochondrial ROS, specifically superoxide anion species (O_2^-). TGCT cells post-LARP1B knockdown were stained with MitoSOX Red which detected O_2^- within the mitochondria of live cells. In combination with LARP1B loss of function, we treated cells with menadione (Mena) as a positive control for ROS generation, which is capable of producing intracellular ROS through redox cycling.

We found that LARP1B depletion resulted in elevated levels of mitochondrial O_2^- production in GCT27 and GCT27CR cells when compared to sh_ctrl, as visualised with increased MitoSOX red fluorescence staining (**Figure 5.13A.**). As expected, fluorescence intensity was strongest with menadione treatment which in combination with LARP1B knockdown resulted in the strongest MitoSOX signal and thus most mitochondrial O_2^- production (**Figure 5.13B.**).

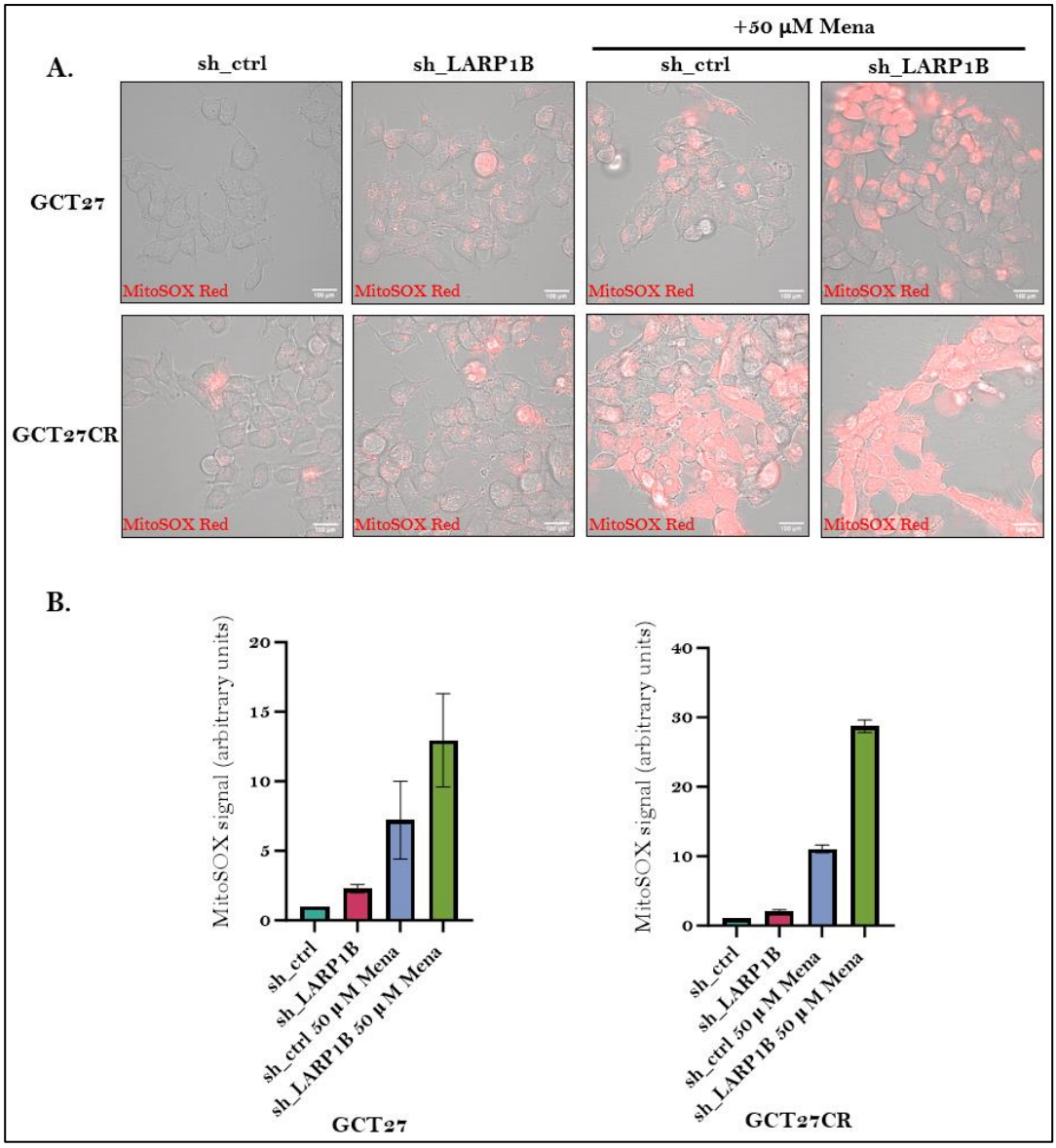

Figure 5.13: LARP1B knockdown resulted in an increase in reactive oxygen species in TGCT cell lines. A. *MitoSOX live cell staining revealed an increase in staining intensity following LARP1B knockdown in the presence and absence of ROS inducer menadione.* ***B.*** *Quantitative analysis of fluorescent staining intensity confirms increase in MitoSOX signal with LARP1B knockdown with and without menadione treatment which was used to induce mitochondrial superoxide anion production. Error bars represent the standard error of mean across biological duplicates. Mena = menadione.*

5.3 Summary of findings

To begin exploring the phenotypic function of LARP1B we depleted LARP1B in TGCT cell lines and where applicable HEK293T cells, and observed effects on cell phenotypes

including proliferation, viability, cytotoxicity, apoptosis, mitochondrial respiration, and reactive oxygen species.

Firstly, we observed a role for LARP1B in maintaining TGCT and HEK293T cell growth and viability. After only 24 hours post-LARP1B knockdown, GCT27 and GCT27CR cells presented with cell rounding and lifting (**Figure 5.2 and 5.3**), associated with significant reduction in proliferation and viability (**Figure 5.5 and 5.6**) as well as increased cytotoxicity and apoptosis (**Figure 5.7 and 5.8**). To further confirm apoptosis in response to LARP1B knockdown, apoptosis markers including PARP and caspases could be detected by western blot.

We also observed a significant reduction in cell proliferation and viability following LARP1B knockdown in HEK293T cells (**Figure 5.10**) which was associated with negligible changes in cytotoxicity and caspase 3/7 activation (**Figure 5.11**). Exogenous LARP1B expression with a LARP1B-Myc/Flag vector significantly increased HEK293T cell proliferation and viability without induction of cytotoxicity or caspase 3/7 activation (**Figure 5.10 and 5.11B.-C.**).

With the knowledge that LARP1 regulates cancer cell metabolism[233], and identification of a plethora of metabolism-associated candidates within the LARP1B interactome (**Results chapter 2**) we investigated the role of LARP1B in TGCT cell metabolism and mitochondrial respiration as a readout for mitochondrial function. As shown in **Figure 5.12**, sh_LARP1B significantly reduced basal OCR in GCT27 and GCT27CR cells in combination with a significant yet small induction of basal glycolysis. These characteristics were coupled with a significant reduction in ATP levels and a significant reduction in maximal respiratory capacities, together indicating abrogated mitochondrial function following LARP1B knockdown. We also observed an increase in intracellular reactive oxygen species, specifically mitochondrial superoxide anions following LARP1B depletion suggestive of oxidative stress induction (**Figure 5.13**).

One of the greatest limitations of this chapter was the lack of stable LARP1B knockdown cell lines. All of our experiments were carried out following transient LARP1B knockdown which adds variability due to transfection techniques. This also prevented us from carrying out rescue experiments by re-expressing LARP1B-Myc/Flag in LARP1B-null cell lines and so we resorted to construct-based overexpression of LARP1B-Myc/Flag in LARP1B wildtype cells. Not only was optimisation of LARP1B knockdown in TGCT cells challenging but optimising LARP1B-Myc/Flag expression also proved difficult. Despite observing a significant reduction in LARP1B mRNA expression following shRNA knockdown, protein levels remained at appreciable levels as shown in **Figure 5.1.** Despite extensive optimisation and use of different RNAi methods (**discussed in Material and Methods 2.3**), we consistently observed this pattern of significant reduction of *LARP1B* mRNA levels but only a small visible reduction in LARP1B protein following LARP1B knockdown. We suspect this is due to a long protein half-life of LARP1B which could be further confirmed by cycloheximide chase to measure degradation kinetics.

6

RESULTS CHAPTER 4: EXPLORING THE INTERPLAY BETWEEN LARP1B AND LARP1

6.1 Introduction

We identified LARP1 within the LARP1B interactome in TGCT cell lines which suggests their interaction (**Results Chapter 2**). We also identified a significant increase in *LARP1* mRNA expression following LARP1B knockdown (**Figure 5.4**). It is interesting to note that LARP1B shRNA knockdown seemingly impacted cellular respiration and metabolism whilst a recent study in our lab demonstrated a key role for LARP1 in the regulation of these same processes in cancer cells[233]. Based on these findings and on our knowledge of paralogous proteins forming distinct relationships, we further investigated the interaction between LARP1B and LARP1. As our earlier results showed a small but significant increase in *LARP1* mRNA expression following LARP1B knockdown, we wanted to determine whether LARP1 knockdown would have a similar effect on LARP1B expression. As such we performed transient siRNA knockdown of LARP1 in our TGCT cell lines and assessed LARP1B protein and mRNA expression. We then investigated the abilities of LARP1 and LARP1B to form direct and/or indirect interactions by performing co-immunoprecipitation (co-IP) studies in the presence and absence of RNAse. To further confirm our co-IP binding, we also immunoprecipitated complexes in HEK293T and OVCAR8 LARP1^{WT} and LARP1^{KO} models. Finally, in addition to expression we explored whether LARP1 depletion would impact LARP1B protein subcellular localisation.

6.2 Results

6.2.1 LARP1 transient siRNA knockdown had variable effects on LARP1B mRNA and protein expression

Our earlier findings revealed a small but significant increase in LARP1 mRNA expression with no visible effects on LARP1 protein (**Figure 5.4**). We wanted to explore whether transient LARP1 knockdown had any impact on LARP1B expression based on these findings and the fact that stable LARP1 knockout in HEK293T cells did not alter LARP1B protein levels (**Figure 4.1**). We performed LARP1 siRNA knockdown in GCT27 and GCT27CR cells using two independent siRNA oligonucleotides termed siLARP1_2 and siLARP1_Q2 for 48 hours and performed qPCR and western blot analysis. Successful LARP1 knockdown in GCT27 is shown in **Figure 6.1A.** with approximately 80% reduction in *LARP1* expression with both siRNA. These findings were associated with a significant reduction in *LARP1B* mRNA expression with siLARP1_2 by approximately

30% and no change with siLARP_Q2 (**Figure 6.1B.**). LARP1 knockdown was also confirmed by a visible reduction in LARP1 protein (**Figure 6.1C.**) whilst LARP1B protein expression remained unchanged, supporting our previous analysis of LARP1B protein expression in HEK293T LARP1^{KO} cells (**Figure 4.1**).

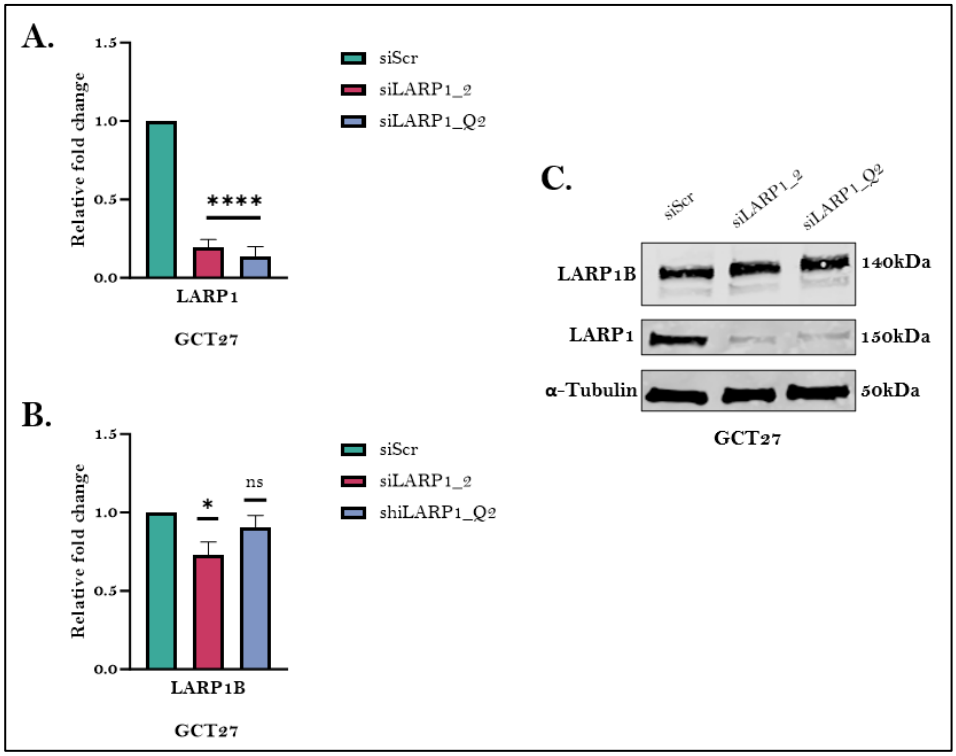

Figure 6.1: LARP1 loss resulted in subtle changes in LARP1B mRNA expression in GCT27 cells. *GCT27 cells were transfected with two independent siRNA against LARP1 followed by qPCR and western blot analysis.* ***A.*** *LARP1 mRNA levels were significantly reduced following transfection with two independent siRNA oligonucleotides whilst* ***B.*** *LARP1B mRNA expression demonstrated a small yet significant reduction with siLARP1_2 but no change with siLARP1_Q2.* ***C.*** *LARP1 knockdown was apparent at the protein level whilst LARP1B protein levels remained unchanged. Error bars represent the standard error of mean across biological triplicates. Western blot is a representative image of biological replicates with approximately 20µg protein loaded/well. Ns P Value= ≥0.05, * P Value= ≤0.05, **** P Value= ≤0.0001. Unpaired student t-test was performed for statistical analysis.*

In GCT27CR cells LARP1 depletion reduced *LARP1* mRNA expression by approximately 70% which corresponded with a significant increase in *LARP1B* mRNA expression with

both siRNA (**Figure 6.2A. and B.**). Levels of LARP1B protein however did not change upon LARP1 knockdown (**Figure 6.2C.**).

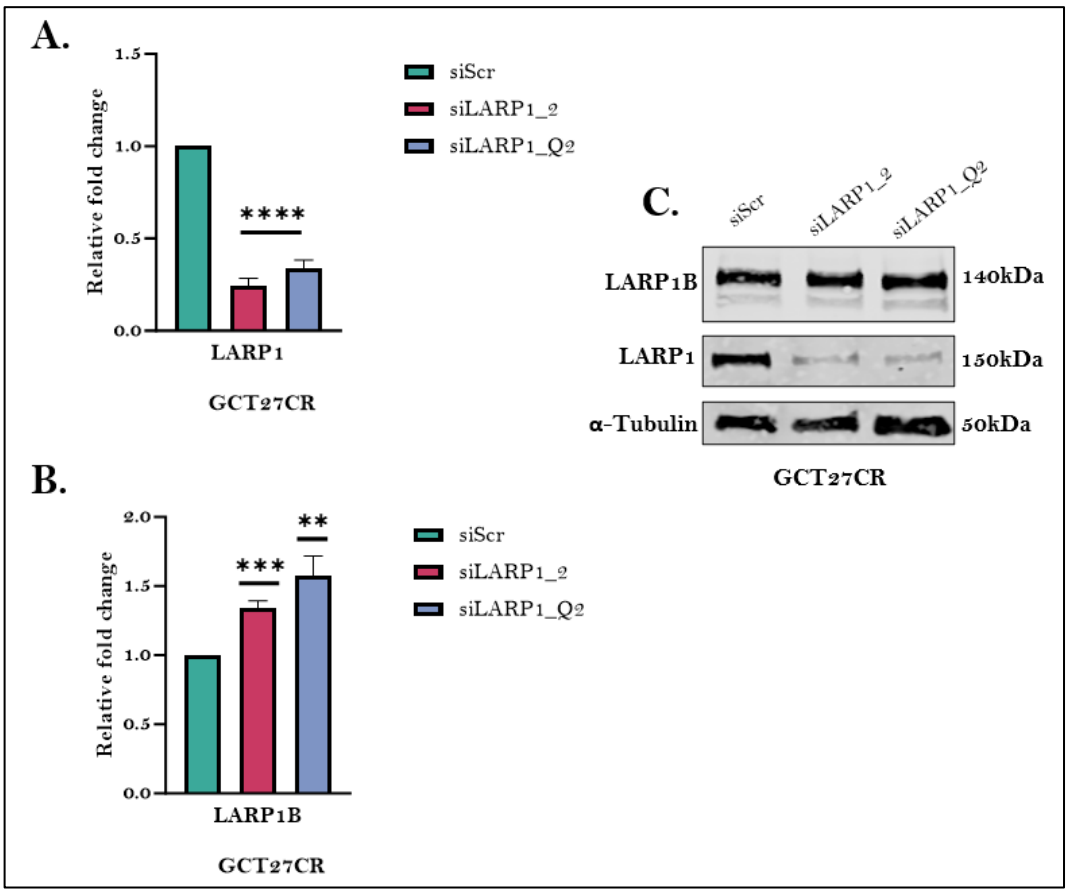

Figure 6.2: LARP1 depletion resulted in minimal changes in LARP1B mRNA expression in GCT27CR cells, contrasting GCT27. *GCT27CR cells were transfected with two independent siRNA against LARP1 followed by qPCR and western blot analysis.* ***A.*** *LARP1 mRNA levels were significantly reduced following transfection with two independent siRNA oligonucleotides whilst* ***B.*** *LARP1B mRNA expression demonstrated a significant increase with both siRNA oligonucleotides* ***C.*** *LARP1 knockdown was apparent at the protein level whilst LARP1B protein levels were sustained as in GCT27 cells. Error bars represent the standard error of mean across biological triplicates. Western blot is a representative image of biological replicates with approximately 20µg protein loaded/well. ** P Value= ≤0.01, *** P Value= ≤0.001, **** P Value= ≤0.0001. Unpaired student t-test was performed for statistical analysis.*

6.2.2 LARP1 stable knockout did not impact LARP1B protein expression or subcellular localisation but reduced *LARP1B* mRNA expression

Transient knockdown of LARP1 in TGCT cell lines demonstrated that under certain conditions *LARP1B* mRNA expression was upregulated with little to no observable impact on LARP1B protein expression. The challenge with this is transient knockdown is short term thus inducing global short-term effects. We therefore looked at LARP1B expression and localisation in HEK293T and OVCAR8 LARP1 CRISPR knockout models.

As shown in **Figure 6.3**, LARP1B protein expression was sustained in HEK293T and OVCAR8 LARP1^{KO} cells when compared to LARP1^{WT} controls. However, qPCR analysis revealed a significant 40% reduction in *LARP1B* expression following LARP1 knockout in HEK293T LARP1^{KO} and a 50% reduction in *LARP1B* expression in OVCAR8 LARP1^{KO} although this was not significant.

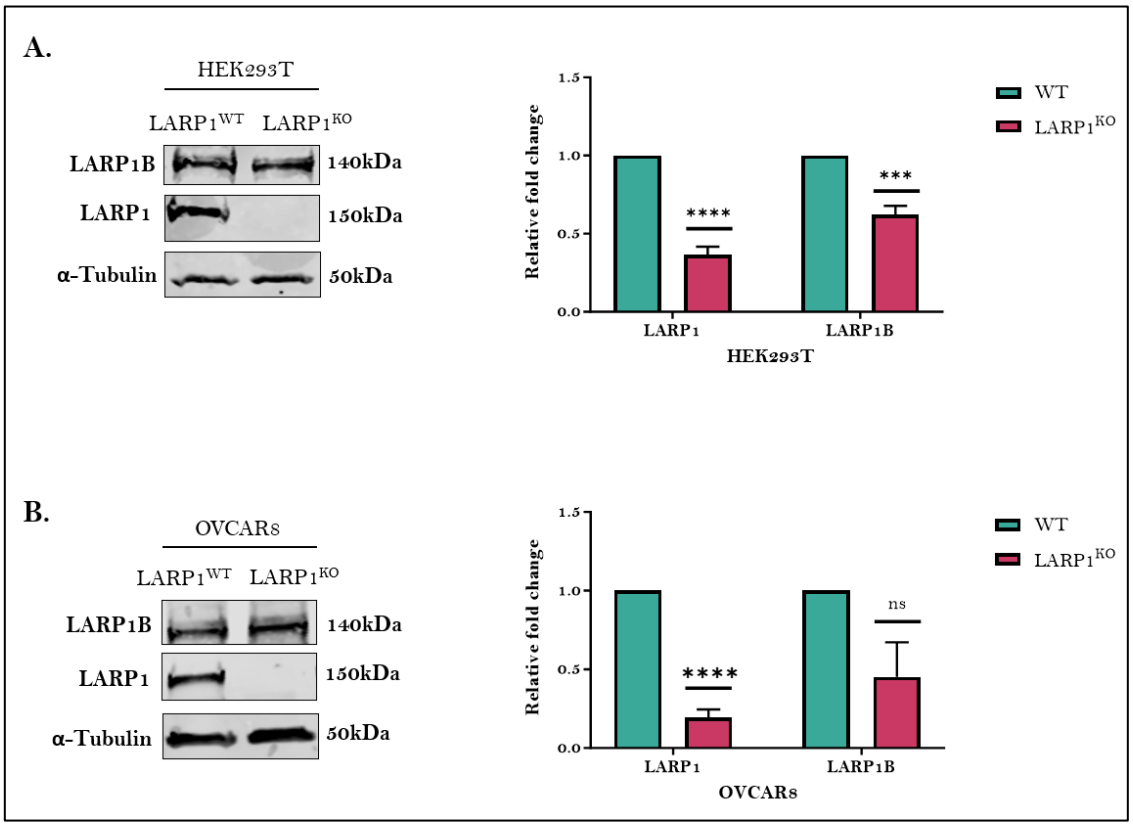

Figure 6.3: LARP1 stable knockout in HEK293T and OVCAR8 did not alter LARP1B protein but reduced LARP1B mRNA levels. A. *In HEK293T cells, western blotting demonstrated complete loss of LARP1 protein expression whilst approximately 40% of mRNA expression remained following LARP1 knockout. LARP1B protein expression was maintained but we observed a significant reduction in LARP1B mRNA expression (right hand panel).* ***B.*** *In OVCAR8 cells, western blotting demonstrated complete loss of LARP1 protein expression whilst*

*approximately 25% of mRNA expression remained following LARP1 knockout (right hand panel). LARP1B protein expression was maintained, and we observed a non-significant reduction of LARP1B mRNA expression. Ns P Value= ≥0.05, *** P Value= ≤0.001, **** P Value= ≤0.0001. Unpaired student t-test was performed for statistical analysis.*

As LARP1 knockout did not induce appreciable effects on LARP1B protein expression we aimed to explore whether there was an effect on LARP1B localisation following LARP1 depletion, focusing on OVCAR8 cell lines. We harvested OVCAR8 LARP1^{WT} and LARP1^{KO} cells and performed subcellular fractionation and immunoblotting as mentioned previously. We observed no change in the localisation of LARP1B between LARP1 wildtype and knockout conditions, with detection of LARP1B in all fractions (**Figure 6.4**). As previously observed in TGCT and HEK293T cells, nuclear fractions were more enriched for LARP1B than cytoplasmic fractions. Again, we observed high LARP1 expression in whole cell and cytoplasmic fractions as well as a small amount of LARP1 in nuclear fractions. α -Tubulin and Lamin A/C confirmed whole cell, cytoplasmic and nuclear compartments.

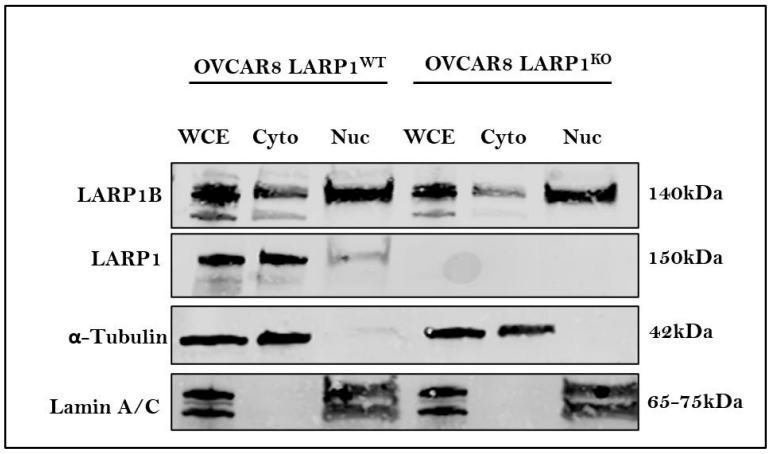

Figure 6.4: LARP1 knockout in OVCAR8 cells did not alter the cellular distribution of LARP1B protein. *OVCAR8 LARP1^{WT} and OVCAR8 LARP1^{KO} cells were subjected to subcellular fractionation and immunoblotting as previously described. As with other cell lines, LARP1B was detected in whole cell, cytoplasmic and nuclear compartments whilst LARP1 was largely restricted to whole cell and cytoplasmic fractions with minimal LARP in nuclear fractions. We did not observe any changes in LARP1B subcellular distribution in LARP1^{KO} conditions. Approximately 30μg of protein was loaded/well.*

We further performed IF analysis in HEK293T LARP1^{WT} and HEK293T LARP1^{KO} cell lines to further corroborate our findings and indeed identified sustained nuclear LARP1B expression (**Figure 6.5A.**). Our IF analysis also confirmed LARP1 depletion compared to HEK293T LARP1^{WT} cells (**Figure 6.5B.**).

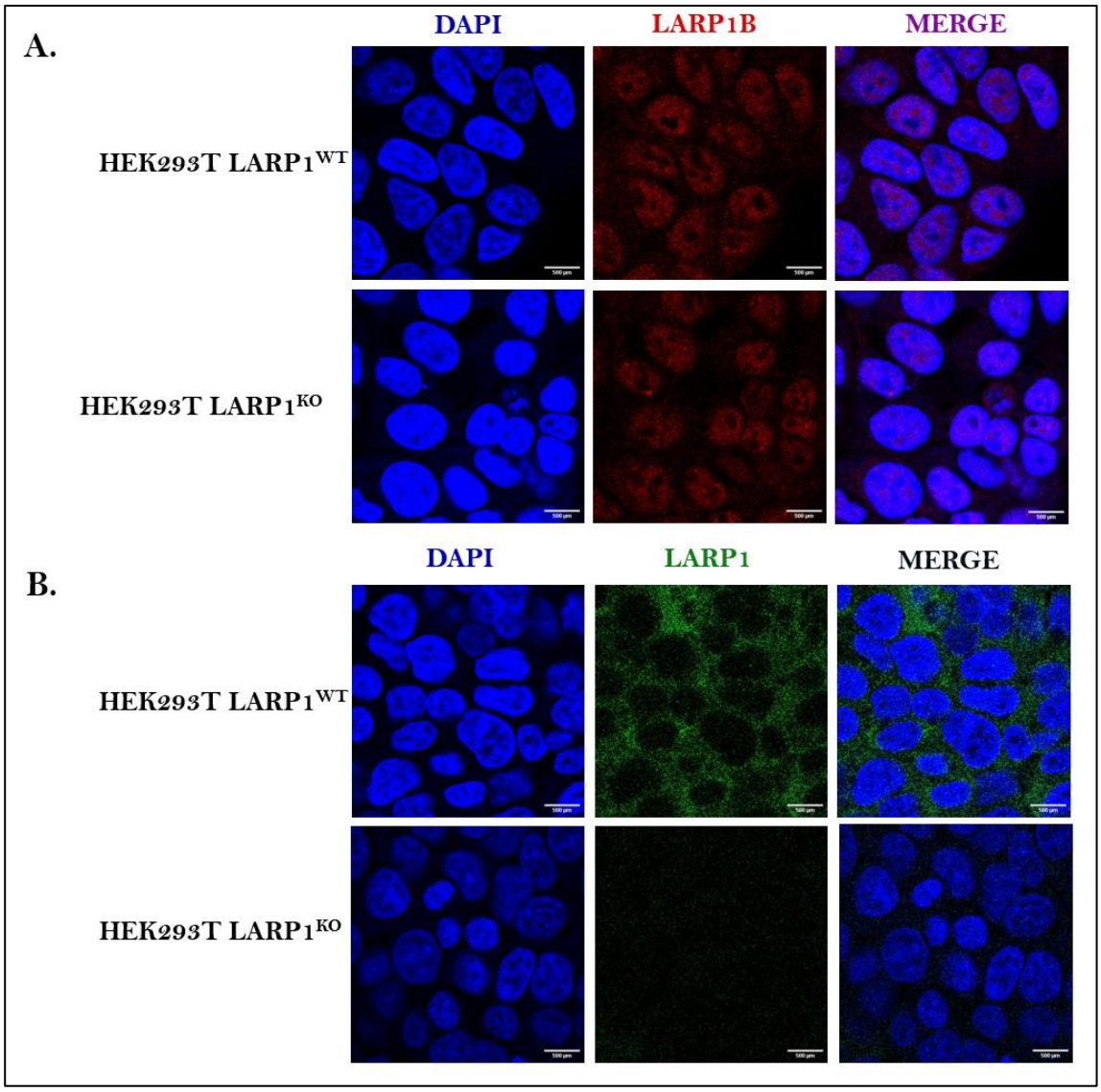

Figure 6.5: Immunofluorescence analysis of HEK293T LARP1^{WT} and HEK293T LARP1^{KO} cells confirmed sustained LARP1B expression and nuclear localisation whilst also validating LARP1 CRISPR knockout. *HEK293T LARP1^{WT} and LARP1^{KO} cell lines were immuno-stained with* ***A.*** *anti-LARP1B (red) or* ***B.*** *anti-LARP1 (green) antibodies DAPI nuclear stain (blue). Cells were viewed under the Zeiss LSM 710 confocal microscope and images were processed using Fiji open-source image processing package. Scale bar = 500µm.*

6.2.3 LARP1B and LARP1 form direct protein-protein interactions that are independent of RNA

Ou earlier investigation into the LARP1B protein interactome identified LARP1B in GCT27 and GCT27CR cell lines. We wanted to confirm these findings and so performed co-IP experiments in TGCT, HEK293t and OVCAR8 cell lines to detect direct and/or indirect protein interactions between LARP1B and LARP1. We used Protein A magnetic affinity beads coated with anti-LARP1B, anti-LARP1 or anti-IgG antibodies to immunoprecipitate protein complexes. To detect whether the interactions between LARP1B and LARP1 were RNA dependent, we performed parallel experiments with RNAse A treatment to degrade RNA.

As shown in **Figure 6.6**, we detected LARP1 in complex with LARP1B and vice versa in both TGCT cell lines (reciprocal interactions highlighted with *) with and without RNAse A treatment. Interestingly, we observed the LARP1B-LARP1 complex at a higher molecular weight than expected at approximately 150kDa. Presence of LARP1B and LARP1 in input samples supports these findings.

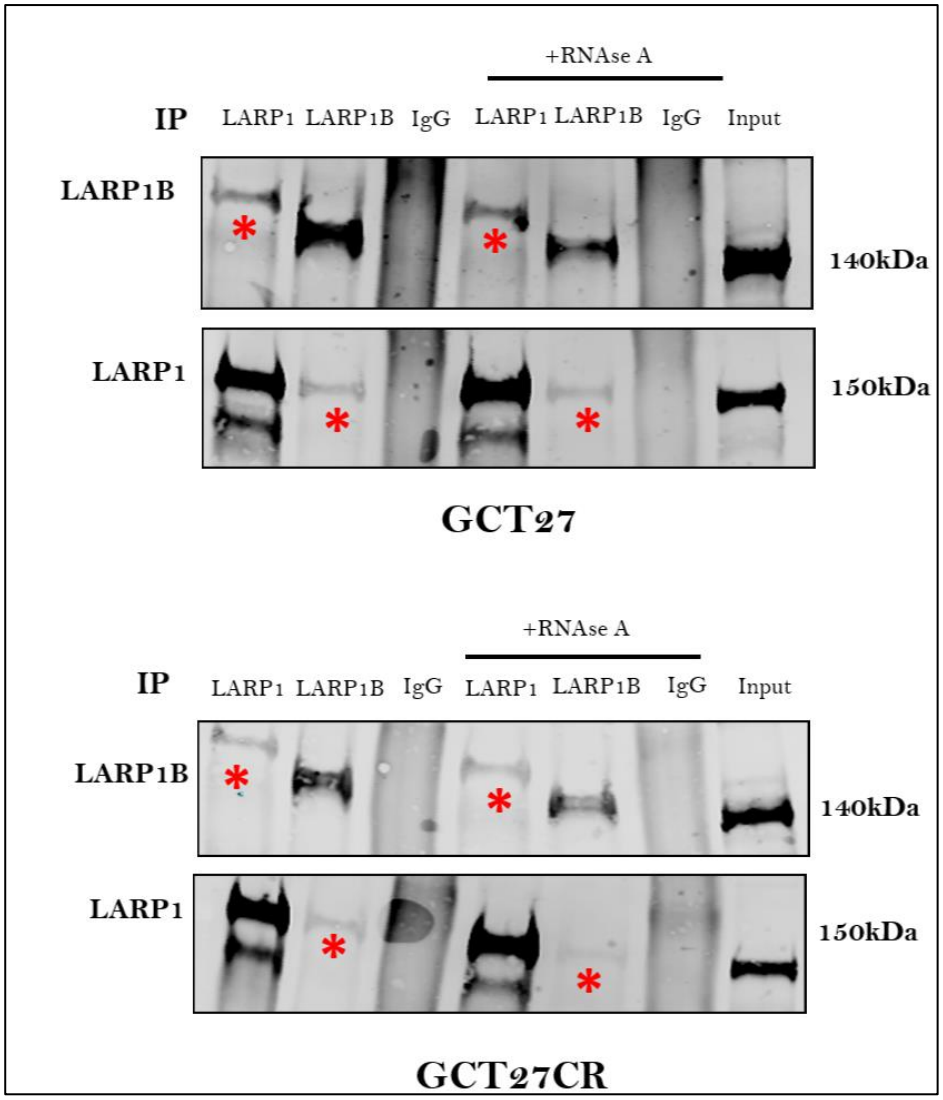

Figure 6.6: LARP1B and LARP1 form protein-protein complexes in TGCT cell lines. *GCT17 and GCT27CR cell lysates were collected for LARP1B and LARP1 co-IP analysis which revealed strong interactions between the proteins in both cell lines. RNAse A treatment did not appear to affect this interaction, suggesting their interaction is not RNA-dependent.*

We also explored these interactions in LARP1 WT and KO models of HEK293T and OVCAR8 cell lines using the same methods (**Figure 6.7**). Firstly, in HEK293T, we observed LARP1B-LARP1 interactions with albeit weaker detection of LARP1 in LARP1B pull downs however a faint band was visible (*). As anticipated, these interactions were completely lost in HEK293T LARP1^{KO} cells (**) due to a loss of endogenous LARP1. Presence of LARP1B in our input samples supports this interaction. In OVCAR8 cell lines we observed similar results with detection of LARP1B in LARP1 pull downs which was absent in LARP1^{KO} cells. LARP1 was not detected in LARP1B pulldowns in OVCAR8^{WT}

or LARP1^{KO} cells which we suspect is due to weak or unstable interactions. Where LARP1B-LARP1 interactions were observed they were again at a higher molecular weight than expected as observed in GCT27 and GCT27CR cells in **Figure 6.6**.

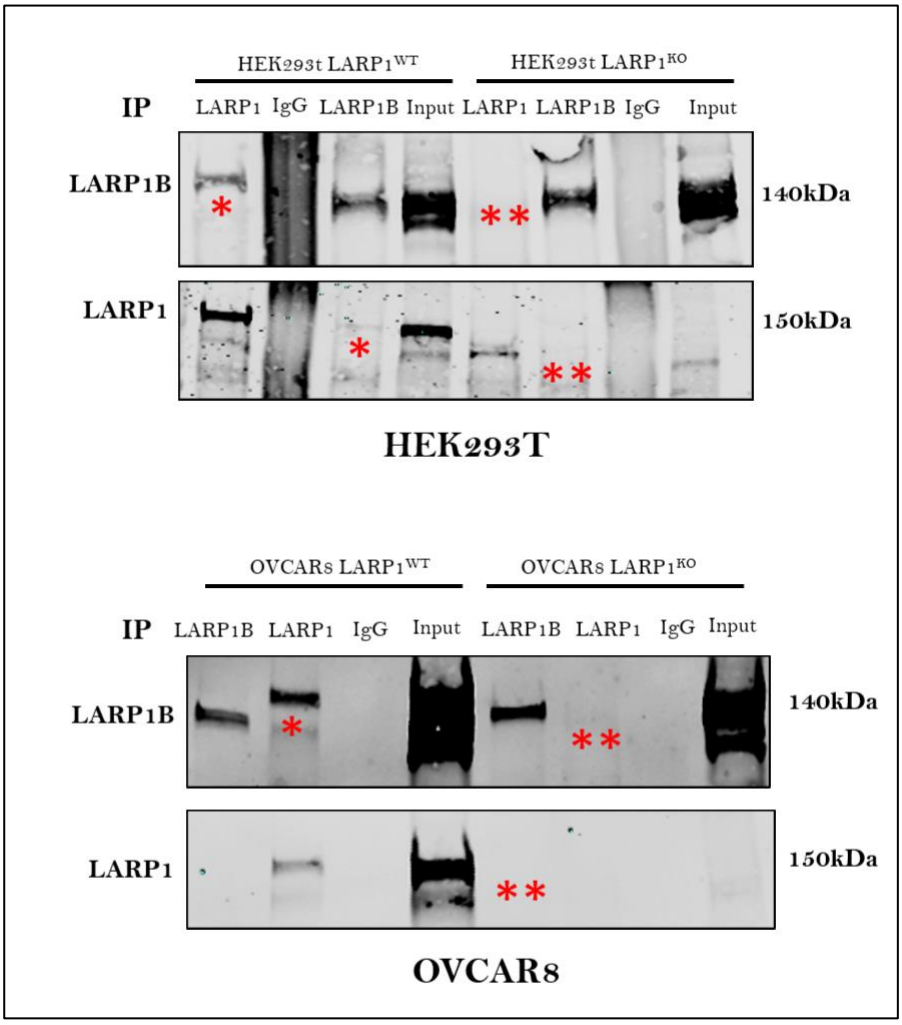

Figure 6.7: LARP1B and LARP1 form protein-protein complexes in HEK293T and OVCAR8 cell lines which are lost upon LARP1 knockout. *HEK293T and OVCAR8 cell lysates were collected for LARP1B and LARP1 co-IP. Reciprocal interactions were most apparent in HEK293T^{WT} and were lost in HEK293T LARP1^{KO} whilst in OVCAR8, reciprocal interactions were weak even in LARP1^{WT}.*

6.3 Summary of findings

Based on the knowledge that paralogous proteins form unique dimeric communications and interactions we explored the effects of LARP1 depletion on LARP1B mRNA and protein expression and subcellular localisation using transient knockdown and an

LARP1^{KO} models. Further, we explored the capabilities of LARP1B and LARP1 in forming direct and/or indirect protein-protein interactions using co-IP experiments.

Transient knockdown of LARP1 using two independent siRNA oligonucleotides demonstrated variable effects on *LARP1B* mRNA expression in TGCT cell lines. Specifically, LARP1 knockdown with siLARP1_2 in GCT27 induced a 30% reduction in *LARP1B* gene expression whilst siLARP1_Q2 had no impact (**Figure 6.1**). In GCT27CR cells, both LARP1 siRNA caused up to a 50% increase in *LARP1B* mRNA expression suggesting opposite dynamics between LARP1B and LARP1 in both cell lines (**Figure 6.2**). Further, despite these contrasting effects at the gene level we did not observe any change in LARP1B protein expression in either cell line.

Our analyses of the interplay between LARP1B and LARP1 so far did not demonstrate changes in LARP1B protein expression (**Figure 6.3**) and so we explored whether LARP1 knockout altered the subcellular localisation of LARP1B. As such, we did not observe changes in LARP1B localisation in OVCAR8 LARP1^{KO} cells compared to LARP1^{WT}, with sustained cytoplasmic and nuclear expression of LARP1B in both cell lines (**Figure 6.4**). These findings were further confirmed by IF in HEK293T LARP1^{WT} and LARP1^{KO} cell lines (**Figure 6.5**).

We identified direct protein-protein interactions between LARP1B and LARP1 in multiple cell lines which were not impacted by RNAse A, suggesting these interactions occur independent of RNA (**Figure 6.6**). These interactions were further confirmed in HEK293T and OVCAR8 LARP1^{KO} models in which LARP1B-LARP1 complexes were not observed following LARP1 depletion (**Figure 6.7**); these interactions were weaker in OVCAR8 compared to HEK293T cells.

A consistent finding in our co-IP experiments is the higher molecular weight of LARP1B when complexed with LARP1. This may be due to LARP1B interacting with post-translationally modified LARP1 perhaps phosphorylated which could increase the molecular weight of the protein complex. Addition of phosphatase in our lysate or lack of phosphatase inhibitors (which were present in our samples) may aid in our understanding of these results. We did not observe changes in these interactions with the addition of

RNAse A suggesting direct protein-protein interactions that are not dependent on the presence of RNA.

7

DISCUSSION, CONCLUSION AND FUTURE WORKS

7.1 Thesis overview

The overarching aim of this project was to provide a comprehensive analysis of the phenotypic function of LARP1B and explore the interplay with other LARP family members, namely LARP1. Prior to this study, there remained a lack of understanding surrounding the expression profile and role of LARP1B in cancer whilst the remaining LARPs have established roles in the development and/or progression of various cancers as highlighted in **Table 1.1**. To complete the puzzle, we performed depletion and overexpression functional analyses and uncovered the LARP1B interactome in TGCT cell lines rich in LARP1B expression.

Our early studies exploring the expression of *LARP1B* mRNA across a subset of tissue and cancer types suggested a key role for LARP1B in testicular tissue and TGCT. Interestingly, single cell transcriptomic sequencing in zebrafish testis identified an enrichment of *larp1b* in round spermatids, deeming it a cell-type specific marker gene for zebrafish spermatids[137]. This finding supports a key role for LARP1B in the testis even amongst different vertebrates. Indeed, we found in a human testicular tissue microarray that normal testicular tissue stained strongly for LARP1B protein including the spermatids, whilst TGCT tissue stained significantly less, suggesting abrogated LARP1B expression during TGCT development. In contrast, normal testicular tissue stained weak for LARP1 whereas TGCT tissue stained strongly for LARP1 although this data was non-significant. Whilst TGCT tissue morphology was visibly attenuated compared to normal tissue, we did not conclude this as the reason for the observed changes in LARP1B expression as despite the anatomical changes, LARP1 expression increased. We then approached TGCT cell lines alongside HEK293T human embryonal kidney cells to further characterise LARP1B.

The LARP1B interactome in TGCT cell lines revealed novel biological processes, functions and expression profiles revealing previously unknown characteristics of LARP1B. We identified a number of nuclear and mitochondria-annotated proteins alongside cytoplasmic proteins, and further confirmed nuclear and mitochondrial localisation of LARP1B by immunofluorescence analysis. Whilst LARP1B demonstrated predominantly nuclear localisation, LARP1 presented with primarily cytoplasmic localisation. This was not an unexpected observation as various online resources such as

UniProt highlight nucleocytoplasmic LARP1B localisation and cytoplasmic LARP1 localisation but had not yet been demonstrated *in vitro*.

LARP1B knockdown and overexpression experiments proved vital in establishing the phenotypic role of LARP1B and demonstrated a significant impact on TGCT and HEK293T cell proliferation and viability following LARP1B depletion. In TGCT cell lines, abrogated cell growth was coupled with cytotoxicity and apoptosis activation whilst in HEK293T cytotoxicity and apoptosis were not activated. It may be that LARP1B depletion abrogates cell proliferation and viability through different means in different cell lines, perhaps even in cancer and non-cancer cell lines. The testes and associated tissue are heavily reliant on functional mitochondrial respiration and ATP production[206, 207]. As we observed apoptosis following LARP1B knockdown, we then investigated mitochondrial function under the same conditions and observed significant reductions in basal oxygen consumption, ATP production and maximal respiration coupled with a significant increase in basal glycolysis. Another key function for the mitochondria in testicular tissue is maintenance of intracellular ROS levels which can have strong adverse effects on germ cell differentiation and sperm function if levels are not regulated[212]. We therefore measured intracellular ROS levels by measuring mitochondrial superoxide and observed a substantial increase in intracellular ROS levels in LARP1B-depleted conditions, specifically superoxide anions.

We also addressed the kinetics between LARP1B and LARP1 and found that under certain conditions LARP1B knockdown significantly increased *LARP1* mRNA expression whilst LARP1 protein levels remained unchanged. Similarly, under certain conditions LARP1 knockdown significantly increased *LARP1B* mRNA expression with no appreciable change in LARP1B protein levels. Interestingly, stable LARP1 knockout in HEK293T and OVCAR8 cells also had no observable changes on LARP1B protein expression but induced a significant reduction in *LARP1B* mRNA expression in HEK293T LARP1^{KO} and insignificant reduction in *LARP1B* mRNA expression in OVCAR8 LARP1^{KO}. Stable LARP1 knockout did not alter LARP1B subcellular localisation. We also observed a direct protein-protein interaction between LARP1B and LARP1 in multiple cell lines independent of RNA and found that LARP1 was enriched within the LARP1B interactome in both GCT27 and GCT27CR cells.

7.2 Discussion

7.2.1 LARP1B protects TGCT cells from oxidative stress induced cellular damage and apoptosis

Mitochondria are rightly named "the cellular powerhouse of the cell", mediating energy production in the form of ATP which is necessary for the execution of biological processes[151]. Mitochondrial function, oxidative phosphorylation and energy production are all reliant on mitochondrial protein translation for which RBPs are indispensable. In fact, RBPs play a key role in maintaining cellular metabolic plasticity through oxidative phosphorylation and ATP synthesis which in turn coordinates downstream cellular responses and biological pathways. This regulation by RBPs is highly complex and requires finetuned communications between cytoplasmic and mitochondrial translation as well as nuclear signalling.[180, 181] In the testis, oxidative phosphorylation is the primary energy consumption means with germ cells heavily relying on OXPHOS during differentiation and maturation. Abrogated OXPHOS is associated with low sperm quality and infertility which can have major clinical implications. [207, 208, 239]

The mitochondria are also the primary site of ROS generation during oxidative phosphorylation with an excessive increase in ROS levels due to an imbalance in homeostatic systems resulting in ROS mediated oxidative stress[240]. In the context of testicular tissue and associated germ cells including sperm, excessive ROS is known to have severe effects on sperm quality due to damages to the structural and functional integrity of sperm, also contributing to male infertility[211].

LARP1B depletion was associated with severe adverse effects on the cellular fitness of TGCT cell lines as evidenced by reduced cell proliferation and viability, increased cytotoxicity and apoptosis, mitochondrial dysfunction, and ROS generation. Combined, these characteristics suggested that LARP1B depletion resulted in ROS-mediated mitochondrial dysfunction and apoptosis of TGCT cell lines. Oxidative stress induced by excessive ROS generation can result in mitochondrial membrane potential depolarisation and oxidative phosphorylation disruption resulting in reduced ATP synthesis and apoptosis through caspase activation[241]; which our findings demonstrate. It is also suggested that in response to ROS insults, cancer cells can promote glycolysis in order to

reduce cellular reliance on oxidative phosphorylation thereby reducing intracellular ROS levels[242]. We observed this phenomenon in TGCT cell lines with a significant reduction in oxidative phosphorylation coupled with a slight yet significant increase in glycolysis following LARP1B depletion. Precisely how LARP1B seemingly regulates oxidative stress in TGCT cells remains to be further explored as it may do so in a number of ways.

Further exploration of our identified LARP1B-bound mitochondrial proteins may reveal the mechanisms by which LARP1B regulates mitochondrial function and oxidative stress. It is interesting to note we identified a select few out of the thirteen known mitochondrial-encoded mitochondrial proteins including Cytochrome B and ATP6, in both TGCT cell lines. This is in addition to a plethora of nuclear-encoded mitochondrial proteins and hints at LARP1B localising and interacting with proteins at these sites, functioning within multiple respiratory complexes. In line with this, we observed mitochondrial localisation of LARP1B in TGCT cell lines and identified multiple candidates which compose different respiratory complexes and possible antioxidants. It is possible that LARP1B regulates these proteins to maintain mitochondrial homeostasis including maintenance of intracellular ROS levels and mitochondrial respiration. Thus, LARP1B depletion would abrogate mitochondrial function resulting in an increase in ROS which in turn alters mitochondrial membrane potential and apoptosis activation. In this study we detected only superoxide anions (O_2^-) however it is possible that LARP1B depletion impacts levels of other ROS species such as H_2O_2 which are also worth investigating.

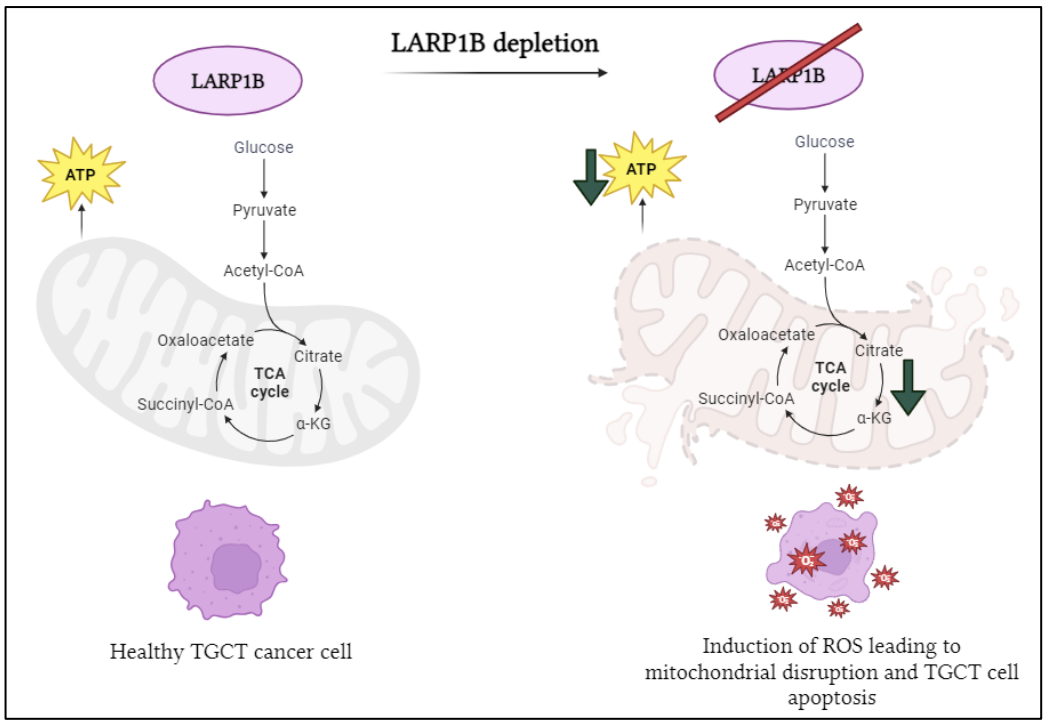

Figure 7.1: Proposed phenotypic role and function of LARP1B. Designed using Biorender.com. *Our findings propose that LARP1B regulates mitochondrial bioenergetics and homeostasis in TGCT cells by maintenance of energy yielding processes namely OXPHOS, and of intracellular ROS levels. Upon LARP1B depletion, OXPHOS capacities are greatly reduced, ATP yields are low and there is an imbalance of intracellular ROS manifesting in oxidative stress induced TGCT cell apoptosis. Original diagram generated using Biorender.*

7.2.2 LARP1B possesses nucleocytoplasmic shuttling capacities and likely corresponding functions

RBPs are ubiquitously expressed within the cell which allows them to accompany mRNA transcripts throughout the RNA life cycle. The subcellular localisation of RBPs largely dictates their function as their nuclear or cytoplasmic residence determines the RNA regulatory process the RBPs are mediating.[7, 13]

Using online resources, we predicted nuclear and cytoplasmic localisation of LARP1B which would contrast known cytoplasmic localisation of LARP1. Both LARPs were predicted to possess nuclear localisation and export sequences with high level of probability suggesting that LARP1B and LARP1 are capable of nuclear-cytoplasmic

shuttling. Our predictions were confirmed with subcellular fractionation of TGCT and HEK293T cell lines which demonstrated predominantly nuclear but also cytoplasmic localisation of LARP1B and predominantly cytoplasmic with minimal nuclear localisation of LARP1. Immunofluorescence analysis supported our subcellular fractionations with a clear overlap of LARP1B with nuclear DAPI and cytoplasmic staining of LARP1. Our LARP1B interactome study supported our findings with a number of nuclear and cytoplasmic candidates identified as potential LARP1B-interactors.

Prior to this study, the subcellular distribution pattern of LARP1B in mammalian cancer cell lines had not been recognised and so it was interesting to find nuclear-cytoplasmic distribution of LARP1B. In our opinion, one of the most interesting nuclear candidates identified was PABPN1, the nuclear isoform of PABP, which has key roles in mRNA transcript polyadenylation within the nucleus and is essential for poly(A) polymerase activity[243]. Within the cytoplasm, PABPN1 is involved in the pioneer round of translation and mRNA deadenylation[244]. Like PABPN1, a number of nuclear annotated candidates possess multiple nucleocytoplasmic cellular functions further supporting the shuttling capacities and diverse RBP functionalities of LARP1B. RBP localisation and nucleocytoplasmic distribution has been attributed to the mRNA in these regions in dictating RBP movements.

Given that nuclear localisation of LARP1B was also observed in non-cancerous HEK293T cells as well as TGCT cancer cell lines, these findings suggest that the observation was not cellular mis-localisation due to disease. Nevertheless, investigation of the subcellular distribution of LARP1B under different conditions would provide us with further information on the nuclear function and nucleocytoplasmic shuttling capabilities of LARP1B. A normal testicular cell line would pose as an improved non-cancer model and induction of various stressors would further reveal to us whether changes in cellular conditions alter LARP1B localisation and thus interactions and function.

7.2.3 LARP1B and LARP1 dynamics hint at compensatory and regulatory functions

LARP1B is likely a product of a gene duplication event resulting in the generation of two full length LARP1 proteins, deeming them protein paralogs[39]. Protein paralogs share a

similar sequence and often biological function whilst also exhibiting their own set of characteristics. By sharing some commonalities paralogs may have redundant, non-redundant or compensatory interactions. Redundancy refers to the ability of paralogous proteins in carrying out the same functions thus contributing to the same biological process which can add a level of genetic robustness. This is despite the evolutionary pressures that cause genes to diverge. Compensation enables one paralog to take on the functions of the other due to changes in expression. As such, paralogous pairs are potential targets of synthetic lethality as targeting both proteins can have a more significant impact on biological functions, than targeting one. [245-248]

We observed distinct subcellular localisation patterns between LARP1B and LARP1 in various cell lines; LARP1B was predominantly nuclear but also demonstrated cytoplasmic localisation whilst LARP1 was largely cytoplasmic with minimal nuclear localisation. The fact that they share localisation whilst also existing in distinct subcellular regions, suggests they possess shared and distinct functionalities. PABP paralogs PABPN1 and PABPC1 demonstrate predominantly nuclear and cytoplasmic localisation respectively, whilst PABPN can also shuttle into the cytoplasm, so both exhibit shared and distinct localisation patterns. Whilst both proteins are capable of binding to polyadenylated RNA they bind and regulate different RNA types with variable degrees of stability and translation efficiency.[249] Thus, it is possible that like PABP paralogs, LARP1B and LARP1 demonstrate similar subcellular distribution patterns which may transpire into both binding similar RNA transcripts but with but with differing binding affinities. Phillippe et al 2020., demonstrated that both LARP1B and LARP1 bind the 5'CAP and regulate TOP mRNAs[49]; this is likely attributed to cytoplasmic LARP1B and LARP1. The function of nuclear LARP1B remains unknown and due to time constraints, we were unable to further explore this in our investigations. Further, a large fraction of nuclear proteins were identified as LARP1B interactors which were not identified within the LARP1 interactome of OVCAR8 cell lines further adding to their functional differences.

We investigated the impact of LARP1 transient and stable depletion on the expression of LARP1B mRNA and protein. Under certain conditions, namely transient siRNA knockdown in GCT27CR cells, LARP1 knockdown significantly increased *LARP1B* mRNA levels. These effects were not observed in GCT27 cell lines or in HEK293T and

OVCAR8 LARP1^{KO} cells. Under the latter conditions, *LARP1B* mRNA expression was in fact reduced albeit non-significantly in OVCAR8. Perhaps this reflects different dynamics between LARP1B and LARP1 under certain conditions i.e., transient vs stable knockdown but also amongst different cell lines. Phillipe et al 2020., demonstrated that LARP1 CRISPR knockout in HEK293T cells led to a significant increase in *LARP1B* mRNA expression[49]. Although this finding contrasts our own, it is interesting that they observed what we found in GCT27CR cells, and it is possible that depending on the surrounding cellular microenvironment, LARP1B is able to compensate for the loss of LARP1 reflected in an increase in mRNA expression. Conversely, it is possible that LARP1 negatively regulates *LARP1B* mRNA which would also be reflected by an increase in LARP1B mRNA expression following LARP1 knockdown. Under no condition of LARP1 depletion did we observe appreciable changes in LARP1B protein expression or subcellular distribution. Perhaps, cytoplasmic LARP1B is capable of overtaking the functions of LARP1 following its loss without observable changes. It is also possible that LARP1 post-transcriptionally regulates LARP1B and so in response to LARP1 knockdown, LARP1B mRNA expression is increased as observed in GCT27CR cells.

A single RNA transcript can be accompanied by a plethora of proteins including RBPs as singular proteins or within larger complexes, which collaborate to perform their RNA regulatory functions[250]. Our co-IP experiments revealed direct protein-protein interactions between LARP1B and LARP1 independent of RNA owing to the maintenance of these interactions following RNAse A treatment. An interesting hypothesis is that the 5'TOP binding and regulatory function attributed to LARP1 may also be attributed to the LARP1B-LARP1 complex. As mentioned, both LARP1B and LARP1 are capable of binding the 5'Cap and TOP sequences[48] and we show here that they form direct protein-protein interactions. LARP1 is also suggested to form homodimers[50] but it is also possible that LARP1 heterodimerises with LARP1B to together perform these mRNA regulatory functions at the 5'Cap and TOP sequences together as one comples. Indeed, there is evidence of protein paralogs heterodimerizing forming highly stable dimeric complexes with different regulatory outcomes to homodimers[251, 252]. This may also explain the apparent high stability of LARP1B and challenges in depleting LARP1B protein.

7.3 Conclusion

In summary, this project characterises LARP1B as regulator of TGCT cell fitness and metabolism by maintaining levels of intracellular mitochondrial ROS perhaps through ROS quenching or maintenance of mitochondrial function and membrane potential. Through loss of function and gain of function experiments, we have identified significant impacts of LARP1B depletion on cell proliferation, viability, survival, mitochondrial function, and oxidative stress which can have significant further implications in the surrounding tumour microenvironment. As evidence suggests highest expression of LARP1B in the testes amongst different mammalian tissue types coupled with significant loss of LARP1B mRNA expression in TGCT, the phenotype we have observed upon LARP1B loss is particularly important for the surrounding testicular microenvironment. If our *in vitro* findings reflect what occurs *in vivo* during TGCT development, the oxidative stress induced due to loss of LARP1B may be a key contributor to TGCT development. Not only is oxidative stress a major contributor to tumorigenesis[253] but also of male infertility which is itself a risk factor for TGCT[193, 211].

7.4 Limitations of the study

This study is the first to describe phenotypic characteristics and functions of LARP1B, particularly in a cancer model. As such, there remains a lack of extensively validated and optimised research tools which was one of the challenges faced in this project. A key limitation in this study was the lack of stable LARP1B knockout cell lines and similarly stable LARP1B-expressing cell lines. It is a well-known fact that transient knockdown and overexpression techniques introduce variability in transfection efficiency which can introduce further variability downstream. Stable cell lines such as LARP1B CRISPR knockout or LARP1B-Myc/Flag stable expression cell lines would overcome the technical variability introduced with transient transfection. This would also enable further optimisation and validation of the anti-LARP1B antibody.

Building on this, the lack of such cell lines prevented us to perform phenotypic rescue experiments by re-expressing LARP1B in LARP1B-null cell lines. Instead, we resorted to re-expressing the LARP1B-Myc/Flag construct in parallel to LARP1B knockdown in

HEK293T cells to compare the phenotypes, but this is not an adequate representation of "rescue experiments".

Finally, all works in this project were performed *in silico* and *in vitro*. Due to the novelty of this study, *in vivo* research models were beyond the scope of this project but would be necessary to confirm the phenotypic and functional role for LARP1B in TGCT. We also lacked normal testicular cell lines which would have posed as a better comparison to TGCT cell lines than HEK293T cells.

7.5 Future works

This project provides the groundwork for extensive further investigation into the role of LARP1B in cancer and normal physiology. As emphasised throughout this thesis, there is little understanding of how LARP1B executes its RNA binding functions in a normal or cancer setting unlike paralog LARP1 which is an established regulator of 5'TOP mRNAs and numerous other transcripts that regulate key cellular processes as discussed. It is therefore imperative to determine the same characteristics for LARP1B.

7.5.1 Determining the complete LARP1B interactome

Due to time constraints, only a single biological replicate was submitted for co-IP MS analysis; to confirm the protein interactors of LARP1B, these experiments would require at least two more repetitions preferably with RNAse treatment to rule out protein-protein interactions mediated by RNA. To support this, RNA-IP followed by next generation sequencing (RIP-Seq) would further reveal the mRNA interactors of LARP1B which together with the co-IP MS candidates would establish a complete interactome in TGCT cell lines.

I am currently in the process of preparing for RIP-seq in OVCAR8 LARP1^{WT} and LARP1^{KO} cell lines which will provide us with vital information on their paralogous relationship and how, if at all, depletion of LARP1 impacts the LARP1B interactome. Co-IP MS and RIP-Seq in LARP1B WT and deficient conditions in various subcellular compartments would also prove critical in determining the genome-wide impact of LARP1B depletion.

Although we set out to explore the interplay of LARP1B with other LARP family members, we focused on LARP1. Interestingly, LARP7 appeared within the LARP1B interactome in GCT27 cells; this interaction would require confirmation by immunoblotting, but it would be interesting to determine LARP1B interactions with other LARP family members.

7.5.2 What are the mechanisms behind LARP1B nucleocytoplasmic shuttling?

There are a number of factors dictating the nucleocytoplasmic shutting of proteins including the recognition of NLS and NES sequences by members of the importin[228] or exportin[229] family, respectively. Through online prediction tools, both LARP1B and LARP1 were suggested to possess such domains and in the context of LARP1B, a number of transportin factors were identified within the LARP1B interactome. Site-directed mutagenesis followed by IF or subcellular fractionation would confirm these localisation and export sequences and their capacities to regulate LARP1B shuttling. The LARP1B amino acid sequence also possesses an arginine-glycine (RG)-rich region located at 149-164aa (**supplementary materials Figure 8.6**). Such sequences are known to act as nuclear localisation signals through recognition by transportin proteins[254] and so mutation of this region may also prove valuable in understanding the cellular distribution patterns of LARP1B.

Could the nuclear localisation of LARP1B be dependent on the presence of nuclear RNA? Is LARP1B binding to pre-RNA? Using RNAse to depolymerise RNAs would confirm whether the nuclear localisation of LARP1B is dependent on the presence of RNA.

7.5.3 What are the conditions regulating LARP1B-LARP1 interactions and what does their dynamics mean?

Our co-IP results revealed direct protein-protein interactions between LARP1B and LARP1 that are not mediated by RNA. We also propose the idea that they may heterodimerise to expand or substantiate their gene regulatory functions such as 5'Cap or

TOP mRNA regulation. To support this hypothesis, proximity ligation assays (PLA) could be performed to detect *in situ* protein-protein interactions.

We observed variable effects on LARP1B and LARP1 mRNA and protein expression following reciprocal knockdowns. Our results hinted at a level of compensation or even regulation of LARP1B on LARP1 and vice versa. What are the conditions for this interaction? To determine whether LARP1B and LARP1 functionally compensate for one another, further loss of function and gain of function experiments in reciprocal wildtype and null conditions i.e., double deficient conditions or LARP1B rescue in LARP1^{KO} cells with LARP1B-Myc/Flag expression construct, would support this aim. Such results would also determine whether LARP1B and LARP1 are synthetic lethal paralogs; a concept proposed by Thompson et al., 2021[248]. Whether LARP1B and LARP1 regulate the mRNA expression of one another could further be confirmed in our RIP-Seq experiments.

8

SUPPLEMENTARY MATERIALS

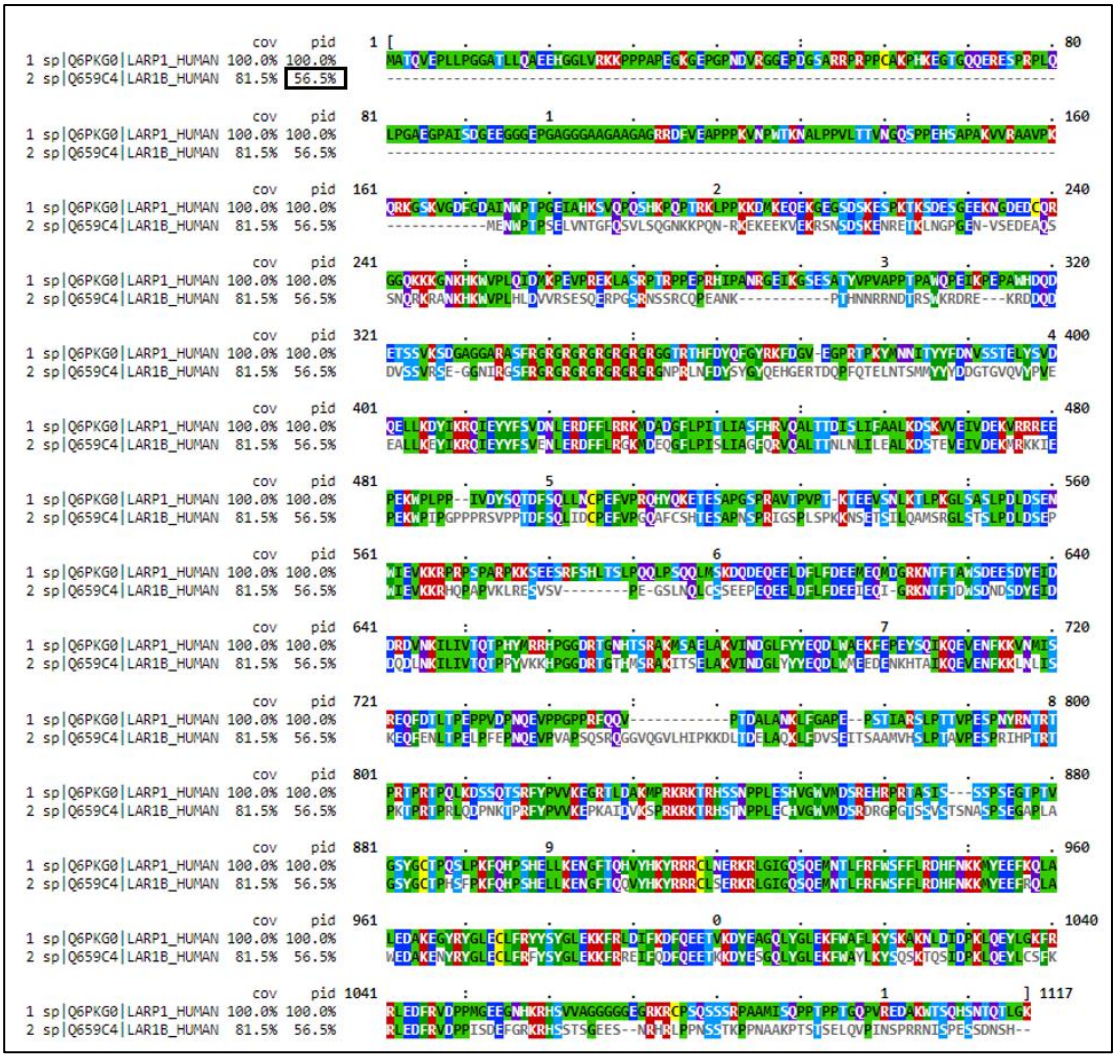

Figure 8.1: LARP1B and LARP1 amino acid sequence alignment reveals 81.5% sequence coverage (cov) and 56.5% percentage identity (pid). *LARP1B isoform 1(Q6PKG0) and LARP1B isoform 1 (Q659C4) amino acid sequences were submitted to Clustal Omega and MView multiple sequence alignment tools for alignment. We identified 81.5% sequence coverage and 56.5% percentage identity shared between the amino acid sequences.*

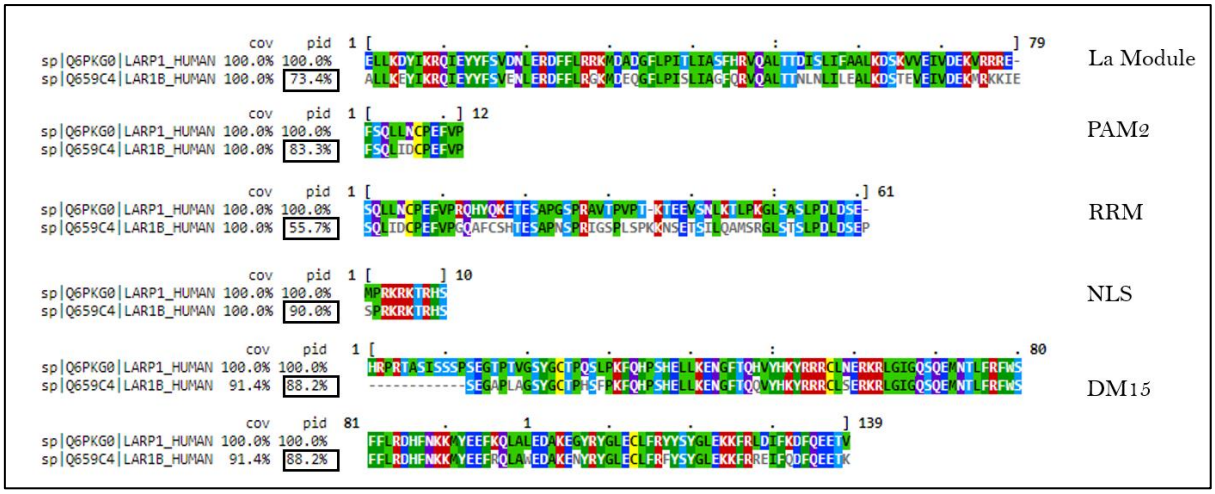

Figure 8.2: LARP1B and LARP1 domains share over 90% sequence coverage (cov) 50% percentage identity (pid). *Sequences encoding LARP1 La Module, PAM2, RRM, NLS and DM15 (isoform 2; Q6PKG0) were aligned against the complete LARP1B isoform 1 (Q659C4) amino acid sequence to determine similarity on Clustal Omega and MView multiple sequence alignment tools.*

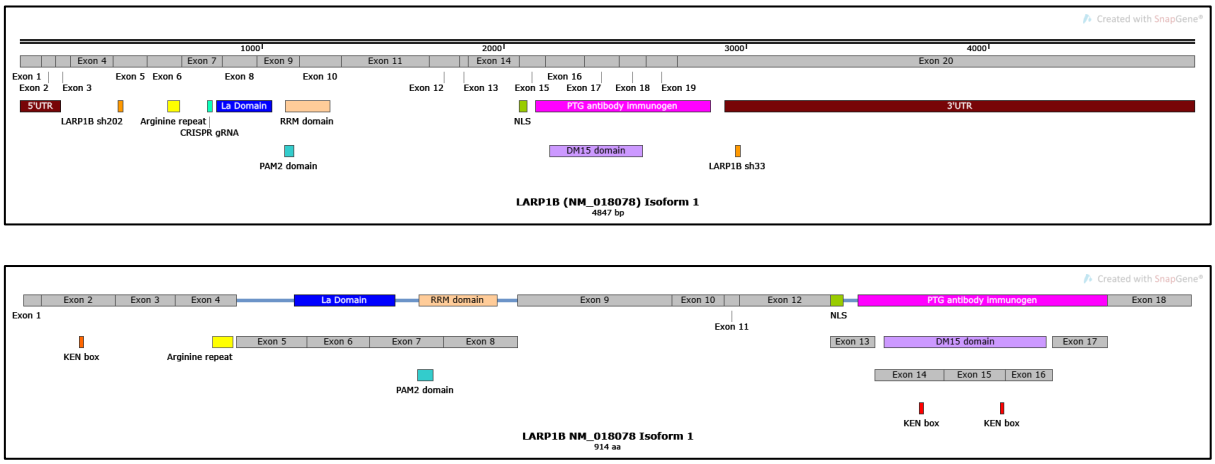

Figure 8.3: LARP1B Isoform 1 (NM_018078) DNA and protein sequence maps annotated with structural domains, antibody immunogens and shRNA targeting sites. *LARP1B isoform sequences were imported into Snap Gene Viewer software for visualisation and annotation. Key domains such as RRM and DM15 domain, arginine repeat, predicted NLS (based on prediction tools described in* ***Results Chapter 2*** *and shRNA sequences are annotated. 5'/3'UTR: 5'/3' un-translated region, sh202/sh33: LARP1B shRNA 202/33, RRM: RNA recognition motif, NLS: nuclear localisation sequence, PTG: Proteintech (antibody) KEN box: KENxxxN motif.*

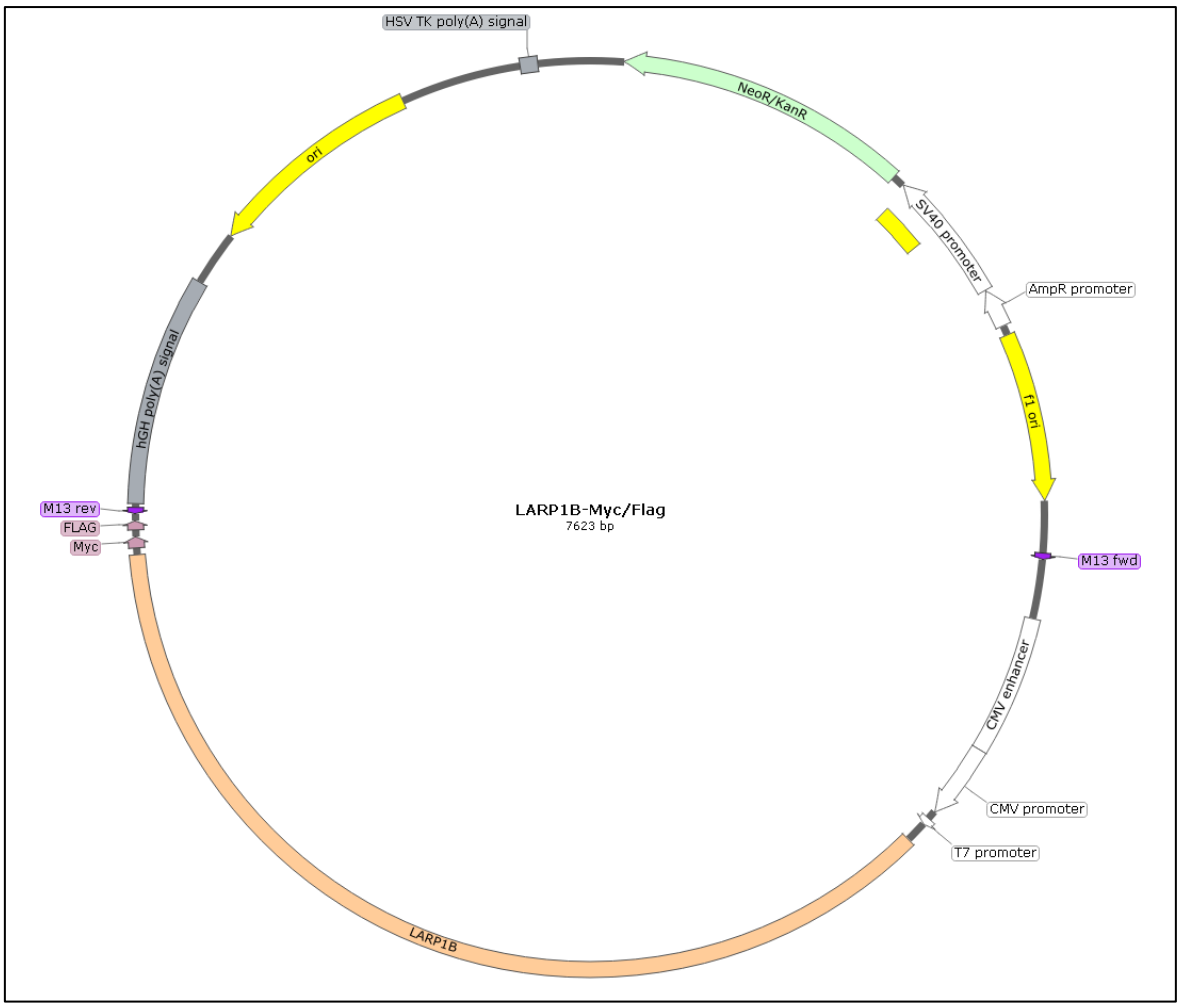

Figure 8.4: LARP1B-Myc/Flag expression construct map. *Expression vector was kindly provided by our collaborator Professor Andrea Bermann for gain of function experiments encoding LARP1B isoform 1 (NM_018078) and Myc-Flag tag. Vector map generated by Snap Gene Viewer software.*

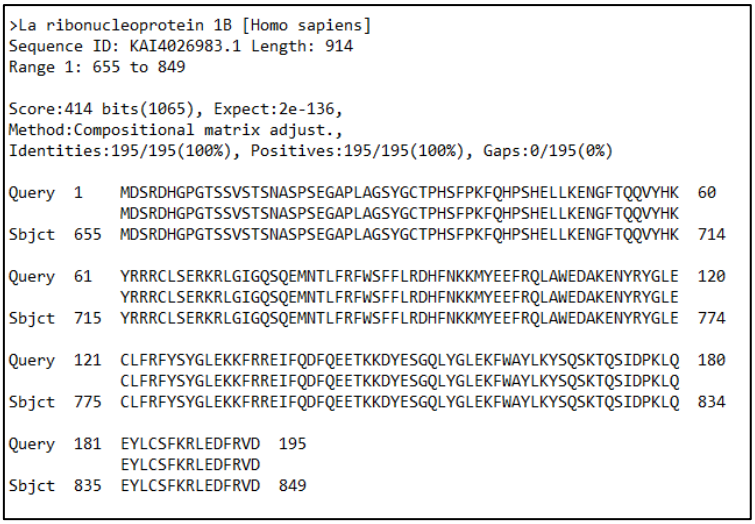

```
>La ribonucleoprotein 1B [Homo sapiens]
Sequence ID: KAI4026983.1 Length: 914
Range 1: 655 to 849

Score:414 bits(1065), Expect:2e-136,
Method:Compositional matrix adjust.,
Identities:195/195(100%), Positives:195/195(100%), Gaps:0/195(0%)

Query  1    MDSRDHGPGTSSVSTSNASPSEGAPLAGSYGCTPHSFPKFQHPSHELLKENGFTQQVYHK  60
            MDSRDHGPGTSSVSTSNASPSEGAPLAGSYGCTPHSFPKFQHPSHELLKENGFTQQVYHK
Sbjct  655  MDSRDHGPGTSSVSTSNASPSEGAPLAGSYGCTPHSFPKFQHPSHELLKENGFTQQVYHK  714

Query  61   YRRRCLSERKRLGIGQSQEMNTLFRFWSFFLRDHFNKKMYEEFRQLAWEDAKENYRYGLE  120
            YRRRCLSERKRLGIGQSQEMNTLFRFWSFFLRDHFNKKMYEEFRQLAWEDAKENYRYGLE
Sbjct  715  YRRRCLSERKRLGIGQSQEMNTLFRFWSFFLRDHFNKKMYEEFRQLAWEDAKENYRYGLE  774

Query  121  CLFRFYSYGLEKKFRREIFQDFQEETKKDYESGQLYGLEKFWAYLKYSQSKTQSIDPKLQ  180
            CLFRFYSYGLEKKFRREIFQDFQEETKKDYESGQLYGLEKFWAYLKYSQSKTQSIDPKLQ
Sbjct  775  CLFRFYSYGLEKKFRREIFQDFQEETKKDYESGQLYGLEKFWAYLKYSQSKTQSIDPKLQ  834

Query  181  EYLCSFKRLEDFRVD  195
            EYLCSFKRLEDFRVD
Sbjct  835  EYLCSFKRLEDFRVD  849
```

Figure 8.5: LARP1B Proteintech antibody immunogen nucleotide BLAST analysis results show complete alignment to LARP1B Isoform 1. *LARP1B immunogen provided by Proteintech was submitted for nucleotide BLAST analysis to determine antibody specificity to targets. Results identified LARP1B protein only including LARP1B Isoform 1 with 100% sequence identity and specificity.*

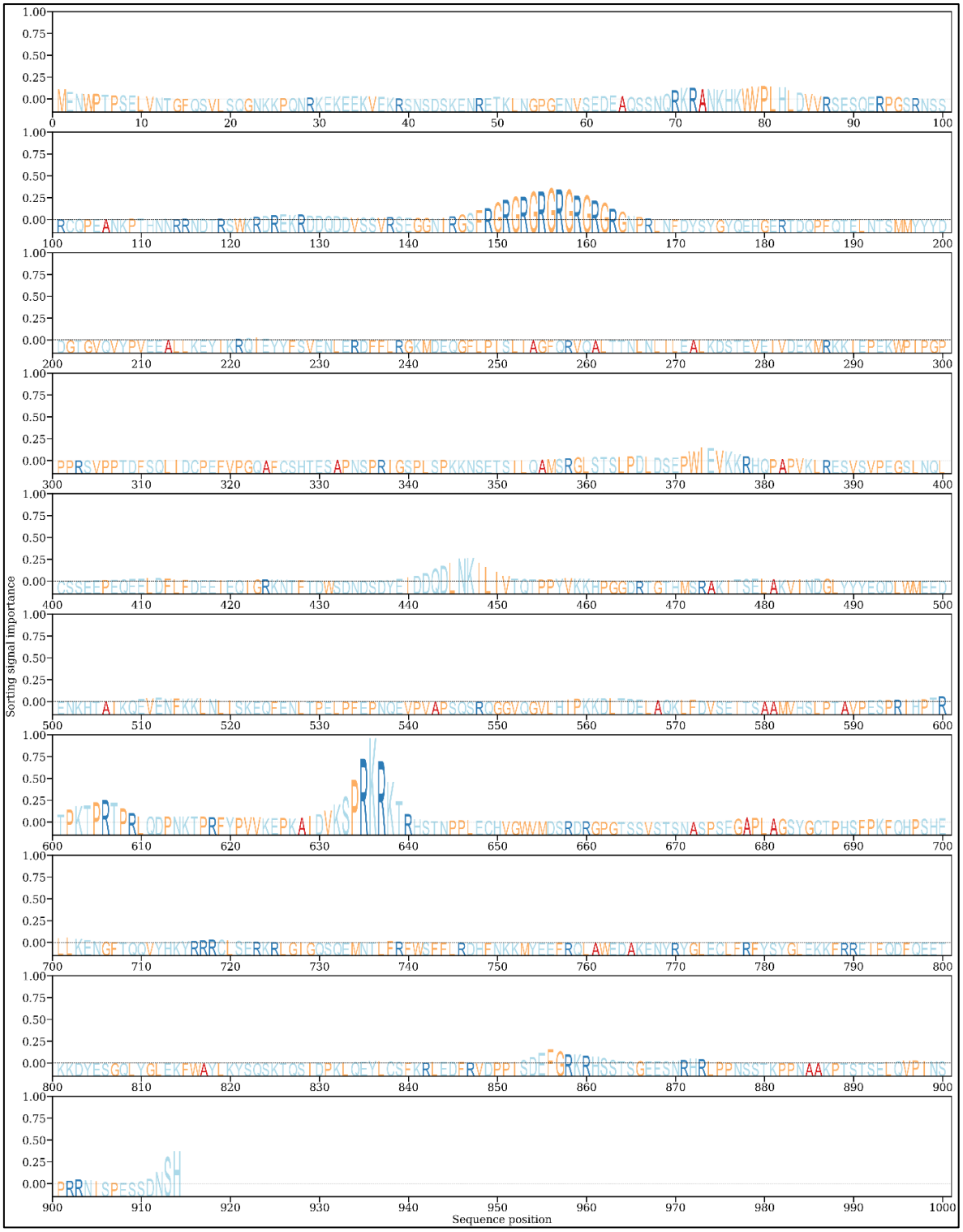

Figure 8.6: DeepLoc 2.0 LARP1B amino acid sequence analysis predicted a potential nuclear localisation sequence (NLS) at 634-643aa and an arginine-glycine (RG)-repeat at 149-164aa which can also function as an NLS. *LARP1B isoform 1 amino acid sequence from UniProt was submitted to DeepLoc 2.0 to predict the presence of NLS domains within LARP1B.*

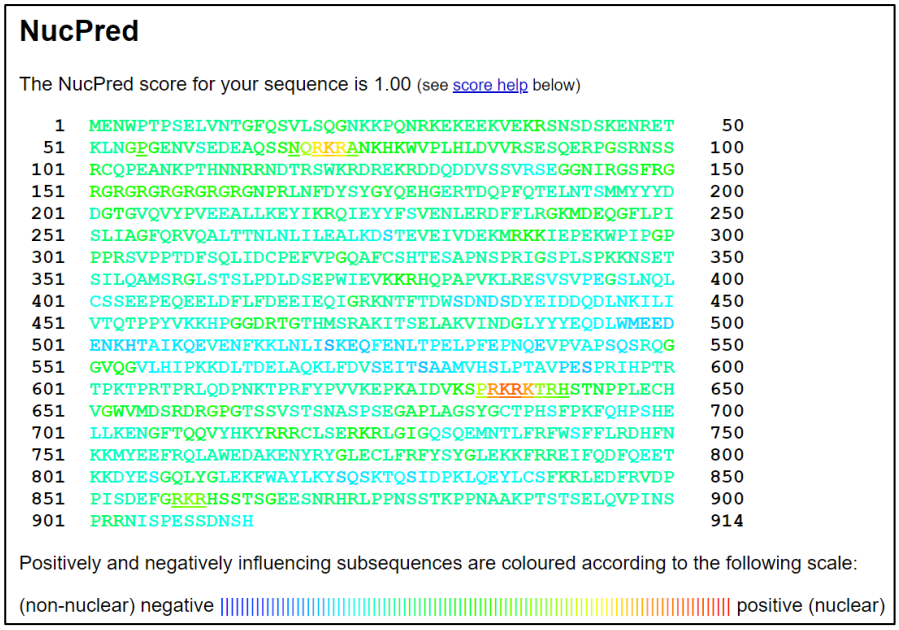

Figure 8.7: NucPred LARP1B amino acid sequence analysis predicted an NLS domain at 634-641aa with a prediction score of 1.00/1.00. *LARP1B isoform 1 amino acid sequence from UniProt was submitted to NucPred sequence predictor to identify the presence of NLS domains within LARP1B to support DeepLoc 2.0 findings in Figure 8.4. A NLS was identified within a region overlapping with DeepLoc 2.0 results.*

Protein Name	Position	Sequence	Score
>LocNES1758938499_0	215-229	LKEYIKRQIEYYFSV	0.011
>LocNES1758938499_0	224-238	EYYFSVENLERDFFL	0.009
>LocNES1758938499_0	254-268	AGFQRVQALTTNLNL	0.420
>LocNES1758938499_0	255-269	GFQRVQALTTNLNLI	0.225
>LocNES1758938499_0	259-273	VQALTTNLNLILEAL	0.152
>LocNES1758938499_0	378-392	RHQPAPVKLRESVSV	0.060
>LocNES1758938499_0	505-519	TAIKQEVENFKKLNL	0.338
>LocNES1758938499_0	520-534	ISKEQFENLTPELPF	0.018
>LocNES1758938499_0	560-574	KKDLTDELAQKLFDV	0.028
>LocNES1758938499_0	834-848	QEYLCSFKRLEDFRV	0.031

Figure 8.8: LocNES LARP1B amino acid sequence analysis predicted ten nuclear export sequences with different prediction scores. *LARP1B isoform 1 amino acide sequence from UniProt was submitted to LocNES NES sequence predictor to identify the presence of possible export sequences. In total ten NESs were predicted with different probabilities depicted as "scores"*

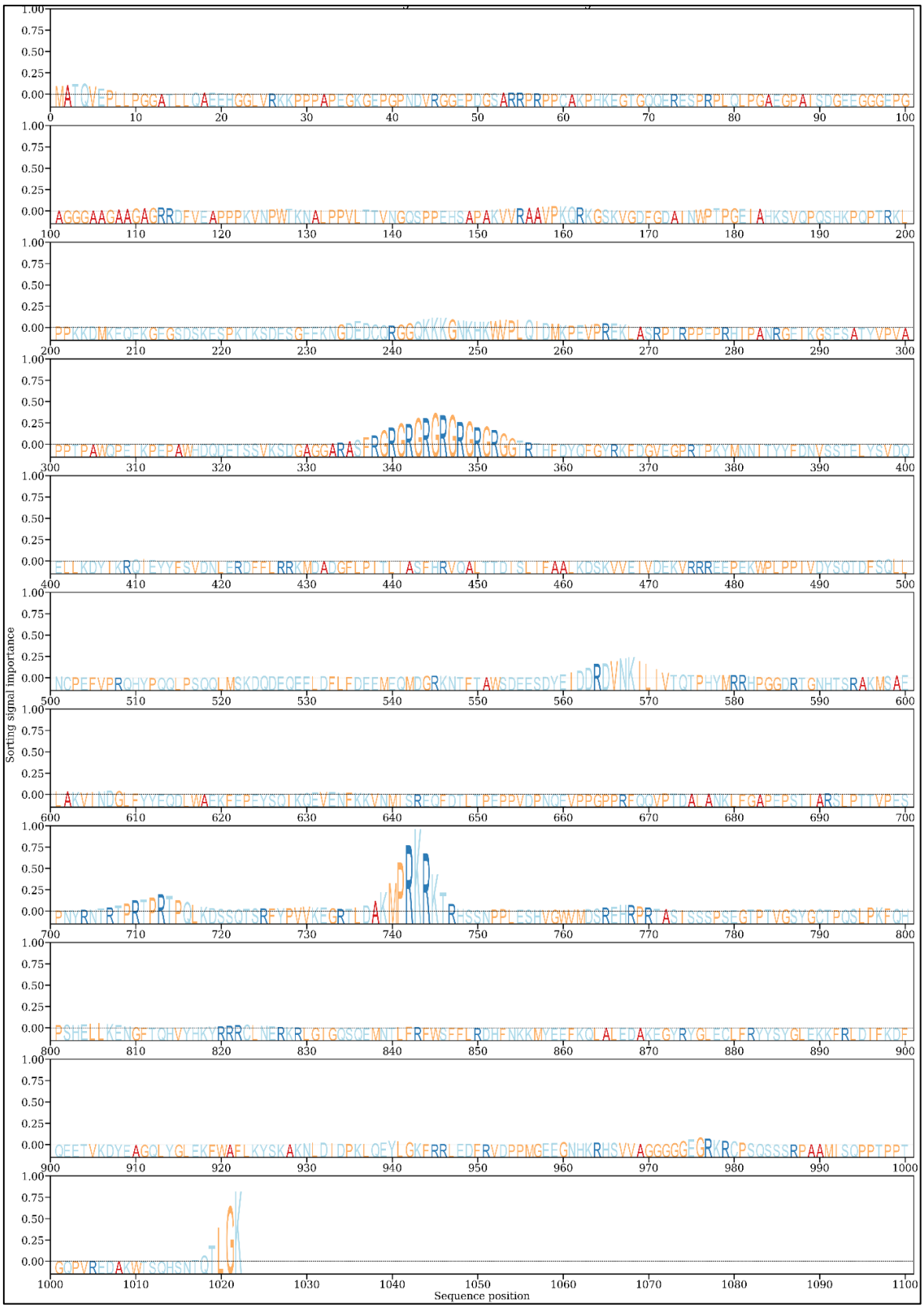

Figure 8.9: DeepLoc 2.0 LARP1 amino acid sequence analysis predicted an NLS at 739-748aa. *LARP1 isoform 2 amino acid sequence from UniProt was submitted to DeepLoc 2.0 to predict the presence of NLS domains within LARP1.*

NucPred

The NucPred score for your sequence is 0.98 (see score help below)

```
   1  MATQVEPLLPGGATLLQAEEHGGLVRKKPPPAPEGKGEPGPNDVRGGEPD   50
  51  GSARRPRPPCAKPHKEGTGQQERESPRPLQLPGAEGPAISDGEEGGGEPG  100
 101  AGGGAAGAAGAGRRDFVEAPPPKVNPWTKNALPPVLTTVNGQSPPEHSAP  150
 151  AKVVRAAVPKQRKGSKVGDFGDAINWPTPGEIAHKSVQPQSHKPQPTRKL  200
 201  PPKKDMKEQEKGEGSDSKESPKTKSDESGEEKNGDEDCQRGGQKKKGNKH  250
 251  KWVPLQIDMKPEVPREKLASRPTRPPEPRHIPANRGEIKGSESATYVPVA  300
 301  PPTPAWQPEIKPEPAWHDQDETSSVKSDGAGGARASFRGRGRGRGRGRGR  350
 351  GRGGTRTHFDYQFGYRKFDGVEGPRTPKYMNNITYYFDNVSSTELYSVDQ  400
 401  ELLKDYIKRQIEYYFSVDNLERDFFLRRKMDADGFLPITLIASFHRVQAL  450
 451  TTDISLIFAALKDSKVVEIVDEKVRRREEPEKWPLPPIVDYSQTDFSQLL  500
 501  NCPEFVPRQHYQKETESAPGSPRAVTPVPTKTEEVSNLKTLPKGLSASLP  550
 551  DLDSENWIEVKKRPRPSPARPKKSEESRFSHLTSLPQQLPSQQLMSKDQD  600
 601  EQEELDFLFDEEMEQMDGRKNTFTAWSDEESDYEIDDRDVNKILIVTQTP  650
 651  HYMRRHPGGDRTGNHTSRAKMSAELAKVINDGLFYYEQDLWAEKFEPEYS  700
 701  QIKQEVENFKKVNMISREQFDTLTPEPPVDPNQEVPPGPPRFQQVPTDAL  750
 751  ANKLFGAPEPSTIARSLPTTVPESPNYRNTRTPRTPRTPQLKDSSQTSRF  800
 801  YPVVKEGRTLDAKMPRKRKTRHSSNPPLESHVGWVMDSREHRPRTASISS  850
 851  SPSEGTPTVGSYGCTPQSLPKFQHPSHELLKENGFTQHVYHKYRRRCLNE  900
 901  RKRLGIGQSQEMNTLFRFWSFFLRDHFNKKMYEEFKQLALEDAKEGYRYG  950
 951  LECLFRYYSYGLEKKFRLDIFKDFQEETVKDYEAGQLYGLEKFWAFLKYS 1000
1001  KAKNLDIDPKLQEYLGKFRRLEDFRVDPPMGEEGNHKRHSVVAGGGGGEG 1050
1051  RKRCPSQSSSRPAAMISQPPTPPTGQPVREDAKWTSQHSNTQTLGK      1096
```

Positively and negatively influencing subsequences are coloured according to the following scale:

(non-nuclear) negative positive (nuclear)

Figure 8.10: ***NucPred LARP1 amino acid sequence analysis predicted an NLS at 739-752aa with a prediction score of 0.98/1.00.*** *LARP1 isoform 2 amino acid sequence from UniProt was submitted to NucPred sequence predictor to identify the presence of NLS domains within LARP1 to support DeepLoc 2.0 findings in Figure 9.6. A NLS was identified within a region overlapping with DeepLoc 2.0 results.*

Protein Name	Position	Sequence	Score
>LocNES635404712_0	297-311	LKEYIKRQIEYYFSV	0.013
>LocNES635404712_0	306-320	EYYFSVENLERDFFL	0.017
>LocNES635404712_0	336-350	AGFQRVQALTTNLNL	0.459
>LocNES635404712_0	337-351	GFQRVQALTTNLNLI	0.219
>LocNES635404712_0	341-355	VQALTTNLNLILEAL	0.128
>LocNES635404712_0	460-474	RHQPAPVKLRESVSV	0.060
>LocNES635404712_0	587-601	TAIKQEVENFKKLNL	0.313
>LocNES635404712_0	602-616	ISKEQFENLTPELPF	0.018
>LocNES635404712_0	642-656	KKDLTDELAQKLFDV	0.028
>LocNES635404712_0	916-930	QEYLCSFKRLEDFRV	0.031

Figure 8.11: LocNES LARP1 amino acid sequence analysis predicted ten nuclear export sequences with different prediction scores. *LARP1 isoform 2 amino acid sequence from UniProt was submitted to LocNES NES sequence predictor to identify the presence of possible export sequences. In total ten NESs were predicted with different probabilities depicted as "scores".*

Protein names	Gene names	Log2 fold change compared to IgG control	Subcellular Location (Protein Atlas annotation)
Nuclear receptor coactivator 5	NCOA5	34.84	Actin filaments;Nucleoplasm (Supported)
Zinc finger CCCH domain-containing protein 13	ZC3H13	33.80	Nucleoplasm (Supported)
Protein timeless homolog	TIMELESS	33.41	Nucleoplasm (Supported)
Splicing factor 3B subunit 2	SF3B2	32.87	Nuclear speckles (Enhanced)
La-related protein 1	LARP1	32.84	Cytosol;Endoplasmic reticulum;Nucleoplasm (Supported)
Chromosome alignment-maintaining phosphoprotein 1	CHAMP1	32.30	Nucleoplasm (Enhanced); Additional: Nuclear bodies
Serum paraoxonase/arylesterase 1	PON1	32.06	N/A
Motile sperm domain-containing protein 2	MOSPD2	31.92	Endoplasmic reticulum (Supported)
Polyadenylate-binding protein 4	PABPC4	31.82	Cytosol (Enhanced)
Aftiphilin	AFTPH	31.60	Cytosol (Supported); Additional: Golgi apparatus;Vesicles
Thyroid hormone receptor-associated protein 3	THRAP3	31.56	Nuclear speckles (Enhanced)
Serine/threonine-protein phosphatase PP1-beta catalytic subunit	PPP1CB	31.35	Nucleoplasm (Supported); Additional: Cytosol
Probable ATP-dependent RNA helicase DDX20	DDX20	31.34	Nuclear bodies (Supported); Additional: Cytosol;Nucleoplasm
La-related protein 1B	LARP1B	31.31	Cytosol (Approved)
Gem-associated protein 4	GEMIN4	31.23	Cytosol;Nuclear bodies (Supported)
Insulin-like growth factor 2 mRNA-binding protein 1	IGF2BP1	31.16	Cytosol (Supported)
Putative helicase MOV-10	MOV10	31.08	Cytosol (Approved)
Myb/SANT-like DNA-binding domain-containing protein 2	MSANTD2	31.01	Nuclear bodies (Supported); Additional: Nucleoplasm
Transformer-2 protein homolog beta	TRA2B	30.99	Nucleoplasm (Enhanced)
Enhancer of rudimentary homolog	ERH	30.89	Nucleoplasm (Approved); Additional: Cytosol
Pericentriolar material 1 protein	PCM1	30.78	Centriolar satellite (Supported); Additional: Cytosol;Nucleoplasm
Methylthioribulose-1-phosphate dehydratase	APIP	30.77	Nucleoplasm (Approved); Additional: Cytosol
G kinase-anchoring protein 1	GKAP1	30.76	Centriolar satellite;Cytosol (Approved)
Cleavage and polyadenylation specificity factor subunit 7	CPSF7	30.42	Nucleoplasm (Supported); Additional: Cytosol
Heterogeneous nuclear ribonucleoprotein U-like protein 2	HNRNPUL2	30.42	Nucleoplasm (Enhanced)
Bcl-2-associated transcription factor 1	BCLAF1	30.34	Nuclear speckles (Enhanced)
Splicing factor 3B subunit 4	SF3B4	30.13	Nuclear speckles (Approved)
BTB/POZ domain-containing protein KCTD3	KCTD3	30.06	Cytosol (Approved)
KH domain-containing, RNA-binding, signal transduction-associated protein 1	KHDRBS1	30.04	Nucleoplasm (Enhanced)
60S ribosomal protein L28	RPL28	30.02	Cytosol;Endoplasmic reticulum (Supported)
rRNA 2-O-methyltransferase fibrillarin	FBL	29.99	Nucleoli fibrillar center (Supported); Additional: Nucleoplasm
Ig heavy chain V-III region	IGHV3-66	29.95	N/A
Heterogeneous nuclear ribonucleoprotein U-like protein 1	HNRNPUL1	29.94	Nucleoplasm (Enhanced)
Serine/arginine-rich splicing factor 10	SRSF10	29.75	Nucleoplasm (Supported)
Histone H1.2	HIST1H1C	29.74	Nucleoli rim;Nucleoplasm (Supported)
Apoptotic chromatin condensation inducer in the nucleus	ACIN1	29.71	Nucleoplasm (Supported); Additional: Cytosol;Plasma membrane
Transformer-2 protein homolog alpha	TRA2A	29.70	Nucleoli (Supported); Additional: Nucleoplasm;Vesicles
Histone deacetylase complex subunit SAP18	SAP18	29.68	Nuclear bodies;Nucleoplasm (Supported); Additional: Cytosol
Scaffold attachment factor B1	SAFB	29.60	Nucleoplasm (Enhanced); Additional: Midbody
Argininosuccinate synthase	ASS1	29.60	Cytosol (Supported); Additional: Nucleoplasm
Protein virilizer homolog	KIAA1429	29.54	Nuclear bodies (Supported); Additional: Nucleoplasm
ATP-dependent RNA helicase DDX18	DDX18	29.51	Mitotic chromosome;Nucleoli;Nucleoli rim (Enhanced)
H/ACA ribonucleoprotein complex subunit 4	DKC1	29.50	Nucleoli fibrillar center (Supported); Additional: Nucleoplasm
U1 small nuclear ribonucleoprotein A	SNRPA	29.50	Nucleoplasm (Supported)
Peroxiredoxin-4	PRDX4	29.49	Endoplasmic reticulum (Supported); Additional: Cytosol
Dihydrolipoyllysine-residue acetyltransferase component of pyruvate dehydrogenase complex, mitochondrial	DLAT	29.49	Mitochondria (Supported)
Histone H1x	H1FX	29.45	Nucleoli;Nucleoplasm (Supported); Additional: Mitotic chromosome;Nucleoli rim

Ribosomal L1 domain-containing protein 1	RSL1D1	29.44	Mitotic chromosome;Nucleoli rim (Enhanced)
RNA-binding protein 45	RBM45	29.37	Nucleoplasm (Supported)
Insulin-like growth factor 2 mRNA-binding protein 2	IGF2BP2	29.33	Cytosol (Enhanced)
Histone H1.4;Histone H1.1	HIST1H1E	29.26	Nuclear speckles (Supported); Additional: Cytosol
Type-1 angiotensin II receptor-associated protein	AGTRAP	29.25	Vesicles (Supported); Additional: Golgi apparatus
DNA replication licensing factor MCM7	MCM7	29.23	Nucleoplasm (Enhanced)
RNA-binding protein with serine-rich domain 1	RNPS1	29.15	Nucleoplasm (Supported)
RNA-binding protein EWS	EWSR1	29.11	Nucleoplasm (Supported); Additional: Nucleoli
DNA topoisomerase 1	TOP1	29.00	Nucleoli fibrillar center;Nucleoplasm (Supported)
Nucleolar protein 56	NOP56	28.98	Nucleoli fibrillar center (Enhanced)
Scaffold attachment factor B2	SAFB2	28.97	Nucleoplasm (Supported); Additional: Nuclear bodies;Vesicles
E3 ubiquitin-protein ligase TRIM4	TRIM4	28.91	Cytosol (Supported); Additional: Plasma membrane
SAFB-like transcription modulator	SLTM	28.90	Nuclear bodies;Nucleoplasm (Enhanced)
Survival motor neuron protein	SMN1	28.87	Cytosol;Nuclear bodies (Supported)
Serine-threonine kinase receptor-associated protein	STRAP	28.82	Cytosol (Enhanced)
Insulin-like growth factor 2 mRNA-binding protein 3	IGF2BP3	28.81	Cytosol (Supported)
Heterogeneous nuclear ribonucleoprotein H2	HNRNPH2	28.81	Nucleoplasm (Enhanced)
Chromatin target of PRMT1 protein	CHTOP	28.79	Nuclear speckles (Supported)
SH3KBP1-binding protein 1	SHKBP1	28.77	Cell Junctions (Approved)
Branched-chain-amino-acid aminotransferase, cytosolic	BCAT1	28.76	N/A
Myb-binding protein 1A	MYBBP1A	28.73	Nucleoli (Supported); Additional: Vesicles
Isoleucine--tRNA ligase, cytoplasmic	IARS	28.70	Cytosol;Nucleoplasm (Approved)
ATP-dependent RNA helicase DDX3X	DDX3X	28.65	Cytosol (Approved); Additional: Nucleoplasm
Interferon-induced, double-stranded RNA-activated protein kinase	EIF2AK2	28.63	Cytosol (Enhanced)
Tubulin alpha-1C chain	TUBA1C	28.55	Microtubules (Supported)
Probable 28S rRNA (cytosine(4447)-C(5))-methyltransferase	NOP2	28.48	Nucleoli (Enhanced)
tRNA-splicing ligase RtcB homolog	RTCB	28.46	Nucleoplasm (Supported); Additional: Cytosol;Vesicles
Protein TFG	TFG	28.44	Vesicles (Supported); Additional: Cytosol
UTP--glucose-1-phosphate uridylyltransferase	UGP2	28.39	Centrosome;Mitochondria (Approved); Additional: Nucleoplasm
Y-box-binding protein 3	YBX3	28.39	Cytosol (Supported)
Pre-mRNA-splicing regulator WTAP	WTAP	28.37	Nuclear speckles (Enhanced)
Signal recognition particle subunit SRP72	SRP72	28.34	N/A
Dolichyl-diphosphooligosaccharide--protein glycosyltransferase 48 kDa subunit	DDOST	28.29	Endoplasmic reticulum (Supported)
Nucleolar protein 58	NOP58	28.23	Nucleoli fibrillar center (Enhanced); Additional: Nucleoplasm
60S ribosomal protein L5	RPL5	28.22	Cytosol;Endoplasmic reticulum (Supported); Additional: Nucleoli;Nucleoli rim
Small nuclear ribonucleoprotein F	SNRPF	28.22	N/A
Complement C5	C5	28.21	N/A
SWI/SNF-related matrix-associated actin-dependent regulator of chromatin subfamily A member 5	SMARCA5	28.21	Nucleoli fibrillar center;Nucleoplasm (Supported)
Dolichyl-diphosphooligosaccharide--protein glycosyltransferase subunit 2	RPN2	28.21	Endoplasmic reticulum (Supported)
YTH domain-containing protein 1	YTHDC1	28.17	Nucleoplasm (Approved); Additional: Plasma membrane
Nucleosome-remodeling factor subunit BPTF	BPTF	28.14	Nucleoplasm (Enhanced)
SRSF protein kinase 1	SRPK1	28.10	Cytosol;Nucleoplasm (Supported); Additional: Plasma membrane
Glycogen phosphorylase, liver form	PYGL	28.07	Cytosol;Plasma membrane (Supported)
Titin	TTN	28.06	N/A
CAD protein	CAD	28.04	Cytosol (Supported)
Serine/arginine-rich splicing factor 9	SRSF9	28.01	Nucleoplasm (Supported); Additional: Nucleoli
Complement C3	C3	28.00	N/A
Sarcoplasmic/endoplasmic reticulum calcium ATPase 2	ATP2A2	28.00	N/A

Vinculin	VCL	27.96	Focal adhesion sites (Enhanced)
Coatomer subunit alpha	COPA	27.91	Cytosol;Nucleoplasm (Approved); Additional: Golgi apparatus
Farnesyl pyrophosphate synthase	FDPS	27.90	Cytosol (Approved); Additional: Nucleoplasm
Double-stranded RNA-binding protein Staufen homolog 1	STAU1	27.88	Cytosol (Enhanced)
Outer dense fiber protein 2	ODF2	27.88	Centrosome (Supported)
U1 small nuclear ribonucleoprotein C	SNRPC	27.87	Nucleoplasm (Enhanced)
Mitogen-activated protein kinase 4	MAPK4	27.86	Golgi apparatus;Nucleoplasm (Approved); Additional: Midbody
Aspartate--tRNA ligase, cytoplasmic	DARS	27.85	Cytosol (Enhanced)
RISC-loading complex subunit TARBP2	TARBP2	27.80	Nucleoplasm (Supported); Additional: Nuclear bodies
Pogo transposable element with ZNF domain	POGZ	27.79	Nucleoplasm (Enhanced)
RNA-binding protein 12B	RBM12B	27.76	Nucleoplasm (Approved)
Ribosomal RNA small subunit methyltransferase NEP1	EMG1	27.75	Nucleoli rim (Supported); Additional: Mitotic chromosome;Nucleoplasm
Serine/arginine-rich splicing factor 1	SRSF1	27.74	Nucleoplasm (Supported)
40S ribosomal protein S20	RPS20	27.74	Cytosol;Endoplasmic reticulum (Supported)
Cullin-associated NEDD8-dissociated protein 1	CAND1	27.74	Cytosol;Golgi apparatus;Nucleoplasm (Enhanced)
Tubulin beta-3 chain	TUBB3	27.69	Microtubules (Approved); Additional: Cytokinetic bridge;Mitotic spindle
UPF0568 protein C14orf166	C14orf166	27.68	Nucleoplasm (Supported)
U5 small nuclear ribonucleoprotein 40 kDa protein	SNRNP40	27.68	Nuclear speckles (Supported)
A-kinase anchor protein 9	AKAP9	27.68	Golgi apparatus (Enhanced); Additional: Centrosome;Vesicles
Histone H1.3	HIST1H1D	27.66	N/A
Nucleolar GTP-binding protein 1	GTPBP4	27.62	Nucleoli;Nucleoli rim (Supported); Additional: Nuclear membrane
Heat shock factor-binding protein 1	HSBP1	27.62	Nucleoli (Supported)
Ribosome biogenesis protein BRX1 homolog	BRIX1	27.57	Mitotic chromosome;Nucleoli (Enhanced)
Ribosomal biogenesis protein LAS1L	LAS1L	27.56	Nucleoplasm (Approved); Additional: Centriolar satellite;Cytosol
Gem-associated protein 7	GEMIN7	27.49	Cytosol;Nucleoplasm (Supported)
Gem-associated protein 2	GEMIN2	27.46	Nuclear bodies;Nucleoplasm (Supported); Additional: Nucleoli
Kinase D-interacting substrate of 220 kDa	KIDINS220	27.44	Nucleoplasm (Approved)
Endoribonuclease Dicer	DICER1	27.44	Cytosol (Supported)
Protein RRP5 homolog	PDCD11	27.40	Nucleoli rim (Supported); Additional: Vesicles
YLP motif-containing protein 1	YLPM1	27.39	Nuclear speckles (Supported)
SNW domain-containing protein 1	SNW1	27.37	Nucleoplasm (Enhanced); Additional: Cytosol
Myosin-10	MYH10	27.35	Actin filaments (Supported); Additional: Cytosol;Mitochondria
Mitochondrial import receptor subunit TOM40 homolog	TOMM40	27.31	Mitochondria (Enhanced); Additional: Cytosol
Apoptosis-inducing factor 1, mitochondrial	AIFM1	27.28	Mitochondria (Supported)
PDZ domain-containing protein 11	PDZD11	27.26	N/A
Cell division cycle 5-like protein	CDC5L	27.22	Nucleoplasm (Supported)
39S ribosomal protein L4, mitochondrial	MRPL4	27.21	N/A
Ankyrin repeat domain-containing protein 11	ANKRD11	27.21	Nucleoplasm (Enhanced); Additional: Cytosol
Nuclear pore membrane glycoprotein 210	NUP210	27.20	N/A
Tubulin beta-6 chain	TUBB6	27.17	Microtubules (Approved); Additional: Cytokinetic bridge;Mitotic spindle
Interferon-induced transmembrane protein 1	IFITM1	27.16	Golgi apparatus (Uncertain); Additional: Cytosol;Plasma membrane
Zinc finger and BTB domain-containing protein 39	ZBTB39	27.10	Vesicles (Approved)
Collagen alpha-1(XVIII) chain;Endostatin	COL18A1	27.09	Golgi apparatus (Approved)
Ragulator complex protein LAMTOR1	LAMTOR1	27.05	Golgi apparatus (Supported); Additional: Plasma membrane;Vesicles
Dynein light chain 1	DYNLL1	27.04	Cytosol;Nucleoplasm (Approved); Additional: Nuclear bodies
Pre-mRNA-splicing factor SLU7	SLU7	27.04	Nucleoplasm (Supported); Additional: Nuclear speckles
Zinc finger RNA-binding protein	ZFR	27.04	Nucleoplasm (Approved)
FACT complex subunit SSRP1	SSRP1	27.03	Cytosol (Uncertain); Additional: Nucleoplasm

CUGBP Elav-like family member 1	CELF1	27.01	Nucleoplasm (Enhanced)
Ras-related GTP-binding protein A	RRAGA	26.99	Golgi apparatus;Vesicles (Approved)
Complement C4-A	C4A	26.99	N/A
Histone-binding protein RBBP7	RBBP7	26.96	Nucleoplasm (Enhanced)
Pleiotropic regulator 1	PLRG1	26.95	Nuclear speckles;Nucleoplasm (Supported); Additional: Nuclear membrane;Nucleoli fibrillar center
N-acetyltransferase 10	NAT10	26.94	Nucleoli (Enhanced); Additional: Midbody
DNA topoisomerase 2-beta	TOP2B	26.90	Nucleoplasm (Enhanced)
RNA binding motif protein, X-linked-like-1	RBMXL1	26.90	Nucleoplasm (Approved)
DNA replication licensing factor MCM4	MCM4	26.89	Nucleoplasm (Enhanced)
Exportin-2	CSE1L	26.88	Nucleoplasm (Enhanced); Additional: Cytosol
Ras-related protein Rab-5C	RAB5C	26.86	Endosomes (Enhanced)
Complement component 1 Q subcomponent-binding protein, mitochondrial	C1QBP	26.86	Plasma membrane (Approved); Additional: Mitochondria
Ribosome production factor 2 homolog	RPF2	26.86	Nucleoli;Nucleoli rim (Supported); Additional: Mitotic chromosome;Nucleoplasm
Tubulin-specific chaperone D	TBCD	26.86	N/A
Zinc finger CCHC domain-containing protein 3	ZCCHC3	26.85	Vesicles (Approved)
U8 snoRNA-decapping enzyme	NUDT16	26.84	Nucleoli;Nucleoplasm (Supported)
Antithrombin-III	SERPINC1	26.77	N/A
Very-long-chain enoyl-CoA reductase	TECR	26.74	Endoplasmic reticulum (Supported)
Polynucleotide 5-hydroxyl-kinase NOL9	NOL9	26.74	Nucleoli (Supported); Additional: Intermediate filaments
Eukaryotic translation initiation factor 4 gamma 1	EIF4G1	26.73	Cytosol (Enhanced)
2,3-cyclic-nucleotide 3-phosphodiesterase	CNP	26.69	Plasma membrane (Approved)
Nuclear cap-binding protein subunit 1	NCBP1	26.64	Cytosol (Supported); Additional: Nucleoplasm
Gem-associated protein 6	GEMIN6	26.61	Nuclear bodies;Nucleoplasm (Supported)
Thioredoxin-related transmembrane protein 1	TMX1	26.60	Endoplasmic reticulum (Supported); Additional: Nucleoli
Tubulin gamma-1 chain	TUBG1	26.59	N/A
Voltage-dependent anion-selective channel protein 3	VDAC3	26.56	Mitochondria (Supported)
Serine/threonine-protein phosphatase 2A 55 kDa regulatory subunit B alpha isoform	PPP2R2A	26.56	Cytosol (Approved)
Regulator of nonsense transcripts 1	UPF1	26.54	Nucleoplasm (Supported); Additional: Cytosol
ELAV-like protein 2	ELAVL2	26.54	Nucleoplasm (Approved); Additional: Cytosol
Peptidyl-prolyl cis-trans isomerase-like 3	PPIL3	26.52	Nucleoplasm (Approved); Additional: Nucleoli
N-acetylserotonin O-methyltransferase-like protein	ASMTL	26.51	Cytosol (Enhanced)
Histone H3	HIST2H3PS2	26.50	Nucleoplasm (Supported)
Pre-mRNA-processing factor 17	CDC40	26.45	Nucleoplasm (Supported)
Cytochrome c oxidase subunit 6C	COX6C	26.45	Mitochondria (Enhanced)
Coatomer subunit beta	COPB1	26.44	Cytosol;Golgi apparatus;Vesicles (Enhanced)
Disks large homolog 5	DLG5	26.41	Cell Junctions (Supported)
Endophilin-A2	SH3GL1	26.37	Cytosol (Enhanced)
Arginine--tRNA ligase, cytoplasmic	RARS	26.35	Cytosol (Supported); Additional: Nucleoli;Nucleoplasm
KH domain-containing, RNA-binding, signal transduction-associated protein 3	KHDRBS3	26.33	Nucleoplasm (Supported)
Cytochrome b5 type B	CYB5B	26.31	Endoplasmic reticulum (Approved); Additional: Centriolar satellite;Cytosol
Double-stranded RNA-binding protein Staufen homolog 2	STAU2	26.31	Nucleoplasm (Supported); Additional: Cytosol
Lysine--tRNA ligase	KARS	26.27	Cytosol (Supported); Additional: Plasma membrane
Splicing factor 3B subunit 1	SF3B1	26.27	Nuclear speckles (Enhanced)
Ribosome-binding protein 1	RRBP1	26.25	Endoplasmic reticulum (Enhanced)
Nuclear pore complex protein Nup93	NUP93	26.22	N/A
Spliceosome RNA helicase DDX39B	DDX39B	26.19	Nuclear speckles (Enhanced)
Nucleolar and coiled-body phosphoprotein 1	NOLC1	26.18	Nucleoli fibrillar center (Enhanced)
Gem-associated protein 8	GEMIN8	26.18	Cytosol;Nucleoplasm (Supported)

ATP synthase subunit g, mitochondrial	ATP5L	26.18	Mitochondria (Supported)
Ragulator complex protein LAMTOR3	LAMTOR3	26.18	N/A
DnaJ homolog subfamily A member 1	DNAJA1	26.16	Cytosol (Supported); Additional: Microtubules
C-1-tetrahydrofolate synthase, cytoplasmic	MTHFD1	26.15	Cytosol (Enhanced)
Heterochromatin protein 1-binding protein 3	HP1BP3	26.14	Nuclear speckles (Supported)
Surfeit locus protein 4	SURF4	26.11	Endoplasmic reticulum;Golgi apparatus;Nuclear membrane (Supported); Additional: Cytosol
Sodium/potassium-transporting ATPase subunit alpha-1	ATP1A1	26.10	N/A
Ras GTPase-activating protein nGAP	RASAL2	26.10	Focal adhesion sites;Plasma membrane (Approved)
Dihydropyrimidinase-related protein 5	DPYSL5	26.10	Nucleoplasm (Approved); Additional: Cytosol
MKI67 FHA domain-interacting nucleolar phosphoprotein	NIFK	26.10	Nucleoli;Nucleoli rim (Enhanced); Additional: Mitotic chromosome
Tubulin alpha-4A chain	TUBA4A	26.10	Microtubules (Enhanced)
Tricarboxylate transport protein, mitochondrial	SLC25A1	26.07	N/A
Spermatogenesis-associated protein 5-like protein 1	SPATA5L1	26.06	Nucleoplasm (Approved); Additional: Nucleoli
Prothrombin	F2	26.06	N/A
Puromycin-sensitive aminopeptidase	NPEPPS	26.05	Cytosol (Supported)
AP-2 complex subunit mu	AP2M1	26.04	Plasma membrane (Supported)
Very-long-chain 3-oxoacyl-CoA reductase	HSD17B12	26.04	N/A
Elongation factor 1-alpha 2	EEF1A2	26.03	Cytosol (Approved); Additional: Nucleoli
39S ribosomal protein L15, mitochondrial	MRPL15	26.03	Mitochondria (Supported)
Dolichyl-diphosphooligosaccharide--protein glycosyltransferase subunit STT3A	STT3A	26.02	N/A
Serine/threonine-protein phosphatase PP1-gamma catalytic subunit	PPP1CC	26.01	Cytosol (Supported); Additional: Vesicles
Nuclear mitotic apparatus protein 1	NUMA1	25.99	Nucleoplasm (Supported); Additional: Cytosol
14-3-3 protein theta	YWHAQ	25.97	Cytosol (Supported); Additional: Nucleoplasm
Protein Hook homolog 1	HOOK1	25.97	N/A
Coatomer subunit delta	ARCN1	25.96	Vesicles (Supported); Additional: Cytosol;Golgi apparatus
NF-kappa-B-activating protein	NKAP	25.95	Nucleoplasm (Supported); Additional: Cytosol
Vesicle-associated membrane protein-associated protein A	VAPA	25.95	Endoplasmic reticulum (Enhanced)
mRNA turnover protein 4 homolog	MRTO4	25.95	Nuclear membrane;Nucleoplasm (Approved); Additional: Nucleoli
Dihydropyrimidinase-related protein 2	DPYSL2	25.94	Cytosol (Supported); Additional: Plasma membrane
5-3 exoribonuclease 2	XRN2	25.93	Nucleoli (Enhanced); Additional: Nucleoplasm
4F2 cell-surface antigen heavy chain	SLC3A2	25.90	Nucleoplasm;Plasma membrane (Approved)
Fragile X mental retardation protein 1	FMR1	25.90	Cytosol (Enhanced)
ER lumen protein-retaining receptor 1	KDELR1	25.88	Golgi apparatus (Supported); Additional: Cytosol;Vesicles
Cytochrome c oxidase subunit 2	MT-CO2	25.88	N/A
Cytochrome c1, heme protein, mitochondrial	CYC1	25.88	Mitochondria (Approved)
U3 small nucleolar RNA-interacting protein 2	RRP9	25.87	Nucleoplasm (Supported)
39S ribosomal protein L2, mitochondrial	MRPL2	25.84	Mitochondria (Supported); Additional: Nucleoplasm
H/ACA ribonucleoprotein complex subunit 1	GAR1	25.83	Nucleoli fibrillar center;Nucleoplasm (Approved)
H/ACA ribonucleoprotein complex subunit 3	NOP10	25.80	Nuclear bodies (Supported)
Ribosome biogenesis regulatory protein homolog	RRS1	25.79	Nucleoli (Supported)
H/ACA ribonucleoprotein complex subunit 2	NHP2	25.79	N/A
Polypyrimidine tract-binding protein 3	PTBP3	25.79	Nucleoplasm (Approved)
T-complex protein 1 subunit eta	CCT7	25.78	Cytosol (Approved)
Protein cornichon homolog 4	CNIH4	25.77	N/A
Fragile X mental retardation syndrome-related protein 1	FXR1	25.76	Cytosol (Enhanced)
60S ribosomal protein L36a-like	RPL36AL	25.75	Cytosol;Endoplasmic reticulum (Approved); Additional: Plasma membrane
E3 ubiquitin-protein ligase Hakai	CBLL1	25.75	Nuclear speckles (Supported)
Complement C1s subcomponent	MASP1	25.74	Cytosol;Nucleoplasm (Enhanced)

IST1 homolog	IST1	25.71	Vesicles (Supported)
Leucine--tRNA ligase, cytoplasmic	LARS	25.69	Cytosol;Nuclear bodies (Approved)
ATPase family AAA domain-containing protein 3A	ATAD3A	25.69	Mitochondria (Enhanced)
Importin-5	IPO5	25.63	Nuclear membrane;Nucleoplasm (Supported); Additional: Cytosol;Golgi apparatus
Nuclear pore complex protein Nup205	NUP205	25.63	N/A
Protein phosphatase 1 regulatory subunit 12B	PPP1R12B	25.60	Actin filaments;Plasma membrane (Approved)
Dynamin-2	DNM2	25.60	Cytosol;Golgi apparatus (Approved)
Glutamine--tRNA ligase	QARS	25.60	Cytosol (Enhanced)
Keratin, type I cytoskeletal 18	KRT18	25.59	Cytosol (Supported)
Histone H3.3	H3F3A	25.58	Nucleoplasm (Supported)
PC4 and SFRS1-interacting protein	PSIP1	25.58	Nucleoplasm (Enhanced)
E3 ubiquitin-protein ligase MIB1	MIB1	25.57	Plasma membrane (Uncertain); Additional: Vesicles
39S ribosomal protein L49, mitochondrial	MRPL49	25.57	N/A
Trifunctional purine biosynthetic protein adenosine-3	GART	25.56	Cytosol (Approved); Additional: Mitochondria
Synaptosomal-associated protein 29	SNAP29	25.55	Cytosol (Supported); Additional: Centrosome
DnaJ homolog subfamily A member 2	DNAJA2	25.53	Cytosol;Nucleoli (Approved); Additional: Intermediate filaments
NADH-cytochrome b5 reductase 3	CYB5R3	25.50	Endoplasmic reticulum (Supported)
Pre-mRNA-splicing factor SPF27	BCAS2	25.50	Centrosome;Nuclear speckles (Supported)
Guanine nucleotide-binding protein-like 3	GNL3	25.48	Nucleoli rim (Enhanced); Additional: Mitotic chromosome;Nuclear bodies
Eukaryotic translation elongation factor 1 epsilon-1	EEF1E1	25.48	Cytosol;Nucleoplasm (Supported)
Serine/threonine-protein phosphatase 2A 65 kDa regulatory subunit A alpha isoform	PPP2R1A	25.47	Cytosol (Approved)
AFG3-like protein 2	AFG3L2	25.46	Mitochondria (Supported)
Pre-mRNA-splicing factor RBM22	RBM22	25.46	Nucleoplasm (Enhanced)
KDEL motif-containing protein 2	KDELC2	25.46	Nucleoplasm (Approved); Additional: Vesicles
Urotensin-2	UTS2	25.45	N/A
Protein BUD31 homolog	BUD31	25.45	Nucleoplasm (Approved); Additional: Centrosome;Microtubules
Protein transport protein Sec61 subunit alpha isoform 1	SEC61A1	25.44	Endoplasmic reticulum (Supported)
Cytochrome c oxidase subunit 4 isoform 1, mitochondrial	COX4I1	25.42	Mitochondria (Supported)
Translocon-associated protein subunit delta	SSR4	25.42	Endoplasmic reticulum (Supported)
Serine/arginine-rich splicing factor 12	SRSF12	25.42	N/A
Cytochrome b-c1 complex subunit 9	UQCR10	25.39	N/A
AP-3 complex subunit delta-1	AP3D1	25.38	Cytosol (Approved)
Putative RNA-binding protein Luc7-like 1	LUC7L	25.37	Nucleoplasm (Approved); Additional: Mitochondria
39S ribosomal protein L44, mitochondrial	MRPL44	25.37	Mitochondria (Approved); Additional: Nuclear bodies;Nucleoplasm;Plasma membrane
39S ribosomal protein L50, mitochondrial	MRPL50	25.36	Mitochondria (Supported); Additional: Cytosol
Protein scribble homolog	SCRIB	25.35	Cell Junctions;Plasma membrane (Enhanced); Additional: Nucleoplasm;Rods & Rings
Peptidyl-prolyl cis-trans isomerase-like 1	PPIL1	25.34	Nucleoli (Supported)
PHD finger protein 6	PHF6	25.33	Nucleoli;Nucleoplasm (Supported)
RuvB-like 1	RUVBL1	25.32	Cytosol;Nucleoplasm (Supported)
60S ribosomal protein L26-like 1	RPL26L1	25.31	Cytosol;Endoplasmic reticulum (Approved); Additional: Nucleoli
Importin-7	IPO7	25.31	Cytosol;Nucleoplasm (Supported)
Mitochondrial carrier homolog 2	MTCH2	25.29	Mitochondria (Approved)
26S proteasome non-ATPase regulatory subunit 2	PSMD2	25.28	N/A
39S ribosomal protein L39, mitochondrial	MRPL39	25.25	Mitochondria (Supported)
Ankyrin repeat domain-containing protein 36C	ANKRD36C	25.25	Cytosol;Nucleoplasm (Approved)
Midkine	MDK	25.25	Vesicles (Approved)
Mitotic spindle assembly checkpoint protein MAD2B	MAD2L2	25.22	Nucleoplasm (Supported)
40S ribosomal protein S28	RPS28	25.20	Cytosol (Approved)

B-cell receptor-associated protein 31	BCAP31	25.13	Endoplasmic reticulum (Enhanced)
Coatomer subunit gamma-1	COPG1	25.13	Golgi apparatus (Supported); Additional: Cytosol;Nucleoplasm
Nucleolar protein 6	NOL6	25.09	Nucleoli (Enhanced); Additional: Nucleoplasm
Transportin-3	TNPO3	25.08	Vesicles (Enhanced)
ATP synthase subunit a	MT-ATP6	25.05	N/A
Signal peptidase complex catalytic subunit SEC11A	SEC11A	25.05	Nuclear membrane (Approved); Additional: Golgi apparatus
Pleckstrin homology-like domain family B member 2	PHLDB2	25.05	Cytosol;Plasma membrane (Supported)
Eukaryotic translation initiation factor 3 subunit I	EIF3I	25.04	Cytosol (Approved)
WD repeat-containing protein 46	WDR46	25.03	Nucleoli (Supported)
Signal peptidase complex subunit 2	SPCS2	25.02	Vesicles (Approved)
Histone H2B type 2-E	HIST2H2BE	25.01	Nucleoplasm (Approved); Additional: Cytosol
ATP-binding cassette sub-family E member 1	ABCE1	24.99	Cytosol (Enhanced)
Histone deacetylase 1;Histone deacetylase 2	HDAC1	24.99	Nucleoplasm (Enhanced)
Transcription intermediary factor 1-beta	TRIM28	24.99	Nucleoplasm (Enhanced)
Antigen KI-67	MKI67	24.98	Nucleoli rim;Nucleoplasm (Enhanced); Additional: Mitotic chromosome;Nuclear bodies
39S ribosomal protein L22, mitochondrial	MRPL22	24.98	Mitochondria (Approved)
Cytochrome b-c1 complex subunit 6, mitochondrial	UQCRH	24.96	N/A
Dolichyl-diphosphooligosaccharide--protein glycosyltransferase subunit DAD1	DAD1	24.96	Cytosol (Uncertain); Additional: Endoplasmic reticulum
Phosphatidylinositol-glycan-specific phospholipase D	GPLD1	24.96	N/A
Eukaryotic translation initiation factor 4E	EIF4E	24.95	Cytoplasmic bodies;Cytosol (Supported); Additional: Nucleoplasm
Translocon-associated protein subunit gamma	SSR3	24.92	N/A
Protein-glutamate O-methyltransferase	ARMT1	24.90	Nuclear bodies (Approved); Additional: Cytosol;Nucleoplasm
Peptidyl-prolyl cis-trans isomerase G	PPIG	24.89	Nuclear speckles (Supported); Additional: Cytosol
CTP synthase 1;CTP synthase 2	CTPS1	24.88	Cytosol (Approved); Additional: Actin filaments
Protein BRICK1	BRK1	24.88	Nuclear speckles (Approved); Additional: Cell Junctions
Solute carrier family 2, facilitated glucose transporter member 1	SLC2A1	24.87	Plasma membrane (Enhanced)
DNA dC->dU-editing enzyme APOBEC-3B	APOBEC3B	24.85	Nucleoplasm (Approved)
39S ribosomal protein L3, mitochondrial	MRPL3	24.85	N/A
Lamin-B1	LMNB1	24.83	Nuclear membrane (Supported)
Transmembrane emp24 domain-containing protein 9	TMED9	24.83	N/A
Elongation of very long chain fatty acids protein 5	ELOVL5	24.82	Endoplasmic reticulum (Enhanced)
Ras-related protein Rab-1A	RAB1A	24.80	Cytosol;Endoplasmic reticulum (Supported)
Probable rRNA-processing protein EBP2	EBNA1BP2	24.80	Nucleoli;Nucleoli rim (Enhanced); Additional: Mitotic chromosome
Mitochondrial import receptor subunit TOM22 homolog	TOMM22	24.80	Mitochondria (Enhanced)
Nuclear pore complex protein Nup160	NUP160	24.78	N/A
Protein FAM98A	FAM98A	24.77	Vesicles (Approved)
Histone H2B type F-S	H2BFS	24.76	Nucleoplasm (Approved); Additional: Cytosol
Neutral amino acid transporter B(0)	SLC1A5	24.73	Plasma membrane (Enhanced)
Tubulin beta-4A chain	TUBB4A	24.73	Microtubules (Supported); Additional: Cytokinetic bridge;Mitotic spindle
ADP-ribosylation factor-like protein 2	ARL2	24.72	Nucleoplasm (Approved); Additional: Cytosol;Focal adhesion sites;Golgi apparatus;Nucleoli
39S ribosomal protein L21, mitochondrial	MRPL21	24.72	Mitochondria;Nucleoplasm (Approved)
Pre-mRNA-splicing factor 38A	PRPF38A	24.72	Nucleoplasm (Enhanced)
Eukaryotic translation initiation factor 3 subunit B	EIF3B	24.71	Cytosol (Approved); Additional: Nucleoplasm
Myeloid leukemia factor 2	MLF2	24.70	Nucleoplasm (Approved); Additional: Cytosol;Plasma membrane
Zinc finger protein 385B	ZNF385B	24.67	Nucleoli fibrillar center (Supported)
Pleckstrin homology domain-containing family A member 7	PLEKHA7	24.60	Cell Junctions;Nucleoplasm (Enhanced); Additional: Cytosol
Eukaryotic translation initiation factor 2 subunit 3	EIF2S3	24.60	N/A
Sterol-4-alpha-carboxylate 3-dehydrogenase, decarboxylating	NSDHL	24.60	Endoplasmic reticulum (Enhanced); Additional: Lipid droplets

60S ribosome subunit biogenesis protein NIP7 homolog	NIP7	24.57	Nucleoli (Supported); Additional: Cytosol;Nucleoplasm
39S ribosomal protein L19, mitochondrial	MRPL19	24.57	Mitochondria (Supported)
Microfibril-associated glycoprotein 4	MFAP4	24.56	Endoplasmic reticulum (Approved)
ER lumen protein-retaining receptor 2	KDELR2	24.53	N/A
Ubiquitin-conjugating enzyme E2 D2	UBE2D2	24.52	Cytosol;Plasma membrane (Approved)
Cilia- and flagella-associated protein 43	CFAP43	24.51	N/A
Hydroxyacyl-coenzyme A dehydrogenase, mitochondrial	HADH	24.50	Mitochondria (Supported)
Erlin-2;Erlin-1	ERLIN2	24.49	Endoplasmic reticulum (Supported)
Magnesium transporter protein 1	MAGT1	24.48	N/A
7-dehydrocholesterol reductase	DHCR7	24.48	Endoplasmic reticulum (Supported)
Cytoplasmic FMR1-interacting protein 1	CYFIP1	24.47	N/A
U2 snRNP-associated SURP motif-containing protein	U2SURP	24.44	Nucleoplasm (Supported)
Vesicle-associated membrane protein 5	VAMP5	24.43	Nucleoplasm;Plasma membrane (Approved)
39S ribosomal protein L43, mitochondrial	MRPL43	24.42	Mitochondria;Nucleoplasm (Approved)
Leucine-rich repeat-containing protein 40	LRRC40	24.42	Nucleoli (Approved)
DNA-directed RNA polymerase II subunit RPB2	POLR2B	24.41	Nucleoplasm (Supported)
Proteasome subunit alpha type-4	PSMA4	24.41	Cytosol;Nucleoplasm (Supported); Additional: Vesicles
Transmembrane emp24 domain-containing protein 2	TMED2	24.41	Vesicles (Supported)
Chromodomain-helicase-DNA-binding protein 6	CHD6	24.40	Nucleoplasm (Supported)
Eukaryotic translation initiation factor 6	EIF6	24.40	Nucleoplasm (Supported)
Myosin-9	MYH9	24.37	Actin filaments;Plasma membrane (Supported); Additional: Cytosol;Nuclear bodies
Sodium/potassium-transporting ATPase subunit beta-3	ATP1B3	24.37	Plasma membrane (Supported)
Ras-related protein Rab-10	RAB10	24.32	N/A
39S ribosomal protein L13, mitochondrial	MRPL13	24.31	N/A
Crooked neck-like protein 1	CRNKL1	24.31	N/A
39S ribosomal protein L17, mitochondrial	MRPL17	24.30	N/A
Protein syndesmos	NUDT16L1	24.29	N/A
RNA-binding protein 25	RBM25	24.24	Nuclear speckles (Enhanced)
Protein transport protein Sec61 subunit beta	SEC61B	24.24	Endoplasmic reticulum (Supported)
Guanine nucleotide-binding protein G(I)/G(S)/G(T) subunit beta-2	GNB2	24.19	Plasma membrane (Supported)
BRCA2 and CDKN1A-interacting protein	BCCIP	24.19	Nucleoplasm (Approved); Additional: Cytosol
Dolichol-phosphate mannosyltransferase subunit 1	DPM1	24.19	N/A
ADP-ribosylation factor-like protein 1	ARL1	24.18	Golgi apparatus (Supported)
Transmembrane and coiled-coil domain-containing protein 1	TMCO1	24.18	Endoplasmic reticulum (Supported)
Delta(24)-sterol reductase	DHCR24	24.18	N/A
Translational activator GCN1	GCN1L1	24.16	Cytosol (Enhanced)
Pachytene checkpoint protein 2 homolog	TRIP13	24.15	Nucleoplasm (Approved)
Eukaryotic translation initiation factor 2 subunit 1	EIF2S1	24.14	Cytosol (Enhanced)
Vacuolar protein sorting-associated protein 33B	VPS33B	24.13	N/A
Copine-3	CPNE3	24.11	Cytosol;Nucleoplasm (Supported)
Nicotinamide phosphoribosyltransferase	NAMPT	24.10	Nuclear speckles (Approved); Additional: Cell Junctions
Guanine nucleotide-binding protein G(I)/G(S)/G(T) subunit beta-1	GNB1	24.10	Plasma membrane (Approved); Additional: Golgi apparatus
T-complex protein 1 subunit epsilon	CCT5	24.09	N/A
26S proteasome non-ATPase regulatory subunit 6	PSMD6	24.07	N/A
Isocitrate dehydrogenase [NAD] subunit beta, mitochondrial	IDH3B	24.06	Mitochondria (Enhanced)
Testis-expressed sequence 10 protein	TEX10	24.05	Nucleoplasm (Approved); Additional: Mitochondria
ADP/ATP translocase 1	SLC25A4	24.05	Mitochondria (Supported)
Alpha-enolase	ENO1	24.05	Cytosol;Plasma membrane (Enhanced)

39S ribosomal protein L51, mitochondrial	MRPL51	24.02	Mitochondria (Supported)
ATP-dependent RNA helicase DHX36	DHX36	24.01	Nucleoplasm (Supported); Additional: Cytosol;Mitochondria
Zinc finger protein RFP	TRIM27	24.01	Nucleoli (Approved); Additional: Nucleoplasm
Solute carrier family 2, facilitated glucose transporter member 3	SLC2A3	24.01	Plasma membrane (Supported)
U4/U6 small nuclear ribonucleoprotein Prp31	PRPF31	23.99	Nucleoplasm (Supported)
CD9 antigen	CD9	23.99	Plasma membrane (Supported)
Putative ATP-dependent RNA helicase DHX33	DHX33	23.98	Nucleoli (Supported)
Phosphatidylserine synthase 1	PTDSS1	23.96	Endoplasmic reticulum (Approved); Additional: Nucleoplasm
HEAT repeat-containing protein 1	HEATR1	23.94	Nucleoli fibrillar center (Enhanced); Additional: Mitochondria
60S ribosomal protein L22-like 1	RPL22L1	23.94	Nucleoli;Nucleoli rim (Approved); Additional: Nucleoplasm
Peptidyl-tRNA hydrolase ICT1, mitochondrial	ICT1	23.94	Mitochondria (Supported); Additional: Nucleoplasm;Plasma membrane
Probable ATP-dependent RNA helicase DDX52	DDX52	23.94	Nucleoli;Nucleoplasm (Supported)
cAMP-dependent protein kinase catalytic subunit gamma	PRKACG	23.93	Cytosol (Approved); Additional: Cytokinetic bridge
Ras GTPase-activating protein-binding protein 1	G3BP1	23.92	Cytosol (Supported)
Dolichyl-diphosphooligosaccharide--protein glycosyltransferase subunit STT3B	STT3B	23.88	Endoplasmic reticulum (Supported)
RNA-binding protein Musashi homolog 2	MSI2	23.87	Cytosol (Supported)
Probable global transcription activator SNF2L1	SMARCA1	23.86	Nucleoplasm (Supported); Additional: Vesicles
Probable ribosome biogenesis protein RLP24	RSL24D1	23.86	Nucleoli;Nucleoli rim;Nucleoplasm (Enhanced)
Plakophilin-4	PKP4	23.85	Cell Junctions (Enhanced); Additional: Plasma membrane
NAD(P) transhydrogenase, mitochondrial	NNT	23.82	Mitochondria (Approved)
39S ribosomal protein L23, mitochondrial	MRPL23	23.82	Mitochondria;Nucleoli fibrillar center (Approved)
Phenylalanine--tRNA ligase alpha subunit	FARSA	23.82	Cytosol (Approved)
DNA replication licensing factor MCM3	MCM3	23.80	Nucleoplasm (Supported)
SURP and G-patch domain-containing protein 2	SUGP2	23.80	Nucleoplasm (Enhanced); Additional: Nuclear bodies
Translocon-associated protein subunit alpha	SSR1	23.79	Endoplasmic reticulum (Supported)
Trifunctional enzyme subunit alpha, mitochondrial	HADHA	23.78	Mitochondria (Enhanced)
Pyrroline-5-carboxylate reductase 1, mitochondrial	PYCR1	23.78	N/A
Calcium-binding mitochondrial carrier protein Aralar2	SLC25A13	23.77	Mitochondria (Supported)
Probable E3 ubiquitin-protein ligase TRIML1	TRIML1	23.77	N/A
U4/U6.U5 tri-snRNP-associated protein 2	USP39	23.77	Nucleoplasm (Supported)
Ras GTPase-activating-like protein IQGAP1	IQGAP1	23.76	Cell Junctions;Plasma membrane (Supported)
ADP-ribosylation factor 5	ARF5	23.76	N/A
E3 ubiquitin-protein ligase TRIM21	TRIM21	23.74	Nucleoplasm (Approved)
U3 small nucleolar RNA-associated protein 15 homolog	UTP15	23.74	Endoplasmic reticulum;Nucleoli (Approved)
F-box/WD repeat-containing protein 11	FBXW11	23.73	Plasma membrane;Vesicles (Approved); Additional: Nucleoplasm
WD repeat-containing protein 43	WDR43	23.68	N/A
G-rich sequence factor 1	GRSF1	23.66	Mitochondria (Enhanced)
DNA mismatch repair protein Msh6	MSH6	23.63	Nucleoplasm (Supported); Additional: Golgi apparatus;Vesicles
Nuclear distribution protein nudE homolog 1	NDE1	23.57	N/A
PCI domain-containing protein 2	PCID2	23.56	Nucleoli;Nucleoplasm (Approved)
Ataxin-10	ATXN10	23.56	Cytosol (Supported); Additional: Plasma membrane
Methylcrotonoyl-CoA carboxylase beta chain, mitochondrial	MCCC2	23.56	Mitochondria (Enhanced)
39S ribosomal protein L47, mitochondrial	MRPL47	23.53	Mitochondria (Supported)
Ubiquitin carboxyl-terminal hydrolase 36	USP36	23.52	Nucleoli;Nucleoli rim (Enhanced); Additional: Nuclear speckles
ADP-ribosylation factor-like protein 6-interacting protein 1	ARL6IP1	23.48	Endoplasmic reticulum (Supported)
ATP-dependent 6-phosphofructokinase, liver type	PFKL	23.47	Mitochondria;Nucleoli (Uncertain)
Ras-related protein Rab-1B	RAB1B	23.46	Golgi apparatus (Supported); Additional: Endoplasmic reticulum
Syntaxin-binding protein 3	STXBP3	23.45	Nucleoplasm (Approved); Additional: Cytosol

Sister chromatid cohesion protein PDS5 homolog A	PDS5A	23.44	Nucleoplasm (Enhanced)
Valine--tRNA ligase	VARS	23.44	Cytosol (Enhanced)
Exportin-T	XPOT	23.40	Nucleoplasm (Enhanced); Additional: Cytosol
Importin-9	IPO9	23.39	Cytosol (Approved); Additional: Vesicles
Importin-11	IPO11	23.39	Nucleoplasm (Supported); Additional: Cytosol
Lysophosphatidylcholine acyltransferase 1	LPCAT1	23.38	Endoplasmic reticulum (Supported); Additional: Lipid droplets
39S ribosomal protein L45, mitochondrial	MRPL45	23.35	Mitochondria (Enhanced)
Structural maintenance of chromosomes protein 4	SMC4	23.34	Cytosol;Nuclear speckles (Supported)
Melanoma-associated antigen D2	MAGED2	23.30	Cytosol;Nucleoli;Nucleoplasm (Enhanced)
Histone H3.1	HIST1H3A	23.29	Nucleoplasm (Supported)
Putative ATP-dependent RNA helicase DHX30	DHX30	23.29	Mitochondria (Supported); Additional: Cytosol
39S ribosomal protein L12, mitochondrial	MRPL12	23.28	Mitochondria (Supported)
RNA-binding protein 3	RBM3	23.26	Nucleoplasm (Enhanced)
Pumilio domain-containing protein KIAA0020	KIAA0020	23.25	Nucleoli (Supported)
Replication factor C subunit 1	RFC1	23.24	Nucleoplasm (Enhanced)
Cyclin-dependent kinase 11A	CDK11A	23.20	Nuclear speckles (Supported); Additional: Cytosol
ATP-binding cassette sub-family F member 1	ABCF1	23.18	Cytosol (Enhanced)
Microsomal glutathione S-transferase 3	MGST3	23.17	Nucleoplasm (Approved)
THO complex subunit 2	THOC2	23.15	Nucleoplasm (Approved)
Fermitin family homolog 2	FERMT2	23.15	Focal adhesion sites (Supported); Additional: Cytosol;Nucleoplasm
Transmembrane protein 14C	TMEM14C	23.04	N/A
Aldehyde dehydrogenase X, mitochondrial	ALDH1B1	23.03	Mitochondria (Supported)
SLIT-ROBO Rho GTPase-activating protein 2B	SRGAP2B	23.02	Cytosol (Approved); Additional: Centrosome
Developmentally-regulated GTP-binding protein 1	DRG1	23.00	Nuclear bodies;Nucleoplasm (Supported); Additional: Cytosol
Tyrosine--tRNA ligase, cytoplasmic	YARS	22.97	Cytosol (Supported); Additional: Nuclear bodies
Transitional endoplasmic reticulum ATPase	VCP	22.97	Cytosol;Nucleoplasm (Enhanced)
Coiled-coil domain-containing protein 77	CCDC77	22.95	Nuclear membrane (Approved)
28S ribosomal protein S35, mitochondrial	MRPS35	22.95	Mitochondria (Approved); Additional: Cytosol
Inosine-5-monophosphate dehydrogenase 2	IMPDH2	22.94	Cytosol (Supported); Additional: Rods & Rings
Superkiller viralicidic activity 2-like 2	SKIV2L2	22.93	Nucleoplasm (Supported)
CCAAT/enhancer-binding protein zeta	CEBPZ	22.93	Vesicles (Approved); Additional: Nucleoplasm
DnaJ homolog subfamily A member 3, mitochondrial	DNAJA3	22.92	Mitochondria (Supported); Additional: Vesicles
Serine/threonine-protein kinase DCLK1	DCLK1	22.90	Nucleoplasm (Approved); Additional: Cytosol
Growth arrest and DNA damage-inducible proteins-interacting protein 1	GADD45GIP1	22.89	Mitochondria (Supported); Additional: Nucleoplasm
Acetyl-CoA carboxylase 1;Biotin carboxylase	ACACA	22.86	Cytosol (Supported); Additional: Actin filaments;Nucleoli fibrillar center
Periphilin-1	PPHLN1	22.85	Nucleoplasm (Supported); Additional: Golgi apparatus
Homeobox protein OTX2	OTX2	22.80	Nucleoplasm (Supported); Additional: Vesicles
U2 small nuclear ribonucleoprotein A	SNRPA1	22.78	Nucleoplasm (Supported); Additional: Nuclear bodies;Nuclear speckles
28S ribosomal protein S5, mitochondrial	MRPS5	22.77	Mitochondria (Supported)
Dual specificity protein kinase CLK3	CLK3	22.76	Nucleoplasm (Supported); Additional: Intermediate filaments
39S ribosomal protein L41, mitochondrial	MRPL41	22.76	Mitochondria (Supported)
39S ribosomal protein L38, mitochondrial	MRPL38	22.74	Mitochondria (Supported)
ATPase family AAA domain-containing protein 3B	ATAD3B	22.73	Mitochondria (Enhanced)
DNA mismatch repair protein Msh2	MSH2	22.71	Nucleoplasm (Supported); Additional: Vesicles
U2 small nuclear ribonucleoprotein B	SNRPB2	22.71	Nuclear speckles (Supported); Additional: Cytoplasmic bodies
Glutamate-rich WD repeat-containing protein 1	GRWD1	22.70	Nucleoli;Nucleoli rim (Enhanced); Additional: Nucleoplasm
AP-1 complex subunit gamma-1	AP1G1	22.69	Golgi apparatus;Vesicles (Enhanced); Additional: Cytosol
Chromodomain-helicase-DNA-binding protein 4	CHD4	22.67	Nucleoplasm (Enhanced)

Methylthioribose-1-phosphate isomerase	MRI1	22.67	Cytosol;Nucleoplasm (Supported); Additional: Nucleoli fibrillar center
DNA replication licensing factor MCM6	MCM6	22.67	Nucleoplasm (Enhanced)
Structural maintenance of chromosomes protein 2	SMC2	22.59	Nucleoplasm (Supported); Additional: Nucleoli
HEAT repeat-containing protein 5B	HEATR5B	22.57	Cytosol;Nuclear speckles;Vesicles (Approved)
N-acylneuraminate cytidylyltransferase	CMAS	22.56	Cytosol (Uncertain); Additional: Nucleoli
Glioma tumor suppressor candidate region gene 2 protein	GLTSCR2	22.55	Nucleoli (Supported)
La-related protein 7	LARP7	22.54	Cytosol;Nucleoplasm (Supported)
pre-rRNA processing protein FTSJ3	FTSJ3	22.52	Nucleoli;Nucleoli rim (Enhanced); Additional: Mitotic chromosome
Eukaryotic translation initiation factor 5B	EIF5B	22.51	Cytosol (Approved); Additional: Plasma membrane
Bromodomain adjacent to zinc finger domain protein 1A	BAZ1A	22.50	N/A
26S proteasome non-ATPase regulatory subunit 12	PSMD12	22.50	Microtubules (Approved); Additional: Cytosol;Nucleoplasm
Glutamine--fructose-6-phosphate aminotransferase [isomerizing] 2	GFPT2	22.46	Vesicles (Approved)
Eukaryotic translation initiation factor 3 subunit E	EIF3E	22.44	Cytosol (Supported)
Pleckstrin homology domain-containing family A member 5	PLEKHA5	22.44	Cytosol;Nucleoplasm (Approved)
E3 ubiquitin-protein ligase TRIP12	TRIP12	22.39	Nuclear speckles (Approved)
Asparagine synthetase [glutamine-hydrolyzing]	ASNS	22.36	Cytosol (Enhanced)
Probable ATP-dependent RNA helicase DDX46	DDX46	22.36	Nuclear speckles (Supported); Additional: Nucleoli fibrillar center
Probable ubiquitin carboxyl-terminal hydrolase FAF-X	USP9X	22.34	Cytosol (Supported)
Something about silencing protein 10	UTP3	22.34	Nucleoli (Supported); Additional: Vesicles
Proteasome activator complex subunit 2	PSME2	22.32	Nucleoplasm (Approved)
Protein transport protein Sec61 subunit gamma	SEC61G	22.31	N/A
Exportin-5	XPO5	22.26	Nucleoplasm (Enhanced); Additional: Cytosol
NADPH--cytochrome P450 reductase	POR	22.25	Vesicles (Approved); Additional: Cytosol;Nucleoplasm
Ras-related protein Rab-3B	RAB3B	22.23	Cell Junctions (Approved)
Rab3 GTPase-activating protein catalytic subunit	RAB3GAP1	22.20	Nucleoplasm (Approved); Additional: Cytosol
Probable ATP-dependent RNA helicase YTHDC2	YTHDC2	22.20	Nucleoplasm (Approved); Additional: Cytoplasmic bodies;Nuclear bodies
GMP synthase [glutamine-hydrolyzing]	GMPS	22.20	Cytosol (Approved)
Cilia- and flagella-associated protein 20	CFAP20	22.19	Nucleoplasm (Supported)
39S ribosomal protein L20, mitochondrial	MRPL20	22.17	Mitochondria (Supported)
Unconventional myosin-Ib	MYO1B	22.17	Plasma membrane (Enhanced)
Pre-mRNA-splicing factor SYF1	XAB2	22.17	Nucleoplasm (Supported); Additional: Vesicles
Phosphatidylinositol glycan anchor biosynthesis class U protein	PIGU	22.16	Nucleoplasm (Approved); Additional: Cytosol
Succinate dehydrogenase [ubiquinone] flavoprotein subunit, mitochondrial	SDHA	22.15	Mitochondria (Supported); Additional: Nucleoli
14-3-3 protein gamma	YWHAG	22.13	Cytosol (Approved)
14-3-3 protein beta/alpha	YWHAB	22.10	Cytosol (Supported)
G patch domain-containing protein 8	GPATCH8	22.09	Nuclear speckles (Approved); Additional: Mitochondria
NADH dehydrogenase [ubiquinone] 1 alpha subcomplex subunit 9, mitochondrial	NDUFA9	22.07	Mitochondria (Approved); Additional: Nucleoplasm
Ribosome biogenesis protein BOP1	BOP1	22.07	Nucleoli;Nucleoli rim (Enhanced); Additional: Mitotic chromosome;Nucleoplasm
Unconventional myosin-Ic	MYO1C	22.07	Nuclear bodies;Plasma membrane (Enhanced)
ATPase family AAA domain-containing protein 2	ATAD2	22.05	Nucleoplasm (Enhanced)
Interferon-inducible double-stranded RNA-dependent protein kinase activator A	PRKRA	22.03	Cytosol (Supported); Additional: Nucleoplasm
Inositol monophosphatase 2	IMPA2	22.02	Nucleoplasm (Approved); Additional: Mitochondria
V-type proton ATPase subunit H	ATP6V1H	22.02	Actin filaments;Cytosol (Supported); Additional: Plasma membrane
Nucleoporin NUP188 homolog	NUP188	22.02	Nucleoplasm (Uncertain); Additional: Cytosol;Nucleoli
CAAX prenyl protease 1 homolog	ZMPSTE24	22.01	N/A
TNF receptor-associated factor 5	TRAF5	21.99	Cytosol (Supported); Additional: Centrosome
Major facilitator superfamily domain-containing protein 10	MFSD10	21.98	Nuclear membrane (Approved); Additional: Nucleoplasm
Saccharopine dehydrogenase-like oxidoreductase	SCCPDH	21.95	Vesicles (Approved)

Protein arginine N-methyltransferase 5	PRMT5	21.93	Cytosol;Nucleoplasm (Supported)
Zinc transporter SLC39A7	SLC39A7	21.92	Endoplasmic reticulum (Supported); Additional: Nucleoplasm
Condensin complex subunit 3	NCAPG	21.91	N/A
Nucleolar protein 11	NOL11	21.90	Nucleoli (Supported)
3-hydroxyacyl-CoA dehydrogenase type-2	HSD17B10	21.88	N/A
Beta-parvin	PARVB	21.87	Actin filaments;Cytosol (Supported)
Transcription factor BTF3	BTF3	21.85	Cytosol (Supported)
Aminopeptidase B	RNPEP	21.85	Golgi apparatus (Approved)
Nuclear pore complex protein Nup107	NUP107	21.84	Nucleoplasm (Uncertain); Additional: Centrosome;Nuclear membrane
Eukaryotic translation initiation factor 4B	EIF4B	21.78	Cytosol (Enhanced)
Spermatid perinuclear RNA-binding protein	STRBP	21.76	N/A
Ubiquitin carboxyl-terminal hydrolase 7	USP7	21.66	Nucleoplasm (Supported); Additional: Nuclear bodies
5-nucleotidase domain-containing protein 2	NT5DC2	21.64	N/A
Lysophospholipid acyltransferase 7	MBOAT7	21.61	Cytosol (Approved)
Cleavage and polyadenylation specificity factor subunit 2	CPSF2	21.60	Nucleoplasm (Approved); Additional: Vesicles
Cytoplasmic dynein 1 light intermediate chain 1	DYNC1LI1	21.58	Centrosome;Cytosol (Supported)
Fanconi anemia group I protein	FANCI	21.56	Nucleoplasm (Enhanced)
Probable ATP-dependent RNA helicase DDX10	DDX10	21.53	Nucleoli (Approved)
Protein SON	SON	21.50	Nuclear speckles (Enhanced)
Lanosterol 14-alpha demethylase	CYP51A1	21.39	Endoplasmic reticulum (Approved)
39S ribosomal protein L40, mitochondrial	MRPL40	21.30	Mitochondria (Supported); Additional: Nucleoli
Probable ATP-dependent RNA helicase DDX47	DDX47	21.30	Nucleoli (Supported)
39S ribosomal protein L30, mitochondrial	MRPL30	21.26	N/A
39S ribosomal protein L28, mitochondrial	MRPL28	21.25	Mitochondria (Supported)
Monocarboxylate transporter 1	SLC16A1	21.24	Cell Junctions;Plasma membrane (Enhanced)
Oxysterol-binding protein-related protein 8	OSBPL8	21.24	Cytosol;Vesicles (Approved)
Coiled-coil domain-containing protein 47	CCDC47	21.21	Endoplasmic reticulum (Enhanced)
Transmembrane emp24 domain-containing protein 5	TMED5	21.20	N/A
Catenin delta-1	CTNND1	21.19	Plasma membrane (Enhanced)
Emerin	EMD	21.14	Nuclear membrane (Enhanced); Additional: Endoplasmic reticulum
Condensin-2 complex subunit D3	NCAPD3	21.13	Nucleoplasm (Supported)
AP-3 complex subunit mu-1	AP3M1	21.12	N/A
ATP-dependent RNA helicase DDX50	DDX50	21.10	Nucleoli (Enhanced)
Actin-related protein 3C	ACTR3C	21.09	N/A
Metaxin-2	MTX2	21.03	Mitochondria (Supported); Additional: Nucleoli
Zinc finger protein 292	ZNF292	21.01	Nuclear membrane;Nucleoplasm (Approved)
Receptor expression-enhancing protein 6	REEP6	21.00	Endoplasmic reticulum (Supported)
Cancer-related nucleoside-triphosphatase	NTPCR	20.98	Cytosol (Approved)
Cytosolic phospholipase A2	PLA2G4A	20.98	Cytosol (Supported); Additional: Vesicles
Coatomer subunit beta	COPB2	20.91	Endoplasmic reticulum (Approved); Additional: Golgi apparatus
Adenylate kinase 2, mitochondrial	AK2	20.88	Mitochondria (Approved)
Cleavage stimulation factor subunit 2 tau variant	CSTF2T	20.85	Nucleoplasm (Enhanced); Additional: Vesicles
Epiplakin	EPPK1	20.83	Intermediate filaments (Enhanced)
Neuroguidin	NGDN	20.83	Mitochondria;Nucleoli (Approved); Additional: Nucleoplasm
Anaphase-promoting complex subunit 7	ANAPC7	20.82	Cytosol;Nucleoplasm (Approved)
AP-2 complex subunit beta;AP-1 complex subunit beta-1	AP2B1	20.80	Vesicles (Supported)
SUMO-activating enzyme subunit 1	SAE1	20.79	Cytosol;Nucleoplasm (Enhanced)
Telomere length regulation protein TEL2 homolog	TELO2	20.78	Cytosol;Nuclear bodies (Supported)

ATP-dependent RNA helicase DDX24	DDX24	20.71	Cytosol;Nucleoli (Approved)
Pentatricopeptide repeat domain-containing protein 3, mitochondrial	PTCD3	20.70	Mitochondria (Supported)
WASH complex subunit 7	KIAA1033	20.66	Nucleoplasm (Enhanced)
E3 ubiquitin-protein ligase UBR4	UBR4	20.63	Nucleoplasm (Supported); Additional: Centrosome;Cytosol
Dynamin-like 120 kDa protein, mitochondrial	OPA1	20.58	Mitochondria;Nucleoplasm (Supported)
S-phase kinase-associated protein 1	SKP1	20.56	Nucleoplasm (Approved); Additional: Cytosol
Electron transfer flavoprotein subunit alpha, mitochondrial	ETFA	20.56	Mitochondria (Enhanced)
Dynamin-1-like protein	DNM1L	20.54	Cytosol (Supported); Additional: Vesicles
RNA-binding protein 28	RBM28	20.46	Nucleoli (Supported)
Mitotic checkpoint serine/threonine-protein kinase BUB1 beta	BUB1B	20.37	Cytosol (Supported)
GTP-binding protein 1	GTPBP1	20.23	Cytosol;Golgi apparatus (Approved); Additional: Nuclear bodies
Kinesin-like protein KIFC1	KIFC1	20.06	Centrosome (Approved)
Protein transport protein Sec61 subunit alpha isoform 2	SEC61A2	19.64	N/A
AT-rich interactive domain-containing protein 3A	ARID3A	19.49	Nucleoplasm (Supported); Additional: Cytosol
Nuclear export mediator factor NEMF	NEMF	19.46	Cytosol;Nucleoplasm (Approved); Additional: Nuclear bodies
Protein deglycase DJ-1	PARK7	19.42	Cytosol;Nucleoplasm (Supported)
Fascin	FSCN1	19.30	Cytosol;Plasma membrane (Approved)
Heterogeneous nuclear ribonucleoprotein Q	SYNCRIP	14.88	Nucleoplasm (Approved); Additional: Cytosol
Interleukin enhancer-binding factor 3	ILF3	13.03	Mitochondria;Nucleoli;Nucleoplasm (Enhanced)
U1 small nuclear ribonucleoprotein 70 kDa	SNRNP70	12.85	Nucleoplasm (Enhanced)
116 kDa U5 small nuclear ribonucleoprotein component	EFTUD2	12.79	Nucleoplasm (Approved); Additional: Cytosol;Vesicles
Polyadenylate-binding protein 1	PABPC1	12.27	Cytosol (Supported)
Protein phosphatase 1 regulatory subunit 12A	PPP1R12A	12.27	Actin filaments;Cytosol (Supported); Additional: Nucleoli;Plasma membrane
Heterogeneous nuclear ribonucleoprotein R	HNRNPR	12.22	Nucleoplasm (Enhanced)
ATP-dependent RNA helicase A	DHX9	11.95	Nucleoplasm (Enhanced); Additional: Nucleoli
Heterogeneous nuclear ribonucleoprotein F	HNRNPF	11.52	Nucleoplasm (Enhanced)
DNA-dependent protein kinase catalytic subunit	PRKDC	11.43	Nucleoplasm (Enhanced)
Heterogeneous nuclear ribonucleoprotein A3	HNRNPA3	11.16	Nucleoplasm (Approved)
U5 small nuclear ribonucleoprotein 200 kDa helicase	SNRNP200	11.14	Nucleoplasm (Supported)
ELAV-like protein 1	ELAVL1	11.06	Nucleoplasm (Supported); Additional: Cytosol;Nucleoli
Heterogeneous nuclear ribonucleoprotein L	HNRNPL	11.02	Nucleoplasm (Enhanced)
Heterogeneous nuclear ribonucleoprotein A0	HNRNPA0	10.91	Nucleoplasm (Enhanced)
Serine/threonine-protein phosphatase PGAM5, mitochondrial	PGAM5	10.85	Mitochondria (Supported)
Probable ATP-dependent RNA helicase DDX17	DDX17	10.74	Nuclear speckles (Supported)
RNA-binding motif protein, X chromosome	RBMX	10.71	Nucleoplasm (Supported)
RNA-binding protein 14	RBM14	10.63	Nuclear speckles (Supported)
Nuclease-sensitive element-binding protein 1	YBX1	10.47	Cytosol (Supported); Additional: Endoplasmic reticulum;Plasma membrane;Vesicles
Heterogeneous nuclear ribonucleoprotein U	HNRNPU	10.46	Nucleoplasm (Supported)
Synergin gamma	SYNRG	10.30	Cytosol (Approved)
TATA-binding protein-associated factor 2N	TAF15	10.12	Nucleoplasm (Enhanced)
Heterogeneous nuclear ribonucleoprotein D-like	HNRNPDL	10.08	Nucleoplasm (Enhanced)
Cytoskeleton-associated protein 4	CKAP4	10.00	N/A
Interleukin enhancer-binding factor 2	ILF2	9.98	Nucleoplasm (Supported); Additional: Cytosol
Pre-mRNA-processing factor 19	PRPF19	9.97	Nuclear speckles (Enhanced)
Heterogeneous nuclear ribonucleoproteins C1/C2	HNRNPC	9.87	Nucleoplasm (Enhanced)
Serine/arginine-rich splicing factor 7	SRSF7	9.76	Nucleoplasm (Enhanced)
Ras-related GTP-binding protein C	RRAGC	9.75	Nucleoplasm;Vesicles (Supported)
Heterogeneous nuclear ribonucleoproteins A2/B1	HNRNPA2B1	9.59	Nucleoplasm (Supported)

Heterogeneous nuclear ribonucleoprotein D0	HNRNPD	9.58	Nucleoplasm (Enhanced)
60S ribosomal protein L6	RPL6	9.53	N/A
Exportin-1	XPO1	9.50	Nuclear membrane;Nucleoplasm (Enhanced); Additional: Cytosol;Vesicles
Heterogeneous nuclear ribonucleoprotein A/B	HNRNPAB	9.45	Nucleoplasm (Enhanced)
60S ribosomal protein L32	RPL32	9.37	Cytosol;Endoplasmic reticulum (Approved)
Nucleolar RNA helicase 2	DDX21	9.37	Mitotic chromosome;Nucleoli rim (Enhanced); Additional: Nucleoplasm
Bifunctional glutamate/proline--tRNA ligase	EPRS	9.33	Cytosol (Enhanced)
Polypyrimidine tract-binding protein 1	PTBP1	9.29	Nucleoplasm (Supported)
RNA-binding protein Raly	RALY	9.29	Nucleoplasm (Enhanced); Additional: Vesicles
DNA topoisomerase 2-alpha	TOP2A	9.28	Nucleoplasm (Supported); Additional: Nucleoli
Clathrin heavy chain 1	CLTC	9.25	Endosomes;Lysosomes (Supported); Additional: Cytosol;Mitotic spindle
Heterogeneous nuclear ribonucleoprotein H	HNRNPH1	9.19	Nucleoplasm (Enhanced)
Heterogeneous nuclear ribonucleoprotein H3	HNRNPH3	9.17	Nucleoplasm (Supported)
60S ribosomal protein L35a	RPL35A	9.14	N/A
Pre-mRNA-splicing factor ATP-dependent RNA helicase DHX15	DHX15	9.09	Nuclear speckles (Enhanced)
Small nuclear ribonucleoprotein Sm D3	SNRPD3	9.08	Nucleoplasm (Supported); Additional: Cytosol;Nuclear bodies
Small nuclear ribonucleoprotein Sm D1	SNRPD1	9.06	N/A
Small nuclear ribonucleoprotein G	SNRPG	9.05	Nucleoplasm (Approved)
Coiled-coil domain-containing protein 61	CCDC61	9.04	Nucleoplasm (Approved)
Cleavage and polyadenylation specificity factor subunit 5	NUDT21	9.01	Nuclear bodies (Supported); Additional: Centriolar satellite
Lupus La protein	SSB	8.99	Nucleoplasm (Approved)
Methionine--tRNA ligase, cytoplasmic	MARS	8.97	Cytosol (Enhanced)
Dolichyl-diphosphooligosaccharide--protein glycosyltransferase subunit 1	RPN1	8.86	Endoplasmic reticulum (Enhanced); Additional: Cytosol
Importin subunit alpha-1	KPNA2	8.83	Nucleoplasm (Enhanced); Additional: Cytosol
Small nuclear ribonucleoprotein-associated protein N	SNRPN	8.83	Nucleoplasm (Approved)
Lamin-B receptor	LBR	8.79	Nuclear membrane (Enhanced)
Polyadenylate-binding protein 2	PABPN1	8.76	Nucleoplasm (Approved); Additional: Nuclear speckles
ATP-citrate synthase	ACLY	8.73	Cytosol (Enhanced); Additional: Nucleoplasm
Small nuclear ribonucleoprotein Sm D2	SNRPD2	8.72	Cytosol (Supported)
Heterogeneous nuclear ribonucleoprotein A1	HNRNPA1	8.65	Nucleoplasm (Supported)
Serpin H1	SERPINH1	8.63	Endoplasmic reticulum (Supported)
Splicing factor, proline- and glutamine-rich	SFPQ	8.59	Nucleoplasm (Enhanced)
40S ribosomal protein S15	RPS15	8.59	Cytosol;Endoplasmic reticulum (Approved)
Small nuclear ribonucleoprotein E	SNRPE	8.47	N/A
40S ribosomal protein S24	RPS24	8.44	Cytosol;Endoplasmic reticulum (Enhanced)
Non-POU domain-containing octamer-binding protein	NONO	8.39	Nucleoplasm (Enhanced); Additional: Nucleoli;Nucleoli fibrillar center
ATP-dependent RNA helicase DDX1	DDX1	8.34	Nucleoplasm (Supported); Additional: Cytosol
Probable ATP-dependent RNA helicase DDX5	DDX5	8.29	Nucleoli;Nucleoplasm (Supported)
40S ribosomal protein S26	RPS26	8.25	Cytosol;Endoplasmic reticulum (Enhanced); Additional: Nucleoli
X-ray repair cross-complementing protein 5	XRCC5	8.21	Nucleoplasm (Supported)
Very-long-chain (3R)-3-hydroxyacyl-CoA dehydratase 3	HACD3	8.21	Endoplasmic reticulum (Enhanced)
Fatty acid synthase	FASN	8.20	Cytosol;Plasma membrane (Enhanced)
60S ribosomal protein L34	RPL34	8.18	Cytosol;Endoplasmic reticulum (Supported); Additional: Nucleoli
ADP/ATP translocase 2	SLC25A5	8.18	Mitochondria (Supported)
Mitochondrial 2-oxoglutarate/malate carrier protein	SLC25A11	8.17	N/A
40S ribosomal protein S11	RPS11	8.13	Cytosol (Approved); Additional: Endoplasmic reticulum;Nucleoli
Histone H3.2	HIST2H3A	8.05	Nucleoplasm (Supported)
Heterogeneous nuclear ribonucleoprotein K	HNRNPK	8.05	Nucleoplasm (Enhanced)

Protein phosphatase 1 regulatory subunit 12C	PPP1R12C	7.98	N/A
X-ray repair cross-complementing protein 6	XRCC6	7.96	Nucleoplasm (Enhanced)
ATP-dependent RNA helicase DDX39A	DDX39A	7.92	Nuclear speckles (Approved)
40S ribosomal protein S6	RPS6	7.91	Cytosol;Endoplasmic reticulum (Enhanced)
Pre-mRNA-processing-splicing factor 8	PRPF8	7.89	Nucleoplasm (Supported)
60S ribosomal protein L14	RPL14	7.89	Cytosol;Endoplasmic reticulum (Supported)
Membrane-associated progesterone receptor component 1	PGRMC1	7.87	Endoplasmic reticulum (Approved); Additional: Nucleoli
TAR DNA-binding protein 43	TARDBP	7.83	Nucleoplasm (Enhanced)
Eukaryotic initiation factor 4A-III	EIF4A3	7.82	Nucleoplasm (Supported)
THO complex subunit 4	ALYREF	7.81	Nuclear speckles;Nucleoplasm (Approved)
60S ribosomal protein L31	RPL31	7.79	N/A
Calnexin	CANX	7.79	Endoplasmic reticulum (Enhanced)
FACT complex subunit SPT16	SUPT16H	7.79	Nucleoplasm (Supported); Additional: Nucleoli fibrillar center
40S ribosomal protein S9	RPS9	7.74	N/A
ATP-dependent 6-phosphofructokinase, platelet type	PFKP	7.74	Cytosol (Supported)
60S ribosomal protein L3	RPL3	7.74	Cytosol;Nucleoli (Supported)
Phosphate carrier protein, mitochondrial	SLC25A3	7.74	Mitochondria (Supported)
Serine/arginine-rich splicing factor 3	SRSF3	7.73	Nucleoplasm (Supported)
40S ribosomal protein S14	RPS14	7.71	Cytosol;Endoplasmic reticulum (Supported)
Vimentin	VIM	7.71	Intermediate filaments (Supported)
Matrin-3	MATR3	7.68	Nucleoplasm (Approved)
Serine/arginine repetitive matrix protein 1	SRRM1	7.61	Nuclear speckles (Enhanced)
60S ribosomal protein L29	RPL29	7.61	Cytosol;Endoplasmic reticulum;Nucleoli (Supported)
26S proteasome non-ATPase regulatory subunit 3	PSMD3	7.59	Nucleoplasm (Approved); Additional: Cytosol
ADP-ribosylation factor 4	ARF4	7.58	N/A
60S ribosomal protein L36a	RPL36A	7.56	Cytosol;Endoplasmic reticulum (Supported); Additional: Plasma membrane
Aminoacyl tRNA synthase complex-interacting multifunctional protein 2	AIMP2	7.55	Cytosol (Approved)
60S ribosomal protein L37a	RPL37A	7.52	Cytosol;Endoplasmic reticulum (Approved)
40S ribosomal protein S3a	RPS3A	7.47	Cytosol;Endoplasmic reticulum;Nucleoli (Enhanced)
Tubulin beta-2B chain	TUBB2B	7.45	Microtubules (Supported); Additional: Cytokinetic bridge;Mitotic spindle
60S ribosomal protein L36	RPL36	7.45	Cytosol (Supported)
Elongation factor Tu, mitochondrial	TUFM	7.44	Mitochondria (Enhanced)
Importin subunit beta-1	KPNB1	7.42	Nuclear membrane (Enhanced); Additional: Cytosol;Nucleoplasm
60S ribosomal protein L23	RPL23	7.42	Cytosol (Supported)
60S ribosomal protein L18a	RPL18A	7.42	Nucleoli (Approved); Additional: Cytosol;Nucleoplasm
Cyclin-dependent kinase 1	CDK1	7.38	Cytosol;Nucleoplasm (Supported)
Tubulin beta-8 chain	TUBB8	7.36	Microtubules (Supported); Additional: Cytokinetic bridge;Mitotic spindle
T-complex protein 1 subunit alpha	TCP1	7.35	N/A
Core histone macro-H2A.1	H2AFY	7.34	Nucleoplasm (Supported)
GTP-binding nuclear protein Ran	RAN	7.33	Nucleoplasm (Enhanced)
40S ribosomal protein S8	RPS8	7.33	Cytosol;Endoplasmic reticulum (Enhanced)
DBIRD complex subunit ZNF326	ZNF326	7.32	Nucleoplasm (Approved); Additional: Golgi apparatus;Vesicles
60S ribosomal protein L23a	RPL23A	7.30	Cytosol;Endoplasmic reticulum;Nucleoli fibrillar center (Approved)
60S ribosomal protein L9	RPL9	7.28	Cytosol;Endoplasmic reticulum (Supported); Additional: Nucleoli
60S ribosomal protein L15	RPL15	7.28	N/A
Cell growth-regulating nucleolar protein	LYAR	7.27	Nucleoli;Nucleoli rim (Enhanced); Additional: Nucleoplasm
Poly(rC)-binding protein 2	PCBP2	7.25	Cytosol;Nucleoplasm (Supported)
60S ribosomal protein L4	RPL4	7.22	Cytosol;Endoplasmic reticulum (Approved); Additional: Nuclear bodies;Nucleoli

Serine/arginine repetitive matrix protein 2	SRRM2	7.21	Nuclear speckles (Enhanced)
60S ribosomal protein L8	RPL8	7.18	Cytosol;Endoplasmic reticulum;Nucleoli (Supported)
60S ribosomal protein L17	RPL17	7.14	Cytosol;Endoplasmic reticulum (Supported)
Ras-related protein Rab-11A	RAB11A	7.14	Centriolar satellite;Vesicles (Enhanced)
60S ribosomal protein L18	RPL18	7.14	Cytosol;Endoplasmic reticulum (Supported); Additional: Nucleoli
Ras-related protein Rab-7a	RAB7A	7.10	Lysosomes (Supported)
60S ribosomal protein L10a	RPL10A	7.10	Cytosol;Endoplasmic reticulum;Nucleoli (Supported)
Luc7-like protein 3	LUC7L3	7.08	Nuclear speckles (Enhanced)
Pinin	PNN	7.06	Nuclear speckles (Supported)
Nucleolin	NCL	7.06	Nucleoli;Nucleoli rim;Nucleoplasm (Enhanced); Additional: Mitotic chromosome
Prohibitin-2	PHB2	7.04	Mitochondria (Enhanced)
L-lactate dehydrogenase A chain	LDHA	7.02	Cytosol (Supported); Additional: Vesicles
Eukaryotic initiation factor 4A-I	EIF4A1	7.01	Cytosol (Approved)
Poly(rC)-binding protein 1	PCBP1	7.00	Nuclear speckles (Supported); Additional: Cytoplasmic bodies;Cytosol;Nucleoplasm
Chromobox protein homolog 3	CBX3	6.97	Nucleoplasm (Supported); Additional: Nuclear bodies
40S ribosomal protein S23	RPS23	6.92	Cytosol (Supported); Additional: Endoplasmic reticulum
Microsomal glutathione S-transferase 1	MGST1	6.92	Mitochondria (Approved); Additional: Endoplasmic reticulum
40S ribosomal protein S2	RPS2	6.88	Cytosol;Endoplasmic reticulum (Approved)
Caspase recruitment domain-containing protein 11	CARD11	6.86	N/A
T-complex protein 1 subunit zeta	CCT6A	6.86	Cytosol (Approved)
Heterogeneous nuclear ribonucleoprotein M	HNRNPM	6.86	Nucleoplasm (Enhanced)
RNA-binding protein FUS	FUS	6.86	Nucleoplasm (Supported)
60S ribosomal protein L27a	RPL27A	6.85	Cytosol;Endoplasmic reticulum (Enhanced)
ATP synthase subunit gamma, mitochondrial	ATP5C1	6.83	N/A
Transmembrane protein 33	TMEM33	6.75	N/A
60S ribosomal protein L21	RPL21	6.72	Cytosol;Endoplasmic reticulum;Nucleoli fibrillar center (Supported)
Elongation factor 1-alpha 1	EEF1A1	6.72	Cytosol (Supported)
40S ribosomal protein S3	RPS3	6.71	Cytosol;Endoplasmic reticulum (Supported)
Guanine nucleotide-binding protein subunit beta-2-like 1	GNB2L1	6.71	Nucleoplasm (Supported); Additional: Cytosol
60S ribosomal protein L26	RPL26	6.71	Cytosol;Endoplasmic reticulum (Approved); Additional: Nucleoli
Microtubule-associated protein 1B	MAP1B	6.70	Cytosol (Enhanced)
60S ribosomal protein L10	RPL10	6.70	Cytosol;Endoplasmic reticulum (Enhanced)
Serine/threonine-protein kinase PRP4 homolog	PRPF4B	6.70	Nuclear speckles (Supported)
40S ribosomal protein S29	RPS29	6.70	Cytosol;Endoplasmic reticulum (Supported)
40S ribosomal protein S17	RPS17	6.65	Cytosol;Endoplasmic reticulum (Approved); Additional: Nucleoli
60S ribosomal protein L13a	RPL13A	6.61	Cytosol;Nucleoli (Approved)
60S acidic ribosomal protein P0	RPLP0	6.61	Cytosol;Endoplasmic reticulum (Supported)
ATP synthase subunit f, mitochondrial	ATP5J2	6.57	Mitochondria (Supported); Additional: Nuclear membrane
Protein LYRIC	MTDH	6.56	Endoplasmic reticulum (Enhanced)
40S ribosomal protein S25	RPS25	6.54	Cytosol;Endoplasmic reticulum (Supported); Additional: Nucleoli
Tubulin beta chain	TUBB	6.52	Microtubules (Supported); Additional: Cytokinetic bridge;Mitotic spindle
40S ribosomal protein S4, X isoform	RPS4X	6.51	N/A
Voltage-dependent anion-selective channel protein 1	VDAC1	6.51	N/A
60S ribosomal protein L11	RPL11	6.49	N/A
40S ribosomal protein S5	RPS5	6.43	Cytosol;Endoplasmic reticulum (Supported)
ADP/ATP translocase 3	SLC25A6	6.42	Mitochondria (Supported)
40S ribosomal protein S10	RPS10	6.35	Cytosol (Approved)
DNA replication licensing factor MCM2	MCM2	6.35	Nucleoplasm (Enhanced)

Leucine-rich repeat-containing protein 59	LRRC59	6.34	Endoplasmic reticulum (Enhanced)
40S ribosomal protein S15a	RPS15A	6.32	N/A
T-complex protein 1 subunit gamma	CCT3	6.29	Cytosol;Plasma membrane (Approved)
40S ribosomal protein S16	RPS16	6.28	Cytosol;Endoplasmic reticulum (Enhanced)
3-beta-hydroxysteroid-Delta(8),Delta(7)-isomerase	EBP	6.27	Endoplasmic reticulum;Nuclear membrane (Supported)
40S ribosomal protein S27	RPS27	6.26	Cytosol;Endoplasmic reticulum (Approved); Additional: Nucleoli
Prohibitin	PHB	6.26	Mitochondria (Supported)
60S ribosomal protein L24	RPL24	6.26	Cytosol;Endoplasmic reticulum (Enhanced)
Eukaryotic translation initiation factor 3 subunit A	EIF3A	6.25	Cytosol;Nucleoplasm (Supported)
60S ribosomal protein L12	RPL12	6.25	Golgi apparatus (Approved)
ATP synthase subunit alpha, mitochondrial	ATP5A1	6.22	Mitochondria (Supported)
Voltage-dependent anion-selective channel protein 2	VDAC2	6.21	Mitochondria (Supported)
T-complex protein 1 subunit beta	CCT2	6.20	Cytosol (Supported)
Tubulin alpha-1A chain	TUBA1A	6.18	Microtubules (Enhanced)
40S ribosomal protein S18	RPS18	6.17	Cytosol (Supported)
Flap endonuclease 1	FEN1	6.16	Nucleoplasm (Enhanced); Additional: Nucleoli
60S ribosomal protein L13	RPL13	6.12	Cytosol;Endoplasmic reticulum;Nucleoli (Enhanced)
60S ribosomal protein L19	RPL19	6.12	Cytosol;Nucleoli (Enhanced)
Signal recognition particle 9 kDa protein	SRP9	6.12	N/A
40S ribosomal protein S13	RPS13	6.06	Endoplasmic reticulum (Approved)
Basigin	BSG	6.04	Vesicles (Approved)
Lamina-associated polypeptide 2, isoforms beta/gamma	TMPO	6.03	Nuclear membrane (Enhanced)
Putative 60S ribosomal protein L39-like 5	RPL39P5	6.03	N/A
Signal recognition particle 14 kDa protein	SRP14	5.99	Nucleoli (Approved); Additional: Nucleoplasm
Splicing factor 3B subunit 6	SF3B6	5.99	Nucleoplasm (Supported)
Protein arginine N-methyltransferase 1	PRMT1	5.96	Nucleoplasm (Supported)
Histone H4	HIST1H4A	5.93	N/A
Activator of 90 kDa heat shock protein ATPase homolog 1	AHSA1	5.90	Cytosol (Supported)
60S acidic ribosomal protein P2	RPLP2	5.88	Cytosol;Nuclear speckles (Approved); Additional: Mitotic spindle
60S ribosomal protein L30	RPL30	5.88	Cytosol;Endoplasmic reticulum (Approved)
D-3-phosphoglycerate dehydrogenase	PHGDH	5.83	Cytosol;Plasma membrane (Enhanced); Additional: Nucleoplasm
Histone H2A type 1-C	HIST1H2AC	5.82	Nucleoplasm (Supported)
Tubulin beta-4B chain	TUBB4B	5.79	Microtubules (Supported); Additional: Cytokinetic bridge;Mitotic spindle
Ras-related protein Rab-6B	RAB6B	5.76	Golgi apparatus (Supported)
Putative RNA-binding protein Luc7-like 2	LUC7L2	5.76	Nucleoplasm (Approved)
ADP-ribosylation factor 1	ARF1	5.76	Cytosol (Approved); Additional: Plasma membrane
40S ribosomal protein S19	RPS19	5.75	Nucleoplasm (Supported)
40S ribosomal protein S30	FAU	5.74	Cytosol;Endoplasmic reticulum (Enhanced); Additional: Nucleoli
26S proteasome non-ATPase regulatory subunit 14	PSMD14	5.73	Nucleoplasm (Supported)
Microtubule-associated protein 4	MAP4	5.73	Cytosol;Microtubules;Plasma membrane (Approved)
L-lactate dehydrogenase B chain	LDHB	5.60	Cytosol (Supported)
60S ribosomal protein L35	RPL35	5.53	Cytosol;Endoplasmic reticulum (Approved)
T-complex protein 1 subunit delta	CCT4	5.52	Cytosol (Supported); Additional: Nucleoplasm
Filamin-A	FLNA	5.49	Actin filaments;Cytosol;Plasma membrane (Enhanced)
Guanine nucleotide-binding protein G(t) subunit alpha-1	GNAT1	5.42	N/A
Ubiquitin-40S ribosomal protein S27a	RPS27A	5.40	Cytosol;Endoplasmic reticulum;Nucleoli (Supported)
Cleavage and polyadenylation specificity factor subunit 6	CPSF6	5.35	Nuclear speckles;Nucleoplasm (Enhanced)
Histone H2A.V;Histone H2A.Z	H2AFV	5.35	N/A

40S ribosomal protein S7	RPS7	5.30	Cytosol;Endoplasmic reticulum (Supported)
Protein DEK	DEK	5.27	Nucleoplasm (Supported); Additional: Cytosol
Actin, cytoplasmic 1	ACTB	5.15	N/A
Glyceraldehyde-3-phosphate dehydrogenase	GAPDH	5.13	Cytosol;Plasma membrane (Enhanced); Additional: Nuclear membrane;Vesicles
Putative heat shock protein HSP 90-beta 2	HSP90AB2P	5.06	N/A
Poly [ADP-ribose] polymerase 1	PARP1	4.99	Nucleoplasm (Supported); Additional: Nucleoli
60S acidic ribosomal protein P1	RPLP1	4.97	Cytosol;Endoplasmic reticulum (Supported)
60S ribosomal protein L7	RPL7	4.89	Cytosol;Endoplasmic reticulum (Approved); Additional: Nucleoli
ATP synthase subunit beta, mitochondrial	ATP5B	4.86	Mitochondria (Enhanced)
Cofilin-1;Cofilin-2	CFL1	4.85	Plasma membrane (Supported)
Actin, alpha skeletal muscle	ACTA1	4.81	N/A
Cytochrome c oxidase subunit 5A, mitochondrial	COX5A	4.79	N/A
Annexin A2;Putative annexin A2-like protein	ANXA2	4.77	Plasma membrane (Approved); Additional: Cytosol
Chromobox protein homolog 5	CBX5	4.72	Nucleoplasm (Enhanced)
Rotatin	RTTN	4.62	Cytosol (Approved); Additional: Centrosome
Splicing factor U2AF 65 kDa subunit	U2AF2	4.60	Nuclear speckles;Nucleoplasm (Supported)
Heat shock protein HSP 90-beta	HSP90AB1	4.59	Cytosol (Supported)
Heat shock protein beta-1	HSPB1	4.51	Cytosol;Plasma membrane (Enhanced)
Splicing factor U2AF 35 kDa subunit	U2AF1	4.50	Nucleoplasm (Enhanced)
60S ribosomal protein L22	RPL22	4.48	Nucleoli (Approved); Additional: Nucleoplasm
Protein disulfide-isomerase A6	PDIA6	4.48	Cytosol;Endoplasmic reticulum (Supported)
26S proteasome non-ATPase regulatory subunit 7	PSMD7	4.43	Nucleoplasm (Enhanced)
78 kDa glucose-regulated protein	HSPA5	4.43	Cytosol (Approved)
Myosin light polypeptide 6	MYL6	4.43	N/A
40S ribosomal protein S12	RPS12	4.42	Cytosol (Supported); Additional: Golgi apparatus;Vesicles
Arf-GAP with coiled-coil, ANK repeat and PH domain-containing protein 2	ACAP2	4.37	Endosomes (Approved)
60S ribosomal protein L27	RPL27	4.30	Nucleoli (Enhanced); Additional: Nucleoplasm
60S ribosomal protein L38	RPL38	4.29	Cytosol;Endoplasmic reticulum (Supported)
ATP synthase subunit O, mitochondrial	ATP5O	4.27	Mitochondria (Approved)
Proteasome activator complex subunit 1	PSME1	4.26	Cytosol (Approved); Additional: Nuclear bodies
Heat shock cognate 71 kDa protein	HSPA8	4.18	Nucleoplasm (Approved); Additional: Vesicles
Elongation of very long chain fatty acids protein 1	ELOVL1	4.14	Endoplasmic reticulum (Supported)
Ribose-phosphate pyrophosphokinase 1	PRPS1	4.12	Vesicles (Approved)
Heat shock 70 kDa protein 1B	HSPA1B	4.11	Cytosol;Vesicles (Approved); Additional: Nucleoplasm
Pyruvate kinase PKM	PKM	4.02	Cytosol (Enhanced)
U3 small nucleolar RNA-associated protein 18 homolog	UTP18	3.99	Nucleoli;Nucleoli rim (Supported); Additional: Nuclear membrane;Nucleoplasm
Heat shock protein HSP 90-alpha	HSP90AA1	3.97	Cytosol (Enhanced)
Peroxiredoxin-6	PRDX6	3.81	Cytosol;Plasma membrane (Supported)
Nucleophosmin	NPM1	3.76	Nucleoli rim (Enhanced); Additional: Nucleoplasm
Plasminogen activator inhibitor 1 RNA-binding protein	SERBP1	3.62	Cytosol (Enhanced)
N-alpha-acetyltransferase 16, NatA auxiliary subunit	NAA16	3.55	Cytosol (Enhanced)
Heat shock 70 kDa protein 6	HSPA6	3.46	Vesicles (Approved); Additional: Nucleoplasm
Elongation factor 2	EEF2	3.36	Cytosol;Plasma membrane (Enhanced)
60S ribosomal protein L7a	RPL7A	3.36	Nucleoli (Approved); Additional: Vesicles
RNA-binding protein 39	RBM39	3.27	Nuclear speckles;Nucleoplasm (Supported); Additional: Centriolar satellite;Microtubules
Ras-related protein Rap-1A	RAP1A	3.22	N/A
Serine/arginine-rich splicing factor 11	SRSF11	3.20	Nuclear speckles (Supported)
60 kDa heat shock protein, mitochondrial	HSPD1	3.15	Mitochondria (Enhanced)

Stress-70 protein, mitochondrial	HSPA9	3.12	Mitochondria (Supported)
Multiple myeloma tumor-associated protein 2	MMTAG2	3.02	Nuclear speckles;Plasma membrane (Approved); Additional: Cytosol
Peroxiredoxin-1	PRDX1	2.67	Mitochondria (Approved)
Elongation factor 1-gamma	EEF1G	2.50	Cytosol (Approved); Additional: Golgi apparatus
Cytoplasmic dynein 1 heavy chain 1	DYNC1H1	2.47	Centrosome;Cytosol (Supported)
Arginine and glutamate-rich protein 1	ARGLU1	2.04	Nucleoplasm (Enhanced); Additional: Cytosol;Mitochondria

Table 8.1: List of enriched candidates identified within the LARP1B protein interactome of GCT27 cells following co-IP MS*. Proteins with a log2 fold change ≥2 are listed along with UniProt annotated Protein name, Gene name, Log2 fold change compared to IgG and Subcellular location. Subcellular location annotations were derived from Metascape annotation analysis which uses UniProt annotations.*

Protein names	Gene names	Log2 fold change compared to IgG control	Subcellular Location (Protein Atlas annotation)
Splicing factor 3B subunit 2	SF3B2	32.66	Nuclear speckles (Enhanced)
Synergin gamma	SYNRG	32.49	Cytosol (Approved)
Chromosome alignment-maintaining phosphoprotein 1	CHAMP1	32.33	Nucleoplasm (Enhanced); Additional: Nuclear bodies
Type-1 angiotensin II receptor-associated protein	AGTRAP	32.02	Vesicles (Supported); Additional: Golgi apparatus
Nucleolar RNA helicase 2	DDX21	31.31	Mitotic chromosome;Nucleoli rim (Enhanced); Additional: Nucleoplasm
Serum paraoxonase/arylesterase 1	PON1	31.10	N/A
Methylthioribulose-1-phosphate dehydratase	APIP	31.05	Nucleoplasm (Approved); Additional: Cytosol
U5 small nuclear ribonucleoprotein 200 kDa helicase	SNRNP200	30.84	Nucleoplasm (Supported)
Histone H1.2	HIST1H1C	30.74	Nucleoli rim;Nucleoplasm (Supported)
Scaffold attachment factor B1	SAFB	30.74	Nucleoplasm (Enhanced); Additional: Midbody
Serine/threonine-protein phosphatase PP1-beta catalytic subunit	PPP1CB	30.72	Nucleoplasm (Supported); Additional: Cytosol
Heterogeneous nuclear ribonucleoprotein H3	HNRNPH3	30.48	Nucleoplasm (Supported)
Serine/threonine-protein phosphatase PGAM5, mitochondrial	PGAM5	30.24	Mitochondria (Supported)
Polyadenylate-binding protein 4	PABPC4	30.20	Cytosol (Enhanced)
Splicing factor 3B subunit 4	SF3B4	30.18	Nuclear speckles (Approved)
Putative helicase MOV-10	MOV10	30.15	Cytosol (Approved)
116 kDa U5 small nuclear ribonucleoprotein component	EFTUD2	30.15	Nucleoplasm (Approved); Additional: Cytosol;Vesicles
Gem-associated protein 4	GEMIN4	30.12	Cytosol;Nuclear bodies (Supported)
Heterogeneous nuclear ribonucleoprotein D-like	HNRNPDL	30.00	Nucleoplasm (Enhanced)
Protein virilizer homolog	KIAA1429	29.96	Nuclear bodies (Supported); Additional: Nucleoplasm
KH domain-containing, RNA-binding, signal transduction-associated protein 1	KHDRBS1	29.96	Nucleoplasm (Enhanced)
Scaffold attachment factor B2	SAFB2	29.95	Nucleoplasm (Supported); Additional: Nuclear bodies;Vesicles
Transformer-2 protein homolog beta	TRA2B	29.86	Nucleoplasm (Enhanced)
ATP-dependent RNA helicase DDX18	DDX18	29.80	Mitotic chromosome;Nucleoli;Nucleoli rim (Enhanced)
H/ACA ribonucleoprotein complex subunit 4	DKC1	29.78	Nucleoli fibrillar center (Supported); Additional: Nucleoplasm
ELAV-like protein 1	ELAVL1	29.72	Nucleoplasm (Supported); Additional: Cytosol;Nucleoli
Heterogeneous nuclear ribonucleoprotein H	HNRNPH1	29.70	Nucleoplasm (Enhanced)
KH domain-containing, RNA-binding, signal transduction-associated protein 3	KHDRBS3	29.64	Nucleoplasm (Supported)
Enhancer of rudimentary homolog	ERH	29.58	Nucleoplasm (Approved); Additional: Cytosol
Serine/arginine-rich splicing factor 10	SRSF10	29.52	Nucleoplasm (Supported)
Peroxiredoxin-4	PRDX4	29.52	Endoplasmic reticulum (Supported); Additional: Cytosol
Nuclease-sensitive element-binding protein 1	YBX1	29.40	Cytosol (Supported); Additional: Endoplasmic reticulum;Plasma membrane;Vesicles
E3 ubiquitin-protein ligase TRIM71	TRIM71	29.28	Actin filaments;Focal adhesion sites;Plasma membrane (Approved)
Cleavage and polyadenylation specificity factor subunit 7	CPSF7	29.11	Nucleoplasm (Supported); Additional: Cytosol
Double-stranded RNA-binding protein Staufen homolog 1	STAU1	28.98	Cytosol (Enhanced)
Pre-mRNA-splicing regulator WTAP	WTAP	28.98	Nuclear speckles (Enhanced)
Histone H1.5	HIST1H1B	28.95	Nucleoplasm (Supported)
Cytoskeleton-associated protein 4	CKAP4	28.93	N/A
Protein RRP5 homolog	PDCD11	28.87	Nucleoli rim (Supported); Additional: Vesicles
Heterogeneous nuclear ribonucleoprotein F	HNRNPF	28.86	Nucleoplasm (Enhanced)
Bcl-2-associated transcription factor 1	BCLAF1	28.80	Nuclear speckles (Enhanced)
RNA-binding protein 45	RBM45	28.80	Nucleoplasm (Supported)
Zinc finger and BTB domain-containing protein 39	ZBTB39	28.76	Vesicles (Approved)
60S ribosomal protein L23	RPL23	28.71	Cytosol (Supported)
Pericentriolar material 1 protein	PCM1	28.70	Centriolar satellite (Supported); Additional: Cytosol;Nucleoplasm
Y-box-binding protein 3	YBX3	28.67	Cytosol (Supported)
Myb/SANT-like DNA-binding domain-containing protein 2	MSANTD2	28.59	Nuclear bodies (Supported); Additional: Nucleoplasm

Pogo transposable element with ZNF domain	POGZ	28.59	Nucleoplasm (Enhanced)
Polypyrimidine tract-binding protein 3	PTBP3	28.58	Nucleoplasm (Approved)
Collagen alpha-1(XVIII) chain;Endostatin	COL18A1	28.54	Golgi apparatus (Approved)
RISC-loading complex subunit TARBP2	TARBP2	28.44	Nucleoplasm (Supported); Additional: Nuclear bodies
Histone H1.3	HIST1H1D	28.36	N/A
Protein lin-28 homolog A	LIN28A	28.35	Cytosol (Supported); Additional: Nucleoli;Rods & Rings
U3 small nucleolar RNA-interacting protein 2	RRP9	28.30	Nucleoplasm (Supported)
SAFB-like transcription modulator	SLTM	28.30	Nuclear bodies;Nucleoplasm (Enhanced)
Histone H1.4	HIST1H1E	28.29	Nuclear speckles (Supported); Additional: Cytosol
Survival motor neuron protein	SMN1	28.27	Cytosol;Nuclear bodies (Supported)
Ribosome-binding protein 1	RRBP1	28.25	Endoplasmic reticulum (Enhanced)
YTH domain-containing protein 1	YTHDC1	28.25	Nucleoplasm (Approved); Additional: Plasma membrane
Signal recognition particle subunit SRP72	SRP72	28.22	N/A
SNW domain-containing protein 1	SNW1	28.20	Nucleoplasm (Enhanced); Additional: Cytosol
Caspase recruitment domain-containing protein 11	CARD11	28.19	N/A
39S ribosomal protein L4, mitochondrial	MRPL4	28.18	N/A
RNA-binding protein 12B	RBM12B	28.14	Nucleoplasm (Approved)
60S ribosomal protein L29	RPL29	28.11	Cytosol;Endoplasmic reticulum;Nucleoli (Supported)
Small nuclear ribonucleoprotein E	SNRPE	28.10	N/A
tRNA-splicing ligase RtcB homolog	RTCB	27.99	Nucleoplasm (Supported); Additional: Cytosol;Vesicles
39S ribosomal protein L15, mitochondrial	MRPL15	27.95	Mitochondria (Supported)
Titin	TTN	27.95	N/A
Nucleolar GTP-binding protein 1	GTPBP4	27.94	Nucleoli;Nucleoli rim (Supported); Additional: Nuclear membrane
LINE-1 retrotransposable element ORF1 protein	L1RE1	27.92	None
Heterogeneous nuclear ribonucleoprotein U-like protein 1	HNRNPUL1	27.92	Nucleoplasm (Enhanced)
Cell division cycle 5-like protein	CDC5L	27.91	Nucleoplasm (Supported)
Serine-threonine kinase receptor-associated protein	STRAP	27.90	Cytosol (Enhanced)
U5 small nuclear ribonucleoprotein 40 kDa protein	SNRNP40	27.90	Nuclear speckles (Supported)
Interferon-induced, double-stranded RNA-activated protein kinase	EIF2AK2	27.89	Cytosol (Enhanced)
Branched-chain-amino-acid aminotransferase, cytosolic	BCAT1	27.87	N/A
Claudin-6	CLDN6	27.86	N/A
Ribosome biogenesis protein BRX1 homolog	BRIX1	27.86	Mitotic chromosome;Nucleoli (Enhanced)
Myb-binding protein 1A	MYBBP1A	27.85	Nucleoli (Supported); Additional: Vesicles
Ribosome production factor 2 homolog	RPF2	27.78	Nucleoli;Nucleoli rim (Supported); Additional: Mitotic chromosome;Nucleoplasm
Chromobox protein homolog 3	CBX3	27.78	Nucleoplasm (Supported); Additional: Nuclear bodies
Myosin-10	MYH10	27.77	Actin filaments (Supported); Additional: Cytosol;Mitochondria
Heat shock factor-binding protein 1	HSBP1	27.73	Nucleoli (Supported)
ATP-dependent RNA helicase DDX1	DDX1	27.72	Nucleoplasm (Supported); Additional: Cytosol
Dihydrolipoyllysine-residue acetyltransferase component of pyruvate dehydrogenase complex, mitochondrial	DLAT	27.70	Mitochondria (Supported)
RNA binding motif protein, X-linked-like-1	RBMXL1	27.68	Nucleoplasm (Approved)
SWI/SNF-related matrix-associated actin-dependent regulator of chromatin subfamily A member 5	SMARCA5	27.68	Nucleoli fibrillar center;Nucleoplasm (Supported)
T-complex protein 1 subunit alpha	TCP1	27.66	N/A
SH3KBP1-binding protein 1	SHKBP1	27.59	Cell Junctions (Approved)
39S ribosomal protein L39, mitochondrial	MRPL39	27.57	Mitochondria (Supported)
Transformer-2 protein homolog alpha	TRA2A	27.55	Nucleoli (Supported); Additional: Nucleoplasm;Vesicles
Protein Hook homolog 1	HOOK1	27.52	N/A
Polyadenylate-binding protein 2	PABPN1	27.52	Nucleoplasm (Approved); Additional: Nuclear speckles
Pleiotropic regulator 1	PLRG1	27.51	Nuclear speckles;Nucleoplasm (Supported); Additional: Nuclear membrane;Nucleoli fibrillar center

G kinase-anchoring protein 1	GKAP1	27.48	Centriolar satellite;Cytosol (Approved)
Nucleosome-remodeling factor subunit BPTF	BPTF	27.36	Nucleoplasm (Enhanced)
DNA replication licensing factor MCM7	MCM7	27.35	Nucleoplasm (Enhanced)
Small nuclear ribonucleoprotein F	SNRPF	27.35	N/A
Coiled-coil domain-containing protein 77	CCDC77	27.32	Nuclear membrane (Approved)
Isoleucine--tRNA ligase, cytoplasmic	IARS	27.30	Cytosol;Nucleoplasm (Approved)
Complement C3	C3	27.27	N/A
Mitogen-activated protein kinase 4	MAPK4	27.26	Golgi apparatus;Nucleoplasm (Approved); Additional: Midbody
La-related protein 1B	LARP1B	27.24	Cytosol (Approved)
39S ribosomal protein L44, mitochondrial	MRPL44	27.24	Mitochondria (Approved); Additional: Nuclear bodies;Nucleoplasm;Plasma membrane
N-acylneuraminate cytidylyltransferase	CMAS	27.22	Cytosol (Uncertain); Additional: Nucleoli
Gem-associated protein 7	GEMIN7	27.17	Cytosol;Nucleoplasm (Supported)
N-acetylserotonin O-methyltransferase-like protein	ASMTL	27.15	Cytosol (Enhanced)
Aspartate--tRNA ligase, cytoplasmic	DARS	27.12	Cytosol (Enhanced)
Dolichyl-diphosphooligosaccharide--protein glycosyltransferase subunit 2	RPN2	27.12	Endoplasmic reticulum (Supported)
Tubulin alpha-4A chain	TUBA4A	27.11	Microtubules (Enhanced)
Protein TFG	TFG	27.09	Vesicles (Supported); Additional: Cytosol
Protein phosphatase 1 regulatory subunit 12C	PPP1R12C	27.04	N/A
ATP synthase subunit gamma, mitochondrial	ATP5C1	27.03	N/A
Disks large homolog 5	DLG5	27.03	Cell Junctions (Supported)
Complement C5	C5	26.96	N/A
PDZ domain-containing protein 11	PDZD11	26.96	N/A
39S ribosomal protein L49, mitochondrial	MRPL49	26.92	N/A
Vinculin	VCL	26.90	Focal adhesion sites (Enhanced)
LINE-1 type transposase domain-containing protein 1	L1TD1	26.90	Vesicles (Enhanced)
Arginine--tRNA ligase, cytoplasmic	RARS	26.81	Cytosol (Supported); Additional: Nucleoli;Nucleoplasm
39S ribosomal protein L13, mitochondrial	MRPL13	26.80	N/A
UPF0568 protein C14orf166	C14orf166	26.77	Nucleoplasm (Supported)
A-kinase anchor protein 9	AKAP9	26.76	Golgi apparatus (Enhanced); Additional: Centrosome;Vesicles
39S ribosomal protein L50, mitochondrial	MRPL50	26.75	Mitochondria (Supported); Additional: Cytosol
39S ribosomal protein L21, mitochondrial	MRPL21	26.75	Mitochondria;Nucleoplasm (Approved)
60S ribosomal protein L5	RPL5	26.74	Cytosol;Endoplasmic reticulum (Supported); Additional: Nucleoli;Nucleoli rim
Sarcoplasmic/endoplasmic reticulum calcium ATPase 2	ATP2A2	26.74	N/A
Ankyrin repeat domain-containing protein 11	ANKRD11	26.71	Nucleoplasm (Enhanced); Additional: Cytosol
Serine/arginine-rich splicing factor 7	SRSF7	26.71	Nucleoplasm (Enhanced)
Pre-mRNA-processing factor 17	CDC40	26.69	Nucleoplasm (Supported)
Ribosome biogenesis regulatory protein homolog	RRS1	26.68	Nucleoli (Supported)
Eukaryotic initiation factor 4A-III	EIF4A3	26.67	Nucleoplasm (Supported)
Protein BRICK1	BRK1	26.65	Nuclear speckles (Approved); Additional: Cell Junctions
Lupus La protein	SSB	26.65	Nucleoplasm (Approved)
H/ACA ribonucleoprotein complex subunit 3	NOP10	26.64	Nuclear bodies (Supported)
Guanine nucleotide-binding protein subunit beta-2-like 1	GNB2L1	26.54	Nucleoplasm (Supported); Additional: Cytosol
N-acetyltransferase 10	NAT10	26.54	Nucleoli (Enhanced); Additional: Midbody
RNA-binding protein EWS	EWSR1	26.51	Nucleoplasm (Supported); Additional: Nucleoli
Protein BUD31 homolog	BUD31	26.48	Nucleoplasm (Approved); Additional: Centrosome;Microtubules
Pre-mRNA-splicing factor RBM22	RBM22	26.47	Nucleoplasm (Enhanced)
Tubulin alpha-1C chain	TUBA1C	26.44	Microtubules (Supported)
Complement C4-A	C4A	26.40	N/A

Putative E3 ubiquitin-protein ligase SH3RF2	SH3RF2	26.37	Nucleoplasm (Enhanced)
Peptidyl-prolyl cis-trans isomerase-like 3	PPIL3	26.35	Nucleoplasm (Approved); Additional: Nucleoli
Guanine nucleotide-binding protein-like 3	GNL3	26.35	Nucleoli rim (Enhanced); Additional: Mitotic chromosome;Nuclear bodies
39S ribosomal protein L19, mitochondrial	MRPL19	26.35	Mitochondria (Supported)
Ras-related GTP-binding protein C	RRAGC	26.35	Nucleoplasm;Vesicles (Supported)
Pre-mRNA-splicing factor SLU7	SLU7	26.34	Nucleoplasm (Supported); Additional: Nuclear speckles
Cell growth-regulating nucleolar protein	LYAR	26.33	Nucleoli;Nucleoli rim (Enhanced); Additional: Nucleoplasm
39S ribosomal protein L2, mitochondrial	MRPL2	26.32	Mitochondria (Supported); Additional: Nucleoplasm
Histone H2A type 2-C	HIST2H2AC	26.30	Nucleoplasm (Supported)
Ribosomal biogenesis protein LAS1L	LAS1L	26.27	Nucleoplasm (Approved); Additional: Centriolar satellite;Cytosol
39S ribosomal protein L43, mitochondrial	MRPL43	26.27	Mitochondria;Nucleoplasm (Approved)
39S ribosomal protein L22, mitochondrial	MRPL22	26.27	Mitochondria (Approved)
39S ribosomal protein L45, mitochondrial	MRPL45	26.19	Mitochondria (Enhanced)
U1 small nuclear ribonucleoprotein C	SNRPC	26.16	Nucleoplasm (Enhanced)
Nucleolar and coiled-body phosphoprotein 1	NOLC1	26.16	Nucleoli fibrillar center (Enhanced)
40S ribosomal protein S29	RPS29	26.12	Cytosol;Endoplasmic reticulum (Supported)
39S ribosomal protein L24, mitochondrial	MRPL24	26.11	N/A
Zinc finger RNA-binding protein	ZFR	26.11	Nucleoplasm (Approved)
Peptidyl-prolyl cis-trans isomerase-like 1	PPIL1	26.11	Nucleoli (Supported)
H/ACA ribonucleoprotein complex subunit 2	NHP2	26.08	N/A
Clathrin heavy chain 1	CLTC	26.08	Endosomes;Lysosomes (Supported); Additional: Cytosol;Mitotic spindle
Eukaryotic translation initiation factor 6	EIF6	26.07	Nucleoplasm (Supported)
39S ribosomal protein L47, mitochondrial	MRPL47	26.06	Mitochondria (Supported)
Probable rRNA-processing protein EBP2	EBNA1BP2	26.03	Nucleoli;Nucleoli rim (Enhanced); Additional: Mitotic chromosome
39S ribosomal protein L37, mitochondrial	MRPL37	26.01	Mitochondria (Supported)
Eukaryotic translation initiation factor 2 subunit 3	EIF2S3	26.01	N/A
YLP motif-containing protein 1	YLPM1	26.01	Nuclear speckles (Supported)
Gem-associated protein 6	GEMIN6	25.99	Nuclear bodies;Nucleoplasm (Supported)
ATP-dependent RNA helicase DDX39A	DDX39A	25.95	Nuclear speckles (Approved)
Nucleolar protein 6	NOL6	25.95	Nucleoli (Enhanced); Additional: Nucleoplasm
Glutamine--tRNA ligase	QARS	25.95	Cytosol (Enhanced)
Nuclear mitotic apparatus protein 1	NUMA1	25.92	Nucleoplasm (Supported); Additional: Cytosol
Pre-mRNA-splicing factor SPF27	BCAS2	25.92	Centrosome;Nuclear speckles (Supported)
Double-stranded RNA-binding protein Staufen homolog 2	STAU2	25.88	Nucleoplasm (Supported); Additional: Cytosol
39S ribosomal protein L9, mitochondrial	MRPL9	25.87	Mitochondria (Supported)
39S ribosomal protein L17, mitochondrial	MRPL17	25.87	N/A
39S ribosomal protein L23, mitochondrial	MRPL23	25.86	Mitochondria;Nucleoli fibrillar center (Approved)
PC4 and SFRS1-interacting protein	PSIP1	25.86	Nucleoplasm (Enhanced)
SRSF protein kinase 1	SRPK1	25.86	Cytosol;Nucleoplasm (Supported); Additional: Plasma membrane
Peptidyl-tRNA hydrolase ICT1, mitochondrial	ICT1	25.85	Mitochondria (Supported); Additional: Nucleoplasm;Plasma membrane
39S ribosomal protein L28, mitochondrial	MRPL28	25.83	Mitochondria (Supported)
E3 ubiquitin-protein ligase Hakai	CBLL1	25.79	Nuclear speckles (Supported)
Stonin-2	STON2	25.78	Cytosol;Nucleoli (Approved)
Histone deacetylase complex subunit SAP18	SAP18	25.77	Nuclear bodies;Nucleoplasm (Supported); Additional: Cytosol
39S ribosomal protein L3, mitochondrial	MRPL3	25.75	N/A
MKI67 FHA domain-interacting nucleolar phosphoprotein	NIFK	25.75	Nucleoli;Nucleoli rim (Enhanced); Additional: Mitotic chromosome
U8 snoRNA-decapping enzyme	NUDT16	25.75	Nucleoli;Nucleoplasm (Supported)
Mitochondrial 2-oxoglutarate/malate carrier protein	SLC25A11	25.74	N/A

Very-long-chain (3R)-3-hydroxyacyl-CoA dehydratase 3	HACD3	25.73	Endoplasmic reticulum (Enhanced)
Aminoacyl tRNA synthase complex-interacting multifunctional protein 2	AIMP2	25.73	Cytosol (Approved)
X-ray repair cross-complementing protein 5	XRCC5	25.73	Nucleoplasm (Supported)
39S ribosomal protein L38, mitochondrial	MRPL38	25.71	Mitochondria (Supported)
Lamin-B receptor	LBR	25.63	Nuclear membrane (Enhanced)
Histone H3.3	H3F3A	25.62	Nucleoplasm (Supported)
CD9 antigen	CD9	25.62	Plasma membrane (Supported)
39S ribosomal protein L30, mitochondrial	MRPL30	25.61	N/A
Regulator of nonsense transcripts 1	UPF1	25.60	Nucleoplasm (Supported); Additional: Cytosol
39S ribosomal protein L20, mitochondrial	MRPL20	25.60	Mitochondria (Supported)
Eukaryotic translation elongation factor 1 epsilon-1	EEF1E1	25.59	Cytosol;Nucleoplasm (Supported)
39S ribosomal protein L41, mitochondrial	MRPL41	25.58	Mitochondria (Supported)
Serine/arginine-rich splicing factor 1	SRSF1	25.57	Nucleoplasm (Supported)
Mitotic spindle assembly checkpoint protein MAD2B	MAD2L2	25.56	Nucleoplasm (Supported)
DNA dC->dU-editing enzyme APOBEC-3B	APOBEC3B	25.54	Nucleoplasm (Approved)
BRI3-binding protein	BRI3BP	25.52	Mitochondria;Nucleoplasm (Approved)
Ras GTPase-activating protein nGAP	RASAL2	25.52	Focal adhesion sites;Plasma membrane (Approved)
UTP--glucose-1-phosphate uridylyltransferase	UGP2	25.49	Centrosome;Mitochondria (Approved); Additional: Nucleoplasm
Core histone macro-H2A.1	H2AFY	25.44	Nucleoplasm (Supported)
AT-rich interactive domain-containing protein 3A	ARID3A	25.42	Nucleoplasm (Supported); Additional: Cytosol
Signal recognition particle 9 kDa protein	SRP9	25.40	N/A
60S ribosome subunit biogenesis protein NIP7 homolog	NIP7	25.37	Nucleoli (Supported); Additional: Cytosol;Nucleoplasm
Ubiquitin carboxyl-terminal hydrolase 36	USP36	25.37	Nucleoli;Nucleoli rim (Enhanced); Additional: Nuclear speckles
Argininosuccinate synthase	ASS1	25.37	Cytosol (Supported); Additional: Nucleoplasm
AFG3-like protein 2	AFG3L2	25.37	Mitochondria (Supported)
Ribosomal protein 63, mitochondrial	MRPL57	25.36	Mitochondria (Supported)
WD repeat-containing protein 43	WDR43	25.36	N/A
Dolichyl-diphosphooligosaccharide--protein glycosyltransferase subunit STT3B	STT3B	25.35	Endoplasmic reticulum (Supported)
Transmembrane protein 33	TMEM33	25.34	N/A
Coiled-coil domain-containing protein 61	CCDC61	25.32	Nucleoplasm (Approved)
Chromodomain-helicase-DNA-binding protein 6	CHD6	25.32	Nucleoplasm (Supported)
Putative ATP-dependent RNA helicase DHX33	DHX33	25.29	Nucleoli (Supported)
Mitochondrial import receptor subunit TOM40 homolog	TOMM40	25.27	Mitochondria (Enhanced); Additional: Cytosol
Histone-binding protein RBBP7	RBBP7	25.25	Nucleoplasm (Enhanced)
Ras-related protein Rab-5C	RAB5C	25.23	Endosomes (Enhanced)
H/ACA ribonucleoprotein complex subunit 1	GAR1	25.21	Nucleoli fibrillar center;Nucleoplasm (Approved)
p21-activated protein kinase-interacting protein 1	PAK1IP1	25.18	Nucleoli (Supported)
Tubulin gamma-1 chain;Tubulin gamma-2 chain	TUBG1;TUBG2	25.15	N/A
Electron transfer flavoprotein subunit alpha, mitochondrial	ETFA	25.15	Centriolar satellite (Supported)
RNA-binding protein with multiple splicing;RNA-binding protein with multiple splicing 2	RBPMS;RBPMS2	25.13	Mitochondria (Enhanced)
AP-2 complex subunit mu	AP2M1	25.12	Nucleoplasm (Supported); Additional: Cytosol
Very-long-chain enoyl-CoA reductase	TECR	25.10	N/A
Pre-mRNA-splicing factor 38A	PRPF38A	25.10	Plasma membrane (Supported)
28S ribosomal protein S30, mitochondrial	MRPS30	25.06	Endoplasmic reticulum (Supported)
Myosin light polypeptide 6	MYL6	25.05	Nucleoplasm (Enhanced)
Pleckstrin homology-like domain family B member 2	PHLDB2	25.05	N/A
AP-3 complex subunit delta-1	AP3D1	25.04	N/A
Myeloid leukemia factor 2	MLF2	25.04	Cytosol;Plasma membrane (Supported)

Inosine-5-monophosphate dehydrogenase 2	IMPDH2	25.04	Cytosol (Approved)
Erlin-2;Erlin-1	ERLIN2	25.03	Nucleoplasm (Approved); Additional: Cytosol;Plasma membrane
Ankyrin repeat domain-containing protein 36C	ANKRD36C	25.01	Cytosol (Supported); Additional: Rods & Rings
Periodic tryptophan protein 1 homolog	PWP1	24.98	Endoplasmic reticulum (Supported)
Microtubule-associated protein 1B	MAP1B	24.96	Cytosol;Nucleoplasm (Approved)
39S ribosomal protein L51, mitochondrial	MRPL51	24.91	Nucleoli rim (Approved); Additional: Golgi apparatus
Tubulin beta-8 chain	TUBB8	24.91	Cytosol (Enhanced)
Alpha-enolase	ENO1	24.90	Mitochondria (Supported)
mRNA turnover protein 4 homolog	MRTO4	24.88	Microtubules (Supported); Additional: Cytokinetic bridge;Mitotic spindle
Protein cornichon homolog 4	CNIH4	24.87	Cytosol;Plasma membrane (Enhanced)
Chromatin target of PRMT1 protein	CHTOP	24.87	Nuclear membrane;Nucleoplasm (Approved); Additional: Nucleoli
Lamina-associated polypeptide 2, isoforms beta/gamma	TMPO	24.83	N/A
FACT complex subunit SPT16	SUPT16H	24.79	Nuclear speckles (Supported)
Protein arginine N-methyltransferase 1	PRMT1	24.79	Nuclear membrane (Enhanced)
Protein LYRIC	MTDH	24.78	Nucleoplasm (Supported); Additional: Nucleoli fibrillar center
Prothrombin;Activation peptide fragment 1	F2	24.77	Nucleoplasm (Supported)
RNA-binding protein with serine-rich domain 1	RNPS1	24.76	Endoplasmic reticulum (Enhanced)
Protein transport protein Sec61 subunit alpha isoform 1	SEC61A1	24.74	N/A
Suppressor of SWI4 1 homolog	PPAN	24.73	Nucleoplasm (Supported)
Coatomer subunit alpha	COPA	24.68	Endoplasmic reticulum (Supported)
39S ribosomal protein L52, mitochondrial	MRPL52	24.67	N/A
E3 ubiquitin-protein ligase MIB1	MIB1	24.65	Cytosol;Nucleoplasm (Approved); Additional: Golgi apparatus
U3 small nucleolar RNA-associated protein 15 homolog	UTP15	24.65	Mitochondria (Supported); Additional: Nucleoplasm
Putative heat shock protein HSP 90-beta 2	HSP90AB2P	24.63	Plasma membrane (Uncertain); Additional: Vesicles
Probable ribosome biogenesis protein RLP24	RSL24D1	24.62	Endoplasmic reticulum;Nucleoli (Approved)
CUGBP Elav-like family member 1	CELF1	24.61	N/A
Crooked neck-like protein 1	CRNKL1	24.61	Nucleoli;Nucleoli rim;Nucleoplasm (Enhanced)
Apoptotic chromatin condensation inducer in the nucleus	ACIN1	24.57	Nucleoplasm (Enhanced)
Dolichyl-diphosphooligosaccharide--protein glycosyltransferase subunit STT3A	STT3A	24.55	N/A
F-box/WD repeat-containing protein 11	FBXW11	24.54	Nucleoplasm (Supported); Additional: Cytosol;Plasma membrane
ER lumen protein-retaining receptor 2	KDELR2	24.53	N/A
WD repeat-containing protein 46	WDR46	24.51	Plasma membrane;Vesicles (Approved); Additional: Nucleoplasm
2,3-cyclic-nucleotide 3-phosphodiesterase	CNP	24.51	N/A
Vacuolar protein sorting-associated protein 33B	VPS33B	24.50	Nucleoli (Supported)
4F2 cell-surface antigen heavy chain	SLC3A2	24.48	Plasma membrane (Approved)
DNA topoisomerase 2-beta	TOP2B	24.48	N/A
39S ribosomal protein L12, mitochondrial	MRPL12	24.41	Nucleoplasm;Plasma membrane (Approved)
Nuclear cap-binding protein subunit 1	NCBP1	24.40	Nucleoplasm (Enhanced)
Endoribonuclease Dicer	DICER1	24.39	Mitochondria (Supported)
Microfibrillar-associated protein 1	MFAP1	24.39	Cytosol (Supported); Additional: Nucleoplasm
Motile sperm domain-containing protein 2	MOSPD2	24.35	Cytosol (Supported)
Coatomer subunit delta	ARCN1	24.32	Nucleoplasm (Supported); Additional: Centrosome
Spermatogenesis-associated protein 5-like protein 1	SPATA5L1	24.30	Endoplasmic reticulum (Supported)
3-beta-hydroxysteroid-Delta(8),Delta(7)-isomerase	EBP	24.28	Vesicles (Supported); Additional: Cytosol;Golgi apparatus
Translocon-associated protein subunit delta	SSR4	24.28	Nucleoplasm (Approved); Additional: Nucleoli
Voltage-dependent anion-selective channel protein 3	VDAC3	24.25	Endoplasmic reticulum;Nuclear membrane (Supported)
Translocon-associated protein subunit gamma	SSR3	24.23	Endoplasmic reticulum (Supported)
Serine/threonine-protein phosphatase PP1-gamma catalytic subunit	PPP1CC	24.22	Mitochondria (Supported)

Fragile X mental retardation syndrome-related protein 1	FXR1	24.15	N/A
Leucine--tRNA ligase, cytoplasmic	LARS	24.13	Cytosol (Supported); Additional: Vesicles
Protein FAM98A	FAM98A	24.10	Cytosol (Enhanced)
T-complex protein 1 subunit gamma	CCT3	24.10	Cytosol;Nuclear bodies (Approved)
Vesicle-associated membrane protein-associated protein A	VAPA	24.10	Vesicles (Approved)
Growth arrest and DNA damage-inducible proteins-interacting protein 1	GADD45GIP1	24.08	Cytosol;Plasma membrane (Approved)
Coatomer subunit beta	COPB1	24.07	Endoplasmic reticulum (Enhanced)
Uncharacterized protein C11orf98	C11orf98	24.04	Mitochondria (Supported); Additional: Nucleoplasm
Endophilin-A2	SH3GL1	24.04	Cytosol;Golgi apparatus;Vesicles (Enhanced)
Protein syndesmos	NUDT16L1	24.01	N/A
Cilia- and flagella-associated protein 43	CFAP43	24.01	Cytosol (Enhanced)
DnaJ homolog subfamily A member 2	DNAJA2	24.01	N/A
Magnesium transporter protein 1	MAGT1	23.99	N/A
Methylcrotonoyl-CoA carboxylase beta chain, mitochondrial	MCCC2	23.99	Cytosol;Nucleoli (Approved); Additional: Intermediate filaments
Nuclear pore complex protein Nup93	NUP93	23.98	N/A
E3 ubiquitin-protein ligase TRIM21	TRIM21	23.96	Mitochondria (Enhanced)
Cyclin-dependent kinase 1	CDK1	23.93	N/A
Cirhin	CIRH1A	23.93	Nucleoplasm (Approved)
Syntaxin-binding protein 3	STXBP3	23.93	Cytosol;Nucleoplasm (Supported)
Gem-associated protein 2	GEMIN2	23.91	Nucleoli fibrillar center (Supported)
Activator of 90 kDa heat shock protein ATPase homolog 1	AHSA1	23.91	Nucleoplasm (Approved); Additional: Cytosol
Sickle tail protein homolog	KIAA1217	23.91	Nuclear bodies;Nucleoplasm (Supported); Additional: Nucleoli
Nuclear pore complex protein Nup205	NUP205	23.88	Cytosol (Supported)
Polynucleotide 5-hydroxyl-kinase NOL9	NOL9	23.86	Cytosol;Nucleoplasm (Approved)
26S proteasome non-ATPase regulatory subunit 14	PSMD14	23.86	N/A
Gem-associated protein 8	GEMIN8	23.84	Nucleoli (Supported); Additional: Intermediate filaments
Eukaryotic translation initiation factor 4 gamma 1	EIF4G1	23.78	Nucleoplasm (Supported)
DNA replication licensing factor MCM2	MCM2	23.77	Cytosol;Nucleoplasm (Supported)
7-dehydrocholesterol reductase	DHCR7	23.76	Cytosol (Enhanced)
Vesicle-associated membrane protein 5	VAMP5	23.73	Nucleoplasm (Enhanced)
Microfibril-associated glycoprotein 4	MFAP4	23.71	Endoplasmic reticulum (Supported)
DNA-directed RNA polymerase II subunit RPB2	POLR2B	23.71	Nucleoplasm;Plasma membrane (Approved)
Midkine	MDK	23.70	Endoplasmic reticulum (Approved)
DNA (cytosine-5)-methyltransferase 3B	DNMT3B	23.70	Nucleoplasm (Supported)
ADP-ribosylation factor-like protein 1	ARL1	23.69	Vesicles (Approved)
Ras-related GTP-binding protein A	RRAGA	23.68	Nucleoplasm (Supported)
DnaJ homolog subfamily A member 1	DNAJA1	23.68	Golgi apparatus (Supported)
pre-rRNA processing protein FTSJ3	FTSJ3	23.66	Golgi apparatus;Vesicles (Approved)
Probable ATP-dependent RNA helicase DDX52	DDX52	23.65	Cytosol (Supported); Additional: Microtubules
ATP synthase subunit g, mitochondrial	ATP5L	23.64	Nucleoli;Nucleoli rim (Enhanced); Additional: Mitotic chromosome
Mitochondrial carrier homolog 2	MTCH2	23.64	Nucleoli;Nucleoplasm (Supported)
Dolichyl-diphosphooligosaccharide--protein glycosyltransferase subunit DAD1	DAD1	23.63	Mitochondria (Supported)
Probable E3 ubiquitin-protein ligase TRIML1	TRIML1	23.63	Mitochondria (Approved)
ATP-dependent DNA helicase Q1	RECQL	23.61	Cytosol (Uncertain); Additional: Endoplasmic reticulum
Heterochromatin protein 1-binding protein 3	HP1BP3	23.59	N/A
IST1 homolog	IST1	23.58	Nucleoplasm (Enhanced)
CTP synthase 1	CTPS1	23.55	Nuclear speckles (Supported)
RuvB-like 1	RUVBL1	23.53	Vesicles (Supported)

Histone deacetylase 1	HDAC1	23.53	Cytosol (Approved); Additional: Actin filaments
Phosphatidylserine synthase 1	PTDSS1	23.52	Cytosol;Nucleoplasm (Supported)
Complement component 1 Q subcomponent-binding protein, mitochondrial	C1QBP	23.51	Nucleoplasm (Enhanced)
Serine/threonine-protein phosphatase 2A 55 kDa regulatory subunit B alpha isoform	PPP2R2A	23.51	Endoplasmic reticulum (Approved); Additional: Nucleoplasm
ATPase family AAA domain-containing protein 3A	ATAD3A	23.49	Plasma membrane (Approved); Additional: Mitochondria
Eukaryotic translation initiation factor 2 subunit 1	EIF2S1	23.47	Cytosol (Approved)
ATP-dependent RNA helicase DDX50	DDX50	23.47	Mitochondria (Enhanced)
DNA mismatch repair protein Msh6	MSH6	23.46	Cytosol (Enhanced)
Annexin A2	ANXA2	23.46	Nucleoli (Enhanced)
Inhibitor of growth protein 3	ING3	23.45	Nucleoplasm (Supported); Additional: Golgi apparatus;Vesicles
Microsomal glutathione S-transferase 3	MGST3	23.44	Plasma membrane (Approved); Additional: Cytosol
ADP-ribosylation factor 1	ARF1	23.43	Nucleoplasm (Enhanced)
Transportin-3	TNPO3	23.40	Nucleoplasm (Approved)
Ras GTPase-activating protein-binding protein 1	G3BP1	23.39	Cytosol (Approved); Additional: Plasma membrane
Developmentally-regulated GTP-binding protein 1	DRG1	23.35	Vesicles (Enhanced)
Exportin-2	CSE1L	23.33	Cytosol (Supported)
ATP synthase subunit O, mitochondrial	ATP5O	23.31	Nuclear bodies;Nucleoplasm (Supported); Additional: Cytosol
Nuclear distribution protein nudE homolog 1	NDE1	23.30	Nucleoplasm (Enhanced); Additional: Cytosol
Calnexin	CANX	23.29	Mitochondria (Approved)
Splicing factor 3B subunit 1	SF3B1	23.29	N/A
ATP-binding cassette sub-family F member 1	ABCF1	23.27	Endoplasmic reticulum (Enhanced)
Melanoma-associated antigen D2	MAGED2	23.27	Nuclear speckles (Enhanced)
Delta(24)-sterol reductase	DHCR24	23.27	Cytosol (Enhanced)
Eukaryotic translation initiation factor 3 subunit I	EIF3I	23.27	Cytosol;Nucleoli;Nucleoplasm (Enhanced)
Phosphatidylinositol-glycan-specific phospholipase D	GPLD1	23.26	N/A
ATP-dependent RNA helicase DDX24	DDX24	23.26	Cytosol (Approved)
Glioma tumor suppressor candidate region gene 2 protein	GLTSCR2	23.25	N/A
Antigen KI-67	MKI67	23.23	Cytosol;Nucleoli (Approved)
DNA mismatch repair protein Msh2	MSH2	23.22	Nucleoli (Supported)
Nucleolar protein 11	NOL11	23.22	Nucleoli rim;Nucleoplasm (Enhanced); Additional: Mitotic chromosome;Nuclear bodies
Peptidyl-prolyl cis-trans isomerase G	PPIG	23.16	Nucleoplasm (Supported); Additional: Vesicles
Elongation of very long chain fatty acids protein 5	ELOVL5	23.13	Nucleoli (Supported)
Ubiquitin-conjugating enzyme E2 D2	UBE2D2	23.12	Nuclear speckles (Supported); Additional: Cytosol
Peroxiredoxin-6	PRDX6	23.11	Endoplasmic reticulum (Enhanced)
Dynamin-2	DNM2	23.09	Cytosol;Plasma membrane (Approved)
HEAT repeat-containing protein 1	HEATR1	23.05	Cytosol;Plasma membrane (Supported)
Coatomer subunit gamma-1	COPG1	23.04	Cytosol;Golgi apparatus (Approved)
Ras-related protein Rab-1B	RAB1B	23.03	Nucleoli fibrillar center (Enhanced); Additional: Mitochondria
Pumilio domain-containing protein KIAA0020	KIAA0020	23.02	Golgi apparatus (Supported); Additional: Cytosol;Nucleoplasm
Transmembrane and coiled-coil domain-containing protein 1	TMCO1	23.02	Golgi apparatus (Supported); Additional: Endoplasmic reticulum
Protein disulfide-isomerase A6	PDIA6	23.01	Nucleoli (Supported)
Periphilin-1	PPHLN1	23.00	Endoplasmic reticulum (Supported)
Tubulin beta-6 chain	TUBB6	22.99	Cytosol;Endoplasmic reticulum (Supported)
Ras-related protein Rab-10	RAB10	22.95	Nucleoplasm (Supported); Additional: Golgi apparatus
Outer dense fiber protein 2	ODF2	22.92	Microtubules (Approved); Additional: Cytokinetic bridge;Mitotic spindle
Tyrosine-protein phosphatase non-receptor type 13	PTPN13	22.92	N/A
26S proteasome non-ATPase regulatory subunit 6	PSMD6	22.91	Centrosome (Supported)
Sodium/potassium-transporting ATPase subunit alpha-1	ATP1A1	22.91	Nucleoplasm (Supported); Additional: Cytosol;Nucleoli fibrillar center

28S ribosomal protein S35, mitochondrial	MRPS35	22.90	N/A
Pleckstrin homology domain-containing family A member 7	PLEKHA7	22.88	N/A
Transmembrane emp24 domain-containing protein 2	TMED2	22.83	Mitochondria (Approved); Additional: Cytosol
Glycogen phosphorylase, liver form	PYGL	22.82	Cell Junctions;Nucleoplasm (Enhanced); Additional: Cytosol
ADP-ribosylation factor-like protein 2	ARL2	22.80	Vesicles (Supported)
Dolichol-phosphate mannosyltransferase subunit 1	DPM1	22.79	Cytosol;Plasma membrane (Supported)
Copine-3	CPNE3	22.78	Nucleoplasm (Approved); Additional: Cytosol;Focal adhesion sites;Golgi apparatus;Nucleoli
Cytochrome c1, heme protein, mitochondrial	CYC1	22.78	N/A
CCAAT/enhancer-binding protein zeta	CEBPZ	22.75	Cytosol;Nucleoplasm (Supported)
Dynamin-1-like protein	DNM1L	22.75	Mitochondria (Approved)
28S ribosomal protein S5, mitochondrial	MRPS5	22.74	Vesicles (Approved); Additional: Nucleoplasm
Dihydropyrimidinase-related protein 2	DPYSL2	22.73	Cytosol (Supported); Additional: Vesicles
Growth/differentiation factor 15	GDF15	22.73	Mitochondria (Supported)
Glutamine--fructose-6-phosphate aminotransferase [isomerizing] 2	GFPT2	22.70	Cytosol (Supported); Additional: Plasma membrane
Probable ATP-dependent RNA helicase DDX47	DDX47	22.67	Golgi apparatus (Enhanced)
Eukaryotic translation initiation factor 3 subunit B	EIF3B	22.65	Vesicles (Approved)
RNA-binding protein 25	RBM25	22.63	Nucleoli (Supported)
PHD finger protein 6	PHF6	22.62	Cytosol (Approved); Additional: Nucleoplasm
ATP-dependent RNA helicase DHX36	DHX36	22.61	Nuclear speckles (Enhanced)
Heat shock 70 kDa protein 1B	HSPA1B	22.59	Nucleoli;Nucleoplasm (Supported)
T-complex protein 1 subunit epsilon	CCT5	22.56	Nucleoplasm (Supported); Additional: Cytosol;Mitochondria
U2 snRNP-associated SURP motif-containing protein	U2SURP	22.56	Cytosol;Vesicles (Approved); Additional: Nucleoplasm
SLIT-ROBO Rho GTPase-activating protein 2B	SRGAP2B	22.56	N/A
Lysophospholipid acyltransferase 7	MBOAT7	22.52	Nucleoplasm (Supported)
Ragulator complex protein LAMTOR1	LAMTOR1	22.52	Cytosol (Approved); Additional: Centrosome
Cytochrome c oxidase subunit 5A, mitochondrial	COX5A	22.49	Cytosol (Approved)
Tubulin alpha-1A chain	TUBA1A	22.44	Golgi apparatus (Supported); Additional: Plasma membrane;Vesicles
DnaJ homolog subfamily A member 3, mitochondrial	DNAJA3	22.44	N/A
Histone H2B type 2-E	HIST2H2BE	22.42	Microtubules (Enhanced)
5-3 exoribonuclease 2	XRN2	22.42	Mitochondria (Supported); Additional: Vesicles
SURP and G-patch domain-containing protein 2	SUGP2	22.41	Nucleoplasm (Approved); Additional: Cytosol
Cleavage and polyadenylation specificity factor subunit 6	CPSF6	22.40	Nucleoli (Enhanced); Additional: Nucleoplasm
Pleckstrin homology domain-containing family A member 5	PLEKHA5	22.40	Nucleoplasm (Enhanced); Additional: Nuclear bodies
Probable global transcription activator SNF2L1	SMARCA1	22.35	Nuclear speckles;Nucleoplasm (Enhanced)
Protein-glutamate O-methyltransferase	ARMT1	22.29	Cytosol;Nucleoplasm (Approved)
60S ribosomal protein L26-like 1	RPL26L1	22.28	Nucleoplasm (Supported); Additional: Vesicles
Testis-expressed sequence 10 protein	TEX10	22.24	Nuclear bodies (Approved); Additional: Cytosol;Nucleoplasm
Oligoribonuclease, mitochondrial	REXO2	22.24	Cytosol;Endoplasmic reticulum (Approved); Additional: Nucleoli
39S ribosomal protein L40, mitochondrial	MRPL40	22.21	Nucleoplasm (Approved); Additional: Mitochondria
Trifunctional enzyme subunit alpha, mitochondrial	HADHA	22.18	Mitochondria (Supported); Additional: Focal adhesion sites;Nucleoli
Epithelial splicing regulatory protein 1	ESRP1	22.18	Mitochondria (Supported); Additional: Nucleoli
Ragulator complex protein LAMTOR3	LAMTOR3	22.18	Mitochondria (Enhanced)
Histone H2B type F-S	H2BFS	22.15	Nuclear bodies (Enhanced); Additional: Nucleoplasm
28S ribosomal protein S18a, mitochondrial	MRPS18A	22.12	N/A
14-3-3 protein theta	YWHAQ	22.11	Nucleoplasm (Approved); Additional: Cytosol
Pre-mRNA-splicing factor SYF1	XAB2	22.10	N/A
Zinc finger protein RFP	TRIM27	22.10	Cytosol (Supported); Additional: Nucleoplasm
Myosin-9	MYH9	22.06	Nucleoplasm (Supported); Additional: Vesicles

Chromobox protein homolog 5	CBX5	22.06	Nucleoli (Approved); Additional: Nucleoplasm
G-rich sequence factor 1	GRSF1	22.05	Actin filaments;Plasma membrane (Supported); Additional: Cytosol;Nuclear bodies
Ribosome biogenesis protein BOP1	BOP1	22.05	Nucleoplasm (Enhanced)
C-1-tetrahydrofolate synthase, cytoplasmic	MTHFD1	22.03	Mitochondria (Enhanced)
U4/U6 small nuclear ribonucleoprotein Prp31	PRPF31	22.01	Nucleoli;Nucleoli rim (Enhanced); Additional: Mitotic chromosome;Nucleoplasm
Protein DEK	DEK	21.98	Cytosol (Enhanced)
ATP-dependent 6-phosphofructokinase, liver type	PFKL	21.93	Nucleoplasm (Supported)
Cytoplasmic FMR1-interacting protein 1	CYFIP1	21.88	Nucleoplasm (Supported); Additional: Cytosol
Ras-related protein Rab-3B	RAB3B	21.87	Mitochondria;Nucleoli (Uncertain)
Signal peptidase complex catalytic subunit SEC11A	SEC11A	21.85	N/A
Monocarboxylate transporter 1	SLC16A1	21.82	Cell Junctions (Approved)
Calcium-binding mitochondrial carrier protein Aralar2	SLC25A13	21.82	Nuclear membrane (Approved); Additional: Golgi apparatus
Fragile X mental retardation protein 1	FMR1	21.81	Cell Junctions;Plasma membrane (Enhanced)
Translational activator GCN1	GCN1L1	21.78	Mitochondria (Supported)
Something about silencing protein 10	UTP3	21.74	Cytosol (Enhanced)
KDEL motif-containing protein 2	KDELC2	21.65	Cytosol (Enhanced)
Eukaryotic translation initiation factor 3 subunit A	EIF3A	21.65	Nucleoli (Supported); Additional: Vesicles
Putative RNA-binding protein Luc7-like 1	LUC7L	21.64	Nucleoplasm (Approved); Additional: Vesicles
Nuclear export mediator factor NEMF	NEMF	21.63	Cytosol;Nucleoplasm (Supported)
NADH-cytochrome b5 reductase 3	CYB5R3	21.61	Nucleoplasm (Approved); Additional: Mitochondria
Replication factor C subunit 1	RFC1	21.58	Cytosol;Nucleoplasm (Approved); Additional: Nuclear bodies
RNA-binding protein 28	RBM28	21.48	Endoplasmic reticulum (Supported)
NADH dehydrogenase [ubiquinone] 1 alpha subcomplex subunit 9, mitochondrial	NDUFA9	21.46	Nucleoplasm (Enhanced)
PCI domain-containing protein 2	PCID2	21.41	Nucleoli (Supported)
Coatomer subunit beta	COPB2	21.41	Mitochondria (Approved); Additional: Nucleoplasm
E3 ubiquitin-protein ligase TRIP12	TRIP12	21.40	Nucleoli;Nucleoplasm (Approved)
Eukaryotic translation initiation factor 5B	EIF5B	21.40	Endoplasmic reticulum (Approved); Additional: Golgi apparatus
S-phase kinase-associated protein 1	SKP1	21.38	Nuclear speckles (Approved)
ADP-ribosylation factor 5	ARF5	21.38	Cytosol (Approved); Additional: Plasma membrane
3-hydroxyacyl-CoA dehydrogenase type-2	HSD17B10	21.38	Nucleoplasm (Approved); Additional: Cytosol
Chromodomain-helicase-DNA-binding protein 4	CHD4	21.35	N/A
DNA replication licensing factor MCM4	MCM4	21.34	N/A
U2 small nuclear ribonucleoprotein A	SNRPA1	21.33	Nucleoplasm (Enhanced)
Cleavage stimulation factor subunit 2 tau variant	CSTF2T	21.31	Nucleoplasm (Enhanced)
Protein scribble homolog	SCRIB	21.25	Nucleoplasm (Supported); Additional: Nuclear bodies;Nuclear speckles
Zinc transporter SLC39A7	SLC39A7	21.21	Nucleoplasm (Enhanced); Additional: Vesicles
Superkiller viralicidic activity 2-like 2	SKIV2L2	21.18	Cell Junctions;Plasma membrane (Enhanced); Additional: Nucleoplasm;Rods & Rings
Zinc finger CCHC domain-containing protein 3	ZCCHC3	21.16	Endoplasmic reticulum (Supported); Additional: Nucleoplasm
Transmembrane protein 14C	TMEM14C	21.16	Nucleoplasm (Supported)
Ribose-phosphate pyrophosphokinase 1	PRPS1	21.13	Vesicles (Approved)
Proteasome subunit alpha type-4	PSMA4	21.11	N/A
Neutral amino acid transporter B(0)	SLC1A5	21.11	Vesicles (Approved)
Protein transport protein Sec61 subunit gamma	SEC61G	21.11	Cytosol;Nucleoplasm (Supported); Additional: Vesicles
Interferon-inducible double-stranded RNA-dependent protein kinase activator A	PRKRA	21.09	Plasma membrane (Enhanced)
Putative RNA-binding protein Luc7-like 2	LUC7L2	21.08	N/A
Importin-7	IPO7	21.05	Cytosol (Supported); Additional: Nucleoplasm
Probable ATP-dependent RNA helicase DDX46	DDX46	21.03	Nucleoplasm (Approved)
Unconventional myosin-Ic	MYO1C	21.00	Cytosol;Nucleoplasm (Supported)

Importin-9	IPO9	20.97	Nuclear speckles (Supported); Additional: Nucleoli fibrillar center
Inositol monophosphatase 2	IMPA2	20.94	Nuclear bodies;Plasma membrane (Enhanced)
Trifunctional purine biosynthetic protein adenosine-3	GART	20.93	Cytosol (Approved); Additional: Vesicles
DNA (cytosine-5)-methyltransferase 3A	DNMT3A	20.91	Nucleoplasm (Approved); Additional: Mitochondria
Exportin-T	XPOT	20.90	Cytosol (Approved); Additional: Mitochondria
Probable ATP-dependent RNA helicase YTHDC2	YTHDC2	20.87	Nucleoplasm (Supported)
Pachytene checkpoint protein 2 homolog	TRIP13	20.86	Nucleoplasm (Enhanced); Additional: Cytosol
HIG1 domain family member 1A, mitochondrial	HIGD1A	20.86	Nucleoplasm (Approved); Additional: Cytoplasmic bodies;Nuclear bodies
Unconventional myosin-Ib	MYO1B	20.82	Nucleoplasm (Approved)
Transcription factor BTF3	BTF3	20.78	Mitochondria (Supported); Additional: Nucleoplasm
Phosphatidylinositol glycan anchor biosynthesis class U protein	PIGU	20.74	Plasma membrane (Enhanced)
Ataxin-10	ATXN10	20.69	Cytosol (Supported)
HEAT repeat-containing protein 5B	HEATR5B	20.68	Nucleoplasm (Approved); Additional: Cytosol
Pre-mRNA-splicing factor CWC22 homolog	CWC22	20.64	Cytosol (Supported); Additional: Plasma membrane
Serine/threonine-protein phosphatase 2A 65 kDa regulatory subunit A alpha isoform	PPP2R1A	20.61	Cytosol;Nuclear speckles;Vesicles (Approved)
U2 small nuclear ribonucleoprotein B	SNRPB2	20.58	Nuclear speckles (Supported); Additional: Cytosol
Catenin delta-1	CTNND1	20.53	Cytosol (Approved)
Probable ATP-dependent RNA helicase DDX10	DDX10	20.52	Nuclear speckles (Supported); Additional: Cytoplasmic bodies
Protein transport protein Sec61 subunit alpha isoform 2	SEC61A2	20.51	Plasma membrane (Enhanced)
Protein deglycase DJ-1	PARK7	20.50	Nucleoli (Approved)
ATPase family AAA domain-containing protein 1	ATAD1	20.48	N/A
Zinc finger protein 292	ZNF292	20.48	Cytosol;Nucleoplasm (Supported)
Tricarboxylate transport protein, mitochondrial	SLC25A1	20.46	Nucleoli rim (Approved); Additional: Mitochondria
V-type proton ATPase subunit H	ATP6V1H	20.45	Nuclear membrane;Nucleoplasm (Approved)
Protein SON	SON	20.44	N/A
26S proteasome non-ATPase regulatory subunit 7	PSMD7	20.42	Actin filaments;Cytosol (Supported); Additional: Plasma membrane
Ezrin	EZR	20.39	Nuclear speckles (Enhanced)
Putative ATP-dependent RNA helicase DHX30	DHX30	20.38	Nucleoplasm (Enhanced)
Structural maintenance of chromosomes protein 4	SMC4	20.37	Plasma membrane (Supported)
Major facilitator superfamily domain-containing protein 10	MFSD10	20.36	Mitochondria (Supported); Additional: Cytosol
Eukaryotic translation initiation factor 4E	EIF4E	20.35	Cytosol;Nuclear speckles (Supported)
Transitional endoplasmic reticulum ATPase	VCP	20.31	Nuclear membrane (Approved); Additional: Nucleoplasm
Nuclear pore complex protein Nup160	NUP160	20.31	Cytoplasmic bodies;Cytosol (Supported); Additional: Nucleoplasm
Neuroguidin	NGDN	20.31	Cytosol;Nucleoplasm (Enhanced)
26S proteasome non-ATPase regulatory subunit 2	PSMD2	20.28	N/A
Glutamate-rich WD repeat-containing protein 1	GRWD1	20.21	Mitochondria;Nucleoli (Approved); Additional: Nucleoplasm
Fascin	FSCN1	20.19	N/A
Cytoplasmic dynein 1 light intermediate chain 1	DYNC1LI1	20.15	Nucleoli;Nucleoli rim (Enhanced); Additional: Nucleoplasm
Exportin-5	XPO5	20.14	Cytosol;Plasma membrane (Approved)
Oxysterol-binding protein-related protein 8	OSBPL8	20.11	Centrosome;Cytosol (Supported)
Probable ubiquitin carboxyl-terminal hydrolase FAF-X	USP9X	20.08	Nucleoplasm (Enhanced); Additional: Cytosol
DNA replication licensing factor MCM3	MCM3	20.08	Cytosol;Vesicles (Approved)
Coiled-coil domain-containing protein 47	CCDC47	19.96	Cytosol (Supported)
NADPH--cytochrome P450 reductase	POR	19.86	Nucleoplasm (Supported)
Apoptosis-inducing factor 1, mitochondrial	AIFM1	19.83	Endoplasmic reticulum (Enhanced)
Telomere length regulation protein TEL2 homolog	TELO2	19.27	Vesicles (Approved); Additional: Cytosol;Nucleoplasm
E3 ubiquitin-protein ligase UBR4	UBR4	19.24	Mitochondria (Supported)
Actin-related protein 3C	ACTR3C	19.21	Cytosol;Nuclear bodies (Supported)

Valine--tRNA ligase	VARS	19.18	Nucleoplasm (Supported); Additional: Centrosome;Cytosol
ATP-citrate synthase	ACLY	19.10	N/A
Epiplakin	EPPK1	19.09	Cytosol (Enhanced)
GTP-binding protein 1	GTPBP1	18.91	Cytosol (Enhanced); Additional: Nucleoplasm
Condensin complex subunit 3	NCAPG	17.42	Intermediate filaments (Enhanced)
Protein phosphatase 1 regulatory subunit 12A	PPP1R12A	15.26	Cytosol;Golgi apparatus (Approved); Additional: Nuclear bodies
Protein timeless homolog	TIMELESS	13.08	N/A
La-related protein 1	LARP1	12.73	Actin filaments;Cytosol (Supported); Additional: Nucleoli;Plasma membrane
ATP-dependent RNA helicase A	DHX9	11.84	Nucleoplasm (Supported)
Nuclear receptor coactivator 5	NCOA5	11.65	Cytosol;Endoplasmic reticulum;Nucleoplasm (Supported)
Thyroid hormone receptor-associated protein 3	THRAP3	11.29	Nucleoplasm (Enhanced); Additional: Nucleoli
Probable 28S rRNA (cytosine(4447)-C(5))-methyltransferase	NOP2	11.00	Actin filaments;Nucleoplasm (Supported)
Insulin-like growth factor 2 mRNA-binding protein 2	IGF2BP2	11.00	Nuclear speckles (Enhanced)
Interleukin enhancer-binding factor 3	ILF3	10.95	Nucleoli (Enhanced)
Splicing factor, proline- and glutamine-rich	SFPQ	10.59	Cytosol (Enhanced)
RNA-binding motif protein, X chromosome	RBMX	10.55	Mitochondria;Nucleoli;Nucleoplasm (Enhanced)
Insulin-like growth factor 2 mRNA-binding protein 3	IGF2BP3	10.46	Nucleoplasm (Enhanced)
Heterogeneous nuclear ribonucleoprotein A0	HNRNPA0	10.29	Nucleoplasm (Supported)
Heterogeneous nuclear ribonucleoprotein A3	HNRNPA3	10.28	Cytosol (Supported)
Heterogeneous nuclear ribonucleoprotein Q	SYNCRIP	10.28	Nucleoplasm (Enhanced)
Heterogeneous nuclear ribonucleoprotein D0	HNRNPD	10.28	Nucleoplasm (Approved)
Heterogeneous nuclear ribonucleoprotein L	HNRNPL	10.16	Nucleoplasm (Approved); Additional: Cytosol
Pre-mRNA-processing factor 19	PRPF19	10.06	Nucleoplasm (Enhanced)
Heterogeneous nuclear ribonucleoprotein A/B	HNRNPAB	10.01	Nucleoplasm (Enhanced)
Cleavage and polyadenylation specificity factor subunit 5	NUDT21	9.79	Nuclear speckles (Enhanced)
Heterogeneous nuclear ribonucleoprotein U	HNRNPU	9.78	Nucleoplasm (Enhanced)
RNA-binding protein 14	RBM14	9.61	Nuclear bodies (Supported); Additional: Centriolar satellite
Interleukin enhancer-binding factor 2	ILF2	9.56	Nucleoplasm (Supported)
Heterogeneous nuclear ribonucleoproteins C1/C2	HNRNPC	9.54	Nuclear speckles (Supported)
Probable ATP-dependent RNA helicase DDX20	DDX20	9.48	Nucleoplasm (Supported); Additional: Cytosol
Probable ATP-dependent RNA helicase DDX17	DDX17	9.43	Nucleoplasm (Enhanced)
Heterogeneous nuclear ribonucleoprotein R	HNRNPR	9.41	Nuclear bodies (Supported); Additional: Cytosol;Nucleoplasm
Ribosomal L1 domain-containing protein 1	RSL1D1	9.36	Nuclear speckles (Supported)
BTB/POZ domain-containing protein KCTD3	KCTD3	9.25	Nucleoplasm (Enhanced)
Non-POU domain-containing octamer-binding protein	NONO	9.24	Mitotic chromosome;Nucleoli rim (Enhanced)
40S ribosomal protein S6	RPS6	9.15	Cytosol (Approved)
DNA-dependent protein kinase catalytic subunit	PRKDC	9.07	Nucleoplasm (Enhanced); Additional: Nucleoli;Nucleoli fibrillar center
Nucleolar protein 56	NOP56	8.94	Cytosol;Endoplasmic reticulum (Enhanced)
Serine/arginine-rich splicing factor 3	SRSF3	8.83	Nucleoplasm (Enhanced)
RNA-binding protein Raly	RALY	8.80	Nucleoli fibrillar center (Enhanced)
Insulin-like growth factor 2 mRNA-binding protein 1	IGF2BP1	8.77	Nucleoplasm (Supported)
Polyadenylate-binding protein 1	PABPC1	8.67	Nucleoplasm (Enhanced); Additional: Vesicles
Serine/arginine-rich splicing factor 9	SRSF9	8.58	Cytosol (Supported)
Histone H1x	H1FX	8.50	Cytosol (Supported)
Heterogeneous nuclear ribonucleoprotein A1	HNRNPA1	8.46	Nucleoplasm (Supported); Additional: Nucleoli
Polypyrimidine tract-binding protein 1	PTBP1	8.41	Nucleoli;Nucleoplasm (Supported); Additional: Mitotic chromosome;Nucleoli rim
Aftiphilin	AFTPH	8.33	Nucleoplasm (Supported)
Nucleolar protein 58	NOP58	8.27	Nucleoplasm (Supported)

Pre-mRNA-splicing factor ATP-dependent RNA helicase DHX15	DHX15	8.23	Cytosol (Supported); Additional: Golgi apparatus;Vesicles
rRNA 2-O-methyltransferase fibrillarin	FBL	8.20	Nucleoli fibrillar center (Enhanced); Additional: Nucleoplasm
Ribosomal RNA small subunit methyltransferase NEP1	EMG1	8.11	Nuclear speckles (Enhanced)
60S ribosomal protein L35a	RPL35A	8.11	Nucleoli fibrillar center (Supported); Additional: Nucleoplasm
60S ribosomal protein L6	RPL6	7.88	Nucleoli rim (Supported); Additional: Mitotic chromosome;Nucleoplasm
Heterogeneous nuclear ribonucleoproteins A2/B1	HNRNPA2B1	7.86	N/A
Lysine--tRNA ligase	KARS	7.75	N/A
Methionine--tRNA ligase, cytoplasmic	MARS	7.74	Nucleoplasm (Supported)
40S ribosomal protein S24	RPS24	7.70	Cytosol (Supported); Additional: Plasma membrane
26S proteasome non-ATPase regulatory subunit 3	PSMD3	7.66	Cytosol (Enhanced)
Bifunctional glutamate/proline--tRNA ligase	EPRS	7.65	Cytosol;Endoplasmic reticulum (Enhanced)
Small nuclear ribonucleoprotein Sm D1	SNRPD1	7.62	Nucleoplasm (Approved); Additional: Cytosol
U1 small nuclear ribonucleoprotein 70 kDa	SNRNP70	7.60	Cytosol (Enhanced)
60S ribosomal protein L10a	RPL10A	7.55	N/A
Microtubule-associated protein 4	MAP4	7.54	Nucleoplasm (Enhanced)
DNA topoisomerase 1	TOP1	7.49	Cytosol;Endoplasmic reticulum;Nucleoli (Supported)
60S ribosomal protein L23a	RPL23A	7.44	Cytosol;Microtubules;Plasma membrane (Approved)
ATP-dependent RNA helicase DDX3X	DDX3X	7.29	Nucleoli fibrillar center;Nucleoplasm (Supported)
Heterogeneous nuclear ribonucleoprotein H2	HNRNPH2	7.21	Cytosol;Endoplasmic reticulum;Nucleoli fibrillar center (Approved)
TATA-binding protein-associated factor 2N	TAF15	7.19	Cytosol (Approved); Additional: Nucleoplasm
Vimentin	VIM	7.19	Nucleoplasm (Enhanced)
60S ribosomal protein L18a	RPL18A	7.17	Nucleoplasm (Enhanced)
Probable ATP-dependent RNA helicase DDX5	DDX5	7.12	Intermediate filaments (Supported)
Zinc finger CCCH domain-containing protein 13	ZC3H13	7.12	Nucleoli (Approved); Additional: Cytosol;Nucleoplasm
Small nuclear ribonucleoprotein Sm D2	SNRPD2	7.10	Nucleoli;Nucleoplasm (Supported)
Heterogeneous nuclear ribonucleoprotein U-like protein 2	HNRNPUL2	6.98	Nucleoplasm (Supported)
60S ribosomal protein L14	RPL14	6.96	Cytosol (Supported)
X-ray repair cross-complementing protein 6	XRCC6	6.89	Nucleoplasm (Enhanced)
THO complex subunit 4	ALYREF	6.82	Cytosol;Endoplasmic reticulum (Supported)
60S ribosomal protein L15	RPL15	6.81	Nucleoplasm (Enhanced)
60S ribosomal protein L8	RPL8	6.80	Nuclear speckles;Nucleoplasm (Approved)
Exportin-1	XPO1	6.75	N/A
Heterogeneous nuclear ribonucleoprotein K	HNRNPK	6.74	Cytosol;Endoplasmic reticulum;Nucleoli (Supported)
60S ribosomal protein L31	RPL31	6.69	Nuclear membrane;Nucleoplasm (Enhanced); Additional: Cytosol;Vesicles
60S ribosomal protein L3	RPL3	6.63	Nucleoplasm (Enhanced)
Histone H3.2	HIST2H3A	6.61	N/A
60S ribosomal protein L34	RPL34	6.61	Cytosol;Nucleoli (Supported)
Pre-mRNA-processing-splicing factor 8	PRPF8	6.60	Nucleoplasm (Supported)
Nucleolin	NCL	6.60	Cytosol;Endoplasmic reticulum (Supported); Additional: Nucleoli
60S ribosomal protein L36a	RPL36A	6.55	Nucleoplasm (Supported)
Small nuclear ribonucleoprotein Sm D3	SNRPD3	6.53	Nucleoli;Nucleoli rim;Nucleoplasm (Enhanced); Additional: Mitotic chromosome
DNA topoisomerase 2-alpha	TOP2A	6.50	Cytosol;Endoplasmic reticulum (Supported); Additional: Plasma membrane
Dolichyl-diphosphooligosaccharide--protein glycosyltransferase subunit 1	RPN1	6.47	Nucleoplasm (Supported); Additional: Cytosol;Nuclear bodies
40S ribosomal protein S8	RPS8	6.46	Nucleoplasm (Supported); Additional: Nucleoli
Spliceosome RNA helicase DDX39B	DDX39B	6.44	Endoplasmic reticulum (Enhanced); Additional: Cytosol
Elongation factor Tu, mitochondrial	TUFM	6.42	Cytosol;Endoplasmic reticulum (Enhanced)
Growth/differentiation factor 3	GDF3	6.41	Nuclear speckles (Enhanced)
60S ribosomal protein L37a	RPL37A	6.39	Mitochondria (Enhanced)

40S ribosomal protein S11	RPS11	6.31	N/A
60S ribosomal protein L17	RPL17	6.31	Cytosol;Endoplasmic reticulum (Approved)
40S ribosomal protein S15	RPS15	6.26	Cytosol (Approved); Additional: Endoplasmic reticulum;Nucleoli
Dynein light chain 1, cytoplasmic	DYNLL1	6.26	Cytosol;Endoplasmic reticulum (Supported)
TAR DNA-binding protein 43	TARDBP	6.26	Cytosol;Endoplasmic reticulum (Approved)
60S ribosomal protein L7a	RPL7A	6.24	Cytosol;Nucleoplasm (Approved); Additional: Nuclear bodies
Heterogeneous nuclear ribonucleoprotein M	HNRNPM	6.23	Nucleoplasm (Enhanced)
60S ribosomal protein L24	RPL24	6.20	Nucleoli (Approved); Additional: Vesicles
Surfeit locus protein 4	SURF4	6.20	Nucleoplasm (Enhanced)
Small nuclear ribonucleoprotein-associated protein N	SNRPN	6.19	Cytosol;Endoplasmic reticulum (Enhanced)
Poly(rC)-binding protein 2	PCBP2	6.16	Endoplasmic reticulum;Golgi apparatus;Nuclear membrane (Supported); Additional: Cytosol
Fatty acid synthase	FASN	6.16	Nucleoplasm (Approved)
Poly [ADP-ribose] polymerase 1	PARP1	6.13	Cytosol;Nucleoplasm (Supported)
60S ribosomal protein L4	RPL4	6.12	Cytosol;Plasma membrane (Enhanced)
40S ribosomal protein S30	FAU	6.10	Nucleoplasm (Supported); Additional: Nucleoli
CAD protein	CAD	6.09	Cytosol;Endoplasmic reticulum (Approved); Additional: Nuclear bodies;Nucleoli
60S ribosomal protein L28	RPL28	6.08	Cytosol;Endoplasmic reticulum (Enhanced); Additional: Nucleoli
40S ribosomal protein S9	RPS9	6.04	Cytosol (Supported)
40S ribosomal protein S14	RPS14	6.03	Cytosol;Endoplasmic reticulum (Supported)
Eukaryotic initiation factor 4A-I	EIF4A1	6.03	N/A
Poly(rC)-binding protein 1	PCBP1	6.00	Cytosol;Endoplasmic reticulum (Supported)
U1 small nuclear ribonucleoprotein A	SNRPA	5.99	Cytosol (Approved)
T-complex protein 1 subunit zeta	CCT6A	5.97	Nuclear speckles (Supported); Additional: Cytoplasmic bodies;Cytosol;Nucleoplasm
U3 small nucleolar RNA-associated protein 18 homolog	UTP18	5.96	Nucleoplasm (Supported)
Keratin, type I cytoskeletal 18	KRT18	5.87	Cytosol (Approved)
Importin subunit alpha-1	KPNA2	5.86	Nucleoli;Nucleoli rim (Supported); Additional: Nuclear membrane;Nucleoplasm
60S ribosomal protein L27a	RPL27A	5.85	Cytosol (Supported)
Dolichyl-diphosphooligosaccharide--protein glycosyltransferase 48 kDa subunit	DDOST	5.84	Nucleoplasm (Enhanced); Additional: Cytosol
60S ribosomal protein L10	RPL10	5.82	Cytosol;Endoplasmic reticulum (Enhanced)
Arf-GAP with coiled-coil, ANK repeat and PH domain-containing protein 2	ACAP2	5.80	Endoplasmic reticulum (Supported)
60S ribosomal protein L30	RPL30	5.79	Cytosol;Endoplasmic reticulum (Enhanced)
Leucine-rich repeat-containing protein 59	LRRC59	5.76	Endosomes (Approved)
Nucleophosmin	NPM1	5.76	Cytosol;Endoplasmic reticulum (Approved)
Matrin-3	MATR3	5.71	Endoplasmic reticulum (Enhanced)
40S ribosomal protein S26	RPS26	5.66	Nucleoli rim (Enhanced); Additional: Nucleoplasm
60S ribosomal protein L13a	RPL13A	5.65	Nucleoplasm (Approved)
Histone H3	HIST2H3PS2	5.64	Cytosol;Endoplasmic reticulum (Enhanced); Additional: Nucleoli
Lamin-B1	LMNB1	5.63	Cytosol;Nucleoli (Approved)
60S ribosomal protein L32	RPL32	5.56	Nucleoplasm (Supported)
Tubulin beta-2B chain	TUBB2B	5.56	Nuclear membrane (Supported)
40S ribosomal protein S23	RPS23	5.54	Cytosol;Endoplasmic reticulum (Approved)
DBIRD complex subunit ZNF326	ZNF326	5.54	Microtubules (Supported); Additional: Cytokinetic bridge;Mitotic spindle
T-complex protein 1 subunit beta	CCT2	5.54	Cytosol (Supported); Additional: Endoplasmic reticulum
ADP/ATP translocase 2	SLC25A5	5.52	Nucleoplasm (Approved); Additional: Golgi apparatus;Vesicles
40S ribosomal protein S2	RPS2	5.51	Cytosol (Supported)
40S ribosomal protein S19	RPS19	5.45	Mitochondria (Supported)
Putative 60S ribosomal protein L39-like 5	RPL39P5	5.45	Cytosol;Endoplasmic reticulum (Approved)
60S acidic ribosomal protein P0	RPLP0	5.45	Nucleoplasm (Supported)

Interferon-induced transmembrane protein 1	IFITM1	5.44	N/A
60S ribosomal protein L18	RPL18	5.44	Cytosol;Endoplasmic reticulum (Supported)
Cytochrome c oxidase subunit 6C	COX6C	5.39	Golgi apparatus (Uncertain); Additional: Cytosol;Plasma membrane
40S ribosomal protein S3	RPS3	5.36	Cytosol;Endoplasmic reticulum (Supported); Additional: Nucleoli
60S ribosomal protein L21	RPL21	5.28	Mitochondria (Enhanced)
ADP/ATP translocase 3	SLC25A6	5.28	Cytosol;Endoplasmic reticulum (Supported)
60S ribosomal protein L12	RPL12	5.20	Cytosol;Endoplasmic reticulum;Nucleoli fibrillar center (Supported)
40S ribosomal protein S4, X isoform	RPS4X	5.14	Mitochondria (Supported)
60S ribosomal protein L9	RPL9	5.11	Golgi apparatus (Approved)
60S ribosomal protein L35	RPL35	5.10	N/A
Voltage-dependent anion-selective channel protein 2	VDAC2	5.08	Cytosol;Endoplasmic reticulum (Supported); Additional: Nucleoli
Actin, cytoplasmic 1	ACTB	5.03	Cytosol;Endoplasmic reticulum (Approved)
Elongation factor 1-alpha 1	EEF1A1	5.01	Mitochondria (Supported)
RNA-binding protein FUS	FUS	4.95	N/A
ATP synthase subunit beta, mitochondrial	ATP5B	4.94	Cytosol (Supported)
60S ribosomal protein L36	RPL36	4.93	Nucleoplasm (Supported)
T-complex protein 1 subunit delta	CCT4	4.92	Mitochondria (Enhanced)
60S ribosomal protein L11	RPL11	4.92	Cytosol (Supported)
60S ribosomal protein L27	RPL27	4.89	Cytosol (Supported); Additional: Nucleoplasm
Tubulin beta chain	TUBB	4.87	N/A
L-lactate dehydrogenase B chain	LDHB	4.85	Nucleoli (Enhanced); Additional: Nucleoplasm
60S ribosomal protein L22	RPL22	4.80	Microtubules (Supported); Additional: Cytokinetic bridge;Mitotic spindle
Voltage-dependent anion-selective channel protein 1	VDAC1	4.80	Cytosol (Supported)
40S ribosomal protein S10	RPS10	4.77	Nucleoli (Approved); Additional: Nucleoplasm
60S ribosomal protein L26	RPL26	4.76	N/A
Actin, alpha skeletal muscle	ACTA1	4.74	Cytosol (Approved)
GTP-binding nuclear protein Ran	RAN	4.68	Cytosol;Endoplasmic reticulum (Approved); Additional: Nucleoli
Complement C1s subcomponent	C1S	4.67	N/A
Rotatin	RTTN	4.62	Nucleoplasm (Enhanced)
Kinase D-interacting substrate of 220 kDa	KIDINS220	4.61	Nucleoplasm (Approved); Additional: Cytosol
ADP-ribosylation factor 4	ARF4	4.56	Cytosol (Approved); Additional: Centrosome
40S ribosomal protein S18	RPS18	4.55	Nucleoplasm (Approved)
40S ribosomal protein S16	RPS16	4.53	N/A
60S acidic ribosomal protein P1	RPLP1	4.46	Cytosol (Supported)
Cytochrome c oxidase subunit 2	MT-CO2	4.42	Cytosol;Endoplasmic reticulum (Enhanced)
Histone H1.0	H1F0	4.42	Cytosol;Endoplasmic reticulum (Supported)
Transcription intermediary factor 1-beta	TRIM28	4.39	N/A
Prohibitin-2	PHB2	4.38	Nuclear bodies;Nucleoplasm (Supported); Additional: Actin filaments;Golgi apparatus
Phosphate carrier protein, mitochondrial	SLC25A3	4.27	Nucleoplasm (Enhanced)
40S ribosomal protein S7	RPS7	4.21	Mitochondria (Enhanced)
ATP synthase subunit alpha, mitochondrial	ATP5A1	4.21	Mitochondria (Supported)
40S ribosomal protein S25	RPS25	4.20	Cytosol;Endoplasmic reticulum (Supported)
40S ribosomal protein S27	RPS27	4.13	Mitochondria (Supported)
Vomeronasal type-1 receptor 5	VN1R5	4.08	Cytosol;Endoplasmic reticulum (Supported); Additional: Nucleoli
Gap junction alpha-1 protein	GJA1	4.04	Cytosol;Endoplasmic reticulum (Approved); Additional: Nucleoli
D-3-phosphoglycerate dehydrogenase	PHGDH	4.04	N/A
Serine/arginine repetitive matrix protein 2	SRRM2	4.04	Cell Junctions;Vesicles (Supported); Additional: Nucleoplasm
40S ribosomal protein S20	RPS20	4.04	Cytosol;Plasma membrane (Enhanced); Additional: Nucleoplasm

40S ribosomal protein S3a	RPS3A	4.03	Nuclear speckles (Enhanced)
Histone H2A type 1-C	HIST1H2AC	4.00	Cytosol;Endoplasmic reticulum (Supported)
Microsomal glutathione S-transferase 1	MGST1	3.99	Cytosol;Endoplasmic reticulum;Nucleoli (Enhanced)
Solute carrier family 2, facilitated glucose transporter member 1	SLC2A1	3.98	Nucleoplasm (Supported)
40S ribosomal protein S15a	RPS15A	3.96	Mitochondria (Approved); Additional: Endoplasmic reticulum
Flap endonuclease 1	FEN1	3.89	Plasma membrane (Enhanced)
Signal recognition particle 14 kDa protein	SRP14	3.88	N/A
Cullin-associated NEDD8-dissociated protein 1	CAND1	3.88	Nucleoplasm (Enhanced); Additional: Nucleoli
L-lactate dehydrogenase A chain	LDHA	3.86	Nucleoli (Approved); Additional: Nucleoplasm
Multiple myeloma tumor-associated protein 2	MMTAG2	3.83	Cytosol;Golgi apparatus;Nucleoplasm (Enhanced)
Ubiquitin-40S ribosomal protein S27a	RPS27A	3.83	Cytosol (Supported); Additional: Vesicles
60S acidic ribosomal protein P2	RPLP2	3.79	Nuclear speckles;Plasma membrane (Approved); Additional: Cytosol
Serpin H1	SERPINH1	3.76	Cytosol;Endoplasmic reticulum;Nucleoli (Supported)
Histone H4	HIST1H4A	3.75	Cytosol;Nuclear speckles (Approved); Additional: Mitotic spindle
60S ribosomal protein L7	RPL7	3.75	Endoplasmic reticulum (Supported)
40S ribosomal protein S5	RPS5	3.73	N/A
60S ribosomal protein L19	RPL19	3.71	Cytosol;Endoplasmic reticulum (Approved); Additional: Nucleoli
Ras-related protein Rab-6B	RAB6B	3.67	Cytosol;Endoplasmic reticulum (Supported)
40S ribosomal protein S12	RPS12	3.65	Cytosol;Nucleoli (Enhanced)
Pyruvate kinase PKM	PKM	3.64	Golgi apparatus (Supported)
Elongation factor 2	EEF2	3.63	Cytosol (Supported); Additional: Golgi apparatus;Vesicles
Plasminogen activator inhibitor 1 RNA-binding protein	SERBP1	3.61	Cytosol (Enhanced)
Heat shock cognate 71 kDa protein	HSPA8	3.58	Cytosol;Plasma membrane (Enhanced)
Tubulin beta-4B chain	TUBB4B	3.54	Cytosol (Enhanced)
Membrane-associated progesterone receptor component 1	PGRMC1	3.53	Nucleoplasm (Approved); Additional: Vesicles
ATP synthase subunit a	MT-ATP6	3.45	Microtubules (Supported); Additional: Cytokinetic bridge;Mitotic spindle
E3 ubiquitin-protein ligase TRIM4	TRIM4	3.45	Endoplasmic reticulum (Approved); Additional: Nucleoli
Ras-related protein Rab-11A	RAB11A	3.43	N/A
Heat shock protein HSP 90-beta	HSP90AB1	3.39	Cytosol (Supported); Additional: Plasma membrane
Histone H2A.V	H2AFV	3.30	Centriolar satellite;Vesicles (Enhanced)
Transmembrane emp24 domain-containing protein 9	TMED9	3.29	Cytosol (Supported)
Elongation factor 1-gamma	EEF1G	3.28	N/A
Solute carrier family 2, facilitated glucose transporter member 3	SLC2A3	3.27	N/A
Very-long-chain 3-oxoacyl-CoA reductase	HSD17B12	3.24	Cytosol (Approved); Additional: Golgi apparatus
Glyceraldehyde-3-phosphate dehydrogenase	GAPDH	3.22	Plasma membrane (Supported)
Heat shock 70 kDa protein 6	HSPA6	3.16	N/A
Heat shock protein beta-1	HSPB1	3.13	Cytosol;Plasma membrane (Enhanced); Additional: Nuclear membrane;Vesicles
Prohibitin	PHB	3.12	Vesicles (Approved); Additional: Nucleoplasm
60S ribosomal protein L13	RPL13	3.06	Cytosol;Plasma membrane (Enhanced)
Probable ATP-dependent RNA helicase DDX41	DDX41	3.05	Mitochondria (Supported)
Receptor expression-enhancing protein 6	REEP6	3.04	Cytosol;Endoplasmic reticulum;Nucleoli (Enhanced)
Protein transport protein Sec61 subunit beta	SEC61B	2.87	Nucleoplasm (Supported); Additional: Nucleoli
ATP synthase subunit f, mitochondrial	ATP5J2	2.82	Endoplasmic reticulum (Supported)
78 kDa glucose-regulated protein	HSPA5	2.82	Endoplasmic reticulum (Supported)
40S ribosomal protein S17	RPS17	2.79	Mitochondria (Supported); Additional: Nuclear membrane
Urotensin-2	UTS2	2.59	Cytosol (Approved)
Ras-related protein Rab-7a	RAB7A	2.56	Cytosol;Endoplasmic reticulum (Approved); Additional: Nucleoli
Heat shock protein HSP 90-alpha	HSP90AA1	2.54	N/A

40S ribosomal protein S13	RPS13	2.52	Lysosomes (Supported)
B-cell receptor-associated protein 31	BCAP31	2.37	Cytosol (Enhanced)
Serine/threonine-protein kinase PRP4 homolog	PRPF4B	2.30	Endoplasmic reticulum (Approved)
Translocon-associated protein subunit alpha	SSR1	2.29	Endoplasmic reticulum (Enhanced)
Filamin-A	FLNA	2.26	Nuclear speckles (Supported)
Peptidyl-prolyl cis-trans isomerase B	PPIB	2.23	Endoplasmic reticulum (Supported)
High mobility group protein B1	HMGB1	2.19	Actin filaments;Cytosol;Plasma membrane (Enhanced)
Cofilin-1	CFL1	2.17	Endoplasmic reticulum (Supported); Additional: Nucleoplasm

Table 8.2: List of enriched candidates identified within the LARP1B protein interactome of GCT27CR cells following co-IP MS. *Proteins with a log2 fold change ≥2 are listed along with UniProt annotated Protein name, Gene name, Log2 fold change compared to IgG and Subcellular location. Subcellular location annotations were derived from Metascape annotation analysis which uses UniProt annotati*

9

References

1. Wang Z-L, Li B, Luo Y-X, Lin Q, Liu S-R, Zhang X-Q, et al. Comprehensive genomic characterization of RNA-binding proteins across human cancers. Cell reports. 2018;22(1):286-98.
2. Gerstberger S, Hafner M, Tuschl T. A census of human RNA-binding proteins. Nature Reviews Genetics. 2014;15(12):829-45.
3. Baltz AG, Munschauer M, Schwanhäusser B, Vasile A, Murakawa Y, Schueler M, et al. The mRNA-bound proteome and its global occupancy profile on protein-coding transcripts. Molecular cell. 2012;46(5):674-90.
4. Mukherjee N, Wessels H-H, Lebedeva S, Sajek M, Ghanbari M, Garzia A, et al. Deciphering human ribonucleoprotein regulatory networks. Nucleic acids research. 2019;47(2):570-81.
5. Zhang B, Babu KR, Lim CY, Kwok ZH, Li J, Zhou S, et al. A comprehensive expression landscape of RNA-binding proteins (RBPs) across 16 human cancer types. RNA biology. 2020;17(2):211-26.
6. Deragon JM, Bousquet-Antonelli C. The role of LARP1 in translation and beyond. Wiley Interdisciplinary Reviews: RNA. 2015;6(4):399-417.
7. Pereira B, Billaud M, Almeida R. RNA-binding proteins in cancer: old players and new actors. Trends in cancer. 2017;3(7):506-28.
8. Musunuru K. Cell-specific RNA-binding proteins in human disease. Trends in cardiovascular medicine. 2003;13(5):188-95.
9. Seufert L, Benzing T, Ignarski M, Müller R-U. RNA-binding proteins and their role in kidney disease. Nature Reviews Nephrology. 2022;18(3):153-70.
10. Masuda K, Kuwano Y. Diverse roles of RNA-binding proteins in cancer traits and their implications in gastrointestinal cancers. Wiley Interdisciplinary Reviews: RNA. 2019;10(3):e1520.
11. Hafner M, Landthaler M, Burger L, Khorshid M, Hausser J, Berninger P, et al. Transcriptome-wide identification of RNA-binding protein and microRNA target sites by PAR-CLIP. Cell. 2010;141(1):129-41.
12. Glisovic T, Bachorik JL, Yong J, Dreyfuss G. RNA-binding proteins and post-transcriptional gene regulation. FEBS letters. 2008;582(14):1977-86.
13. Salem ES, Vonberg AD, Borra VJ, Gill RK, Nakamura T. RNAs and RNA-binding proteins in immuno-metabolic homeostasis and diseases. Frontiers in Cardiovascular Medicine. 2019;6:106.
14. Sarkar S, Horn G, Moulton K, Oza A, Byler S, Kokolus S, et al. Cancer development, progression, and therapy: an epigenetic overview. International journal of molecular sciences. 2013;14(10):21087-113.
15. Takeshima H, Ushijima T. Accumulation of genetic and epigenetic alterations in normal cells and cancer risk. NPJ precision oncology. 2019;3(1):7.
16. García-Cárdenas JM, Guerrero S, López-Cortés A, Armendáriz-Castillo I, Guevara-Ramírez P, Pérez-Villa A, et al. Post-transcriptional regulation of colorectal cancer: a focus on RNA-binding proteins. Frontiers in molecular biosciences. 2019;6:65.
17. Arteaga CL, Sliwkowski MX, Osborne CK, Perez EA, Puglisi F, Gianni L. Treatment of HER2-positive breast cancer: current status and future perspectives. Nature reviews Clinical oncology. 2012;9(1):16-32.

18. Spector NL, Blackwell KL. Understanding the mechanisms behind trastuzumab therapy for human epidermal growth factor receptor 2–positive breast cancer. Journal of Clinical Oncology. 2009;27(34):5838-47.
19. Sung H, Ferlay J, Siegel RL, Laversanne M, Soerjomataram I, Jemal A, et al. Global cancer statistics 2020: GLOBOCAN estimates of incidence and mortality worldwide for 36 cancers in 185 countries. CA: a cancer journal for clinicians. 2021;71(3):209-49.
20. Hanahan D, Weinberg RA. Hallmarks of cancer: the next generation. cell. 2011;144(5):646-74.
21. Jewer M, Findlay SD, Postovit L-M. Post-transcriptional regulation in cancer progression: microenvironmental control of alternative splicing and translation. Journal of cell communication and signaling. 2012;6:233-48.
22. Zhang M, Matyunina LV, Walker LD, Chen W, Xiao H, Benigno BB, et al. Evidence for the importance of post-transcriptional regulatory changes in ovarian cancer progression and the contribution of miRNAs. Scientific reports. 2017;7(1):8171.
23. Kechavarzi B, Janga SC. Dissecting the expression landscape of RNA-binding proteins in human cancers. Genome biology. 2014;15:1-16.
24. Wurth L. Versatility of RNA-binding proteins in cancer. International Journal of Genomics. 2012;2012.
25. Heinonen M, Bono P, Narko K, Chang S-H, Lundin J, Joensuu H, et al. Cytoplasmic HuR expression is a prognostic factor in invasive ductal breast carcinoma. Cancer research. 2005;65(6):2157-61.
26. Wang J, Wang B, Bi J, Zhang C. Cytoplasmic HuR expression correlates with angiogenesis, lymphangiogenesis, and poor outcome in lung cancer. Medical oncology. 2011;28(Suppl 1):577-85.
27. Wu X, Gardashova G, Lan L, Han S, Zhong C, Marquez RT, et al. Targeting the interaction between RNA-binding protein HuR and FOXQ1 suppresses breast cancer invasion and metastasis. Communications biology. 2020;3(1):193.
28. Abdelmohsen K, Gorospe M. Posttranscriptional regulation of cancer traits by HuR. Wiley Interdisciplinary Reviews: RNA. 2010;1(2):214-29.
29. Zong F-Y, Fu X, Wei W-J, Luo Y-G, Heiner M, Cao L-J, et al. The RNA-binding protein QKI suppresses cancer-associated aberrant splicing. PLoS genetics. 2014;10(4):e1004289.
30. Mohibi S, Chen X, Zhang J. Cancer the 'RBP'eutics–RNA-binding proteins as therapeutic targets for cancer. Pharmacology & therapeutics. 2019;203:107390.
31. Hanahan D. Hallmarks of cancer: new dimensions. Cancer discovery. 2022;12(1):31-46.
32. Hong S. RNA binding protein as an emerging therapeutic target for cancer prevention and treatment. Journal of cancer prevention. 2017;22(4):203.
33. Kang D, Lee Y, Lee J-S. RNA-binding proteins in cancer: functional and therapeutic perspectives. Cancers. 2020;12(9):2699.
34. Perone Y, Farrugia AJ, Rodríguez-Meira A, Győrffy B, Ion C, Uggetti A, et al. SREBP1 drives Keratin-80-dependent cytoskeletal changes and invasive behavior in endocrine-resistant ERα breast cancer. Nature communications. 2019;10(1):2115.
35. Chaudhury A, Chander P, Howe PH. Heterogeneous nuclear ribonucleoproteins (hnRNPs) in cellular processes: Focus on hnRNP E1's multifunctional regulatory roles. Rna. 2010;16(8):1449-62.
36. Peng W, Furuuchi N, Aslanukova L, Huang Y-H, Brown SZ, Jiang W, et al. Elevated HuR in pancreas promotes a pancreatitis-like inflammatory microenvironment that facilitates tumor development. Molecular and cellular biology. 2018;38(3):e00427-17.
37. Stavraka C, Blagden S. The La-related proteins, a family with connections to cancer. Biomolecules. 2015;5(4):2701-22.

38. Maraia RJ, Mattijssen S, Cruz-Gallardo I, Conte MR. The La and related RNA-binding proteins (LARPs): structures, functions, and evolving perspectives. Wiley Interdisciplinary Reviews: RNA. 2017;8(6):e1430.
39. Deragon J-M. Distribution, organization an evolutionary history of La and LARPs in eukaryotes. RNA biology. 2021;18(2):159-67.
40. Kershaw CJ, Costello JL, Castelli LM, Talavera D, Rowe W, Sims PF, et al. The yeast La related protein Slf1p is a key activator of translation during the oxidative stress response. PLoS genetics. 2015;11(1):e1004903.
41. Bousquet-Antonelli C, Deragon J-M. A comprehensive analysis of the La-motif protein superfamily. Rna. 2009;15(5):750-64.
42. Berman AJ, Thoreen CC, Dedeic Z, Chettle J, Roux PP, Blagden SP. Controversies around the function of LARP1. RNA biology. 2021;18(2):207-17.
43. Al-Ashtal HA, Rubottom CM, Leeper TC, Berman AJ. The LARP1 La-Module recognizes both ends of TOP mRNAs. RNA biology. 2021;18(2):248-58.
44. Hopkins TG, Mura M, Al-Ashtal HA, Lahr RM, Abd-Latip N, Sweeney K, et al. The RNA-binding protein LARP1 is a post-transcriptional regulator of survival and tumorigenesis in ovarian cancer. Nucleic acids research. 2016;44(3):1227-46.
45. Lahr RM, Fonseca BD, Ciotti GE, Al-Ashtal HA, Jia J-J, Niklaus MR, et al. La-related protein 1 (LARP1) binds the mRNA cap, blocking eIF4F assembly on TOP mRNAs. Elife. 2017;6:e24146.
46. Mura M, Hopkins TG, Michael T, Abd-Latip N, Weir J, Aboagye E, et al. LARP1 post-transcriptionally regulates mTOR and contributes to cancer progression. Oncogene. 2015;34(39):5025-36.
47. Ogami K, Oishi Y, Sakamoto K, Okumura M, Yamagishi R, Inoue T, et al. mTOR- and LARP1-dependent regulation of TOP mRNA poly (A) tail and ribosome loading. Cell reports. 2022;41(4).
48. Philippe L, van den Elzen AM, Watson MJ, Thoreen CC. Global analysis of LARP1 translation targets reveals tunable and dynamic features of 5′ TOP motifs. Proceedings of the National Academy of Sciences. 2020;117(10):5319-28.
49. Philippe L, Vasseur J-J, Debart F, Thoreen CC. La-related protein 1 (LARP1) repression of TOP mRNA translation is mediated through its cap-binding domain and controlled by an adjacent regulatory region. Nucleic acids research. 2018;46(3):1457-69.
50. Hong S, Freeberg MA, Han T, Kamath A, Yao Y, Fukuda T, et al. LARP1 functions as a molecular switch for mTORC1-mediated translation of an essential class of mRNAs. Elife. 2017;6:e25237.
51. Burrows C, Abd Latip N, Lam S-J, Carpenter L, Sawicka K, Tzolovsky G, et al. The RNA binding protein Larp1 regulates cell division, apoptosis and cell migration. Nucleic acids research. 2010;38(16):5542-53.
52. Fonseca BD, Zakaria C, Jia J-J, Graber TE, Svitkin Y, Tahmasebi S, et al. La-related protein 1 (LARP1) represses terminal oligopyrimidine (TOP) mRNA translation downstream of mTOR complex 1 (mTORC1). Journal of Biological Chemistry. 2015;290(26):15996-6020.
53. Lahr RM, Mack SM, Héroux A, Blagden SP, Bousquet-Antonelli C, Deragon J-M, et al. The La-related protein 1-specific domain repurposes HEAT-like repeats to directly bind a 5′ TOP sequence. Nucleic acids research. 2015;43(16):8077-88.
54. Beauchamp EM, Abedin SM, Radecki SG, Fischietti M, Arslan AD, Blyth GT, et al. Identification and targeting of novel CDK9 complexes in acute myeloid leukemia. Blood, The Journal of the American Society of Hematology. 2019;133(11):1171-85.
55. Zhang Y, Cai W, Zou Y, Zhang H. Knockdown of KCNQ1OT1 inhibits proliferation, invasion, and drug resistance by regulating miR-129-5p-Mediated LARP1 in osteosarcoma. BioMed Research International. 2020;2020.

56. Wu M, Kong C, Cai M, Huang W, Chen Y, Wang B, et al. Hsa_circRNA_002144 promotes growth and metastasis of colorectal cancer through regulating miR-615-5p/LARP1/mTOR pathway. Carcinogenesis. 2021;42(4):601-10.
57. Xu Z, Xu J, Lu H, Lin B, Cai S, Guo J, et al. LARP1 is regulated by the XIST/miR-374a axis and functions as an oncogene in non-small cell lung carcinoma. Oncology Reports. 2017;38(6):3659-67.
58. Chen J, Li X, Yang L, Zhang J. Long Non-coding RNA LINC01969 promotes ovarian cancer by regulating the miR-144-5p/LARP1 axis as a competing endogenous RNA. Frontiers in Cell and Developmental Biology. 2021;8:625730.
59. Zhu X, Du T, Chen X, Hu P. Circ-PDZD8 promotes cell growth and glutamine metabolism in non-small cell lung cancer by enriching LARP1 via sequestering miR-330-5p. Thoracic Cancer. 2023.
60. Kato M, Goto Y, Matsushita R, Kurozumi A, Fukumoto I, Nishikawa R, et al. MicroRNA-26a/b directly regulate La-related protein 1 and inhibit cancer cell invasion in prostate cancer. International journal of oncology. 2015;47(2):710-8.
61. Zhang W, Cao C, Shen J, Shan S, Tong Y, Cai H, et al. Long non-coding RNA LINC01270 is an onco-promotor in lung adenocarcinoma by upregulating LARP1 via sponging miR-326. Bioengineered. 2022;13(6):14472-88.
62. Li M, Yin B, Chen M, Peng J, Mu X, Deng Z, et al. Downregulation of the lncRNA ASB16-AS1 decreases LARP1 expression and promotes clear cell renal cell carcinoma progression via miR-185-5p/miR-214-3p. Frontiers in Oncology. 2021;10:617105.
63. Cui Z, He J, Zhu J, Ni W, Liu L, Bian Z, et al. O-GlcNAcylated LARP1 positively regulated by circCLNS1A facilitates hepatoblastoma progression through DKK4/β-catenin signalling. Clinical and Translational Medicine. 2023;13(4):e1239.
64. Jiang F, Fang D-B, Lin J, Chen Q, Zhu L-X, Yu H-Z. Correlation of LARP1 and E-cadherin expression with prognosis of intrahepatic cholangiocarcinoma. International Journal of Clinical and Experimental Pathology. 2018;11(7):3559.
65. Ramani K, Robinson AE, Berlind J, Fan W, Abeynayake A, Binek A, et al. S-adenosylmethionine inhibits La ribonucleoprotein domain family member 1 in murine liver and human liver cancer cells. Hepatology. 2022;75(2):280-96.
66. Xie C, Huang L, Xie S, Xie D, Zhang G, Wang P, et al. LARP1 predict the prognosis for early-stage and AFP-normal hepatocellular carcinoma. Journal of translational medicine. 2013;11:1-10.
67. Ye L, Lin S-t, Mi Y-s, Liu Y, Ma Y, Sun H-m, et al. Overexpression of LARP1 predicts poor prognosis of colorectal cancer and is expected to be a potential therapeutic target. Tumor Biology. 2016;37:14585-94.
68. Plissonnier M-L, Cottarel J, Piver E, Kullolli M, Centonze FG, Pitteri S, et al. LARP1 binding to hepatitis C virus particles is correlated with intracellular retention of viral infectivity. Virus research. 2019;271:197679.
69. Engeland CE, Oberwinkler H, Schümann M, Krause E, Müller GA, Kräusslich H-G. The cellular protein lyric interacts with HIV-1 Gag. Journal of virology. 2011;85(24):13322-32.
70. Karlas A, Machuy N, Shin Y, Pleissner K-P, Artarini A, Heuer D, et al. Genome-wide RNAi screen identifies human host factors crucial for influenza virus replication. Nature. 2010;463(7282):818-22.
71. Suzuki Y, Chin W-X, Han QE, Ichiyama K, Lee CH, Eyo ZW, et al. Characterization of RyDEN (C19orf66) as an interferon-stimulated cellular inhibitor against dengue virus replication. PLoS pathogens. 2016;12(1):e1005357.
72. Lee S, Lee Y-s, Choi Y, Son A, Park Y, Lee K-M, et al. The SARS-CoV-2 RNA Interactome. Molecular cell. 2021;81(13):2838-50. e6.

73. Werneck-de-Castro JP, Peçanha FLM, Silvestre DH, Bernal-Mizrachi E. The RNA-binding protein LARP1 is dispensable for pancreatic β-cell function and mass. Scientific reports. 2021;11(1):2079.
74. Jia J-J, Lahr RM, Solgaard MT, Moraes BJ, Pointet R, Yang A-D, et al. mTORC1 promotes TOP mRNA translation through site-specific phosphorylation of LARP1. Nucleic acids research. 2021;49(6):3461-89.
75. Gao T, Nie Y, Guo J. Hypermethylation of the gene LARP2 for noninvasive prenatal diagnosis of β-thalassemia based on DNA methylation profile. Molecular biology reports. 2012;39:6591-8.
76. Haiyuni MY, Aziee S, Nasir A, Abdullah WZ, Johan MF. LARP2 DNA Methylation in Transfusion-dependent Haemoglobin E-Beta (HbE/β) and β-Thalassaemia Major Patients. Malaysian Journal of Medicine & Health Sciences. 2019;15(3).
77. Wolin SL, Cedervall T. The la protein. Annual review of biochemistry. 2002;71(1):375-403.
78. Kuehnert J, Sommer G, Zierk AW, Fedarovich A, Brock A, Fedarovich D, et al. Novel RNA chaperone domain of RNA-binding protein La is regulated by AKT phosphorylation. Nucleic acids research. 2015;43(1):581-94.
79. Sommer G, Dittmann J, Kuehnert J, Reumann K, Schwartz P, Will H, et al. The RNA-binding protein La contributes to cell proliferation and CCND1 expression. Oncogene. 2011;30(4):434-44.
80. Schwartz EI, Intine RV, Maraia RJ. CK2 is responsible for phosphorylation of human La protein serine-366 and can modulate rpL37 5′-terminal oligopyrimidine mRNA metabolism. Molecular and cellular biology. 2004;24(21):9580-91.
81. Fan H, Sakulich AL, Goodier JL, Zhang X, Qin J, Maraia RJ. Phosphorylation of the human La antigen on serine 366 can regulate recycling of RNA polymerase III transcription complexes. Cell. 1997;88(5):707-15.
82. Pan J, Tong S, Kong L, Zhu J, Tang J. La protein contributes to cells proliferation and migration and serves as a potential therapeutic target for hepatocellular carcinoma. Asia-Pacific Journal of Clinical Oncology. 2020;16(5):e228-e35.
83. Petz M, Them NC, Huber H, Mikulits W. PDGF enhances IRES-mediated translation of Laminin B1 by cytoplasmic accumulation of La during epithelial to mesenchymal transition. Nucleic acids research. 2012;40(19):9738-49.
84. Heise T, Kota V, Brock A, Morris AB, Rodriguez RM, Zierk AW, et al. The La protein counteracts cisplatin-induced cell death by stimulating protein synthesis of anti-apoptotic factor Bcl2. Oncotarget. 2016;7(20):29664.
85. Harley JB, Alexander EL, Bias WB, Fox OF, Provost TT, Reichlin M, et al. Anti-Ro (SS-A) and anti-La (SS-B) in patients with Sjögren's syndrome. Arthritis & Rheumatism: Official Journal of the American College of Rheumatology. 1986;29(2):196-206.
86. Provost TT, Reichlin M. Antinuclear antibody—negative systemic lupus erythematosus: I. Anti-Ro (SSA) and anti-La (SSB) antibodies. Journal of the American Academy of Dermatology. 1981;4(1):84-9.
87. Tseng C-E, Buyon JP. Neonatal lupus syndromes. Rheumatic Disease Clinics of North America. 1997;23(1):31-54.
88. Yang R, Gaidamakov SA, Xie J, Lee J, Martino L, Kozlov G, et al. La-related protein 4 binds poly (A), interacts with the poly (A)-binding protein MLLE domain via a variant PAM2w motif, and can promote mRNA stability. Molecular and cellular biology. 2011;31(3):542-56.
89. Mattijssen S, Maraia RJ. LARP4 is regulated by tumor necrosis factor alpha in a tristetraprolin-dependent manner. Molecular and Cellular Biology. 2016;36(4):574-84.

90. Coleman JC, Tattersall L, Yianni V, Knight L, Yu H, Hallett S, et al. The RNA binding proteins LARP4A and LARP4B promote sarcoma and carcinoma growth and metastasis. bioRxiv. 2023:2023.04. 11.536377.
91. Lewis BM, Cho CY, Her H-L, Hunter T, Yeo GW. LARP4 Is an RNA-Binding Protein That Binds Nuclear-Encoded Mitochondrial mRNAs To Promote Mitochondrial Function. bioRxiv. 2022:2022.10. 24.513614.
92. Lu M, Gong B, Wang Y, Li J. CircBNC2 affects epithelial ovarian cancer progression through the miR-223-3p/LARP4 axis. Anti-Cancer Drugs. 2022;34(3):384-94.
93. Egiz M, Usui T, Ishibashi M, Zhang X, Shigeta S, Toyoshima M, et al. La-related protein 4 as a suppressor for motility of ovarian cancer cells. The Tohoku Journal of Experimental Medicine. 2019;247(1):59-67.
94. Bai SW, Herrera-Abreu MT, Rohn JL, Racine V, Tajadura V, Suryavanshi N, et al. Identification and characterization of a set of conserved and new regulators of cytoskeletal organization, cell morphology and migration. BMC biology. 2011;9(1):1-18.
95. Seetharaman S, Flemyng E, Shen J, Conte MR, Ridley AJ. The RNA-binding protein LARP4 regulates cancer cell migration and invasion. Cytoskeleton. 2016;73(11):680-90.
96. Schäffler K, Schulz K, Hirmer A, Wiesner J, Grimm M, Sickmann A, et al. A stimulatory role for the La-related protein 4B in translation. Rna. 2010;16(8):1488-99.
97. Grimm C, Pelz J-P, Schneider C, Schäffler K, Fischer U. Crystal structure of a variant PAM2 motif of LARP4B bound to the MLLE domain of PABPC1. Biomolecules. 2020;10(6):872.
98. Yin W, Chen J, Wang G, Zhang D. MicroRNA-106b functions as an oncogene and regulates tumor viability and metastasis by targeting LARP4B in prostate cancer. Molecular Medicine Reports. 2019;20(2):951-8.
99. Li Y-H, Long M-M, Dai S-D, Wang Z-C. LARP4B gene mutation is involved in the development of neurofibroma. Clinical and Experimental Dermatology. 2023;48(4):394-5.
100. Koso H, Yi H, Sheridan P, Miyano S, Ino Y, Todo T, et al. Identification of RNA-binding protein LARP4B as a tumor suppressor in glioma. Cancer Research. 2016;76(8):2254-64.
101. Dermit M, Dodel M, Lee FC, Azman MS, Schwenzer H, Jones JL, et al. Subcellular mRNA localization regulates ribosome biogenesis in migrating cells. Developmental cell. 2020;55(3):298-313. e10.
102. Cai L, Fritz D, Stefanovic L, Stefanovic B. Binding of LARP6 to the conserved 5′ stem–loop regulates translation of mRNAs encoding type I collagen. Journal of molecular biology. 2010;395(2):309-26.
103. Zhang Y, Stefanovic B. mTORC1 phosphorylates LARP6 to stimulate type I collagen expression. Scientific reports. 2017;7(1):41173.
104. Zhang Y, Stefanovic B. Akt mediated phosphorylation of LARP6; critical step in biosynthesis of type I collagen. Scientific reports. 2016;6(1):22597.
105. Danchuk S, Delafontaine P, Higashi Y. Mir-1976 Downregulation and Phosphorylation of LARP6 are Associated with Insulin-like Growth Factor-1 (IGF1)-induced Collagen Upregulation in Vascular Smooth Muscle Cells. The FASEB Journal. 2019;33(S1):522.9-.9.
106. Martino L, Pennell S, Kelly G, Busi B, Brown P, Atkinson RA, et al. Synergic interplay of the La motif, RRM1 and the interdomain linker of LARP6 in the recognition of collagen mRNA expands the RNA binding repertoire of the La module. Nucleic acids research. 2015;43(1):645-60.

107. Vukmirovic M, Manojlovic Z, Stefanovic B. Serine-threonine kinase receptor-associated protein (STRAP) regulates translation of type I collagen mRNAs. Molecular and cellular biology. 2013;33(19):3893-906.
108. Challa AA, Stefanovic B. A novel role of vimentin filaments: binding and stabilization of collagen mRNAs. Molecular and cellular biology. 2011;31(18):3773-89.
109. Manojlovic Z, Stefanovic B. A novel role of RNA helicase A in regulation of translation of type I collagen mRNAs. Rna. 2012;18(2):321-34.
110. Manojlovic Z, Blackmon J, Stefanovic B. Tacrolimus (FK506) prevents early stages of ethanol induced hepatic fibrosis by targeting LARP6 dependent mechanism of collagen synthesis. PLoS One. 2013;8(6):e65897.
111. Cai L, Fritz D, Stefanovic L, Stefanovic B. Nonmuscle myosin-dependent synthesis of type I collagen. Journal of molecular biology. 2010;401(4):564-78.
112. Long X, Liu X, Deng T, Chen J, Lan J, Zhang S, et al. LARP6 suppresses colorectal cancer progression through ZNF267/SGMS2-mediated imbalance of sphingomyelin synthesis. Journal of Experimental & Clinical Cancer Research. 2023;42(1):1-18.
113. Shao R, Scully Jr SJ, Yan W, Bentley B, Mueller J, Brown C, et al. The novel lupus antigen related protein acheron enhances the development of human breast cancer. International journal of cancer. 2012;130(3):544-54.
114. Chen L, Su Y, Yin B, Li S, Cheng X, He Y, et al. LARP6 regulates keloid fibroblast proliferation, invasion, and ability to synthesize collagen. Journal of Investigative Dermatology. 2022;142(9):2395-405. e7.
115. Markert A, Grimm M, Martinez J, Wiesner J, Meyerhans A, Meyuhas O, et al. The La-related protein LARP7 is a component of the 7SK ribonucleoprotein and affects transcription of cellular and viral polymerase II genes. EMBO reports. 2008;9(6):569-75.
116. Eichhorn CD, Yang Y, Repeta L, Feigon J. Structural basis for recognition of human 7SK long noncoding RNA by the La-related protein Larp7. Proceedings of the National Academy of Sciences. 2018;115(28):E6457-E66.
117. Zhang F, Yan P, Yu H, Le H, Li Z, Chen J, et al. L ARP7 is a BRCA1 ubiquitinase substrate and regulates genome stability and tumorigenesis. Cell Reports. 2020;32(4).
118. Ji X, Lu H, Zhou Q, Luo K. LARP7 suppresses P-TEFb activity to inhibit breast cancer progression and metastasis. Elife. 2014;3:e02907.
119. Sui X, Sui Y, Wang Y. LARP7 in papillary thyroid carcinoma induces NIS expression through suppression of the SHH signaling pathway. Molecular medicine reports. 2018;17(6):7521-8.
120. Cheng Y, Jin Z, Agarwal R, Ma K, Yang J, Ibrahim S, et al. LARP7 is a potential tumor suppressor gene in gastric cancer. Laboratory investigation. 2012;92(7):1013-9.
121. Alazami AM, Al-Owain M, Alzahrani F, Shuaib T, Al-Shamrani H, Al-Falki YH, et al. Loss of function mutation in LARP7, chaperone of 7SK ncRNA, causes a syndrome of facial dysmorphism, intellectual disability, and primordial dwarfism. Human mutation. 2012;33(10):1429-34.
122. Kang SA, Pacold ME, Cervantes CL, Lim D, Lou HJ, Ottina K, et al. mTORC1 phosphorylation sites encode their sensitivity to starvation and rapamycin. Science. 2013;341(6144):1236566.
123. Smith EM, Benbahouche NEH, Morris K, Wilczynska A, Gillen S, Schmidt T, et al. The mTOR regulated RNA-binding protein LARP1 requires PABPC1 for guided mRNA interaction. Nucleic acids research. 2021;49(1):458-78.
124. Schmidt N, Lareau CA, Keshishian H, Ganskih S, Schneider C, Hennig T, et al. The SARS-CoV-2 RNA–protein interactome in infected human cells. Nature microbiology. 2021;6(3):339-53.
125. Gentilella A, Moron-Duran FD, Fuentes P, Zweig-Rocha G, Riano-Canalias F, Pelletier J, et al. Autogenous control of 5′ TOP mRNA stability by 40S ribosomes. Molecular cell. 2017;67(1):55-70. e4.

126. Clifford RJ, Zhang J, Meerzaman DM, Lyu MS, Hu Y, Cultraro CM, et al. Genetic variations at loci involved in the immune response are risk factors for hepatocellular carcinoma. Hepatology. 2010;52(6):2034-43.
127. Li L, Liu H, Hu X, Huang Y, Wang Y, He Y, et al. Identification of key genes in non-alcoholic fatty liver disease progression based on bioinformatics analysis. Molecular medicine reports. 2018;17(6):7708-20.
128. Wang M, Jiang F, Wei K, Wang J, Zhou G, Wu C, et al. Development and validation of a RNA binding protein-associated prognostic model for hepatocellular carcinoma. Technology in cancer research & treatment. 2021;20:15330338211004936.
129. Alur V, Raju V, Vastrad B, Tengli A, Vastrad C, Kottursheti S. Integrated bioinformatics analysis reveals novel key biomarkers and potential candidate small molecule drugs in gestational diabetes mellitus. Bioscience reports. 2021;41(5):BSR20210617.
130. Cormier KW, Larsen B, Gingras A-C, Woodgett JR. Interactomes of Glycogen Synthase Kinase-3 Isoforms. Journal of Proteome Research. 2023;22(3):977-89.
131. Liu X, Salokas K, Tamene F, Jiu Y, Weldatsadik RG, Öhman T, et al. An AP-MS- and BioID-compatible MAC-tag enables comprehensive mapping of protein interactions and subcellular localizations. Nature communications. 2018;9(1):1188.
132. Zhang Y, Huang N-q, Yan F, Jin H, Zhou S-y, Shi J-s, et al. Diabetes mellitus and Alzheimer's disease: GSK-3β as a potential link. Behavioural brain research. 2018;339:57-65.
133. Wang Y, Feng W, Xue W, Tan Y, Hein DW, Li X-K, et al. Inactivation of GSK-3β by metallothionein prevents diabetes-related changes in cardiac energy metabolism, inflammation, nitrosative damage, and remodeling. Diabetes. 2009;58(6):1391-402.
134. Liang X, Wang P, Chen B, Ge Y, Gong AY, Flickinger B, et al. Glycogen synthase kinase 3β hyperactivity in urinary exfoliated cells predicts progression of diabetic kidney disease. Kidney International. 2020;97(1):175-92.
135. Huang Y, Kim JK, Do DV, Lee C, Penfold CA, Zylicz JJ, et al. Stella modulates transcriptional and endogenous retrovirus programs during maternal-to-zygotic transition. Elife. 2017;6:e22345.
136. Hwang H, Chen S, Ma M, Divyanshi, Fan H-C, Borwick E, et al. Phase transition of maternal RNAs during vertebrate oocyte-to-embryo transition. bioRxiv. 2023:2023.05.11.540463.
137. Qian P, Kang J, Liu D, Xie G. Single cell transcriptome sequencing of Zebrafish testis revealed novel spermatogenesis marker genes and stronger Leydig-germ cell paracrine interactions. Frontiers in genetics. 2022;13:851719.
138. Doss MX, Wagh V, Schulz H, Kull M, Kolde R, Pfannkuche K, et al. Global transcriptomic analysis of murine embryonic stem cell-derived brachyury+ (T) cells. Genes to Cells. 2010;15(3):209-28.
139. Zhang C-J, Li Z-T, Shen K-J, Chen L, Xu D-F, Gao Y. Characterization of progression-related alternative splicing events in testicular germ cell tumors. Asian Journal of Andrology. 2021;23(3):259.
140. Huang Z-G, He R-Q, Mo Z-N. Prognostic value and potential function of splicing events in prostate adenocarcinoma. International journal of oncology. 2018;53(6):2473-87.
141. del Valle Torrado M, Labarta JD, Migliorini A. Interstitial deletion of the long arm of chromosome 4 in a patient with mental retardation and abnormal phenotype. Journal of Medical Genetics. 1982;19(6):477.
142. Mitchell JA, Packman S, Loughman WD, Fineman RM, Zackai E, Patil SR, et al. Deletions of different segments of the long arm of chromosome 4. American journal of medical genetics. 1981;8(1):73-89.

143. Wakui K, Nishida T, Masuda J-i, Itoh T, Katsumata D, Ohno T, et al. De novo interstitial deletion of 4q [46, XX, del (4)(q27q28. 2)] with intact blood group-MN locus, confining its locus to 4q28. 2–4q31. 1. Japanese journal of human genetics. 1991;36(2):149-53.
144. Khungwanmaythawee K, Sornjai W, Paemanee A, Jaratsittisin J, Fucharoen S, Svasti S, et al. Mitochondrial changes in β0-thalassemia/Hb E disease. PLoS One. 2016;11(4):e0153831.
145. Fibach E, Dana M. Oxidative stress in β-thalassemia. Molecular diagnosis & therapy. 2019;23:245-61.
146. Bian J, Zhang D, Wang Y, Qin H, Yang W, Cui R, et al. Mitochondrial quality control in hepatocellular carcinoma. Frontiers in Oncology. 2021;11:713721.
147. Kim J-a, Wei Y, Sowers JR. Role of mitochondrial dysfunction in insulin resistance. Circulation research. 2008;102(4):401-14.
148. Ghosh S, Körte A, Serafini G, Yadav V, Rodenfels J, editors. Developmental energetics: Energy expenditure, budgets and metabolism during animal embryogenesis. Seminars in Cell & Developmental Biology; 2023: Elsevier.
149. Lin C-S, Liu L-T, Ou L-H, Pan S-C, Lin C-I, Wei Y-H. Role of mitochondrial function in the invasiveness of human colon cancer cells. Oncology reports. 2018;39(1):316-30.
150. Wu CW, Yin PH, Hung WY, Li AFY, Li SH, Chi CW, et al. Mitochondrial DNA mutations and mitochondrial DNA depletion in gastric cancer. Genes, Chromosomes and Cancer. 2005;44(1):19-28.
151. Yin P, Lee H, Chau G, Wu Y, Li S, Lui W, et al. Alteration of the copy number and deletion of mitochondrial DNA in human hepatocellular carcinoma. British Journal of Cancer. 2004;90(12):2390-6.
152. Brand M, Orr A, Perevoshchikova I, Quinlan C. The role of mitochondrial function and cellular bioenergetics in ageing and disease. British Journal of Dermatology. 2013;169(s2):1-8.
153. Zhang W, Zhang S-L, Hu X, Tam KY. Targeting tumor metabolism for cancer treatment: is pyruvate dehydrogenase kinases (PDKs) a viable anticancer target? International journal of biological sciences. 2015;11(12):1390.
154. Vander Heiden MG, Cantley LC, Thompson CB. Understanding the Warburg effect: the metabolic requirements of cell proliferation. science. 2009;324(5930):1029-33.
155. Nolfi-Donegan D, Braganza A, Shiva S. Mitochondrial electron transport chain: Oxidative phosphorylation, oxidant production, and methods of measurement. Redox biology. 2020;37:101674.
156. Wang Y, Patti GJ. The Warburg effect: a signature of mitochondrial overload. Trends in Cell Biology. 2023.
157. Jaworska M, Szczudło J, Pietrzyk A, Shah J, Trojan SE, Ostrowska B, et al. The Warburg effect: a score for many instruments in the concert of cancer and cancer niche cells. Pharmacological Reports. 2023:1-15.
158. Ashton TM, McKenna WG, Kunz-Schughart LA, Higgins GS. Oxidative phosphorylation as an emerging target in cancer therapy. Clinical Cancer Research. 2018;24(11):2482-90.
159. Ren L, Meng L, Gao J, Lu M, Guo C, Li Y, et al. PHB2 promotes colorectal cancer cell proliferation and tumorigenesis through NDUFS1-mediated oxidative phosphorylation. Cell Death & Disease. 2023;14(1):44.
160. Al-Masri M, Paliotti K, Tran R, Halaoui R, Lelarge V, Chatterjee S, et al. Architectural control of metabolic plasticity in epithelial cancer cells. Communications Biology. 2021;4(1):371.

161. Jia D, Lu M, Jung KH, Park JH, Yu L, Onuchic JN, et al. Elucidating cancer metabolic plasticity by coupling gene regulation with metabolic pathways. Proceedings of the National Academy of Sciences. 2019;116(9):3909-18.
162. McGuirk S, Audet-Delage Y, St-Pierre J. Metabolic fitness and plasticity in cancer progression. Trends in cancer. 2020;6(1):49-61.
163. Matia-González AM, Jabre I, Laing EE, Gerber AP. Oxidative stress induces coordinated remodeling of RNA-enzyme interactions. Iscience. 2021;24(7):102753.
164. Sies H, Belousov VV, Chandel NS, Davies MJ, Jones DP, Mann GE, et al. Defining roles of specific reactive oxygen species (ROS) in cell biology and physiology. Nature Reviews Molecular Cell Biology. 2022;23(7):499-515.
165. Irrcher I, Ljubicic V, Hood DA. Interactions between ROS and AMP kinase activity in the regulation of PGC-1α transcription in skeletal muscle cells. American Journal of Physiology-Cell Physiology. 2009;296(1):C116-C23.
166. Li M-y, Zhu X-l, Zhao B-x, Shi L, Wang W, Hu W, et al. Adrenomedullin alleviates the pyroptosis of Leydig cells by promoting autophagy via the ROS–AMPK–mTOR axis. Cell death & disease. 2019;10(7):489.
167. Li F, Li J, Wang P-H, Yang N, Huang J, Ou J, et al. SARS-CoV-2 spike promotes inflammation and apoptosis through autophagy by ROS-suppressed PI3K/AKT/mTOR signaling. Biochimica et Biophysica Acta (BBA)-Molecular Basis of Disease. 2021;1867(12):166260.
168. Sênos Demarco R, Jones DL. Mitochondrial fission regulates germ cell differentiation by suppressing ROS-mediated activation of epidermal growth factor signaling in the Drosophila larval testis. Scientific reports. 2019;9(1):19695.
169. Turner DJ, Turner M. RNA binding proteins as regulators of oxidative stress identified by a targeted CRISPR-cas9 single guide RNA library. The CRISPR Journal. 2021;4(3):427-37.
170. Birben E, Sahiner UM, Sackesen C, Erzurum S, Kalayci O. Oxidative stress and antioxidant defense. World allergy organization journal. 2012;5:9-19.
171. Liu S, Qiu Y, Xiang R, Huang P. Characterization of H2O2-Induced Alterations in Global Transcription of mRNA and lncRNA. Antioxidants. 2022;11(3):495.
172. Jeong SM, Hwang S, Seong RH. Transferrin receptor regulates pancreatic cancer growth by modulating mitochondrial respiration and ROS generation. Biochemical and biophysical research communications. 2016;471(3):373-9.
173. Chetram MA, Bethea DA, Odero-Marah VA, Don-Salu-Hewage AS, Jones KJ, Hinton CV. ROS-mediated activation of AKT induces apoptosis via pVHL in prostate cancer cells. Molecular and cellular biochemistry. 2013;376:63-71.
174. Wang Y, Chen P, Chen X, Gong D, Wu Y, Huang L, et al. ROS-induced DCTPP1 upregulation contributes to cisplatin resistance in ovarian cancer. Frontiers in Molecular Biosciences. 2022;9:838006.
175. Xue D-F, Pan S-T, Huang G, Qiu J-X. ROS enhances the cytotoxicity of cisplatin by inducing apoptosis and autophagy in tongue squamous cell carcinoma cells. The international journal of biochemistry & cell biology. 2020;122:105732.
176. Itoh T, Terazawa R, Kojima K, Nakane K, Deguchi T, Ando M, et al. Cisplatin induces production of reactive oxygen species via NADPH oxidase activation in human prostate cancer cells. Free radical research. 2011;45(9):1033-9.
177. Barroeta PH, O'Sullivan MJ, Zisterer DM. The role of the Nrf2/GSH antioxidant system in cisplatin resistance in malignant rhabdoid tumours. Journal of Cancer Research and Clinical Oncology. 2023;149(11):8379.
178. Silva MM, Rocha CRR, Kinker GS, Pelegrini AL, Menck CFM. The balance between NRF2/GSH antioxidant mediated pathway and DNA repair modulates cisplatin resistance in lung cancer cells. Scientific reports. 2019;9(1):17639.

179. Lee RG, Rudler DL, Rackham O, Filipovska A. Is mitochondrial gene expression coordinated or stochastic? Biochemical Society Transactions. 2018;46(5):1239-46.
180. Qin W, Myers SA, Carey DK, Carr SA, Ting AY. Functional proximity mapping of RNA binding proteins uncovers a mitochondrial mRNA anchor that promotes stress recovery. BioRxiv. 2020:2020.11. 17.387209.
181. Ma J, Sun L, Gao W, Li Y, Dong D. RNA binding protein: coordinated expression between the nuclear and mitochondrial genomes in tumors. Journal of Translational Medicine. 2023;21(1):512.
182. Gopalakrishna S, Pearce SF, Dinan AM, Rosenberger FA, Cipullo M, Spåhr H, et al. C6orf203 is an RNA-binding protein involved in mitochondrial protein synthesis. Nucleic acids research. 2019;47(17):9386-99.
183. Antonicka H, Sasarman F, Nishimura T, Paupe V, Shoubridge EA. The mitochondrial RNA-binding protein GRSF1 localizes to RNA granules and is required for posttranscriptional mitochondrial gene expression. Cell metabolism. 2013;17(3):386-98.
184. Abdelmohsen K, Kuwano Y, Kim HH, Gorospe M. Posttranscriptional gene regulation by RNA-binding proteins during oxidative stress: implications for cellular senescence. 2008.
185. Tanaka M, Sasaki K, Kamata R, Hoshino Y, Yanagihara K, Sakai R. A novel RNA-binding protein, Ossa/C9orf10, regulates activity of Src kinases to protect cells from oxidative stress-induced apoptosis. Molecular and Cellular Biology. 2009;29(2):402-13.
186. Dell'Orco M, Sardone V, Gardiner AS, Pansarasa O, Bordoni M, Perrone-Bizzozero NI, et al. HuD regulates SOD1 expression during oxidative stress in differentiated neuroblastoma cells and sporadic ALS motor cortex. Neurobiology of Disease. 2021;148:105211.
187. Guo CC, Czerniak B. Somatic-type malignancies in testicular germ cell tumors. Human Pathology. 2022;127:123-35.
188. Doghish AS, Moustafa HAM, Elballal MS, Sallam A-AM, El-Dakroury WA, Mageed SSA, et al. The potential role of miRNAs in the pathogenesis of testicular germ cell tumors-A Focus on signaling pathways interplay. Pathology-Research and Practice. 2023:154611.
189. Farnetani G, Fino MG, Cioppi F, Riera-Escamilla A, Tamburrino L, Vannucci M, et al. Long-term effect of cytotoxic treatments on sperm DNA fragmentation in patients affected by testicular germ cell tumor. Andrology. 2023.
190. Alvin M. Matsumoto WJB. William's Textbook of Endocrinology (Thirteenth Edition). Thirteenth ed. United Kingdom: Elsevier; 2016.
191. Paxton S, Peckham M, Knibbs A. The Leeds histology guide. 2003.
192. Caggiano C, Cavallo F, Giannattasio T, Cappelletti G, Rossi P, Grimaldi P, et al. Testicular germ cell tumors acquire cisplatin resistance by rebalancing the usage of DNA repair pathways. Cancers. 2021;13(4):787.
193. Baroni T, Arato I, Mancuso F, Calafiore R, Luca G. On the origin of testicular germ cell tumors: from gonocytes to testicular cancer. Frontiers in endocrinology. 2019;10:343.
194. Looijenga LH, Van Agthoven T, Biermann K. Development of malignant germ cells-the genvironmental hypothesis. International Journal of Developmental Biology. 2013;57(2-3-4):241-53.
195. Boisen K, Main K, Rajpert-De Meyts E, Skakkebaek N. Are male reproductive disorders a common entity? The testicular dysgenesis syndrome. Annals of the New York academy of sciences. 2001;948(1):90-9.
196. Fukawa T, Kanayama Ho. Current knowledge of risk factors for testicular germ cell tumors. International Journal of Urology. 2018;25(4):337-44.
197. Das MK, Haugen ØP, Haugen TB. Diverse roles and targets of miRNA in the pathogenesis of testicular germ cell tumour. Cancers. 2022;14(5):1190.

198. Skakkebaek N, Berthelsen J, Giwercman A, Müller J. Carcinoma-in-situ of the testis: possible origin from gonocytes and precursor of all types of germ cell tumours except spermatocytoma. International journal of andrology. 1987;10(1):19-28.
199. Akyüz M, Topaktaş R, Ürkmez A, Koca O, Öztürk Mİ. Evaluation of germ-cell neoplasia in situ entity in testicular tumors. Turkish Journal of Urology. 2019;45(6):418.
200. Skotheim RI, Abeler VM, Nesland JM, Fosså SD, Holm R, Wagner U, et al. Candidate genes for testicular cancer evaluated by in situ protein expression analyses on tissue microarrays. Neoplasia. 2003;5(5):397-404.
201. Chovanec M, Hanna N, Cary KC, Einhorn L, Albany C. Management of stage I testicular germ cell tumours. Nature Reviews Urology. 2016;13(11):663-73.
202. Schmidtova S, Kalavska K, Kucerova L. Molecular mechanisms of cisplatin chemoresistance and its circumventing in testicular germ cell tumors. Current Oncology Reports. 2018;20:1-12.
203. Litchfield K, Levy M, Huddart RA, Shipley J, Turnbull C. The genomic landscape of testicular germ cell tumours: from susceptibility to treatment. Nature Reviews Urology. 2016;13(7):409-19.
204. Bragado P, Armesilla A, Silva A, Porras A. Apoptosis by cisplatin requires p53 mediated p38α MAPK activation through ROS generation. Apoptosis. 2007;12:1733-42.
205. Zhang J, Wang Q, Wang M, Jiang M, Wang Y, Sun Y, et al. GASZ and mitofusin-mediated mitochondrial functions are crucial for spermatogenesis. EMBO reports. 2016;17(2):220-34.
206. Lord T, Nixon B. Metabolic changes accompanying spermatogonial stem cell differentiation. Developmental cell. 2020;52(4):399-411.
207. Park Y-J, Pang M-G. Mitochondrial functionality in male fertility: from spermatogenesis to fertilization. Antioxidants. 2021;10(1):98.
208. Shih HJ, Chang CY, Huang IT, Tsai PS, Han CL, Huang CJ. Testicular torsion–detorsion causes dysfunction of mitochondrial oxidative phosphorylation. Andrology. 2021;9(6):1902-10.
209. Saleh RA, HCLD AA. Oxidative stress and male infertility: from research bench to clinical practice. Journal of andrology. 2002;23(6):737-52.
210. Agarwal A, Sekhon LH. The role of antioxidant therapy in the treatment of male infertility. Human fertility. 2010;13(4):217-25.
211. Chianese R, Pierantoni R. Mitochondrial reactive oxygen species (ROS) production alters sperm quality. Antioxidants. 2021;10(1):92.
212. Asadi N, Bahmani M, Kheradmand A, Rafieian-Kopaei M. The impact of oxidative stress on testicular function and the role of antioxidants in improving it: a review. Journal of clinical and diagnostic research: JCDR. 2017;11(5):IE01.
213. Aziz N, Saleh RA, Sharma RK, Lewis-Jones I, Esfandiari N, Thomas Jr AJ, et al. Novel association between sperm reactive oxygen species production, sperm morphological defects, and the sperm deformity index. Fertility and sterility. 2004;81(2):349-54.
214. Barik G, Chaturvedula L, Bobby Z. Role of oxidative stress and antioxidants in male infertility: An interventional study. Journal of human reproductive sciences. 2019;12(3):204.
215. Quinn P, Payne A. Oxygen-mediated damage of microsomal cytochrome P-450 enzymes in cultured leydig cells. Role in steroidogenic desensitization. Journal of Biological Chemistry. 1984;259(7):4130-5.
216. Liu Z, Lin H, Ye S, Liu Q-y, Meng Z, Zhang C-m, et al. Remarkably high activities of testicular cytochrome c in destroying reactive oxygen species and in triggering apoptosis. Proceedings of the National Academy of Sciences. 2006;103(24):8965-70.

217. Silva EC, Cárcano FM, Bonatelli M, Zaia MG, Morais-Santos F, Baltazar F, et al. The clinicopathological significance of monocarboxylate transporters in testicular germ cell tumors. Oncotarget. 2018;9(29):20386.
218. Bonatelli M, Silva EC, Cárcano FM, Zaia MG, Lopes LF, Scapulatempo-Neto C, et al. The Warburg effect is associated with tumor aggressiveness in testicular germ cell tumors. Frontiers in endocrinology. 2019;10:417.
219. Hammond SM, Caudy AA, Hannon GJ. Post-transcriptional gene silencing by double-stranded RNA. Nature Reviews Genetics. 2001;2(2):110-9.
220. Tang Z, Li C, Kang B, Gao G, Li C, Zhang Z. GEPIA: a web server for cancer and normal gene expression profiling and interactive analyses. Nucleic acids research. 2017;45(W1):W98-W102.
221. Győrffy B. Survival analysis across the entire transcriptome identifies biomarkers with the highest prognostic power in breast cancer. Computational and structural biotechnology journal. 2021;19:4101-9.
222. Győrffy B. Discovery and ranking of the most robust prognostic biomarkers in serous ovarian cancer. Geroscience. 2023:1-10.
223. Győrffy B, Surowiak P, Budczies J, Lánczky A. Online survival analysis software to assess the prognostic value of biomarkers using transcriptomic data in non-small-cell lung cancer. PloS one. 2013;8(12):e82241.
224. Posta M, Győrffy B. Analysis of a large cohort of pancreatic cancer transcriptomic profiles to reveal the strongest prognostic factors. Clinical and Translational Science.
225. Kovács SA, Fekete JT, Győrffy B. Predictive biomarkers of immunotherapy response with pharmacological applications in solid tumors. Acta Pharmacologica Sinica. 2023:1-11.
226. Atlas THP. The Human Protein Atlas 2023 [Available from: https://www.proteinatlas.org/ENSG00000138709-LARP1B/tissue#expression_summary.
227. Mattijssen S, Kozlov G, Fonseca BD, Gehring K, Maraia RJ. LARP1 and LARP4: up close with PABP for mRNA 3'poly (A) protection and stabilization. RNA biology. 2021;18(2):259-74.
228. Lu J, Wu T, Zhang B, Liu S, Song W, Qiao J, et al. Types of nuclear localization signals and mechanisms of protein import into the nucleus. Cell communication and signaling. 2021;19(1):1-10.
229. Xu D, Farmer A, Collett G, Grishin NV, Chook YM. Sequence and structural analyses of nuclear export signals in the NESdb database. Molecular biology of the cell. 2012;23(18):3677-93.
230. Miyamoto Y, Yamada K, Yoneda Y. Importin α: a key molecule in nuclear transport and non-transport functions. The journal of biochemistry. 2016;160(2):69-75.
231. Özdaş S, Canatar Ip. Targeting of nucleo-cytoplasmic transport factor exportin 1 in malignancy. Medicine International. 2022;2(1):1-8.
232. Faber GP, Nadav-Eliyahu S, Shav-Tal Y. Nuclear speckles–a driving force in gene expression. Journal of cell science. 2022;135(13):jcs259594.
233. Chettle J, Dedeic Z, Fischer R, Vendrell I, Campo L, Easton A, et al. LARP1 regulates metabolism and mTORC1 activity in cancer. bioRxiv. 2022:2022.09. 04.506559.
234. Yamada Y, Takayama Ki, Fujimura T, Ashikari D, Obinata D, Takahashi S, et al. A novel prognostic factor TRIM44 promotes cell proliferation and migration, and inhibits apoptosis in testicular germ cell tumor. Cancer science. 2017;108(1):32-41.
235. Fu Y, Sun S, Bi J, Kong C, Shi D. An RNA-binding protein-related risk signature can predict the prognosis and tumor immunity of patients with testicular germ cell tumors. American Journal of Translational Research. 2022;14(5):2825.

236. Roška J, Wachsmannová L, Hurbanová L, Šestáková Z, Mueller T, Jurkovičová D, et al. Differential gene expression in cisplatin-resistant and-sensitive testicular germ cell tumor cell lines. Oncotarget. 2020;11(51):4735.
237. Niles AL, Moravec RA, Hesselberth PE, Scurria MA, Daily WJ, Riss TL. A homogeneous assay to measure live and dead cells in the same sample by detecting different protease markers. Analytical biochemistry. 2007;366(2):197-206.
238. Ježek J, Cooper KF, Strich R. Reactive oxygen species and mitochondrial dynamics: the yin and yang of mitochondrial dysfunction and cancer progression. Antioxidants. 2018;7(1):13.
239. Nakada K, Sato A, Yoshida K, Morita T, Tanaka H, Inoue S-I, et al. Mitochondria-related male infertility. Proceedings of the National Academy of Sciences. 2006;103(41):15148-53.
240. Murphy MP. How mitochondria produce reactive oxygen species. Biochemical journal. 2009;417(1):1-13.
241. Cheng M-H, Pan C-Y, Chen N-F, Yang S-N, Hsieh S, Wen Z-H, et al. Piscidin-1 induces apoptosis via mitochondrial reactive oxygen species-regulated mitochondrial dysfunction in human osteosarcoma cells. Scientific Reports. 2020;10(1):5045.
242. Movahed ZG, Rastegari-Pouyani M, Hossein Mohammadi M, Mansouri K. Cancer cells change their glucose metabolism to overcome increased ROS: One step from cancer cell to cancer stem cell? Biomedicine & Pharmacotherapy. 2019;112:108690.
243. Kerwitz Y, Kühn U, Lilie H, Knoth A, Scheuermann T, Friedrich H, et al. Stimulation of poly (A) polymerase through a direct interaction with the nuclear poly (A) binding protein allosterically regulated by RNA. The EMBO journal. 2003;22(14):3705-14.
244. Banerjee A, Apponi LH, Pavlath GK, Corbett AH. PABPN 1: molecular function and muscle disease. The FEBS journal. 2013;280(17):4230-50.
245. Ghosh S, O'Connor TJ. Beyond paralogs: the multiple layers of redundancy in bacterial pathogenesis. Frontiers in cellular and infection microbiology. 2017:467.
246. Ewen-Campen B, Mohr SE, Hu Y, Perrimon N. Accessing the phenotype gap: enabling systematic investigation of paralog functional complexity with CRISPR. Developmental cell. 2017;43(1):6-9.
247. Dandage R, Landry CR. Paralog dependency indirectly affects the robustness of human cells. Molecular systems biology. 2019;15(9):e8871.
248. Thompson NA, Ranzani M, van der Weyden L, Iyer V, Offord V, Droop A, et al. Combinatorial CRISPR screen identifies fitness effects of gene paralogues. Nature communications. 2021;12(1):1302.
249. Nicholson-Shaw AL, Kofman ER, Yeo GW, Pasquinelli AE. Nuclear and cytoplasmic poly (A) binding proteins (PABPs) favor distinct transcripts and isoforms. Nucleic acids research. 2022;50(8):4685-702.
250. Lou T-F, Weidmann CA, Killingsworth J, Hall TMT, Goldstrohm AC, Campbell ZT. Integrated analysis of RNA-binding protein complexes using in vitro selection and high-throughput sequencing and sequence specificity landscapes (SEQRS). Methods. 2017;118:171-81.
251. Rivero-Hinojosa S, Pugacheva EM, Kang S, Méndez-Catalá CF, Kovalchuk AL, Strunnikov AV, et al. The combined action of CTCF and its testis-specific paralog BORIS is essential for spermatogenesis. Nature Communications. 2021;12(1):3846.
252. Angus-Hill ML, Schlichter A, Roberts D, Erdjument-Bromage H, Tempst P, Cairns BR. A Rsc3/Rsc30 zinc cluster dimer reveals novel roles for the chromatin remodeler RSC in gene expression and cell cycle control. Molecular cell. 2001;7(4):741-51.
253. Kuo C-L, Ponneri Babuharisankar A, Lin Y-C, Lien H-W, Lo YK, Chou H-Y, et al. Mitochondrial oxidative stress in the tumor microenvironment and cancer immunoescape: foe or friend? Journal of Biomedical Science. 2022;29(1):74.

254. Bourgeois B, Hutten S, Gottschalk B, Hofweber M, Richter G, Sternat J, et al. Nonclassical nuclear localization signals mediate nuclear import of CIRBP. Proceedings of the National Academy of Sciences. 2020;117(15):8503-14.